FLUID MIGRATION THROUGH GEOMEMBRANE SEAMS AND THROUGH THE INTERFACE BETWEEN GEOMEMBRANE AND GEOSYNTHETIC CLAY LINER

Madalena Barroso

Thèse en cotutelle

présentée à

L' UNIVERSITE GRENOBLE I – JOSEPH FOURRIER

Ecole Doctorale Terre-Univers-Environnement

et

FACULDADE DE CIÊNCIAS E TECNOLOGIA DA UNIVERSIDADE DE COIMBRA

Pour l'obtention du titre de

DOCTEUR

Spécialité: Sciences de la terre et de l'univers et de l'environnement

par

Madalena C. P. BARROSO

CONTRIBUTION A L'ETUDE DES TRANSFERTS DE MASSE AU NIVEAU DES JOINTS DE GEOMEMBRANE ET A L'INTERFACE ENTRE GEOMEMBRANE ET GEOSYNTHETIQUE BENTONITIQUE

CONTRIBUIÇÃO PARA O ESTUDO DA MIGRAÇÃO DE FLUIDOS ATRAVÉS DAS JUNTAS DE GEOMEMBRANA E ATRAVÉS DA INTERFACE ENTRE GEOMEMBRANA E GEOSSINTÉTICO BENTONÍTICO

FLUID MIGRATION THROUGH GEOMEMBRANE SEAMS AND THROUGH THE INTERFACE BETWEEN GEOMEMBRANE AND GEOSYNTHETIC CLAY LINER

Soutenue le 23 Mars 2005

Jury

Patrick PIERSON	Directeur de thèse
Luís LEMOS	Directeur de thèse
Maria de Lurdes LOPES	Rapporteur
Bernard PERRIN	Rapporteur
Nathalie TOUZE-FOLTZ	Examinatrice
Maria da Graça LOPES	Examinatrice
Gaétan POTIÉ	Examinateur

Thèse préparée au sein de *Laboratório Nacional de Engenharia Civil* (LNEC), au Cemagref et en cotutelle à l'Université Joseph Fourrier et l'Université de Coimbra

ACKNOWLEDGEMENS

This dissertation has been developed under a co-operation agreement (*cotutelle*) between the University Joseph Fourrier (*Laboratoire Interdisciplinaire de Recherche Impliquant la Géologie et la Mécanique de l'Université Joseph Fourier* – Lirigm) and the University of Coimbra (*Faculdade de Ciências e Tecnologia* – FCTUC). The *Laboratório Nacional de Engenharia Civil* (LNEC) and the *Institut de Recherche pour I'Ingénierie de l'Agriculture et de l'Environnement* (Cemagref) were also involved in this co-operation. The work was surpervised, in France, by Professor Patrick Pierson and Mrs. Nathalie Touze-Foltz (PhD), and, in Portugal, by Professor Luís Lemos and Professor Maria da Graça Alfaro Lopes.

First, I would like to express my gratitude to the LNEC, in the person of its Director, Professor Francisco Correia Nunes, for all the resources and facilities offered.

Thanks are extended to Lirigm, to Cemagref, and to FCTUC, not only for the resources and facilities offered, but also for always welcoming me.

I am grateful to Professor Patrick Pierson, to Mrs. Nathalie Touze-Foltz (PhD), to Professor Luís Lemos and to Professor Maria da Graça Alfaro Lopes for their supervision, support, and never failing encouragement. Their advice was always constructive and therefore much valued and appreciated. Also their kindness sincerely touched me, and their commitment inspired me. I have been impressed by their dedication from the heart.

I wish to express my gratitude to Professor Bernard Perrin, professor at *Université Paul Sabatier*, Toulouse and to Professor Maria de Lurdes Lopes, professor at *Faculdade de Engenharia da Universidade do Porto* for accepting to be reviewers of my dissertation.

This work would not have been possible without the invaluable, and excellent, technical support provided by many people at LNEC, Lirigm and Cemagref. In particular, I am indebted to Mr. Luís Pinto for his help with the running of the tests carried out at LNEC amongst many other things. A great debt is owed to Mr. Augusto Lopes, former technician at LNEC, and to Mr. Yves Orengo, research engineer at Lirigm, for actually turning the designs into reality. Thanks are also extended to Mr. Roland Gallo and Mr. Didier Croissant for their assistance during the laboratory tests carried out at Cemagref.

I am also grateful to Mr. Alvaro Ribeiro and Mr. Sylvain Moreau for their expert advice on uncertainty calculations, to Mrs. Laura Caldeira (PhD) and Mr. Bilé Serra (PhD) for letting me use the test facilities, respectively, for performing the large-scale tests and for measuring the hydraulic conductivity of the geosynthetic clay liners, and to Mrs. Graça Tomé for revising the English.

Thanks must also go to the colleagues from the Engineering Geology Division of LNEC for their kind co-operation, support and friendship. Special thanks are due to Mr. Filipe Telmo Jeremias (PhD), head of Division, for all his support and encouragement.

I would also like to acknowledge the assistance provided by Ms. Lara Martins, Ms. Marta Gamboa, Mr. Olivier Darlot, Ms. Feriel Mesmoudi and Ms. Aurore Bessières during the period of training in LNEC or in Cemagref.

I have benefited from the discussions with other researchers and engineers, in particular with Mr. Fernando Pardo de Santayana (PhD), Mr. Kent von Maubeuge and Mr. François Cartaud (PhD). Particular thanks go to Professor Kerry Rowe who welcomed me at Queen's University for a two week period that was of particular interest and benefit for my work.

I wish to express, as well, my appreciation to NAUE, SIPLAST and LINTECO, for providing the geosynthetics, and to RESIOESTE for providing the soil used in the experimental works carried out.

I also would like to express my gratitude to *Fundação Calouste Gulbenkian* for the provision of a grant for the missions in France, and to NAUE for the financial support provided for the modifications made in the test facility used for carrying out the large-scale tests in LNEC, as well as for purchasing some laboratory test accessories.

My final thanks must go to my family, who have shown so much care over the entire duration of this study. I owe particular thanks to José, Beatriz and Tomás for their unfailing love and support.

ABSTRACT

Composite liners are used to limit the contamination migration from landfills. Their successful performance is closely related with the geomembrane as it provides the primary barrier to diffusive and advective transport of contaminants. Critical issues on the performance of the geomembranes are the seams between geomembrane panels and the inevitable defects resulting, for instance, from inadequate installation activities.

In landfills, where high density polyethylene geomembranes are usually used, seams are typically made by the thermal-hot dual wedge method. A literature review on quality control of the seams showed that, in situ, fluid-tightness of seams is evaluated in qualitative terms (pass/failure criteria), despite their importance to ensure appropriate performance of the geomembranes as barriers.

In addition, a synthesis of studies on geomembrane defects indicated that defects varying in density from 0.7 to 15.3 per hectare can be found in landfills. Defects represent preferential flow paths for leachate. Various authors have developed analytical solutions and empirical equations for predicting the flow rate through composite liners due to defects in the geomembrane. The validity of these methods for composite liners comprising a geomembrane over a geosynthetic clay liner (GCL) over a compacted clay liner (CCL) has never been studied from an experimental point of view.

To address the problem of fluid migration through the geomembrane seams, an attempt is made to provide a test method, herein termed as “gas permeation pouch test”, for assessing the quality of the thermal-hot dual wedge seams. This test consists of pressurising the air channel formed by the double seam with a gas to a specific pressure and, then, measuring the decrease in pressure over time. From the pressure decrease, both the gas permeation coefficients, in steady state conditions, and the time constant, in unsteady state conditions, can be estimated. Experiments were carried out both in laboratory and in field conditions to study the suitability of this test to assess the quality of the seams in situ. The results obtained suggest that it is possible to assess the quality of the geomembrane seams from a non-destructive test conducted in situ by determining the time constant.

To address the problem of fluid migration through geomembrane defects, composite liners comprising a geomembrane with a circular hole over a GCL over a CCL were simulated in tests at three scales. Flow rates at the interface between the geomembrane and the GCL were measured. Correspondent interface transmissivity was estimated based on final flow rates and observation of the wetted area. A parametric study was performed to evaluate the influence of the prehydration of the GCL, the hydraulic head on top of the liner and the confining stress over the liner system, on the flow rate through composite liners due to defects in the geomembrane, as well as to check the feasibility of an extrapolation of the results obtained on small-scale tests to field conditions. It was found that the transmissivity does not seem to be affected by the prehydration of the GCLs when low confining stresses were used. It also does not seem to be influenced by the increase in confining stress when non-prehydrated GCLs are used. Finally, the transmissivity does not seem to be significantly affected by the increase in hydraulic head. The results also suggest that predictions on flow rates though composite liners due to defects in the geomembrane, which are based on transmissivity values obtained in small scale tests, are conservative.

Lastly, based on the transmissivities obtained in this study, empirical equations for predicting the flow rate through composite liners consisting of a geomembrane over a GCL over a CCL are proposed. Flow rates calculated using these equations are in better agreement with the flow rates measured experimentally than the empirical equations reported in literature. The new empirical equations provide design engineers with simple and accurate tools for calculating the flow rates through the above mentioned type of composite liners.

RESUME

Les étanchéités composites sont utilisées pour limiter la migration des lixiviats à travers les barrières d'installations de stockage de déchets. Leur efficacité est étroitement liée à la géomembrane car cette-ci agit comme une barrière primaire contre le transport diffusif et advectif des contaminants. Un point essentiel pour une bonne performance des géomembranes est la bonne qualité des soudures entre les lés de géomembranes ainsi que l'absence de défauts.

Dans les barrières d'installations de stockage de déchets, où des géomembranes en polyéthylène haute densité sont le plus couramment utilisées, les soudures sont souvent effectuées par la méthode du double cordon. Une synthèse de la littérature sur le contrôle de la qualité des soudures, a démontré que, sur site, l'étanchéité des soudures est évaluée en termes qualitatifs (critères d'admission/défaillance), malgré leur importance pour assurer la performance adéquate des géomembranes en tant que barrières.

D'autre part, une synthèse des études sur les défauts dans les géomembranes a démontré que leur densité est comprise en moyenne entre 0,7 à 15,3 par hectare dans les barrières d'installations de stockage de déchets. Les défauts représentent des passages préférentiels d'écoulement pour les lixiviats. Plusieurs auteurs ont développé des solutions analytiques et des équations empiriques pour prévoir l'écoulement au travers des étanchéités composites dus à des défauts dans la géomembrane. La validité de ces équations pour les étanchéités composites comportant une géomembrane associée à un géosynthétique bentonitique (GSB) placé sur une couche d'argile compactée (CCL) n'a jamais été étudiée, du point de vue expérimental.

Une méthode d'essai a été élaborée pour évaluer la qualité des soudures effectuées par la méthode du double cordon, ici désignée comme "essais de perméabilité au gaz sur poche". Cet méthode d'essai consiste à pressuriser le conduit d'air résultant de l'élaboration du double cordon avec un gaz jusqu'à une pression spécifique et mesurer la réduction de la pression au cours du temps. A partir de la réduction de la pression on peut estimer les coefficients de perméation au gaz, en régime permanent, ainsi que la constante de temps, en régime transitoire. Des essais ont été effectués à la fois au laboratoire, et en extérieur avec des soudures exposées, pour étudier l'adéquation de cet essai à l'évaluation de la qualité des soudures sur site. Les résultats obtenus suggèrent qu'il est possible d'évaluer la qualité des soudures de géomembrane à partir d'un essai non-destructif effectué sur site moyennant la détermination de la constante de temps.

Des essais à trois échelles différentes ont été réalisés avec des étanchéités composites comportant une géomembrane avec un trou circulaire surmontant un GSB pour étudier le problème de la migration des liquides au travers des défauts dans la géomembrane. Les débits à l'interface entre la géomembrane et le GSB ont été mesurés et la transmissivité de l'interface correspondante a été estimée. Une étude paramétrique a été effectuée pour évaluer l'influence de la pré-hydratation du GSB, de la charge hydraulique et de la contrainte mécanique appliquées sur l'étanchéité composite, ainsi que pour évaluer la viabilité de l'extrapolation des résultats obtenus dans des essais à petite échelle aux conditions de terrain. On a observé que la transmissivité ne semble pas être affectée par la pré-hydratation des GSB quand des contraintes de confinement réduites ont été utilisées. La transmissivité ne semble pas non plus être influencée par l'augmentation de la contrainte de confinement quand on utilise des GSB, qui n'ont pas été préalablement hydratés. Finalement, la transmissivité ne semble pas être significativement affectée par l'augmentation de la charge hydraulique. Les résultats suggèrent aussi que les prévisions relatives aux débits au travers des étanchéités composites liés à l'existence de défauts dans la géomembrane, et basées sur les valeurs de transmissivité obtenues dans des essais à petite échelle représentent la limite supérieure des débits pouvant être observés.

Finalement, à partir des valeurs de transmissivité obtenues dans cette étude, on a développé des équations empiriques pour prévoir le débit au travers des étanchéités composites comportant une géomembrane, un GSB et une CCL. Les débits calculés en utilisant les nouvelles équations proposées sont plus proches des résultats de mesure que les équations empiriques existantes. Ces nouvelles équations empiriques représentent donc pour l'ingénieur un outil validé par l'expérimentation de prévision des débits à travers les étanchéités composites.

RESUMO

Os sistemas de confinamento de fundo e taludes dos aterros de resíduos incluem barreiras múltiplas, tipicamente constituídas por uma geomembrana, geralmente de polietileno de alta densidade (PEAD), um geossintético bentonítico (GCL) e uma camada de solo argiloso compactada (CCL). O sucesso destas barreiras depende, em grande medida, do desempenho das geomembranas pois estas constituem a barreira activa à migração de poluentes. Os principais aspectos, que podem comprometer o desempenho das geomembranas, são as juntas (união entre painéis adjacentes) e os orifícios.

A revisão bibliográfica sobre o controlo de qualidade das juntas in situ indicou que a estanqueidade das juntas é avaliada, através de critérios qualitativos (passa/não passa), não obstante a importância das mesmas para assegurar o desempenho adequado das geomembranas.

Por outro lado, a revisão bibliográfica sobre orifícios nas geomembranas mostrou que estes são inevitáveis e que, nos aterros de resíduos, o seu número pode variar entre 0,7 a 15,5 por hectare. Os orifícios representam caminhos preferenciais para a migração de poluentes. Várias equações analíticas e empíricas têm sido desenvolvidas, para calcular o fluxo de contaminantes que migra através de orifícios nas geomembranas. Porém, a validade destes métodos, para barreiras múltiplas constituídas por geomembrana, GCL e CCL, nunca foi estudada de um ponto de vista experimental.

Para estudar o problema da estanqueidade das juntas realizadas por termofusão, com dupla soldadura (método geralmente utilizado para nas geomembranas de PEAD), desenvolveu-se um ensaio, o qual foi designado por "ensaio de permeância em bolsa de gás". Este ensaio consiste em pressurizar o canal entre os dois lados da dupla soldadura com um determinado gás. A qualidade das juntas foi avaliada com base em dois parâmetros, determinados a partir do decréscimo de pressão no interior da junta, ao longo do tempo. O primeiro parâmetro, a permeância, foi calculado em regime permanente. O segundo, " parâmetro τ", foi estimado em regime transitório. Foram realizados ensaios em laboratório assim como ao ar livre, a fim de estudar a adequabilidade do método para avaliar a qualidade das juntas in situ. Os resultados obtidos sugerem que é possível avaliar a qualidade das juntas através de ensaios de permeância em bolsa de gás in situ, mediante a determinação do parâmetro τ.

Para estudar o problema da migração de fluidos através de orifícios na geomembrana, realizaram-se ensaios em três escalas, com vista a medir o fluxo que migra através de um orifício na geomembrana e calcular a correspondente transmissividade entre a mesma e o GCL. Este trabalho teve por objectivos estudar a influência da pré-hidratação dos GCLs, da tensão confinante e da carga hidráulica sobre a migração de fluidos através dos orifícios da geomembranas assim como comparar os resultados obtidos a diferentes escalas e avaliar a validade dos resultados obtidos, em ensaios laboratoriais, para as condições em que a geomembrana se encontra em serviço. Os resultados sugerem que a transmissividade não é significativamente influenciada pela pré-hidratação dos GCLs quando a tensão confinante é reduzida. Por outro lado, o aumento da tensão confinante influenciou apenas os resultados dos ensaios realizados com provetes pré-hidratados. A transmissividade não foi, igualmente, influenciada pelo aumento da carga hidráulica. Os resultados sugerem, também, que o cálculo do fluxo que migra através de orifícios de geomembrana, realizado com base nos valores da transmissividade, obtidos em ensaios de pequena escala, é conservativo.

Por fim, com base nos valores de transmissividade obtidos neste estudo, desenvolveram-se equações empíricas para calcular o fluxo que migra através de barreiras múltiplas constituídas por uma geomembrana, um GCL e uma camada de solo argiloso compactada. Os fluxos calculados utilizando as novas equações foram relativamente semelhantes aos obtidos experimentalmente e, comparativamente, mais precisos do que os fluxos calculados com base nas equações empíricas disponíveis na literatura, o que constitui um melhoramento nas ferramentas existentes.

TABLE OF CONTENTS

Appendixes:

LIST OF FIGURES

LIST OF TABLES

NOTATIONS

Roman

a	=	area of circular defect in geomembrane (m^2)
A, A_p, A_Q	=	constants (dimensionless)
b	=	width of defect of infinite length (m)
B, B_p, B_Q	=	constants (dimensionless)
C	=	$H_f + H_L - h_a$ (m)
C_c	=	contact condition factor, also called contact quality factor (dimension is variable), for axi-symmetric case
C_{td}	=	contact condition factor, also called contact quality factor (dimension is variable), for two-dimensional case
c_f	=	concentration of penetrant molecules in fluid in contact with geomembrane (kg m^{-3})
c_g	=	concentration of diffusing molecules in geomembrane (kg m^{-3})
D	=	diffusion coefficient (m^2 s^{-1})
E_{peel}	=	seam efficiency in peel (%)
E_{shear}	=	seam efficiency in shear (%)
f	=	mass flux of penetrant molecules through the geomembrane (kg m^{-2} s^{-1})
f_{CO2L}	=	mass flux of carbon dioxide through the geomembrane by unit of seam length (kg m^{-2} s^{-1})
f_G	=	mass flux of gas G determined for Δp_G when the specimen is immersed in gas (mol m^{-2} s^{-1} for geomembrane area unit or mol s^{-1} for pouch specimen)
f_G'	=	mass flux of gas G determined for $\Delta p'_G$ when the specimen is immersed in liquid (mol m^{-2} s^{-1} for geomembrane area unit or mol s^{-1} for pouch specimen)
f_{N2}	=	mass flux of nitrogen through the geomembrane (kg m^{-2} s^{-1})
f_{N2L}	=	mass flux of nitrogen through the geomembrane by unit of seam length (kg m^{-2} s^{-1})
f_W	=	mass flux of water vapour determined (mol m^{-2} s^{-1} for geomembrane area unit or mol s^{-1} for pouch specimen)
F, E	=	coefficient, value dependent on boundary conditions (m)
g	=	acceleration due to gravity (m s^{-2})
h	=	hydraulic head interface (m)
h_a	=	hydraulic head in aquifer or at bottom of foundation layer (m)
H_f	=	thickness of the foundation layer (m)
H_{GCL}	=	thickness of the GCL (m)
H_L	=	thickness of the soil layer (CCL or GCL)(m)
H_S	=	equivalent thickness of the soil liner (GCL+CCL) (m)
h_s	=	specific hydraulic head in interface at $r = R_c$ (m)
h_w	=	elevation of the water body above a specific datum (m)
i	=	hydraulic head gradient (m)
I_0	=	modified Bessel function of zero order (dimensionless)
I_1	=	modified Bessel function of first order (dimensionless)
IP	=	plasticity index (%)
i_s	=	mean gradient across soil layer and foundation layer (dimensionless)
k	=	saturated hydraulic conductivity (m s^{-1})
K	=	unsaturated hydraulic conductivity (m s^{-1})
K_0	=	modified Bessel function of zero order (dimensionless)

K_1 = modified Bessel function of first order (dimensionless)

k_f = hydraulic conductivity of foundation layer (m s^{-1})

k_{GCL} = hydraulic conductivity of geosynthetic clay liner (m s^{-1})

k_i = hydraulic conductivity of interface (m s^{-1})

k_L = hydraulic conductivity of soil layer (CCL or GCL) (m s^{-1})

k_s = equivalent hydraulic conductivity (GCL+CCL) (m s^{-1})

k_x, k_y, k_z = hydraulic conductivity, repectively, in x-direction, y-direction and z-direction (m s^{-1})

L = seam length (m)

L_0 = melt depth (m)

LL = liquid limit (%)

LP = plastic limit (%)

L_{td} = length of the geomembrane seam, or length of two-dimensional defect in geomembrane (defect of infinite length or damaged wrinkle) (m)

m = van Genuchten model parameter (dimensionless)

M_f = mass of dry filter paper (g)

M_w = mass of water in the filter paper (g)

n = number of moles of specific element (mol)

n = van Genuchten model parameter (dimensionless)

n_G = number of moles of gas G (mol)

n_{G+W} = number of moles of gas G and water W (mol)

n_{N2} = number of moles of nitrogen (mol)

n_W = number of moles of water (mol)

$\underline{P}$ = coefficient of permeability of the geomembrane to a specific element (m^2 s^{-1})

P_0 = $\dfrac{\text{No. of } (\omega, \gamma_d) \text{ points above line of optimums}}{\text{Total No. of } (\omega, \gamma_d) \text{ measurements}} \times 100$

p_{atm} = atmospheric pressure (Pa)

P_{CO2L} = permeance to carbon dioxide by unit of seam length (mol m^{-1} s^{-1} Pa^{-1})

P_G = permeance to gas G (mol m^{-2} s^{-1} Pa^{-1} for characterizing geomembrane area unit or mol s^{-1} Pa^{-1} for characterizing pouch specimen)

p_{G+W} = gas and water vapour pressure in pouch (Pa)

p_{Gin} = gas G absolute pressure inside the pouch (total or partial pressure depending on the gas composition, monoconstituent or not) (Pa)

$p_{Gin}(\infty)$ = absolute final gas pressure in the pouch (Pa)

$p_{Gin}(0)$ = absolute initial gas pressure in pouch (Pa)

p_{Gout} = gas pressure outside pouch specimen (Pa)

p_{N2} = nitrogen pressure in pouch (Pa)

p_{N2out} = nitrogen pressure outside pouch specimen (Pa)

P_{N2} = permeance to nitrogen (mol s^{-1} Pa^{-1})

P_{N2L} = permeance to nitrogen by unit of seam length (mol m^{-1} s^{-1} Pa^{-1})

P_W = permeance to water vapour (mol m^{-2} s^{-1} Pa^{-1} for characterizing geomembrane area unit or mol s^{-1} Pa^{-1} for characterizing pouch specimen)

p_{Wout} = pressure of liquid outside the pouch specimen (Pa)

$\underline{P_{N2}}''$ = coefficient of permeability to nitrogen (mol s^{-1} m^{-1} Pa^{-1})

$\underline{P_W}''$ = coefficient of permeability to water vapour (mol s^{-1} m^{-1} Pa^{-1})

$\underline{P_G}''$ = coefficient of permeability to a specific gas G (mol s^{-1} m^{-1} Pa^{-1})

$\underline{P_G'}$ = coefficient of permeability to a specific gas G (mol m^2 s^{-1} kg^{-1})

$\overline{P_{CO2L}}$ = mean cabon dioxide permeance by unit of seam length (mol m^{-1} s^{-1} Pa^{-1})

$\overline{p_{G+W}}$ = mean gas and water vapour pressure in pouch during the time interval Δt (Pa)

$\overline{P_{GL}}$ = mean gas G permeance of pouch specimen by unit of seam length determined for time interval Δt (mol s^{-1} m^{-1} Pa^{-1})

$\overline{P_G}$ = mean gas G permeance of pouch specimen determined for time interval Δt (mol m^{-2} s^{-1} Pa^{-1} for characterizing geomembrane area unit or mol s^{-1} Pa^{-1} for characterizing pouch specimen)

$\overline{p_{Gin}}$ = mean gas G pressure inside the pouch during the time interval Δt (Pa)

$\overline{P_{N2L}}$ = mean nitrogen permeance by unit of seam length (mol m^{-1} s^{-1} Pa^{-1})

$\overline{P_{N2}}$ = mean nitrogen permeance of pouch specimen determined for time interval Δt (mo m^{-2} s^{-1} Pa^{-1} for characterizing geomembrane area unit or mol s^{-1} Pa^{-1} for characterizing pouch specimen)

$\overline{P_{WL}}$ = mean water vapour permeance of pouch specimen by unit of seam length determined for time interval Δt (mol s^{-1} m^{-1} Pa^{-1})

$\overline{P_W}$ = mean water vapour permeance of pouch specimen determined for time interval Δt (mol m^{-2} s^{-1} Pa^{-1} for characterizing geomembrane area unit or mol s^{-1} Pa^{-1} for characterizing pouch specimen)

$\overline{p_W}$ = mean water vapour pressure in pouch during the time interval Δt (Pa)

Q = rate of flow through defect in geomembrane component of a composite liner (m^3 s^{-1})

Q_a = $2.85 Q_R \left[log \frac{k_i}{k_{GCL}} \right]^{-0.73}$ (m^{2}s^{-1})

Q_L = rate of flow per unit length (m^{2}s^{-1})

Q_r = radial rate of flow in transmissive layer for a axi-symmetric problem (m^{3}s^{-1})

Q_R = rate of flow predicted using Equation (4.30) (m^{2}s^{-1})

Q_s = rate of flow into soil liner (soil layer and foundation layer) (m^{3}s^{-1})

Q_x = rate of flow in interface for two-dimensional problem (m^{3}s^{-1})

r = radial distance (m)

r = specific humidity (water vapour kg dry air kg^{-1})

R = Universal Gas Constant (8.3143 m^3 Pa mol^{-1} K^{-1})

R_c = radius of test cell or system studied in axi-symmetric case (m)

r_0 = radius of defect in geomembrane (m)

s = thickness of interface (m)

s_t = seam thickness (m)

S_{gf} = partitioning coefficient (dimensionless)

T = absolute temperature (K)

$T_{seam\ in\ peel}$ = seam peel strength (N)

$T_{seam\ in\ shear}$ = seam shear strength (N)

$T_{unseamed\ sheet}$ = sheet tensile strength (N)

t = time (s)

t_0 = delay time (s)

t_g = thickness of geomembrane (m)
u = uncertainty
v = Darcian velocity (m s^{-1})
V = inner volume of pouch specimen (m^3)
WTR = water vapour transmission rate
x = horizontal distance (m)
X_c = width of test cell or system studied in damaged wrinkle case (m)
X_w = limit width for validity of two-dimensional solutions (m)
z = spatial dimension parallel to the direction of diffusion (m)
z = vertical distance (m)
$Z(t)$ = $\left[\frac{p_{Gin}(t) - p_{Gout}}{p_{Gin}(0) - p_{Gout}}\right]$

Greek

α = van Genuchten model parameter (m^{-1})
β = $\sqrt{\frac{k_s}{(H_L + H_f)\theta}}$ (m^{-1})
χ = exponent of hydraulic head in empirical equation (dimensionless)
$\partial c_g/\partial z$ = concentration gradient of diffusing molecules in geomembrane (kg m^{-4})
$\partial h_w/\partial x$ = hydraulic head gradient in the x-direction (dimensionless)
$\partial h_w/\partial y$ = hydraulic head gradient in the y-direction (dimensionless)
$\partial h_w/\partial z$ = hydraulic head gradient in the z-direction (dimensionless)
ε = $\frac{R\,T P_G}{V}$ (s^{-1})
γ_d = dry unit weight (kN m^{-3})
$(\gamma_d)_{max}$ = maximum dry unit weight (kN m^{-3})
γ_w = unit weight of water (kN m^{-3})
η = dynamic viscosity of water (kg m^{-1} s^{-1})
κ = exponent of soil layer hydraulic conductivity in empirical equation (dimensionless)
λ = factor in hydraulic gradient expression (dimensionless)
μ = exponent in hydraulic gradient expression (dimensionless)
π = constant = 3.14159265…
θ = transmissivity of the interface (m^2 s^{-1})
ρ_w = density of water (kg m^{-3})
τ = time constant (hour)
τ_{CO2} = time constant for carbon dioxide (hour)
τ_{N2} = time constant for nitrogen (hour)
ω = gravimetric water content (%)
ω_f = water content of the filter paper (%)
ω_{opt} = optimum water content (%)
ξ = exponent of defect area or width in empirical equation (dimensionless)
ψ = total potential or suction (m)
ψ_c = suction for which $K=k/2$ (m)

ψ_g = gravitational potential (m)
ψ_m = matric potential (m)
ψ_p = pressure potential (m)
ψ_o = osmotic potential (m)
Θ = volumetric water content (dimensionless)
Θ_r = residual volumetric water content (dimensionless)
Θ_s = volumetric water content at saturation (dimensionless)
Ω_0, Ω_1 = constants (dimensionless)

Differences

Δc_f = concentration difference of penetrant molecule in adjacent fluids on either side of the geomembrane (kg m^{-3})
Δc_g = concentration difference of penetrant molecule in the geomembrane (kg m^{-3})
Δn = number of moles difference (mol)
Δp_G = partial pressure difference of penetrant molecule *G* in adjacent fluids on both sides of geomembrane for specimen immersed in gas (Pa)
$\overline{\Delta p_G}$ = mean pressure difference during time interval Δt for specimen immersed in gas (Pa)
$\Delta p_G'$ = partial pressure difference of penetrant molecule G in adjacent fluids on both sides of geomembrane for specimen immersed liquid (Pa)
$\overline{\Delta p_G}'$ = mean pressure difference during time interval Δt for specimen immersed in liquid (Pa)
Δp_W = water partial pressure difference (Pa)
Δt = time interval (s)
δt = infinitesimal time interval (s)

Abbreviations

CCL: Compacted Clay Liner
CEMAGREF: Institut de Recherche pour l'Ingénierie de l'Agriculture et de l'Environnement
ECC: Excellent Contact Conditions
GCL CC: GCL Contact Conditions
GCL: Gosynthetic Clay Liner
GM: Geomembrane
GSYS: Geomembrane Yield Strength
LIRIGM: Laboratoire Interdisciplinaire de Recherche Impliquant la Géologie et la Mécanique de l'Université Joseph Fourier
LNEC: Laboratório Nacional de Engenharia Civil
PLCS: Primary Leachate Collection System
SLCS: Secondary Leachate Collection System
USEPA: United States Environmental Protection Agency

1 INTRODUCTION

1.1 BACKGROUND

As mankind becomes increasingly aware of the environment, more questions are asked as to the possible environmental effects of our waste management systems. The disposal of waste may lead to contamination of the air, surface water, or groundwater. Over the past two decades it has become necessary to design and construct safe waste disposal facilities or landfills. Modern landfills are designed with a barrier system intending to control contaminant movement from any waste facility to levels that will result in negligible impact to the environment. This system often includes composite liners, consisting either of a geomembrane over a compacted clay liner, of a geomembrane over a geosynthetic clay liner, or of a geomembrane over a geosynthetic clay liner over a compacted clay liner.

The effectiveness of composite liners in service conditions is closely related with the performance of geomembranes, as they provide the primary resistance for contaminants to migrate from the site. The performance of the geomembrane is linked with the seams quality and the unavoidable defects occurring mainly due to inadequate construction activities, such as, puncture, tears, cuts, etc.

Seams need both to be fluid-tight and have a mechanical strength of the same order of magnitude as geomembrane panels. In landfills, where geomembranes are mainly seamed by the thermal-hot dual wedge method, the fluid-tightness of the seams is typically evaluated in qualitative terms, in spite of the recognised vulnerability of those areas. A more accurate tool to evaluate the quality of the seams by quantitative measurement of their fluid-tightness arises as a need.

As regards the unavoidable defects in the geomembrane, their impact can be minimised by proper design of the landfill liner. For that, it is of primary importance to predict the flow rates through composite liners due to defects in the geomembrane. A number of attempts has been made to predict the flow rates by calculations based on fundamental parameters that govern the problem. Even though several tools are available (empirical equations, analytical equations, numerical codes), experimental data for validating those tools are scarce.

1.2 RESEARCH OBJECTIVES

The aim of this dissertation is to study the quality of geomembrane seams from a fluid-tightness point of view, and to evaluate the flow rates through composite liners due to defects in the geomembrane.

With regard to seams, the study concentrates on high density polyethylene geomembranes made by the thermal-hot dual wedge method. The main objectives of the research carried out can be summarised as follows:

- To design and carry out a series of small-scale laboratory tests, termed here as "gas permeation pouch tests", for assessing quantitatively the quality of the geomembrane seams, as well as for studying the aptness of the pressurised dual method, usually used on site to evaluate the thermal-hot dual wedge seams quality;

- To design and carry out large-scale gas permeation pouch tests, both in laboratory and in field conditions, to study the suitability of performing this test in situ to assess the quality of thermal-hot dual wedge geomembrane seams;

- To carry out mechanical tests to investigate a possible correlation between gas permeation test results and mechanical strength of the seams.

As to flow rates, the study concentrates on composite liners consisting of a geomembrane over a geosynthetic clay liner (GCL) over a compacted clay liner (CCL). The amount of liquid flow at the interface between the geomembrane and the GCL seems to depend on many factors, namely: the hydraulic conductivity of the GCL (saturated or unsaturated), the liquid head acting on top of the composite liner, the confining stress over the liner system, the contact conditions between the geomembrane and the GCL, the thickness of the lining system (GCL and CCL), the type and location of the defect in the geomembrane, etc. A parametric study is conducted to find the relative importance of some of the most important parameters governing the flow rate through composite liners due to geomembrane defects. The research objectives were the following:

- To carry out a series of laboratory tests to examine the suitability of the filter paper method for evaluating the suction of the GCLs; suction is required to estimate the water retention curves, from which it is possible to infer the unsaturated hydraulic conductivity of the GCLs;

- To design and carry out a series of small-scale laboratory tests to examine the influence of prehydration of the GCLs, of the confining stress, and of the hydraulic head on flow rates through composite liners due to defects in geomembranes;

- To design and carry out intermediate and large scale tests for complementing the small-scale tests and for checking the feasibility of an extrapolation of the results obtained on small-scale tests to field conditions;

- To develop empirical equations for predicting the flow rate through composite liners due to defects in the geomembrane.

1.3 OUTLINE OF THE DISSERTATION

This dissertation is organised in seven chapters. After the present chapter of introduction, Chapter 2 focuses on landfills and composite bottom liners. Emphasis will be given to critical issues related with a successful performance of geomembranes (seams and defects) and to the factors affecting the hydraulic performance of the geosynthetic clay liners.

Chapter 3 addresses the theoretical background on mass transport through intact geomembranes. The governing equations for determining the permeation coefficients of the geomembranes are given in the chapter. A summary of previous experimental studies on geomembrane permeation to gases and water vapour is also presented.

Chapter 4 contains the basic theory on water flow through both saturated and unsaturated porous media. The predictive methods for assessing the unsaturated hydraulic conductivity are described. Emphasis is given to methods based on water retention curves, often represented by the van Genuchten parameters. A literature review on water retention curves for GCLs is included. Also in Chapter 4, the existing analytical solutions and empirical equations to predict the flow rate through composite liners are discussed. Finally, the chapter presents a synthesis of previous studies on flow through composite liners consisting of a geomembrane and of a GCL.

Chapter 5 describes the experimental work on gas flow through geomembrane seams. Materials, equipment, and test procedures are described. The results obtained are reported and discussed.

Chapter 6 presents the experimental work on water retention curves and on flow rates through composite liners due to geomembranes defects, including a description of specimens, equipments and test procedures. The results obtained are shown and discussed. These are followed by the development of empirical equations for predicting the flow rate through composite liners consisting of a geomembrane over a GCL over a CCL.

Chapter 7 summarises the conclusions drawn from the work described in this thesis, and highlights various recommendations for future research.

2 LANDFILLS AND COMPOSITE LINERS

2.1 INTRODUCTION

The disposal of waste materials is a matter of increasing public concern. The major component of solid waste disposal systems in almost every country is the landfill. During the last three decades, the practice of landfilling has developed into fully engineering facilities subject to stringent regulations in order to protect the environment. To limit contaminant migration to levels that will result in negligible impact on the environment, several different types of lining systems can be used for waste containment. The simplest liner consists of either a geomembrane, a CCL or a GCL. Whereas any of these materials can be used as a barrier by itself, modern landfills usually combine two or more components, for example, a geomembrane over a CCL, a geomembrane over a GCL, or geomembrane over a GCL over a CCL, creating a composite liner.

In a composite liner, the geomembrane provides the primary resistance to advective contaminant flow (also termed leakage, and herein simply referred to as flow) as well as to diffusion of some contaminants. The clay component of the composite liner, CCL or GCL, serves to reduce the flow through inevitable holes or defects in the geomembrane. It also provides some attenuation of contaminants that can diffuse through intact geomembranes or transfer through holes in the geomembranes.

Some of the significant issues in the design of composite liners are (Rowe 1999): (1) contaminant transport (advective and diffusive transport); (2) service life of the engineered waste disposal systems (i.e. how long can it be relied upon to control transport to the design level); (3) geotechnical problems (e.g. stability, differential settlement, bearing capacity); and (4) natural attenuation of contaminants (e.g. sorption, biodegradation, and dilution).

In the scope of the present work, emphasis will be given to the first point: the potential for advective and diffusive transport. This topic is linked with the problem of vulnerable areas of geomembranes, namely the seams between geomembrane panels, and the unavoidable defects (holes, tears, cuts, etc.). This chapter focuses on landfill composite bottom liners. First, it makes an overview of landfills and their design approaches. Then, it addresses the materials used in composite liners, namely geomembrane liners, GCLs and CCLs, as well as the main critical issues related with their successful performance in landfills.

2.2 LANDFILLS

2.2.1 Historical perspective

Landfilling, in various forms, has been a common practice for a while. However, until the late seventies little attention was given to the impact of landfilled waste on the environment. From that time to the nineties landfill design philosophy changed towards the containment and isolation of the waste, giving rise to the development of engineered waste disposal systems, followed by an extensive use of geosynthetics. The focus of the present decade seems to be on mechanical and biological waste treatment, increasing use of leachate recirculation and bioreactor technology, as the knowledge of these concepts increases, as well as the benefits

related to the reduction of long term costs and liabilities (Bouazza et al. 2002a). The evolution of the municipal solid waste landfills in developed countries is summarized in Table 2.1.

Table 2.1 - Summary of municipal solid waste landfill evolution (from Bouazza et al. 2002a)

Dates	Development	Problems	Improvements
1970s	Sanitary landfills	Health/nuisance	Daily cover, better compaction, engineered approach to containment
Late 1980s to early 1990s	Engineered landfills, recycling	Ground and groundwater contamination	Engineered liners, covers, leachate and gas collection systems, increasing regulation
1990s	Improved siting and containment, waste diversion and re-use	Stability, gas migration	Incorporation of technical and socio-political factors into siting process, development of new lining materials, new cover systems, increase post-closure use
2000s	Improved waste treatment	?	Increasing emphasis on mechanical and biological waste treatment, leachate recirculation and bioreactors

Modern landfills include three liner components: bottom, side, and cover liners. The bottom liner is used to prevent or reduce the advective and diffusive contaminant migration into the surrounding environment. The side slope liner has basically the same functions as the bottom liner, while the cover system controls water and gas movement and minimizes odours, disease vectors and other nuisances. Cover systems are also used to meet erosion, aesthetic, and post-closure development criteria.

The most stringent of the mentioned systems is the bottom liner. It typically includes an active barrier and a passive barrier. The active barrier incorporates the drainage system (drainage systems and filters) and the active confinement of the landfill (geomembrane, usually high density polyethylene), whereas the passive barrier comprises the passive confinement (CCL and/or GCL) and the attenuation layer (geological barrier).

The design solution for landfill lining systems depends on regulations and on characteristics of the site. Regulations can vary from country to country or even within the country, depending on waste management strategies and practices, as well as public concern and political will. It depends also on the type of landfills, which are typically classified into three groups according to the wastes: inert, non hazardous (e.g. municipal solid wastes), and industrial hazardous (European Directive No. 1999/31/EC).

2.2.2 Design approaches

The design of a landfill liner system can be made either on a prescriptive basis or on a performance basis (Manassero et al. 1998). In the first case, the requirements for a minimum lining system profile are specified through regulations, whereas in the second approach it must take into account numerous parameters such as: transport parameters and service life of the mineral barriers, drainage layers, geosynthetics, and also the main characteristics of the waste. The objective is to evaluate the leachate quality and production over the landfill activity and after closure (Manassero et al. 2000).

Both approaches present advantages and disadvantages. As regards prescriptive design approach, the main benefits can be summarised as follows (Estrin & Rowe 1995): (1) minimises the effort of approval for the regulator by providing a process which basically allows a check list comparison to be made between the proposed design and the prescriptive design requirements; (2) makes it easy for proponents since the regulator can easily determine if the proponent's application complies with the prescriptive specifications; and (3) ensures a minimum environmental protection. However, it might be either insufficient to assure minimisation of environmental impacts at long term, or overly conservative (Rowe et al. 1995).

The main benefits of the performance design approach include (Estrin & Rowe 1995): (1) allowing landfill designer to bring updated engineering concepts in designing to achieve these performance standards, which promotes both theoretical and practical research investigation and the application of evolving technology in the field; (2) need of a detailed evaluation of the proposed design prior to approval; and (3) the lining systems can be adapted to the specific characteristics of the waste and the considered site. The drawbacks of this approach can be listed as follows (Manassero et al. 1998): (1) the reliability of the design model must be validated; (2) the reliability of each input parameter for modelling the behaviour of landfill lining performance and the time and space variability of the contaminant targets must be checked; and (3) evaluation of some projects can be very difficult.

Most regulations around the world follow the prescriptive design approach. Table 2.2 presents a summary of regulatory requirements for landfill liner design in different countries. The performance design approach has been used in some countries such as Canada and USA.

Many European Countries follow the European Directive No. 1999/31/EC. It establishes that the protection of soil and water (groundwater and superficial water) must be achieved by combining a geological barrier with an artificial sealing layer (usually assumed as a geomembrane). The geological barrier must have a hydraulic conductivity (k) less than 10^{-9} m s^{-1} and be at least 1 m thick. For hazardous waste, bottom lining systems must consist of an artificial sealing layer plus a geological barrier with $k \leq 10^{-9}$ m s^{-1} and be at least 5 m thick.

Nevertheless, according to the European Directive, if the geological barrier does not fulfil the aforementioned conditions other materials may artificially complement it, provided that a technically equivalent protection can be achieved. Moreover, the minimum thickness of the equivalent barrier must be 0.5 m, and the system has to incorporate a drainage layer with a minimum thickness of 0.5 m. The Directive, however, does not illustrate how technical equivalence is to be justified. As result, different design solutions can be considered.

In Portugal, the bottom liner systems implemented in large MSW landfills usually include an active barrier comprising a drainage layer (≥ 0.5 m) and a HDPE geomembrane 2 mm thick, and a passive barrier consisting of a GCL over a CCL ($k < 10^{-9}$ m s^{-1}, thickness ≥ 0.5 m), as Figure 2.1 shows.

In France, bottom liner active barriers also comprise a drainage layer and a geomembrane, but for passive barriers the criterion is more stringent. The passive barrier must include 1 m of compacted clay liner ($k \leq 10^{-9}$ m s^{-1}) over 5 m of compacted soil ($k \leq 10^{-6}$ m s^{-1}), as Figure 2.2 (a) shows. However, because the GCLs have become more and more widespread in this country, the equivalence issue has arisen. According to MEDD (2002), equivalent solutions can be achieved by using either a GCL over 1 m of compacted soil ($k \leq 10^{-9}$ m s^{-1}) over 5 m of compacted soil ($k \leq 10^{-5}$ m s^{-1}), or a GCL over 0.5 m of compacted soil ($k \leq 10^{-9}$ m s^{-1}) over 5 m of compacted soil ($k \leq 10^{-6}$ m s^{-1}), as Figure 2.2 (b) and (c) depicts. For

hazardous wastes the compacted clay liner below the geomembrane must be at least 5 m thick and have a $k \leq 10^{-9}$ m s^{-1}.

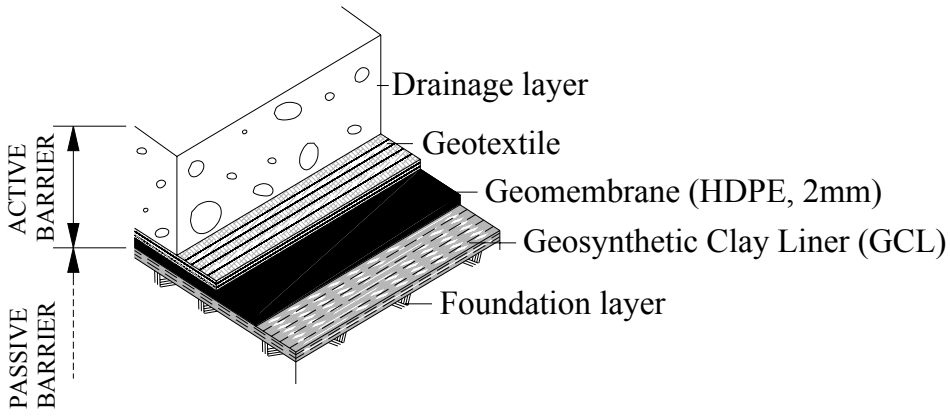

Figure 2.1– Schematic drawing of the composite liner used at Portuguese MSW landfills

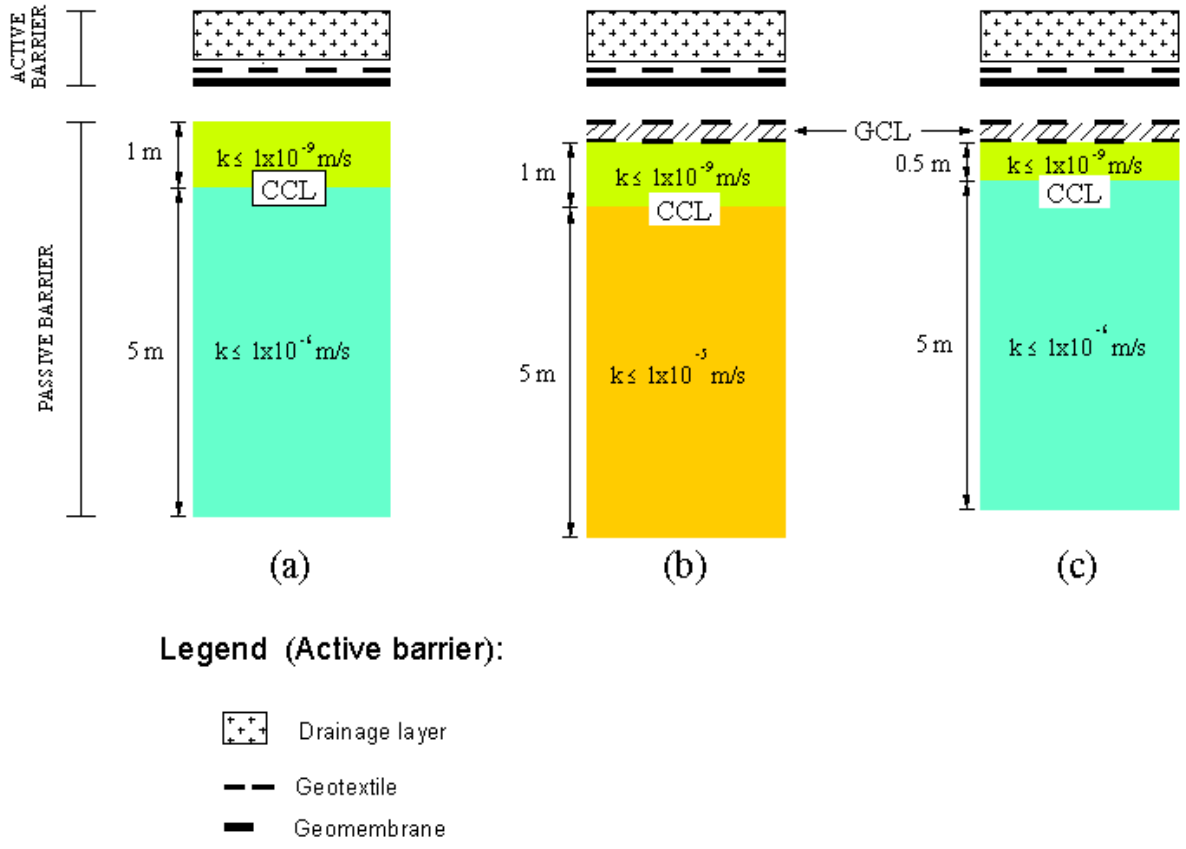

Figure 2.2 – Schematic drawing of composite liners in French MSW landfills

At present, landfills have composite liners that can be either single or double (Figure 2.3). Double composite liners include a drainage layer (also termed in literature as leakage detection layer or leakage detection system) placed between the primary and the secondary liners. This drainage layer can be constituted either by a granular layer or by a geonet, and aims to control the leachate that goes through the primary liner system.

Double composite liners are mainly used in hazardous landfills in the USA. According to Koerner (2000), 24 % of MSW landfills in USA and 14 % of landfills worldwide have been designed with double lining systems.

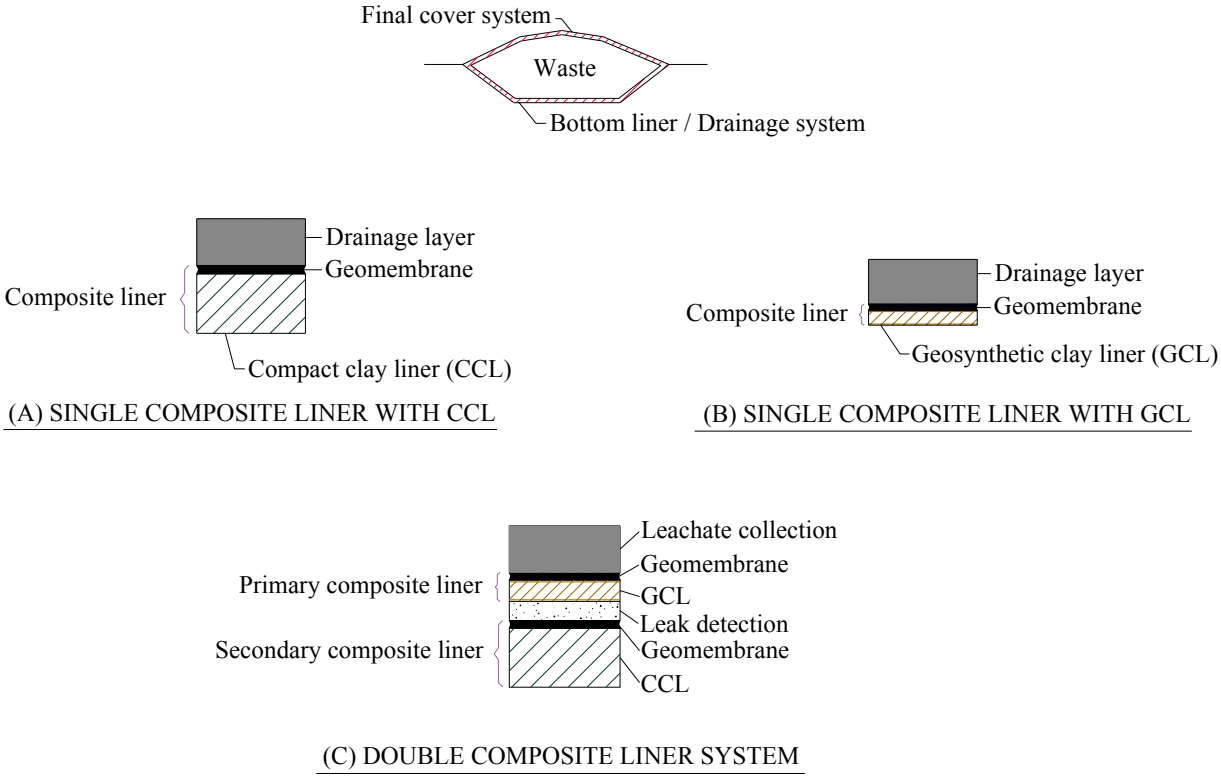

Figure 2.3 – Examples of single and double composite liner systems (adapted from Daniel 1998)

The materials typically used in composite liners to reduce the contaminant migration to levels that will result in negligible impact on environment, namely geomembranes, geosynthetic clay liners and compacted clay liners, as well as the critical aspects of their successful performance, will be addressed in the following sections.

Table 2.2 – Typical bottom liner systems in different countries (modified from Manassero et al. 2000 and Bouazza et al. 2002a)

Country	Waste type	Bottom liner (confinement)
Europe: Directive 1999/31/CE (Portugal)	Non-Hazardous	Geological barrier ($\geq$ 1 m, $k \leq 10^{-9}$ m s^{-1} or equivalent but $\geq$ 0.5 m) + artificial sealing layer
	Hazardous	Geological barrier ($\geq$ 5 m, $k \leq 10^{-9}$ m s^{-1} or equivalent but $\geq$ 0.5 m) + artificial sealing layer
	Inert	Geological barrier ($\geq$ 1m, $k \leq 10^{-7}$ m s^{-1} or equivalent but $\geq$ 0.5 m) + artificial sealing layer
France	Non-Hazardous	Geological barrier ($\geq$ 1 m clay, $k \leq 10^{-9}$ m s^{-1} + 5 m soil, $k \leq 10^{-6}$ m s^{-1}) + geomembrane
	Hazardous	Geological barrier ($\geq$ 5 m clay, $k \leq 10^{-9}$ m s^{-1}) + geomembrane
Germany	Non-Hazardous	Geological barrier + mineral layer ($\geq$ 0.75 m clay, $k \leq 10^{-10}$ m s^{-1}) + geomembrane (2.5 mm thick)
	Hazardous	Compacted clay liner ($\geq$ 3 m) + mineral layer ($\geq$ 1.5 m) + geomembrane (2.5 mm thick)
	Inert	Compacted clay liner ($\geq$ 0.5 m)
Austria	Non-Hazardous	Geological barrier (5 m, $k \leq 10^{-7}$ m s^{-1} or 3 m, $k \leq 10^{-8}$ m s^{-1}) or equivalent artificial mineral barrier + Compacted clay liner (0.75 m, $k \leq 10^{-9}$ m s^{-1}) + geomembrane (2.5 mm thick)
	Inert	Compacted clay liner ($\geq$ 0.5 m, $k \leq 10^{-9}$ m s^{-1})
USA (USEPA)	Non-Hazardous	Compacted clay liner ($\geq$ 0.6 m, $k \leq 10^{-9}$ m s^{-1}) + geomembrane (1.5 mm thick if made of HDPE)
	Hazardous	Double liner: compacted clay ($\geq$ 0.9 m, $k \leq 10^{-9}$ m s^{-1}) + geomembrane + granular layer (0.3 m, $k \geq 10^{-4}$ m s^{-1}) + geomembrane
Canada		
British Columbia	Non-Hazardous	Compacted clay liner ($\geq$ 2 m, natural attenuation landfill) + compacted clay liner ($\geq$ 1 m, engineered landfill)
Ontario	N.H.-larger landfills	Double liner: compacted clay liner ($\geq$ 0.75 m) + geomembrane, 1m soil subgrade*
	N.H.-smaller landfills	Compacted clay liner ($\geq$ 0.75 m) + geomembrane, 3m soil subgrade*
Quebec	Non-Hazardous	Compacted clay liner ($\geq$ 0.6 m) + double geomembrane separated by a leak detection layer (0.6 m subsoil)
Australia		
NSW State	Non-Hazardous	Compacted clay liner ($\geq$ 0.9 m)*
	N.H. or Hazardous	Compacted clay liner ($\geq$ 0.9 m) + geomembrane (to be used in areas of significant threat to the environment)*
Victoria State	Non-Hazardous	Compacted clay liner (0.6 m) + geomembrane
Japan	Non-Hazardous (fly ash)	Low permeability soil or GCL, sand-cement-bentonite mix, asphalt layer, double geomembrane

*These are not prescribed requirements, but rather design-guidelines. It is possible to demonstrate that natural k at the site is sufficiently low so that an engineered liner is not required.

2.3 COMPOSITE LINERS: MATERIALS

2.3.1 Geomembranes liners

2.3.1.1 Definition and raw materials

According to IGS (2000), a geomembrane is defined as a planar, relatively impermeable, polymeric (synthetic or natural) sheet used in contact with soil, rock, and/or any other geotechnical material in civil engineering applications.

The geomembrane can be produced from polymeric or bituminous materials. However, bituminous geomembranes are rarely used in waste containment applications for bottom liners. Thus, in this work, the term geomembrane will be used specifically to describe materials that are made of polymeric resins.

Polymeric geomembranes are made from synthetic polymers derived mainly from oil-based products. Polymers used for geomembranes can be thermoplastic, thermoset, or a combination of both. Thermoplastic polymers when heated become soft and pliable without any substantial change in their inherent properties, and when cooled revert back to their original properties. Thermoset polymers once cooled remain solid upon the subsequent application of heat (Koerner 1998).

A wide range of polymers can be used for geomembrane production. Most of the time only one polymer is used for a given product. However, to improve specific properties, two or more polymers can be blended (Ingold 1994). The most common polymers used for manufacturing geomembranes are listed in Table 2.3. In landfill bottom liners, HDPE is usually used, mainly because it is typically compatible with leachate and it presents a satisfactory long-term performance. Nevertheless, as discussed during the 7th International Conference on Geosynthetics, held in Nice in 2002, the door could be opened to other materials (Giroud & Touze-Foltz 2003).

Table 2.3 - Common types of geomembranes

Polymers	Abbreviation	Type of compound
High density polyethylene	HDPE	Thermoplastic
Low density polyethylene	LDPE	Thermoplastic
Very low density polyethylene	VLDPE	Thermoplastic
Linear low density polyethylene	LLDPE	Thermoplastic
Polypropylene	PP	Thermoplastic
Ethylene propylene diene monomer	EPDM	Thermoset
Chlorinated polyethylene	CPE	Thermoplastic/thermoset
Polyvinyl chloride	PVC	Thermoplastic
Chlorosulfonated polyethylene	CSPE	Thermoplastic/ thermoset
Ethylene interpolymer alloy	EIA	Thermoplastic

Polymers in their pure form are not suitable for geomembrane production. Afterwards, they are mixed with various additives to produce a final product with the required properties. Thus,

the primary resin is formulated with additives, fillers, extruders and/or other agents. The additives are used as ultraviolet light absorbers (UV), antioxidants, thermal stabilisers, plasticisers, biocides, flame-retardants, lubricants, forming agents, or antistatic agents (Ingold 1994, Koerner 1998).

A primary performance objective for geomembranes as liners is the protection of the groundwater quality. The success of their performance is closely related to the quality of the seams and to the presence of inevitable defects caused by inadequate construction activities. Seams and potential defects are two key issues in landfill construction and operation. In this context, Section 2.3.1.2 describes the main seaming methods presently available, discusses the parameters that may affect seams quality, and presents an overview of the seams quality control, whereas Section 2.3.1.3 focuses on defects, their origin, density and size.

2.3.1.2 Geomembrane seams

2.3.1.2.1 Field seaming methods

A variety of bonding systems is used in the seaming of geomembranes. Selection of the best method depends on the type of geomembrane as Table 2.4 shows. Seaming methods currently available include (Koerner 1998): extrusion welding, thermal fusion or melt bonding, chemical fusion and adhesive seaming (Figure 2.4).

Table 2.4 - Field seaming methods for various geomembrane types

Type of geomembrane	Seaming method			
	Extrusion (fillet and flat)	Thermal fusion (hot wedge and hot air)	Chemical fusion (chemical and bodied)	Adhesive (chemical and contact)
HDPE	√	√		
VLDPE	√	√		
PP		√		
PVC		√	√	√
CSPE-R		√	√	√
EIA-R		√	√	√

R = reinforced

Extrusion methods

Extrusion methods are used exclusively for seaming polyethylene geomembranes, specifically in the following cases: patches, poorly accessible areas (e.g. around pipes), and in case of extremely short seam lengths. A ribbon of molten parent material is extruded either between the adjacent overlapped sheets to form a flat weld, or over the top of the adjoining sheets to form a fillet. Seaming rate and temperature both play important roles in achieving an acceptable seam. Excessive melting weakens the geomembrane and too little melting results in inadequate extrudate flow across the seam interface and, consequently, in poor seam strength (Koerner 1998).

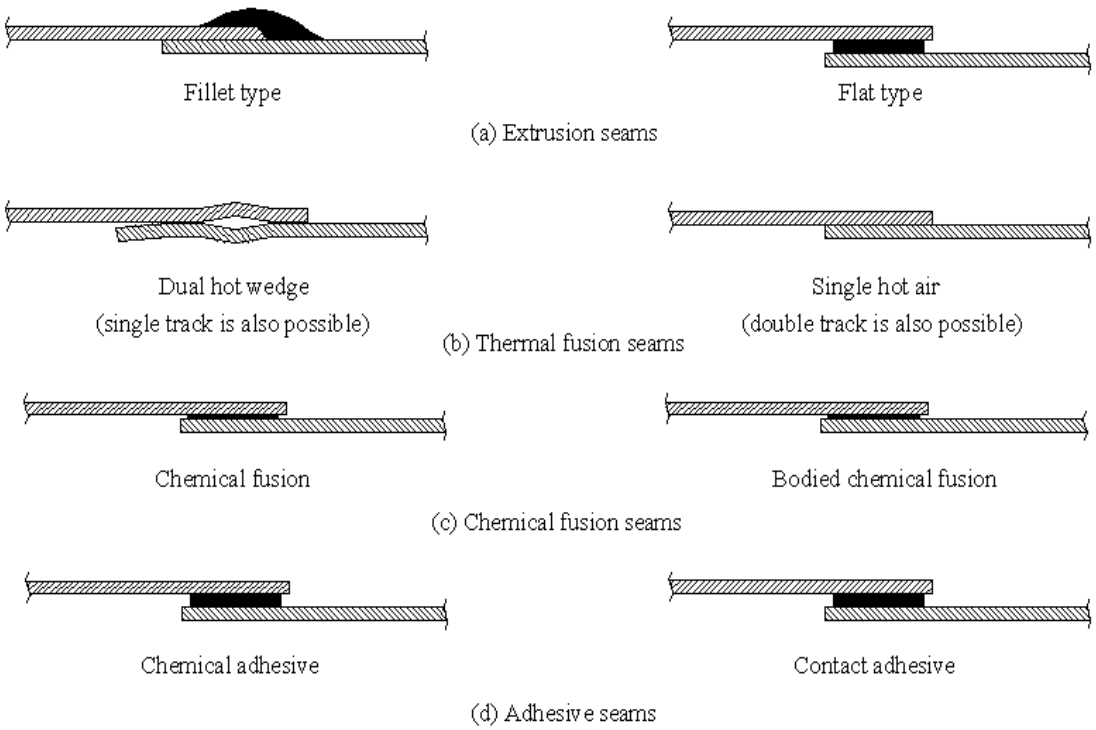

Figure 2.4 - Methods of seaming (based on Daniel & Koerner 1993)

Thermal fusion methods

There are two thermal fusion methods: hot wedge and hot air. On both, the surface portions of the opposing surfaces are truly melted. By hot wedge seaming a wedge of hot steel is passed between the overlapped sections of adjacent membrane, melting the sheet. Then, pressure rollers bring the molten surfaces together to form the final seam. Both single hot wedge and dual hot wedge systems are available. The dual hot wedge seam forms a continuous air channel between two seams. This air channel can be used to evaluate the continuity of the seam by pressurising it and monitoring any drop in air pressure that may signify a leak in the seam. The seaming parameters (speed, temperature, and roller force) are adjustable and continuously monitored. The adjustments are done according to the weather conditions. Too much melting weakens the geomembrane and inadequate melting results in low seam strength. The hot air method consists of using a device provided with a resistance heater, a blower and temperature control, to force hot air into two sheets to melt the opposite surfaces. Pressure is applied to the seamed area to bond the two sheets. Like in the hot wedge method, both single and dual seams can be made (Daniel & Koerner 1993).

Chemical fusion methods

There are two chemical fusion seam types: chemical fusion and bodied chemical fusion. The first uses a liquid solvent applied between the two sheets to be assembled. After a few seconds to soften the geomembrane surfaces, they are pressed together firmly with rollers on a firm base to make complete contact and bond the sheets. Bodied chemical fusion seams are

identical to chemical fusion seams except that 1 % to 20 % of the parent lining resin or compound is dissolved in the solvent and then used to produce the seam. The solvent liquid is applied between the two opposite surfaces, which are then pressed together to make complete contact (Daniel & Koerner 1993).

Adhesive methods

There are two chemical adhesive methods: chemical adhesive and contact adhesive. The first method uses an adherent (dissolved bonding agent) that is left after the seam has been completed and cured, becoming an additional element in the seam system. In the second method, contact adhesives are bonding agents applied to mating surfaces. As soon as they reach the proper degree of tackiness, a roller presses the two sheets already assembled. As in the chemical adhesive method, the adherent becomes an additional element in the system (Koerner 1998).

For chemical-resistant materials such as HDPE, solvent and adhesive systems are very unusual if not non-existent. The adhesive layer formed in these systems is generally more susceptible to chemical attack and may result in subsequent failure at the seam. Hot air methods are usually regarded also with reservation. Actually, consistent results are difficult to reach on field since the techniques significantly rely on temperature. Long-term durability is affected as well, due to the intense heating process that often oxidises the geomembrane surfaces.

Hence, hot wedge and extrusion methods are presently considered as the most reliable seaming methods (Koerner 1998).

2.3.1.2.2 Factors affecting HDPE seams quality

Consistent quality in fabricating field seams is paramount to geomembrane performance. There are many factors that may affect seams quality. Some are uncontrollable such as the weather conditions, others, like preparation of geomembrane surfaces to be joined, can be controlled. Nevertheless, first of all, the quality of the seams depends on the quality of the geomembrane itself. Site conditions are also very important. Site must be cleaned and care must be taken to ensure that the welding machine can function as intended. In addition, seam interfaces cannot be dirty or wet. All dirt must be removed before the seaming starts. The expertise of the seaming crew and appropriate project design specifications are other important issues in seams quality.

In landfills, HDPE geomembranes are usually seamed by thermal fusion methods, namely by dual hot wedge. The welding machines can be either entirely controlled by micro-processor or the seaming parameters, such as seaming speed, wedge temperature and contact pressure of the hot wedge, have to be adjusted according to the ambient temperature and to the temperature of the membrane surface.

As pointed out by Rollin & Fayoux (1991) machine parameters are determinant on seam quality. For example, it is known that a change in sheet temperature affects the seam quality and that by varying speed it is possible to compensate for that quality change. Some attempts were made to correlate the seam quality and the seaming parameters (e.g. Rollin & Fayoux 1991, Rollin et al. 1989). However, since many factors can influence the seam quality, definition of proper range of force, speed and temperature for each seam is very

difficult, as underlined by Struve (1994). Thus, trial seams or qualifying seams on field are usually mandatory as pre-qualifying experience for personal, equipment, and procedures for making seams on identical geomembrane material and under the same weather conditions as the actual field production seams will be made. Trial seams should be done every four hours, whenever personal or equipment is changed, and when climatic conditions reflect significant changes in geomembrane temperature (Peggs 1997).

2.3.1.2.3 Quality control of the seams

Due to their vulnerability, seams require a strict quality control. They need to be both fluid-tight and have strength of the same order of magnitude as geomembrane panels. The quality control of HDPE field seams is usually done on the basis of non-destructive and destructive test methods. Non-destructive test methods aim to evaluate the fluid-tightness, whereas the destructive test methods measure the relative strength of the bond.

Non-destructive seam tests

In non-destructive test methods the goal is to check 100% of the seams. Several non-destructive test methods can be used to identify geomembrane seams discontinuities, including visual observation, air lance, pressurised dual seam, vacuum box, electrical methods, ultrasonic methods, etc. Table 2.5 shows the main test methods used to control seams.

In landfill applications, the most used methods are pressurised dual seam, for thermal fusion seams, and vacuum box, for extrusion seams. Both of them can only be used to measure the continuity of seams. They provide only qualitative information (pass/fail) about fluid-tightness of the seams, despite the main reason to make geomembrane seams is to make the lining system fluid-tight.

Destructive seam tests

Destructive seam tests are carried out on field seamed samples, typically taken on a random basis. Tests are usually performed both in the field and in laboratory. Sampling frequency generally ranges from one sample per 150 m to one sample per 500 m of seam length, depending on local specifications and QCA plans.

There are two destructive test methods that are widely used in testing bond strength of seamed geomembranes: the shear test and the peel test (Figure 2.5). HDPE geomembranes can be tested according to ASTM D 4437. Shear strength testing is performed by applying a force across the seam in a direction parallel to the plane of the bond, thus subjecting the bond interface to a shearing force. Peel testing is performed by applying a load such that the bonded interface is subjected to a peeling force that attempts to separate the two sheets that have been seamed together. The first test is used to assess the shear resistance of the seam, while the second is used to evaluate the adhesion strength between two welded geomembranes or between the extruded polymer and the sheets (Daniel & Koerner 1993).

Table 2.5 – Non-destructive geomembrane seam testing methods (based on Rollin et al. 2002a, *Comité Français des Géosynthétiques* 2003).

Test method	Description	Applicability	Comments
Air lance	A jet of compressed air is directed through a nozzle beneath the upper edge of the overlapped seams. If a portion of seam leaks, either air flows under the geomembrane and inflates it, or makes the geomembrane vibrate. An audible sound changes when unbounded areas are encountered.	Mostly for flexible geomembranes; best for thin geomembranes (thinner than 1mm).	Results not very reproducible; very high operator dependency.
Pressurised dual seam	The gap existent in the double seams is pressurised by air injection during a certain period. If no drop on the pressure gauge occurs during that time interval, the seam is acceptable.	All type of geomembranes seamed with double hot wedge or double hot air.	Fast method. Sensitive to the seam parameters.
Vacuum box	A soap solution is sprayed on the top of the seam. A transparent box is placed on the seam and vacuum is made in the box. If no bubbles or froth appear, the seam is acceptable.	Mostly for stiff geomembranes; mainly, for HDPE of which the thickness exceeds 1 mm.	Slow method; often difficult to make a vacuum-tight joint; mainly for patches.
Electric wire	A copper or stainless wire is placed between the overlapped sheets and embedded into the completed seam. A charged probe of high-voltage (~20000 V) is connected to one end of the wire and slowly moved over the whole seam. An audible alarm rings when a defect is encountered.	All types of geomembranes seamed.	High operator dependency.
Electrical sparking	A conduction wire is inserted into the seam during seaming process. By applying a suitable voltage above the seams, leakage to ground transmits a spark, accompanied by an audible alarm signal.	All geomembranes, for areas where vacuum cannot be used such as corners.	Difficult to set up accurately over large areas; results not always reliable.
Ultrasonic pulse echo	Compares the measured thickness of the seam to the thickness that it should have. A high-frequency pulse (5-15 MHz) is sent into the upper geomembrane, which will not be reflected at the bottom of the lower one if an unbounded area is present.	Only for nonreinforced geomembranes; not applicable to extrusion fillet seams.	Qualitative result.
Ultrasonic impedance plane	A continuous wave (160-185 kHz) is transmitted through the seam by means of a transducer in contact with the geomembrane and a characteristic dot pattern is displayed on a monitor. The location of the dot pattern indicates if the seam is bonded or not. Calibration of the dot pattern is required to indicate a good seam.	Has potential for all types of geomembranes.	Qualitative result.
Ultrasonic shadow	It uses two roller transducers, one sends a multi-frequency pulse into the upper geomembrane and the other receives the signal from the lower geomembrane on the other side of the seam. The analyses of the displayed results (amplitude versus time) indicate the quality of the seam.	Not applicable to reinforced geomembranes; can be used for all types of seams.	Best suited to semicrystalline geomembranes.
Mechanical probe test	Uses a stiff probe under the top edge of a seam to detect unbounded areas, which are easier to split than the properly welded areas.	All geomembranes and all seams with well-defined edge.	Depends largely on sensitivity of the operator.

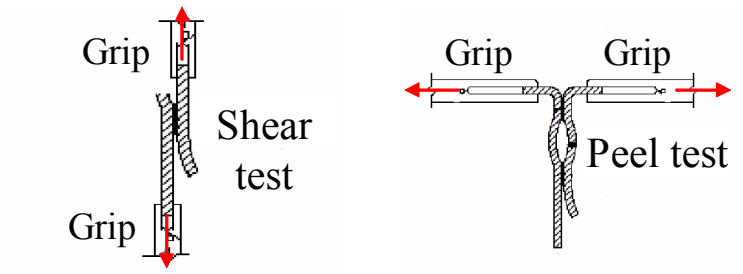

Figure 2.5 - Scheme of the specimens used in shear and peel tests

For HDPE geomembranes, the seam strength is the maximum force attained divided by either the original specimen width, resulting in units of force per unit width, or the original cross sectional area, resulting in units of stress. Usually, forces per unit width are used as this absolute strength value can readily be compared to other test results (Daniel & Koerner 1993).

Within the scope of the QC/QA activities, acceptance criteria are traditionally defined based on shear and peel efficiencies and on the location of the failure in the peel test. Shear elongation and peel separation were recently added to the acceptance criteria of the seams, although they are not often monitored during the tests.

Shear and peel efficiencies can be evaluated as follows (Daniel & Koerner 1993):

$$E_{shear} = \frac{T_{seam\ in\ shear}}{T_{unseamed\ sheet}} 100 \qquad (2.1)$$

$$E_{peel} = \frac{T_{seam\ in\ peel}}{T_{unseamed\ sheet}} 100 \qquad (2.2)$$

where E_{shear} and E_{peel} are the seam efficiency, respectively, in shear and in peel (%), T_{seam} is the seam shear strength (force or stress units), T_{peel} is the seam peel strength (force or stress units), and $T_{unseamed\ sheet}$ is sheet tensile strength (force or stress units).

Minimum allowable seam shear and seam peel strengths efficiencies are usually required as seam acceptance criteria. For example, USEPA (Daniel & Koerner 1993) suggests a minimum seam of 95 % of the specified yield strength of the geomembrane (GSYS) in shear, and of 62 % of the GSYS in peel. Other suggested values of shear and peel seam efficiencies can be found in the literature. Table 2.6 summarises some of these quantitative acceptance criteria for HDPE thermal fusion seams.

As for the location of the failure in a peel test, it is usually required that the specimen breaks outside the seam (failure in the adjacent sheet geomembrane on either side of the seam) in what is often termed Film Tearing Bond (FTB).

Table 2.6 - Quantitative acceptance criteria for HDPE geomembrane seams (thermal fusion seams)

	Haxo & Kamp (1990)	USEPA (Daniel & Koerner 1993)	Peggs (1994a, b)		Koerner (1998)	Benneton & Gerard (2002)
			Very good seam	Good seam		
Shear efficiency regarding GSYS	> 90-110 %	> 95 %	> 95 %	> 90 %	> 90-100 %	> 90 %
Shear elongation (at break)	> 50 %	-	> 500 %	> 100 %	-	-
Peel efficiency regarding GSYS	> 60-70 %	> 62 %	> 80 %	> 70 %	> 50-80 %	> 65 %
Peel separation	-	-	0 %	< 10 %	-	-

Note: GSYS = yield strength of the geomembrane

According to Peggs (1996b, 1997), shear and peel strengths are meaningless, only peel separation and elongation provide useful information. Elongation determines if seaming process has adversely affected the adjacent geomembrane. For HDPE geomembranes, seams that break at high stress level but at low strain may seem suitable at first glance, but brittle behaviour is an indicator of long-term problems for the seam. In addition, if during a peel test, a specimen separates partially along the bonded interface before failing through the bottom geomembrane, but with adequate strength, it may conventionally be considered to be acceptable. However, if that specimen is examined under a microscope it will be seen that the separated surfaces have a large number of crazes, which can reduce the stress cracking resistance of the geomembrane. Thus, in his most recent publications, Peggs suggests zero peel separation for acceptable seams.

Recently, Benneton & Gerard (2002) performed a research for the French Chapter of IGS (CFG) to study if the common used acceptance criterion for geomembrane seams are suitable taking into account the evolution of the resins. They tested five types of geomembranes (HDPE and bituminous) according to French standards NF P 84-502.1, for shear test, and NF P 84-502.2, for peel test (dumbbell shapes). Their main conclusions can be summarised as follows: (1) both types of test must be performed (shear and peel); (2) shear strength should present a minimum seam efficiency of 90 % of GSYS; peel strength for extrusion seams should present a minimum seam efficiency of 60 % of GSYS; (3) peel strength for fusion seams should present a minimum seam efficiency of 65 %; (4) adhesive failures should not be allowed.

Other methods for assessing seams quality

Other methods for assessing seams quality include microscopic analysis, impact strength test, incremental peel strength along the length of the seam, and thickness of the finished seam track. Microscope analyses are used to complement the information given by mechanical tests. They are used to observe molecular abnormalities, to identify micro stress cracks within the bonded sheets, to detect unbounded areas and to observe slow crack growth phenomena (Rollin et al. 1994). In the impact test a drop-weight apparatus is used to produce proper immediate failure. The mean failure energy can be reported as the seam failing or passing upon application of an adequate drop-weight mean energy. This test provides additional information about the behaviour of the seams under dynamic conditions as the ones usually encountered during the installation process (Rollin et al. 1994). The incremental peel test has

some qualitative value, but the need to manually assist the propagation of the peeling may lead to diverting the separation plane away from its natural vector. Therefore, optimistic results may be achieved (Peggs 1994b).

In Germany, the thickness of the finished seam track has also been used for assessing seam quality, for hot wedge weld seams. Luders (2000) presented a process model developed from experimental results on hot wedge weld seams. The aim of the model was to establish a quality criterion that would allow the inherent quality of acceptable seams to be expressed differentially and to identify it in terms of valid limits. Another goal of the model was to find a functional relationship between the adjustable parameters of the machine and those process parameters that indicate suitable seam quality under field conditions. The criterion of quality used by this author to validate his model was the failure time in long-term peel tests, which was correlated to the reduction in seams thickness (s_t). According to Luders (2000), good seams can be achieved for seam thickness reduction ratio (s_t/L_0) between 0.5 and 0.9, where L_0 is the melt depth.

2.3.1.2.4 Summary of Section 2.3.1.2

In landfills, HDPE geomembranes are typically used. This type of geomembranes is generally seamed by thermal fusion methods, namely by the dual hot wedge method. Seaming machine parameters such as seaming speed, wedge temperature, and contact pressure of the hot wedge are determinant on the quality of the seams.

Due to the application of heat and pressure during the seaming process, seams are vulnerable areas that require a strict quality control. It is necessary to ensure that seams are both fluid-tightness and present a mechanical strength of the same order of magnitude as the non-seamed geomembrane.

The mechanical strength of HDPE seams is quantitatively evaluated through shear and peel tests, whereas their fluid-tightness is usually assessed via pressurised dual seam tests. Pressurised dual seam tests measure the continuity of the seams (pass/failure criteria), but only provide qualitative information about fluid-tightness, which is the main reason for making the seams.

Therefore, a tool for controlling the fluid-tightness of the seams from a quantitative point of view appears to be necessary. In this context, a test method for studying the quality of the seams and the influence of the seaming parameters was developed in the present work. It will be described in Chapter 5.

The second critical issue for geomembranes as liners refers to defects (e.g. holes, tears, cuts, lack of seam bond, and burns). These defects, through which the liquid flow, are also termed as leaks. Data collected from liner leak detection and location systems have shown that defects always occur, even in liners constructed according to a strict construction quality program.

The methods used to locate and detect defects in geomembrane liners, as well as the origins, density and size of the defects will be discussed in Section 2.3.1.3.

2.3.1.3 Geomembrane defects

2.3.1.3.1 Methods to detect and locate defects in geomembrane liners

The methods to detect and locate defects in geomembrane liners (liner leak location and detection systems) have become more and more widespread, although the control of the geomembrane liners is not mandatory in current state-of-practice, conversely to the control of the seams (see Section 2.3.1.2.3).

There are two categories of methods. The first one is able to detect and locate potential leak paths, such as unintended openings, perforations, breaches, tears, punctures, seam defects, etc. It basically includes electrical leak location (ELL) methods. The second category comprises the methods that only detect the presence of defect and do not locate them. It comprises: flood testing, infrared thermography, dye and chemical tracer testing, and gas tracers methods (*Comité Français des Géosynthétiques* 2003).

Electrical leak location methods were developed in the early eighties and have been used successfully in electrically-insulating geomembranes such as PE, PP, CSPE and bituminous geomembranes installed in several types of facilities (Rollin et al. 2004). These methods locate defects in the geomembrane liner by applying an electrical potential across the geomembrane and then locate areas where the electrical current flows through discontinuities in the liner (Swyka et al. 1999; Peggs 2001; Rollin et al. 2004) as Figure 2.6 schematically presents. Common electrical leak location methods include water puddle and water lance methods, wading, electrically conductive geomembrane, soil-covered geomembrane system and grid system.

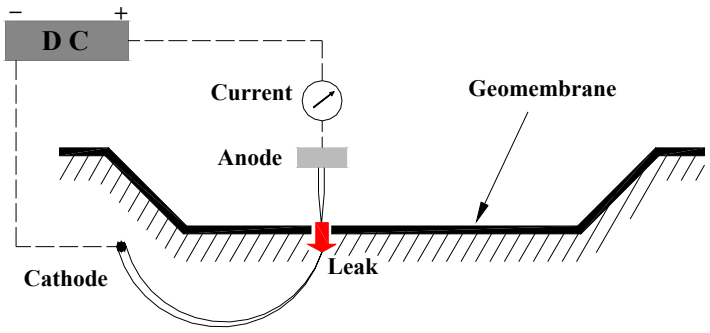

Figure 2.6 – Scheme of the electrical leak location methods (adapted from Rollin et al. 1999)

Water puddle and water lance

In the water puddle and water lance methods, a positively charged stream of water is directed on the surface of the exposed geomembrane (Figure 2.7). When the water contacts the negatively charged subgrade through a defect in the liner, the current flows and is recorded. These methods are appropriate to survey a dry uncovered geomembrane during its installation when placed over an electrically conductive subgrade. The advantage of these methods is the possibility to detect defects in geomembrane sheets and seams as work progresses. Other advantage is that the larger leak paths do not mask smaller ones. The disadvantage is that they can only be used with uncovered geomembranes. In addition, the presence of wrinkles and

steep slopes may inhibit the survey speed if there is no contact between the liner and the conductive soil layer (Rollin et al. 2004).

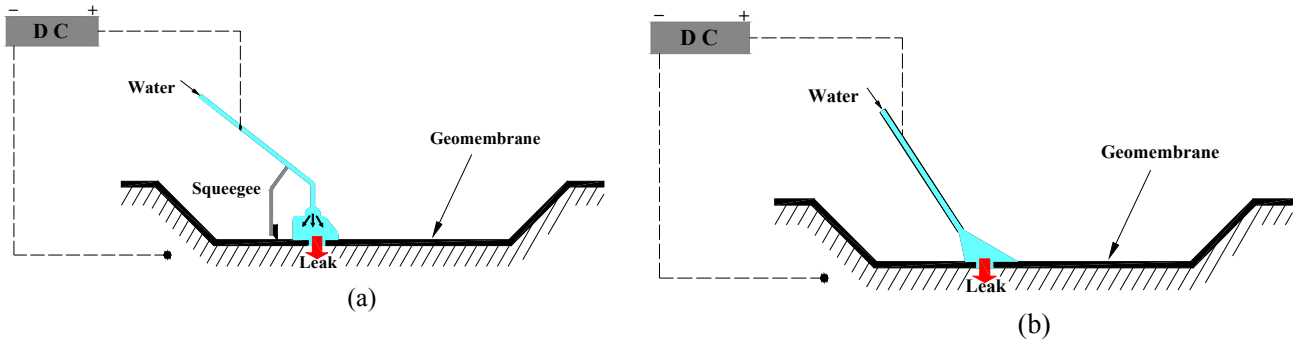

Figure 2.7 –Scheme of the (a) water puddle and (b) water lance systems (adapted from ASTM D 6747)

Wading (water-covered geomembrane)

In this method, a handheld probe is traversed through the water that covers the geomembrane to measure its iso-potential contours while a constant potential gradient is applied between the water above the geomembrane and the leaked water, or subgrade, below the geomembrane (Figure 2.8). The main advantages of this technique are that it detects leak paths in covered geomembranes and can be used in in-service facilities. The shortcoming is that it needs to flood the geomembrane with water, which makes impossible its use as work progresses during the construction phase. On the other hand, larger leak paths can mask smaller ones (ASTM D 6747).

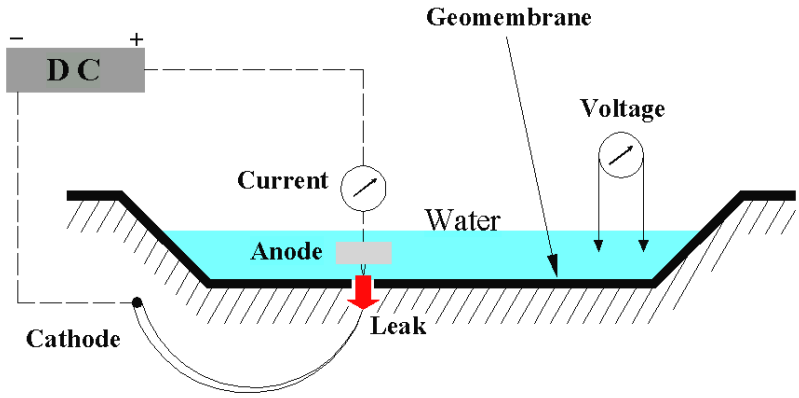

Figure 2.8 – Scheme of the water-covered geomembrane system (modified from ASTM D 6747)

Electrically conductive geomembrane

In this method, a conductive geomembrane, manufactured by co-extruding a layer of electrically conductive polyethylene material on the underside, is installed in the field in such

a way that the conductive side is against the subgrade and the non-conductive side on top (Figure 2.9). The geomembrane can be spark-tested for defects using an electrical device to induce electrical discharges from a positive electrode, which is swept across the top of the geomembrane, to the negatively charged conductive layer at the bottom of the geomembrane. When there is a defect, a closed circuit is created and a spark is produced. The main advantages of this method are that it can be performed during construction, no water pumping is required, primary and secondary liners can be tested, and all slopes can be tested. The main drawbacks include: the presence of wrinkles and steep slopes inhibits the survey speed; seams may also interrupt the continuity of the conductive layer; it can only be used with dry exposed geomembranes (*Comité Français des Géosynthétiques 2003,* ASTM D 6747).

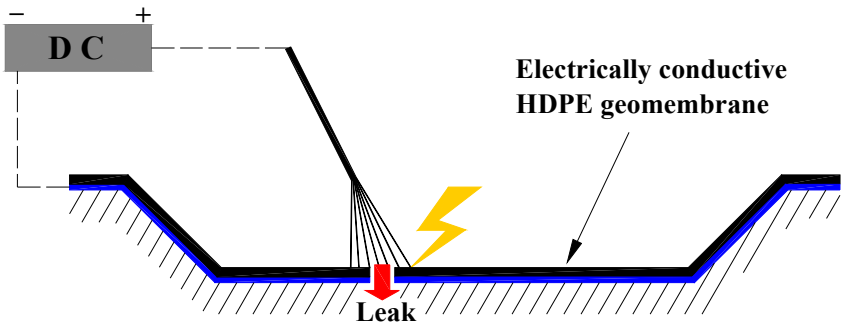

Figure 2.9 – Scheme of the conductive HDPE geomembrane leak location system (adapted from *Comité Français des Géosynthétiques 2003*)

Soil-covered geomembrane system

This technique tests the geomembrane after the protective soil layer placement (Figure 2.10). It is similar to the water-covered geomembrane method except that the geomembrane is covered with soil during the survey, and point by point measurements are carried out on the surface of the soil (ASTM D 6747). This method needs an electrically conductive layer below the geomembrane. The main advantage of this technique is that it locates defects that occur during the placement of the protective cover soil, whereas the main disadvantage is that the soil must have some moisture to make proper contact (Rollin et al. 2004).

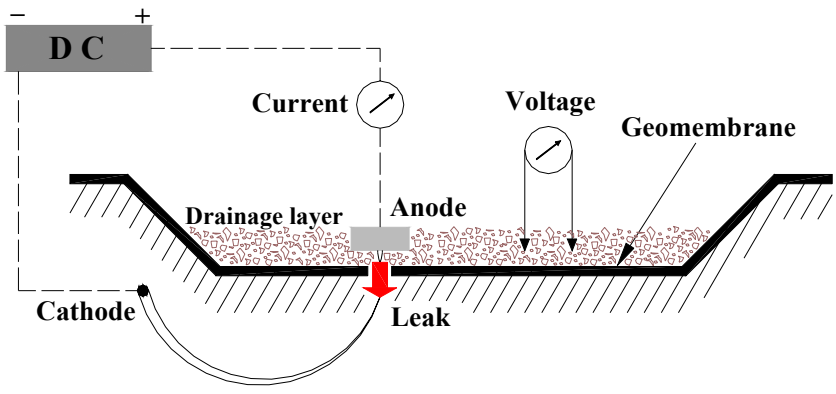

Figure 2.10 – Scheme of the soil-covered geomembrane system (adapted from *Comité Français des Géosynthétiques 2003*)

Grid system (permanent in situ system)

This permanent system requires an electrically conductive grid of electrodes below the geomembrane and liquid or humidity above the liner. Defects are detected by performing potential measurement by means of a widely spaced grid of electrodes under the lined area (Figure 2.11). This method can give updated information during operation and post-closure phases. In addition, it can be used under cover soil and with liquid stored in application. The main disadvantage is that it cannot be used during construction.

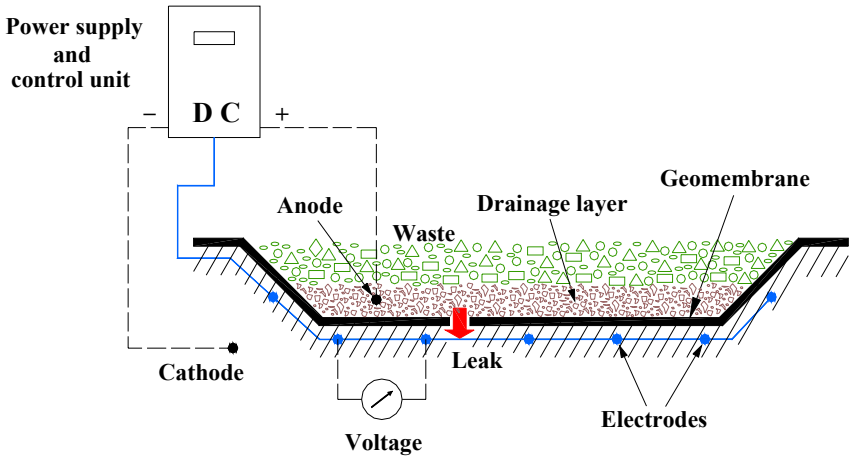

Figure 2.11 – Scheme of the permanent monitoring system

With respect to systems that only detect the defects, different methods can be used. In *flood testing* a liquid, water or leachate, is introduced into the landfill cell and the secondary drainage layer, referred to as secondary leachate collection system (SLCS), is monitored to assess if the primary liner is leak-proof. This is a simple method but it requires a significant amount of time to complete and a large liquid resource (Swyka et al. 1999).

Infrared thermography basically works by measuring geomembrane surface temperatures, using, for example, an infrared camera. The relatively low value of thermal conductivity possessed by HDPE geomembranes provides a thermal barrier. Usually, the geomembranes are at higher temperature than the subgrade during the day and vice versa at night. Thus, hot or cold air flowing through a defect in the geomembrane would generate temperature variations (*Comité Français des Géosynthétiques 2003*). According to Peggs (1996a), this method can not be used for soil and waste covered liners.

Fluorescent dyes and chemical tracers have also been used to detect defects. They can be introduced into a suspect location within the landfill and the secondary system monitored for breakthrough time. A short breakthrough time would indicate that the dye or tracer required some travel time prior to reaching the breach. This technique can only be used when there is a SLCS. In addition, results obtained are somewhat subjective due to the unknown variables in the collection systems. Furthermore, it is believed to be impractical for pinpointing the location of a defect (Swyka et al. 1999).

In *gas tracing* methodology, a tracer injection system pumps air (tagged with volatile tracer) below the geomembrane. The tracer is then allowed to diffuse for a nominal amount of time. Then, its presence is observed in the air in the layer above the geomembrane with the use of a

portable air sampling apparatus. Samples collected on a uniform geometric grid above the geomembrane area are analysed with a field mobilised gas chromatograph (Touze-Foltz 2001). This method can be used for uncovered geomembranes and for geomembranes covered by around 0.5 m of drainage soils (Swyka et al. 1999).

2.3.1.3.2 Cause of defects

Defects in the geomembrane result generally from construction activities e.g. improper seaming, punctures by stones in the support or cover material, dropped objects, tears, excessive stresses caused by equipment traffic, failures from subsidence or shear failures of the supporting soil after installation, imperfect connections between geomembranes and appurtenances, etc.

Several syntheses of studies on geomembrane defects have been published. For example, Rollin et al. (2002b), reviewing the information from Colucci & Lavagnolo (1995), Darilek et al. (1989), Laine & Darilek (1993), and Rollin et al. (1999), collected data from more than 150 electrical surveys, corresponding to more than 1.5 million square meters. The data analysed pointed out that 65 % of defects were related to seaming and 35 % were located in the sheet of the geomembrane itself. Many surveys analysed by these authors were conducted after a conventional construction quality assurance plan had been implemented. The liners surveyed included steel tanks, concrete tanks, basins and ponds, uncovered primary and secondary landfill liners and soil covered landfill liners. It must be noted that this study does not distinguish between covered and uncovered geomembranes, although the main cause of defects in a facility appears to be related with the status of the geomembranes (covered/uncovered).

For covered geomembranes, it seems that most defects appear during the placement of the primary leachate collection system (PLCS). For example, results presented by Nosko & Touze-Foltz (2000) from electrical damage detection systems installed at more than 300 sites, from 16 countries, covering over 3 250 000 m^2, showed that the majority of the damages (71%) were caused by stones during PLCS installation, 16 % by heavy equipment, 6 % by inadequate seams, 6% by the workers, and 1% by cuts (Figure 2.12). Similar conclusions were drawn by Colucci & Lavagnolo (1995) from the analysis of 30 leak location surveys conducted in Italy, covering more than 300 000 m^2. According to these authors, the number and the quality of the defects were related to the quality of the subgrade material, the quality of the cover material, the accuracy in their installation and the quality of the liner installation.

As for the effects of the subgrade materials, it must be pointed out that modern landfills often incorporate a GCL. Although there is no data available on this topic, when the geomembrane is placed over a GCL, it can be expected that a negligible number of defects be caused by the underneath materials.

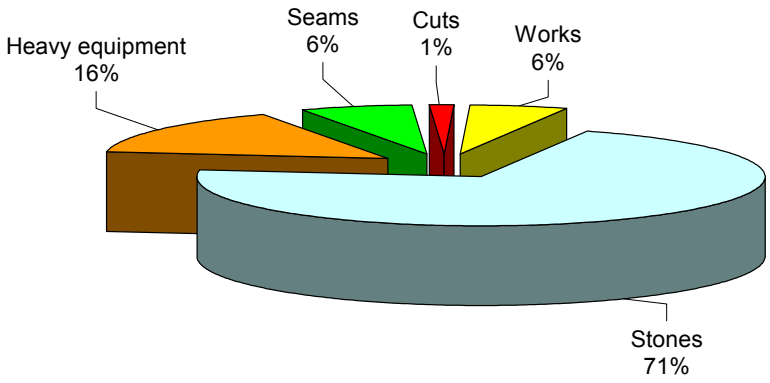

Figure 2.12 – Cause of defects in geomembrane liners after installation of the cover layer (data from Nosko & Touze-Foltz 2000)

Concerning uncovered liners, different causes of defects have been indicated. The results reported by Rollin et al. (1999) from an electrical leak location system used in exposed geomembrane liners installed in basins, ponds and landfills, showed that 55 % of the damages occurred in seams (fillet extrusion seams for HDPE), followed by the holes due to the poor quality of the subgrade (25 %), as illustrated in Figure 2.13. These results are related to surveys conducted on 9 sites located in France and Canada, between 1994 and 1998, covering more than 225 000 m^2. Different results were presented by Peggs (2001) from a water lance survey performed on 645 000 m^2 of exposed LLDPE geomembrane on a mining tailing management facility. In this facility, punctures caused by the subgrade materials beneath the geomembranes were the main cause of defects (38.2 %). Only 16.8 % of the defects were found on geomembrane seams (Figure 2.13). However, results by Peggs (2001) concern just one facility, thus comparison with mean results obtained from several sites might be questionable.

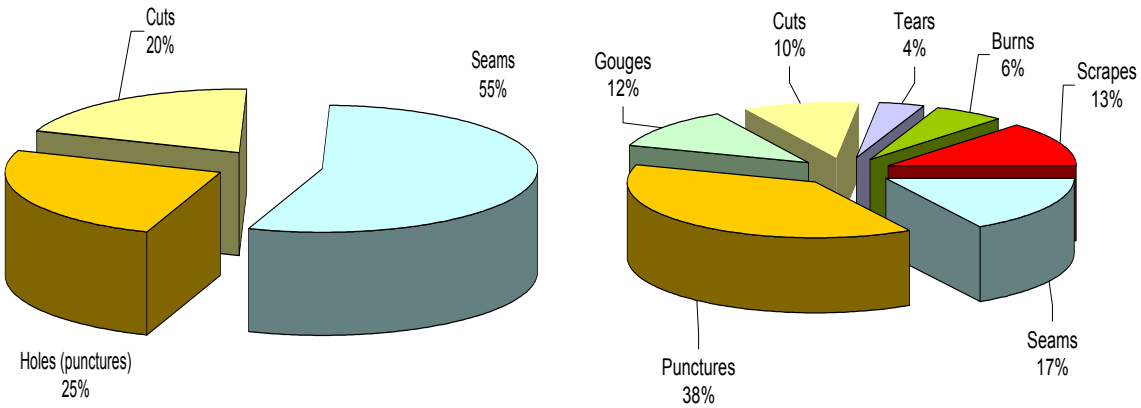

Rollin et al. (1999) Peggs (2001)

Figure 2.13 - Cause of defects in geomembrane liners in uncovered liners

2.3.1.3.3 Defects density

Another issue related with this topic is the defects density per liner area, i.e. number of defects per hectare (Colucci & Lavagnolo 1995). The variation of defect density as a function of the area of the facility surveyed is plotted in Figure 2.14. It can be observed that the density of defects tends to decrease as the surveyed area increases. However, it must be noted that there are many uncertainties regarding the varying conditions found in different sites (different types of geomembranes, different facilities, covered and uncovered geomembranes, etc). According to Colucci & Lavagnolo (1995), the reasons for the higher defects densities found in small installations can be summarised as follows: (1) smaller facilities have proportionally more complex features (corners, sumps, penetration); (2) small facilities tend to have higher percentage of hand seaming (extrusions); (3) large facilities have a stricter construction quality program; (4) large installations generally receive less traffic. Similar observations have been drawn by other authors, such as, for example, Rollin et al. (1999, 2004).

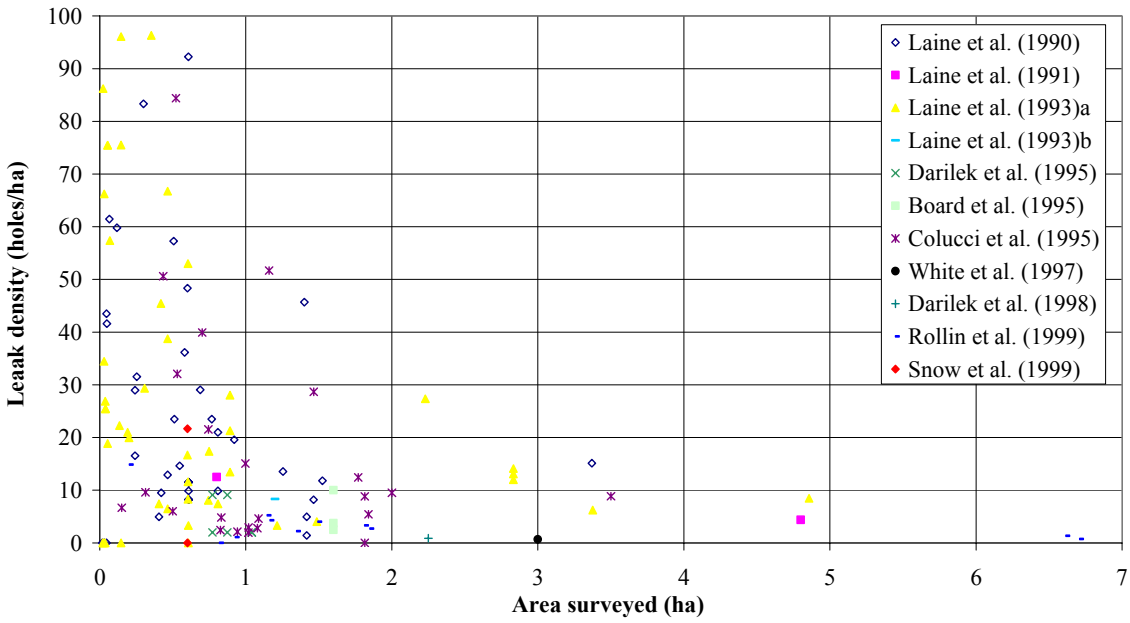

Figure 2.14 – Variation of defect density as a function of the area surveyed (Touze-Foltz 2001)

Table 2.7 shows defect densities presented by different authors for covered and uncovered geomembranes. It can be seen that they range from 0.7 to 15.3 defects/ha for covered geomembrane liners and from 2 to 5.5 defects/ha for uncovered ones. Analysis of the data presented in Table 2.7 is quite difficult because the number of sites as well as the area surveyed vary significantly from one study to the other, which influences the results. For example, the density reported by Peggs (2001) is related to a single large facility, and as previously mentioned, large facilities tend to present lower defect density. Thus, the defect density reported by this author might not be representative for small landfills. In addition, for uncovered geomembrane liners, the defect density reported by Rollin et al. (1999) is relatively lower than the one from the others, but it is mainly related to surveys carried out on sites

where a geotextile was installed between the subgrade material and the geomembrane. Also, it refers to sites where a very strict CQA programme was implemented.

It should be noted that relatively higher defect densities can be found on small containment facilities with complex features to deal with, and where the geomembrane is placed directly on the subgrade-soil. For example, Laine et al. (1989) reported a mean density of 26 defects/ha from surveys conducted on small containment facility (less than 2 ha). Also, results of surveys conducted in two small lagoons (less than 1 ha) showed a mean density of 45 defects/ha (Barroso 2001). In this case, the high defect density observed was mainly due to inadequate installation of the geomembrane.

Table 2.7 includes the mean values obtained by Touze-Foltz (2001) from a synthesis of studies involving electrical leak location systems. For uncovered geomembrane liners, the author analysed the surveys conducted by Laine (1991), Board & Laine (1995), and Rollin et al. (1999). For covered geomembranes, surveys assessed included: Laine & Mosley (1993), Board & Laine (1995), Colucci & Lavagnolo (1995), White & Barker (1997), Darilek & Miller (1998), Snow et al. (1999). This author reports a mean defect density of 2.8 per hectare after installation of the geomembrane and 11.9 per hectare after placement of the granular drainage layer. This result confirms that the majority of the defects occur during placement of the granular layer above the geomembrane.

Table 2.7 – Reported defect density (modified from Touze-Foltz 2001)

Reference	Area surveyed (ha)	Status of geomembrane	Defects on geomembrane sheet (%)	Defects on geomembrane seams (%)	Mean defect density (defect/ha)
Laine & Mosley (1993)	1	Covered	20	80	8.3
Board & Laine (1995)	2	Covered	31	69	5.5
Colucci & Lavagnolo (1995)	25	Covered	85	45	15.3
White & Barker (1997)	1	Covered	100	0	0.7
Darilek & Miller (1998)	1	Covered	100	0	0.9
Snow et al. (1999)	2	Covered	100	0	10.9
Nosko & Touze-Foltz (2000)	325	Covered	93.7	6.3	12.9
Touze-Foltz (2001)	108.8	Covered	81.5	18.5	11.9
Laine (1991)	2	Uncovered	-	-	5.5
Board & Laine (1995)	1	Uncovered	17	83	3.8
Rollin et al. (1999)	22	Uncovered	45	55	2.5
Touze-Foltz (2001)	31.3	Uncovered	42	58	2.8
Peggs (2001)	64.5	Uncovered	83.2	16.8	2.0

As previously mentioned, Rollin et al. (2002b) also performed a synthesis of studies involving electrical leak location systems. Their results were not included in Table 2.7 because they do not distinguish between the surveys conducted with covered and uncovered geomembrane liners. The defect density estimated by these authors was 17.4 defects/ha.

Another interesting aspect recently pointed out refers to defects occurred in the long term. Needham et al. (2004) reported data from electrical leak detection surveys using permanent systems. Data were obtained from 88 cells and 18 leachate lagoon at 55 landfill sites in Eastern Europe, Belgium and the United Kingdom, covering approximately 1 022 000 m^2.

Results were reviewed from a survey company over a 7-year period, from 1996 to 2003. According to these authors, the number of defects was 1 460 (14.3 defects/ha), with 74 % located during the initial leak survey at the end of liner construction and 26 % of the defects being detected in subsequent surveys. As regards the defects detected on later surveys reported by Needham et al. (2004), most of them (78 %) were caused by stone puncturing in consequence of traffic movement over empty cells. Needham et al. (2004) do not include detailed information about the cause of the defects, however reported data draw attention to the possibility of damages occurring during operation of the landfill.

Results of a permanent in situ system (grid system) at a landfill in UK since installation in 1995 are also reported by Needham et al. (2004). A liner area of 5.5 ha is covered by this system. The monitoring at that landfill site has so far given a defect density of 16 holes/ha. Of these holes, 27 % were detected after completion of the liner, before waste disposal started in the cell or after landfilling began. In addition, there is no evidence of gradual development of holes from 1995 to 2003. Based on these results, the authors concluded that once a liner is covered by several meters of waste, the agents for future development of holes in liner (e.g. stress cracking) are limited and they are unlikely to develop for at least the first decade of the service of the geomembrane liner.

2.3.1.3.4 Type and size of defects

Table 2.8 presents data reported by different authors about type and size of defects. It can be seen that Colucci & Lavagnolo (1995) found that approximately 50 % of all detected defects were smaller than 1 cm^2 with larger defects being the holes and tears. Rollin et al. (1999) found that the smallest defects (< 0.02 cm^2) represented 43% of the detected defects and were mainly associated with seam failures, whereas the largest defects (> 0.1 cm^2), representing 22.4 % of the total, were more related to holes and cuts. Nosko & Touze-Foltz (2000) observed that 50 % of the defects fall into a range of 0.5 to 2.0 cm^2, 24.9 % of the defects varied from 2.0 to 10 cm^2, 14.3 % exceeded 10 cm^2, and 10.8 % were less than 0.5 cm^2. An interesting aspect of their study is that the defects related with heavy equipment were typically larger than 10 cm^2, whereas the majority of the defects related to seams (83 %) were less than 2 cm^2. In addition, Peggs (2001) found that the most common defect was a puncture between 0.2 and 1 cm in diameter.

It can be observed that the sizes of the defects reported by Rollin et al. (1999) are smaller than those from other authors included in Table 2.8. This is due to the fact that their results are related to uncovered geomembrane liners and defects in geomembranes can be much larger after placement of the overlying drainage materials, as pointed out by Colucci & Lavagnolo (1995), Nosko & Touze-Foltz (2000), and Peggs (2001).

From Table 2.8, the following general comments can be made: (1) the majority of the holes are smaller than 10 cm^2, which would correspond to a circular hole of 3.6 cm in diameter; (2) seams are not bonded over lengths ranging from 1 mm to more than 1 m; (3) cuts can reach more than 1 m; and (4) most tears are smaller than 1 m long.

Table 2.8– Defect size as a function of defect type

Reference	Size	Holes	Tears/burns/ equipment	Cuts/ scraps/ gouges	Seams	Sites	Area surveyed (ha)
Colucci & Lavagnolo (1995)	0-0.2 cm^2	44	31	12	11	25	27.6
	0.2-1 cm^2	37	49	21	4		
	1-5 cm^2	60	49	2	8		
	5-10 cm^2	22	11	0	4		
	10-100 cm^2	10	22	0	1		
	100-1000 cm^2	15	4	0	0		
	1000-8400 cm^2	0	5	0	0		
Rollin et al. (1999)	<0.02 cm^2	3	-	0	18	11	24.1
	0.02-0.1 cm^2	6	-	4	7		
	> 0.1 cm^2	3	-	6	2		
Nosko & Touze-Foltz (2000)	< 0.5 cm^2	332		5	115	300	325
	0.5-2 cm^2	1720	236	36	105		
	2-10 cm^2	843	153	18	30		
	> 10 cm^2	90	496	-	15		
Peggs (2001)	< 0.1 cm	10	0	4	2	1	63.4
	0.2-1 cm	28	9	7	5		
	1-5 cm	7	2	21	3		
	5-10 cm	0	1	5	3		
	10-50 cm	1	0	2	1		
	50-100 cm	0	0	0	3		
	> 100 cm	0	0	2	2		
	unknown	4	1	5	3		

2.3.1.3.5 Summary of Section 2.3.1.3

In landfills, the main cause of defects in geomembrane liners is the placement of the primary leachate collection system (PLCS). Inadequate seams and the quality of the subgrade materials can also be very important causes of defects.

Regarding the number and density of defects, reported data suggest that they depend on the size of the facility. Small defect densities were found in larger facilities. This can be attributed mainly to the proportionally less complex features (corners, sumps, pipes penetration, etc.) of the larger facilities, as well as to the small percentage of hand seaming. The implementation of strict CQA programmes also seems to have a great impact on the number of defects. Large defect densities are usually reported for sites constructed without CQA programmes (Rollin et al. 2002b, Needham et al. 2004). A frequency ranging from 0.7 to 15.3 defects/ha can be expected in landfills. In addition, a recent study involving permanent in situ system of leaks detection also showed that additional defects might be expected during landfill operation.

A wide range of sizes of defects has been reported in literature. Defect dimensions appear to change from less than one millimetre to more than one meter. Nevertheless, the majority of the defects seem to be smaller than 10 cm^2.

The issue of the size of the defects is very important in the scope of present work as, in order to carry out experimental work to measure the flow rate through composite liners due to a

hole in a geomembrane (Chapter 6), a hole size as representative as possible of the field conditions should be used. Based on discussion addressed and taking into account the dimensions of our laboratory model (boundary effects needed to be avoided), a circular hole 3 mm in diameter was used in the tests carried out in this study.

As mentioned before, another material used in composite liners to limit the advective flow, which occurs mainly through geomembrane defects, is the GCL. The main characteristics of this component, as well as the main factors affecting its performance a barrier will be addressed in Section 2.3.2.

2.3.2 Geosynthetic Clay Liners

2.3.2.1 Definition and raw materials

There are many ways to classify geosynthetic clay liners, such as geocomposite clay liner (IGS 2000), clay geosynthetic barriers (term adopted in International Symposium Nuremberg held in 2002), bentonite mats, bentonite blankets, prefabricated bentonite blankets, etc. The term geosynthetic clay liner (GCL) was adopted in the present work because it is the most commonly used.

The use of GCLs is relatively recent. It appears that it was first used in 1986 in the USA. Its development and use have gained widespread popularity, which have been followed by intensive research. Some topics that have been under research in the GCLs field are: hydraulic conductivity, diffusion characteristics and chemical compatibility (e.g. Petrov et al. 1997a, b; Petrov & Rowe 1997; Rowe 1998; Lake & Rowe 2000; Jo et al. 2001; Vasko et al. 2001, Katsumi et al. 2004); mechanical behaviour (e.g. Triplett & Fox 2001; Fox et al. 2002; Zanzinger & Alexiew 2002; Bonaparte et al. 2002; Oliveira & Lopes 2002); gas migration (e.g. Didier et al. 2000; Vangpaisal et al. 2002; Bouazza et al. 2002b; Vangpaisal & Bouazza 2004); and durability (e.g. Alexiew 2000; Egloffstein 2001, 2002; Southen & Rowe 2002, 2004; Southen et al. 2004).

GCLs are factory-manufactured hydraulic barriers typically consisting of a layer of a thin bentonite (powdered or granular) sandwiched between two geotextiles or bonded to a geomembrane. Bentonite is the critical component of the GCLs and gives rise to very low hydraulic conductivity of the product. Geotextiles and geomembranes components have two major functions. First, they keep the bentonite layer in place in its non-hydrated state during transportation, handling and installation, and second, keep the bentonite in place after hydration during service life of the products.

Bentonite is a natural clay that appears largely as product of weathering, through a chemical transformation from volcanic ash that was deposited, either during the cretaceous period in marine environments (sodium bentonites), or during the tertiary period in fresh water environments (calcium bentonites). The most widespread member of this group is the montmorillonite, a three-layer clay mineral from the dioctahedrical smectite group. According to Egloffstein (2001, 2002), high quality bentonites contain 75 to 90 % of montmorillonite by weight. Similar values are suggested by Bouazza et al. (2002a), who refers to 60 to 90 % of montmorillonite. Additionally to montmorillonite, bentonites also contain other minerals such as quartz, feldspars, mica, cristobalite, carbonates, and other clay and nonclay minerals.

For industrial applications, bentonite can be classified as sodium or calcium, depending on the dominant exchangeable cation. To improve the hydraulic performance of calcium bentonites,

they can be activated, i.e primary calcium ions are replaced by sodium ions, and then are used in GCLs manufacturing as well.

Structurally, montmorillonites are three-layer minerals consisting of an alumina sheet sandwiched between two silica sheets (tetrahedron-octahedron-tetrahedron sheets), as Figure 2.15 shows. In the tetrahedron sheet, one silicon atom is surrounded by four oxygen atoms linked to a six-ring net. In the octahedron sheet, one aluminium atom is surrounded by six oxygen atoms (OH-groups). Bonding between the shared interior oxide anions and the cations in the tetrahedron and octahedron sheets links the layers together and yields the unique sheet structure of clay minerals. This structure differs somewhat, due to isomorphous substitutions in tetrahedron and octahedron sheets (Si^{4+} by Al^{3+}in tetrahedron sheet, and Al^{3+} by Mg^{2+}, Fe^{2+} or Li^{+} in octahedron sheet), resulting in a slight overall negative charge in the surfaces of silicate sheets (Egloffstein, 1997). In addition, montmorillonite has a large-specific surface area accessible to water (750-800 m^2 g^{-1}) and a large cation exchange capacity, between 100 to 150 meq/100g (Gomes 1986).

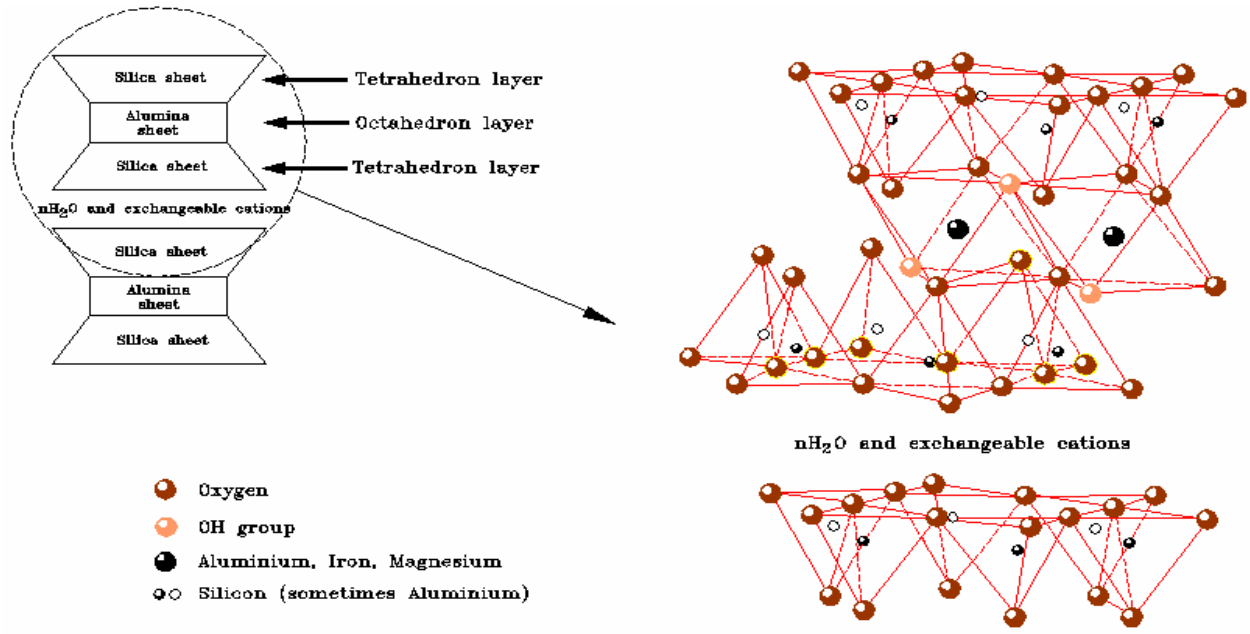

Figure 2.15 – Structure and form of the three-layer clay mineral (various sources)

During the hydration, these combined characteristics of montmorillonite result in adsorption of a large number of hydrated cations (exchangeable cations, such as Ca^{2+}, Mg^{2+}, Na^{+}) as well as water molecules to balance the excess negative charge (Gomes 1986). The adsorption of water molecules and cations results in significant swelling of montmorillonite. These molecules are considered immobile relative to those in bulk pore water (i.e. non-adsorbed water), and act similarly to the solid phase in terms of impact on the flow. When the volume of bound water molecules increases, the fraction of the pore space of freely flowing bulk water decreases and flowing paths become smaller and irregular (Jo et al. 2001). Consequently, hydrated bentonite provides a barrier to fluid flow, typical exhibiting a low hydraulic conductivity to water. According to Bouazza (2002), sodium bentonites and sodium activated-bentonites, can swell ten to fifteen times their volume, whereas calcium bentonites swell two to four times their volume.

Regarding geosynthetic components of the GCLs (geotextiles or geomembranes), several options have been adopted by the different manufacturers. In geotextile-supported GCLs, different combinations of woven and nonwoven can be used. They vary in their manufacturing and in their mass per unit area. The needle punched geotextiles typically range from 100 g m^{-2} to 800 g m^{-2} mass per unit area, and woven ones vary from light products to 200 g m^{-2} slit film. The raw materials are usually either polypropylene, or high density polyethylene. The way they are used also depends on manufacture. Some products include one woven on top and one non-woven geotextile at the bottom, while in other products the non-woven geotextile is on the top and the woven geotextile at the bottom. The products with a geomembrane backing can also vary in type, raw material, thickness, and surface texture.

2.3.2.2 Geotextile-supported GCLs

Geotextile-supported GCLs can be grouped into three main categories (Figure 2.16): needlepunched, stitch-bonded, or adhesive-bonded. In needlepunched products, the bentonite is held in place between the carrier and cover geotextiles by a process of needlepunching. The geotextile on at least one side must be a needlepunched geotextile without a woven component. The needlepunching process punches fibres from this geotextile through the bentonite and embeds these fibres into the bottom geotextile. In stitch-bond products, the bentonite is held in place between the carrier and cover geotextiles by process of stitching. Finally, in adhesive products, the bentonite is covered with adhesive that glues it to geotextiles (Koerner 1997).

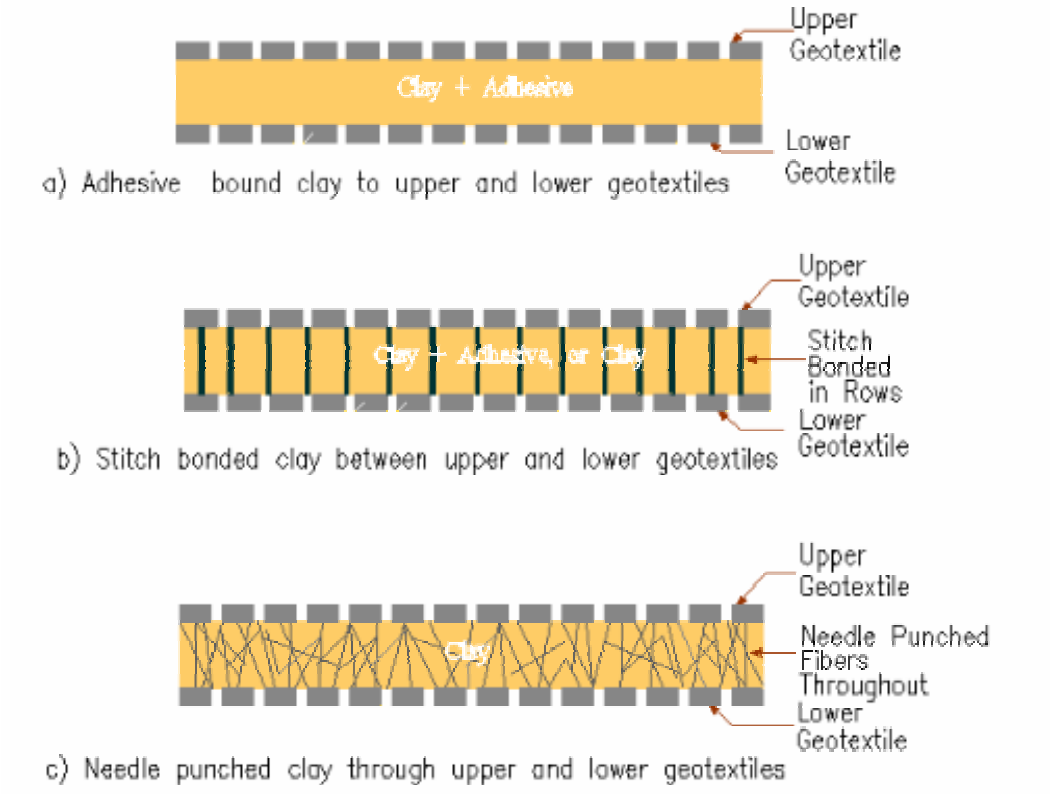

Figure 2.16 – Scheme of the geotextile based GCLs (modified from Koerner 1998)

Needlepunched and stitch-bonded products are often considered as reinforced products in opposition to adhesive-bonded products. The reinforcement is achieved differently in the different types of GCLs. The needlepunching process causes some fibres from the upper geotextile to extend through the bentonite and lower geotextile, bonding the entire product together (von Maubeuge & Heerten 1994). The fibres that are punched through the lower geotextile either rely on natural entanglement and friction to keep the product together, or are heated, causing its fusion to the lower geotextile. In this case, a robust bond between the two geotextiles and bentonite potentially occurs, and they are sometimes termed as thermal locked GCLs. The reinforcement can be also attained by sewing the geotextiles and bentonite all together with parallel rows of stitch bonded yarns (Bouazza 2002).

2.3.2.3 Geomembrane-supported GCLs

In geomembrane-supported GCLs (Figure 2.17), the bentonite is bonded to a geomembrane using a non-polluting adhesive and a thin open weave spun-bonded geotextile is adhered to the bentonite during installation, for protection purposes (Bouazza 2002). This type of GCL is not as much used as geotextile-supported products.

Figure 2.17 – Scheme of the geomembrane based GCLs (modified from Rollin et al. 2002a)

It must be pointed out that new products or modified products have been arising in the market. New products include (Rollin et al. 2002a): prehydrated, thermally treated, double layered GCLs, GCLs with geotextile composite, GCL with the upper geotextile impregnated with bentonite, products that combine different bonding methods (e.g. adhesive plus stitch bonding), etc.

The effectiveness of geotextile-supported GCLs (hereafter designed just as GCLs) as supplementary barriers in landfills is closely related to the hydraulic conductivity of the bentonite, and with the amount of lateral flow at the interface between them and the geomembrane (Bonaparte et al. 2002). The main factors affecting the hydraulic performance of GCLs, such as hydration conditions, permeant liquid and the confining stress are briefly discussed in Section 2.3.2.4. The flow at the interface between the GCL and the geomembrane will be addressed in Chapter 4.

2.3.2.4 Hydraulic performance

2.3.2.4.1 Hydration conditions

The influence of the hydration conditions on the hydraulic conductivity of GCLs has been addressed by several researchers, such as Daniel et al. (1993), Didier & Comeaga (1997), Petrov et al. (1997a), Petrov & Rowe (1997), Ruhl & Daniel (1997), Shackelford et al. (2000), Vasko et al. (2001), Shan & Lai (2002), Katsumi et al. (2004). Results obtained have shown that, in general, prehydrating the GCLs under the same normal stress than the permeation test results in lower hydraulic conductivity than the one obtained in nonprehydrated conditions. The term prehydrated means that the GCL is initially hydrated in deionised, distilled or tap water, prior to permeation with a chemical solution, whereas the term nonprehydrated means that the GCL is wetted and permeated using the same chemical solution (Ruhl & Daniel 1997, Katsumi et al. 2004).

The prehydration water content that would prevent alterations in hydraulic conductivity of GCLs due to a permeant has been also investigated. For example, Daniel et al. (1993) carried out tests in which the bentonite component of a geomembrane-suported GCL was prehydrated to water contents of 50 %, 100 % or 125 %, before being permeated with benzene, gasoline, methanol, methyl ter-butil ether (MTBE) or trichloroethylene (TCE). Air dry specimens (17 %) and saturated specimens (145 %) were also tested. The results obtained are summarised in Figure 2.18. Hydraulic conductivities for the specimens prehydrated to water contents of 125 % and 145 % were not included in this figure because no flow was observed. It was found that the hydraulic conductivity of the GCLs was not affected by the hydrocarbons solutions when the prehydration water content exceeded 100 %.

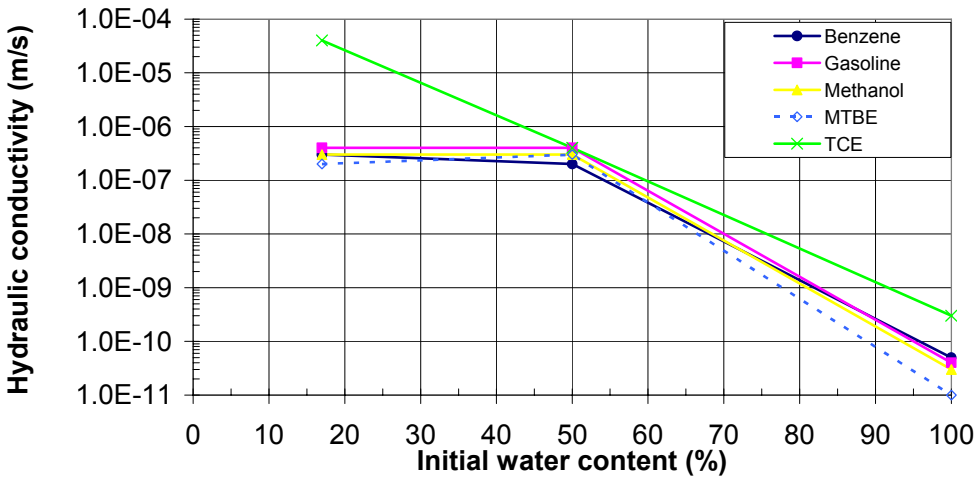

Figure 2.18 - Effect of initial water content on the hydraulic conductivity of a GCL permeated with different permeants (data from Daniel et al. 1993)

Similar investigations were conducted by Vasko et al. (2001). They evaluated how prehydration water content affected the hydraulic conductivity of GCLs permeated with salt solutions ($CaCl_2$), with different concentrations, expressed in terms of molarities (M). Results obtained are shown in Figure 2.19. It can be observed that for the low concentration (0.025 M), the prehydration water content was found to have no influence on hydraulic

conductivity. For concentrations higher than 0.1 M, lower hydraulic conductivities were obtained with higher prehydration water content. The hydraulic conductivity dropped two orders of magnitude as the prehydration water content increased from 9 % to 200 %, and remained constant as the prehydration water content increased.

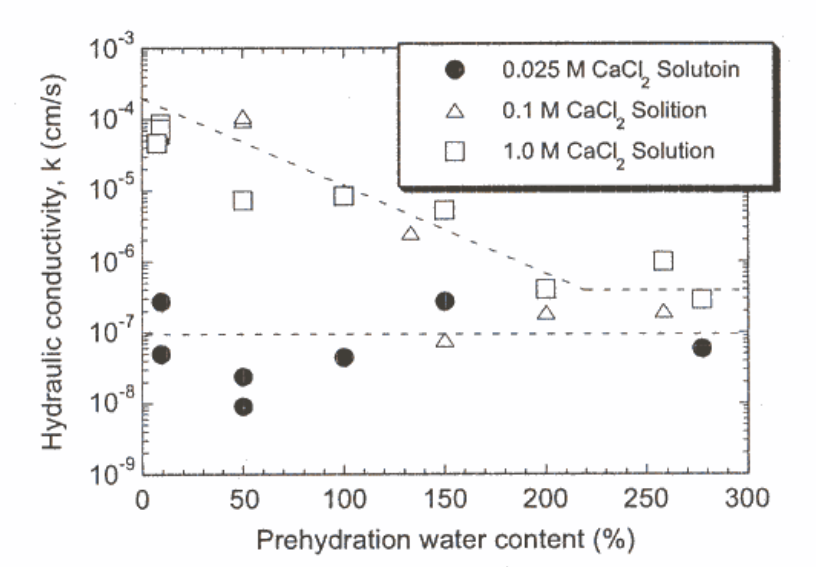

Figure 2.19 – Hydraulic conductivity versus prehydration water content for GCLs permeated with $CaCl_2$ solutions with different concentrations (Vasko et al. 2001)

According to Vasko et al. (2001), the advantages accrued by prehydration followed by permeation with a non-wetting organic liquid, as the hydrocarbons solutions used by Daniel et al. (1993), are not obtained when the permeant liquid is a wetting aqueous solution. The difference might be attributed to the different hydration mechanisms involved when the GCL is in contact with wetting or non-wetting permeants.

Shan & Lai (2002) performed hydraulic conductivity tests and swelling tests on two GCLs with various hydrating liquids (tap water, acid water, seawater, MSW leachate, and gasoline). The tests were conducted using hydrated and nonprehydrated specimens. The results obtained showed that the hydraulic conductivity of GCLs depends both on hydrating and permeating liquid. As long as GCLs are hydrated or permeated with aqueous solutions, their hydraulic conductivity will remain low. They concluded that GCLs can serve as effective hydraulic barriers for application in landfills and secondary containment systems where acid water, seawater, or leachate, instead of fresh water, is the hydration liquid.

To summarise, it seems that the hydraulic conductivity of the GCLs is controlled by the hydrating and the permeating liquids. Moreover, the hydration of GCLs with water (prehydration) prior to permeation with liquids other than water appears to result in a lower hydraulic conductivity than the one obtained in nonprehydrating conditions. With this respect, the *Comité Français des Géosynthétiques* (1998) recommends that these products should be prehydrated before achieving service conditions. A minimum prehydration of 100 % is suggested. The water necessary to reach this water content can be sprayed on the GCL or absorbed from the underlying soil (*Comité Français des Géosynthétiques 1998*). Nevertheless, it is not recommended that the prehydration be made before confining the GCLs.

2.3.2.4.2 Permeant liquid

The permeant liquid can significantly affect the hydraulic conductivity of GCLs. A synthesis of studies addressing this topic was presented by Rowe (1998). This author reviewed data reported by Petrov et al. (1997b), Petrov & Rowe (1997), Ruhl & Daniel (1997), and Rad et al. (1994). Information collected refers to eight GCL (six geotextile based and two geomembrane based products) and seven permeants: distilled water, tap water, two different synthetic leachates, two real MSW leachates, and a simulated hazardous waste leachate. The main findings reported by Rowe (1998) can be summarised as follows: (1) specimens permeated with tap water and distilled water showed similar results; (2) the hydraulic conductivity increases with the concentration of salts in the permeating solution; and (3) specimens permeated with a real or synthetic landfill leachate might have a hydraulic conductivity of an order of magnitude higher than that with water.

It must be pointed out that all studies analysed by Rowe (1998) have concentrated on the GCL short term behaviour. Further analysis conducted by Shackelford et al. (2000), on some of these studies, indicated that the termination of hydraulic conductivity tests involving prehydrated GCLs before chemical equilibrium is established may result in measured hydraulic conductivities unconservatively low.

Shackelford et al. (2000) also discussed the factors and testing considerations affecting the hydraulic conductivity of the GCLs permeated with liquids other than water, in what they termed as non-standard liquids. They concluded that the non-standard liquids containing both high concentration of monovalent cations and low concentration of divalent cations can cause important increases in the hydraulic conductivity of the GCLs (more than one order of magnitude) provided that the test is performed sufficiently long to allow for exchange of adsorbed cations. Furthermore, the GCLs characteristics that influence their hydraulic conductivity to liquids other than water are the aggregate size distribution, content of montmorillonite, thickness of the adsorbed layer, prehydration and void ratio of the mineral content.

Later studies regarding the effect of the permeant liquid on hydraulic conductivity of the GCLs were conducted by other authors. For example, Jo et al. (2001) examined the influence of salt solutions of various concentrations, cation valence, and pH on swelling and hydraulic conductivity of non-prehydrated GCLs. Their results indicate that lower swell and high hydraulic conductivity were associated to an increase in concentration and an increase in cation valence. They also observed that pH only influenced hydraulic conductivity and swelling when it was either very low (< 2), or very high (>13). Another finding reported by these authors refers that the results of free swell tests can be used as a practical screening method for compatibility testing with inorganic solutions. This conclusion is consistent with the conclusion drawn by Shan & Lai (2002), according to which the results of free swell tests can be used to foresee the effect of the hydration liquid or the permeant on the hydraulic conductivity of the GCLs.

Katsumi et al. (2004) investigated also how multi-salt solutions ($CaCl_2$ + NaCl) affected the hydraulic conductivity of non-prehydrated powdered and granular bentonites. Reported results show that the permeability of both GCLs (powdered and granular) was affected by the chemical solutions. Nevertheless, the results suggest that the powdered bentonite was less affected than the granular bentonite, particularly at high concentrations. For powdered bentonite, the hydraulic conductivity presented an increase in permeability from 1 to 2 orders of magnitude, whereas for granular GCL the hydraulic conductivity increased from 1 to 4 orders of magnitude. According to these authors, it is likely that the pores between the

granules may not be blocked due to a lower level of swelling of the bentonite, especially for high concentrations, resulting in an increase in hydraulic conductivity.

To summarise, literature review carried out has shown that hydraulic conductivity of GCLs increases as the concentration and cation valence of the permeant liquid increases. This seems to be related to the swelling capacity of these products. In addition, studies focused on the effect of multi-salt solutions on hydraulic conductivity of non-prehydrated powdered and granular bentonites, showed that the hydraulic conductivity of the granular bentonite was more affected by the multi-salt solutions than the powdered bentonite. This was attributed to the fact that in granular bentonite the pores between the granules may not be blocked due to a lower level of swelling of the bentonite causing an increase in hydraulic conductivity.

2.3.2.4.3 Confining stress

The influence of the confining stress on the hydraulic conductivity of GCLs has been examined by several investigators. Estornell & Daniel (1992) conducted hydraulic conductivity tests with water on three geosynthetic clay liners (stitch-bond, adhesive bounded geotextiles based product, and adhesive bounded geomembrane supported GCL). Tests were carried out on a flexible–wall permeameter. Confining stresses used ranged from 14 to 91 kPa. The results obtained showed that the hydraulic conductivity decreases with increasing confining stress. Similar trend is indicated by Daniel (1996), who anticipates that increasing the confining stress consolidates the GCL to a lower porosity, reducing the permeability.

Petrov et al. (1997b) evaluated how low (3-4 kPa), intermediate (34-37 kPa) and high static confining stresses (109-117 kPa) affected the hydraulic conductivity of a needlepunched GCL. The GCL consisted of a powdered sodium bentonite sandwiched between a needlepunched carrier geotextile reinforced by a woven geotextile, and a needlepunched cover geotextile. Specimens were confined prior to hydration and were hydrated and permeated with either distilled water, or tap water. Except two tests, which were carried out on a double-ring permeameter, in general tests were conducted in a computer controlled constant flow rate fixed-ring permeameter. Results showed that the hydraulic conductivity decreases as the confining stresses increases. These authors attributed the reduction in GCL hydraulic conductivity to lower bulk void ratios resulting from higher confining stresses. They also showed that a linear relationship exists between the logarithm of the hydraulic conductivity and the bulk void ratio.

Petrov & Rowe (1997) showed that void ratios are dependent on both the magnitude of the confining stress and the level of bentonite hydration at the time of application of the confining stresses. Within the scope of their research on chemical compatibility of GCLs with salt solutions and leachates, Petrov & Rowe (1997) observed that applying static confining stresses prior to bentonite hydration produced significantly lower void ratios at a given confining stress than applying increasing confining stresses after allowing the GCL to fully hydrate under a low confining stress. According to the authors, these results emphasise the hydraulic advantages of maximising the overburden stress prior to GCL hydration.

Shackelford et al. (2000) re-plotted published data by Petrov & Rowe (1997) on hydraulic conductivity of GCLs permeated with various NaCl solutions in a bi-logarithm scale. Re-plotted data showed that there is also a strong correlation between the logarithm of hydraulic conductivity and the logarithm of bulk void ratio. More importantly, it highlights

that both bulk void ratio and cation concentration influence the hydraulic conductivity of the GCLs, for a given permeant.

To sum up, hydraulic conductivity decreases as confining stress increases as can be seen in Figure 2.20, which compiled data from various sources. This figure also includes some results of hydraulic conductivity tests carried out in the present work to assist the interpretation of the experimental work on flow rates through composite liners involving a GCL, what will be presented in Chapter 6.

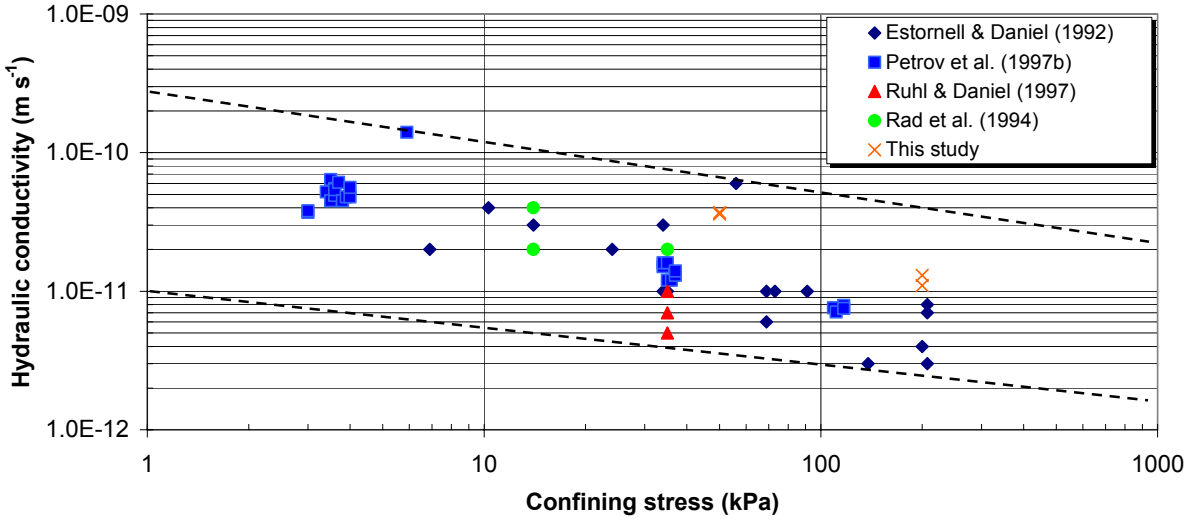

Figure 2.20 - Variation of hydraulic conductivity in function of confining stress

Another type of barrier that can be employed in composite liners to limit the advective flow in lining systems is a CCL (compacted clay liner). Similar to the others types of lining materials, the critical aspects of its successful performance will be briefly discussed in following Section 2.3.3.

2.3.3 Compacted Clay Liners

Compacted clay liners consist of natural mineral soils, bentonite-soil blends, and other materials placed and compacted in lifts. They are designed to work effectively as hydraulic barriers. The critical issue of this liner is its hydraulic conductivity. A value less than 10^{-9} m s^{-1} is typically required for this property (Daniel 1993).

Construction of a CCL with a hydraulic conductivity less than 10^{-9} m s^{-1} requires the use of suitable soils. It has been considered that the soil ability to achieve a specific hydraulic conductivity depends on its plasticity characteristics, water content, and particle size.

Plasticity characteristics are quantified by liquid limit (LL), plastic limit (PL) and plasticity index (PI). The liquid limit is defined as the minimum moisture content, in percentage of oven-dried weight, at which a soil mixture can flow. The plastic limit is the minimum moisture content at which a soil can be moulded. The plastic index (PI=LL-PL) defines the range of moisture contents over which a soil exhibits plastic behaviour. The PI of the soil is

perhaps the single most frequently used indicator of the suitability of a natural soil for use in a CCL. A minimum value around 10 % for PI is often recommended (Oweis & Khera 1998).

Water content refers to the amount of free water contained in a given amount of soil. Its measurement is useful for assessing whether a clay soil needs pre-processing (moisture adjustment or soil amendments) to yield a specific density or hydraulic conductivity (USEPA 1998).

In regard to particle size, a minimum percentage of fines (typically ≥ 50 % passing no. 200 sieve, which has an opening size equal to 75 μm) is usually specified. A minimum of clay (fraction finer than 2 μm) is also sometimes required, such as ≥ 20 to 25 % (Bonaparte et al. 2002). In addition, care must be taken as regards the percent gravel (particles unable to pass through the openings of a no. 4 sieve, opening size equal to 4.75 mm), in cases where a CCL functions as a bottom layer to a geosynthetic, as gravel can cause puncturing in geosynthetics. Controlling the maximum particle size and angularity of the gravel should help avoiding puncturing. It also prevents gravel from creating preferential flow paths. It is recommended to use soil liners with particles and rock fragments smaller than 19 mm (USEPA 1998). Bouazza (2002) recommended a maximum 12 mm stone size in subgrade when the latter is overlaid by GCLs.

The approach outlined regarding the soil ability to achieve a specific hydraulic conductivity is not supported by the findings included in the database assembled to analyse the field performance of CCLs, particularly to address the question of whether GCLs are meeting the purpose of having a hydraulic conductivity less than 10^{-9} m s^{-1}. Practically, no correlation was found between the hydraulic conductivity and the typically measured soil index properties, such as liquid limit, plasticity index, percentage of clay, percentage of fine. This indicates that CCLs having a field hydraulic conductivity less than 10^{-9} m s^{-1} can be constructed with a relatively wide range of clayey soils. This database consisted of 89 CCLs (81 test pads plus 8 actual bottom liners), all of them with specifications to achieve a hydraulic conductivity less than 10^{-9} m s^{-1} (Daniel 1998, Benson et al. 1999, Bonaparte et al. 2002).

Other important conclusions drawn based on information gathered with this database can be summarised as follows (Daniel 1998, Benson et al. 1999, Bonaparte et al. 2002): (i) the primary emphasis should be given to ensure compaction wet of the line of optimum (i.e. curve connecting the peaks of compaction curves developed using a range of compactive energy – Figure 2.21); (ii) the most important control parameter in hydraulic performance of the CCLs was not found to be water content or density, but rather a parameter termed P_0 (Figure 2.22), which represents the percentage of field-measured water content-density points that lie on or above the line of optimums; a P_0 of at least 70 to 80 % is suggested to achieve a hydraulic conductivity less than 10^{-9} m s^{-1} (shaded zone in Figure 2.23); (iii) liners that are thick or have a higher number of lifts have a significantly better chance of achieving a lower field hydraulic conductivity; and (iv) 25 % of 89 CCLs failed to achieve a large-scale hydraulic conductivity less than 10^{-9} m s^{-1}, confirming the difficulty that is often found in achieving the required low hydraulic conductivity in field.

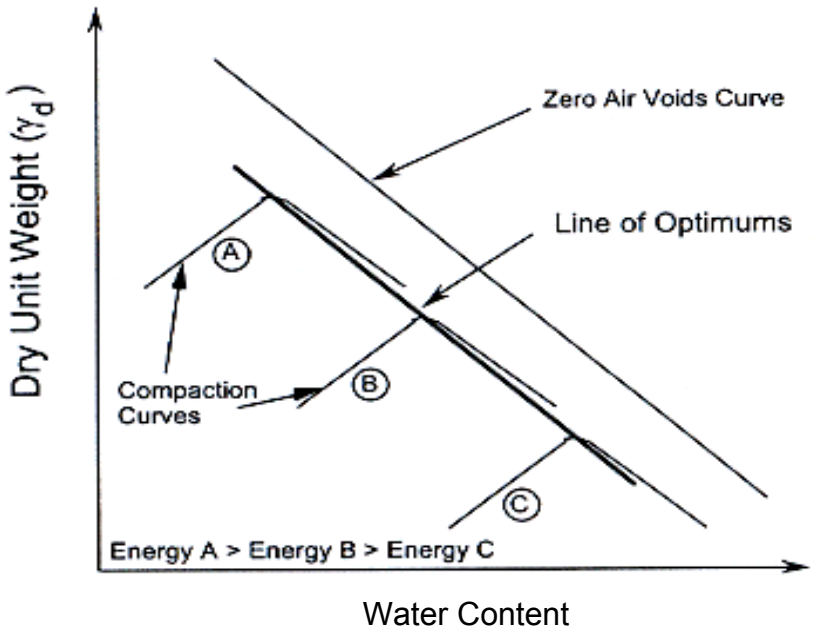

Figure 2.21 – Line of optimums (Daniel 1998, Bonaparte et al. 2002)

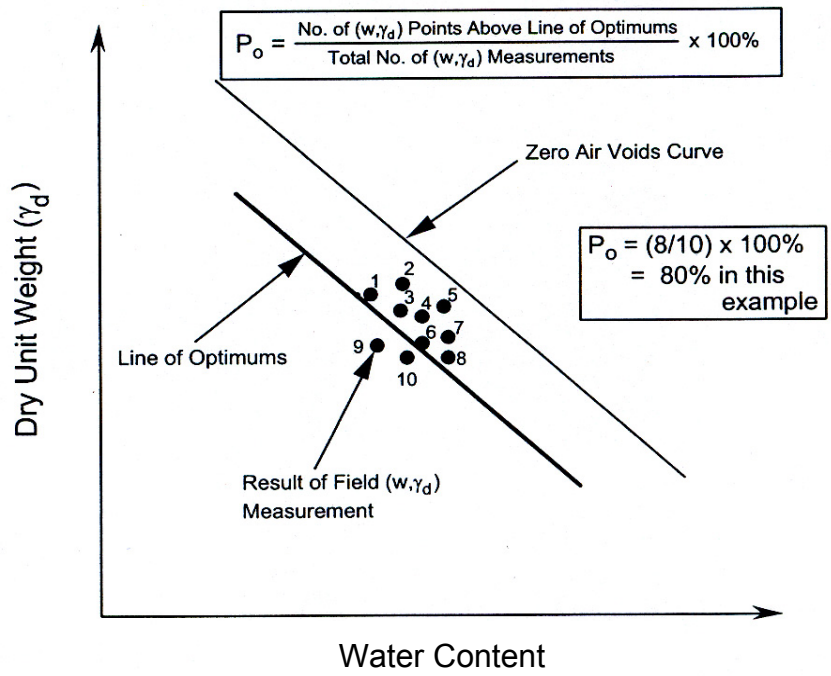

Figure 2.22 – Definition of percent of points wet of optimums: P_0 (cited by Benson et al. 1999, Daniel 1998, Bonaparte et al. 2002)

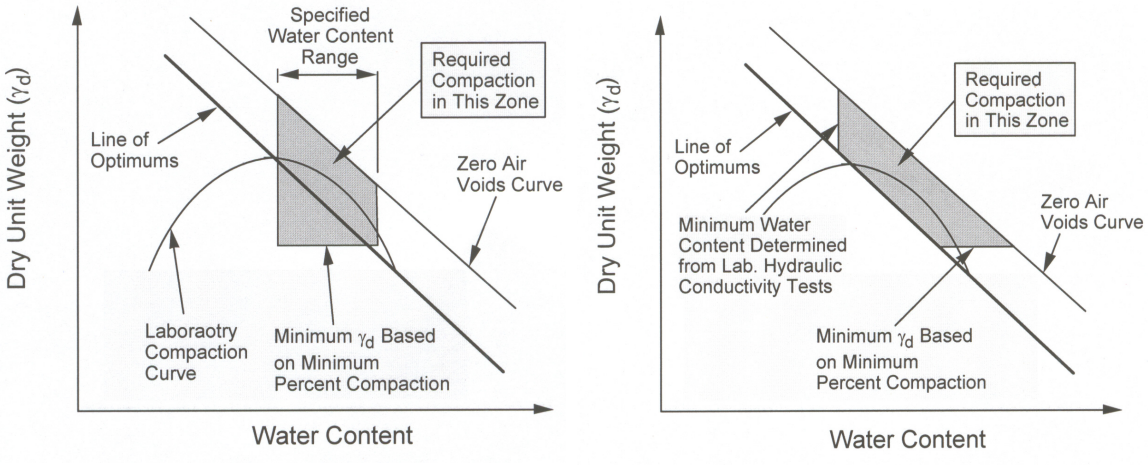

(A) Typical type of specification currently used **(B) Recommended compaction specification**

Figure 2.23 – Water content-density specifications showing: (A) traditional (but not recommended) type of specification, and (B) the recommended type of specification emphasizing compaction to water content-density values on or above the line of optimums (Bonaparte et al. 2002)

The discussion addressed in Section 2.3.3 was focused on hydraulic conductivity. However, it must be taken into account that as P_0 increases, the shear strength, including interface shear strength with geosynthetics, often decreases. Thus, design specifications must ensure that the soil also has proper strength. Other factors such as bearing capacity are also important issues. The engineer must ensure that all criteria, and not only hydraulic conductivity, are satisfied, as emphasised in Bonaparte et al. (2002).

2.4 SUMMARY AND CONCLUSIONS

An extended literature review on landfills and composite liners has been presented in this chapter. Critical issues for a successful performance of the lining materials (geomembranes, geosynthetic clay liners, and compacted clay liners) in landfills have been discussed.

As for geomembranes, their performance is closely related with the seams and the unavoidable defects occurring mainly because of inadequate construction activities. Seams need to be both fluid-tight and have a mechanical strength of the same order of magnitude as geomembrane panels. Thus, they require a strict quality control. However, from a fluid-tightness point of view, their construction quality control is usually based on qualitative criteria (pass/failure), despite the importance of ensuring satisfactory fluid-tightness at the seams.

A literature review on origins, density, and typical sizes of the defects has been presented. It was found that in landfills the majority of defects occur during placement of the cover materials, although inadequate seams as well as the quality of the subgrade materials have been pointed out as very important causes of defects. Mean densities ranging from 0.7 to 15.3 defects/ha can be expected in landfills. In addition, a recent study with permanent in situ systems highlighted that additional defects can appear during landfill operation. Defects

dimensions from less than one millimetre to more than one meter can be encountered, although most defects are smaller than 10 cm^2.

Successful performance of geosynthetic clay liners in landfills is closely related with their hydraulic conductivity, which is highly dependent on the nature of the hydrating and permeating liquid, as well as on the confining stress. Data collected from the literature have shown that prehydration, i.e. hydration with water prior to permeation, usually results in a lower hydraulic conductivity than the one obtained using non-prehydrated GCLs. To guarantee the hydraulic performance of this type of liner, a minimum prehydration of 100 % is suggested by *Comité Français des Géosynthétiques* (1998). Changes in hydraulic conductivity are related with the type and concentration of the permeant liquid. Typically, the hydraulic conductivity of GCLs increases with the increase in the concentration and cation valence of the permeant liquid. It could also be observed that the hydraulic conductivity of the GCLs decreases as the confining stress increases.

With respect to compacted clay liners, the critical issue is their hydraulic conductivity. To perform properly, a hydraulic conductivity less than 10^{-9} m s^{-1} is usually required. The ability of CCL to achieve that value depends mainly on the soil characteristics and on the field compaction procedures. Current technical specifications for construction of CCLs recommend that the primary emphasis should be given to ensure compaction to water content-density values on or above the line of optimums.

The discussions addressed in this chapter highlighted the need for a tool to assess the fluid-tightness of seams from a quantitative point of view. In the present work (Chapter 5) an attempt is made to provide a test method for assessing the quality of the seams by a quantitative measurement. In addition, it could be seen that geomembrane defects appear to be unavoidable. In this framework, experimental work for quantifying the flow rates through composite liners involving GCLs due to defects in the geomembrane is carried out and will be presented in Chapter 6.

3 FLUID MIGRATION THROUGH GEOMEMBRANES

3.1 INTRODUCTION

Geomembranes are used in a wide range of engineering applications as active barriers to control fluid migration. Despite their low permeability, gases, vapours, liquids and dissolved species can migrate through the geomembranes. Therefore, tests are necessary to evaluate the permeation coefficients of the geomembranes to the fluids with which they are in contact in service conditions.

This chapter presents some basic equations for determining the permeation coefficients of the geomembranes. Next, it discusses the factors that affect the migration through intact geomembranes and the laboratory methods used for assessing the permeation coefficients. Finally, it presents a summary of previous experimental studies on geomembrane permeation to gases and water vapour.

3.2 DEFINITIONS AND BASIC EQUATIONS

The concept of permeability in the conventional sense (i.e. according to Darcy law) is not applicable to geomembranes, since they are nonporous materials. However, gases and liquids can migrate through the intact geomembranes by an activated diffusion process, different from the liquid convection process occurring through the pores of porous soils. The transport of a given permeant is usually considered to occur by steps or jumps over a series of potential barriers, following the least resistant path. For gases, this transport process involves three steps (Haxo et al. 1984, Rogers 1985, Haxo 1990): (1) partition or absorption of the permeant in the upstream surface of the geomembrane; (2) diffusion of the permeant through the geomembrane under a concentration gradient; and (3) partition or desorption of the permeant from the downstream surface of the geomembrane into the ambient medium. It should be noted that the extent of each step depends on various parameters among which the most important ones are the permeant-geomembrane interaction and the temperature (Sangam & Rowe 2001b).

The driving force for this migration process is the activity or chemical potential of the permeant, which decreases continuously towards the permeation. In the case of gas migration through geomembranes, concentration is usually the major chemical potential to be considered (Haxo 1990).

In step 1, adsorption consists of removal of the permeant molecule from the fluid and its dispersion on or into the polymer. The permeating molecule is distributed by two or more phases. The process may involve absorption and incorporation in microvoids, cluster formation, solvation-shell formation, etc. (Rogers 1985).

When a geomembrane is in contact with a fluid enough time to reach equilibrium, a relationship at the interface fluid/geomembrane is established (Rowe 1998, Sangam & Rowe 2001b) between the final concentration in the geomembrane, c_g (kg m^{-3}) and the equilibrium concentration in the fluid, c_f (kg m^{-3}). For low penetrant concentrations (Rogers 1985), or where the penetrant does not interact with the polymers, as is usually the case of HDPE geomembranes, c_g is directly proportional to c_f (Rowe 1998):

$$c_g = S_{gf} c_f \tag{3.1}$$

in which S_{gf} is the partitioning coefficient. It might be described as the extent to which a permeating species is distributed between the geomembrane and an adjacent medium.

In step 2, the sorbed permeant at the geomembrane surface will diffuse within the material. Roughly, diffusion can be defined as the process that tends to remove differences in concentration by means of random molecular motions (Park 1986).

The diffusion of the permeating molecules in a geomembrane can be modelled by Fick's first law, which can be expressed as follows:

$$f = -D \frac{\partial c_g}{\partial z} \tag{3.2}$$

in which f is the permeant mass flux passing through a unit area of geomembrane surface (kg m^{-2} s^{-1}), D is the diffusion coefficient (m^2 s^{-1}), z is the spatial dimension parallel to the direction of diffusion (m), and $\partial c_g/\partial z$ is the concentration gradient (kg m^{-4}). Diffusion coefficient describes the degree of mobility of the dissolved permeant within the geomembrane.

Step 3 is similar to the first step with an inverted process. It consists in permeant desorption from the geomembrane to the outer solution.

From an experimental point of view, it is much more difficult to measure the concentration change in the geomembrane than to measure the concentration in the fluid on both sides of the geomembrane. Therefore, it is more practical to express the diffusion equations in terms of concentration in adjacent fluids (Sangam & Rowe 2001b).

Substituting Equation (3.1) into Equation (3.2) and considering the equilibrium concentration difference Δc_f (kg m^{-3}) of the penetrant molecules in the adjacent fluids of a thin geomembrane, the mass flux, f, across geomembrane is given by:

$$f = -D \frac{\partial c_g}{\partial z} = -D \frac{\Delta c_g}{t_g} = -D S_{gf} \frac{\Delta c_f}{t_g} = -\underline{P} \frac{\Delta c_f}{t_g} \tag{3.3}$$

in which t_g is the geomembrane thickness (m); and $\underline{P}$ is generally designated as coefficient of permeability (m^2 s^{-1}). $\underline{P}$ characterizes mass transfer from one fluid to another through the tested geomembrane. It depends on D and on the partitioning coefficient S_{gf}:

$$\underline{P} = S_{gf} D \tag{3.4}$$

It should be noted that $\underline{P}$ refers to the three steps of the migration process, whereas D refers only to the second step that is diffusion in the geomembrane. Thus, in this case, the permeability coefficient $\underline{P}$ depends on experimental test conditions, such as the concentrations, temperature, etc.

For a gas G, if the quantity of gas is expressed in number of moles instead of mass, Equation (3.3) can also be written as follows:

$$f_G = -\underline{P_G}' \frac{\Delta c_f}{t_g} \tag{3.5}$$

in which f_G is the mass diffusive flux of gas G, expressed in mol m^{-2} s^{-1}, and $\underline{P_G}'$ is the coefficient of permeability to gas G, expressed in mol m^2 s^{-1} kg^{-1}.

In a gas, a change of the partial pressure in fluid is accompanied by a change in the molar concentration in fluid (Haxo & Pierson 1991). Thus, Equation (3.5) can then be written as follows:

$$f_G = -\underline{P_G}'' \frac{\Delta p_G}{t_g} \tag{3.6}$$

in which Δp_G is the partial pressure difference of gas G in adjacent fluids (Pa), and $\underline{P_G}''$ is the coefficient of permeability of the geomembrane to gas G expressed in mol s^{-1} m^{-1} Pa^{-1}.

It is possible to experimentally infer the value of $\underline{P_G}''$ by performing steady state experiments in which the partial pressures are known in the fluid on both sides of the geomembrane (Δp_G) and f_G can be determined, as Chapter 5 will show. The permeability is then calculated as follows:

$$\underline{P_G}'' = \frac{f_G \, t_g}{\Delta p_G} \tag{3.7}$$

Characterising the permeability of a geomembrane by a coefficient of permeability presents several drawbacks. First, previous studies on this topic have shown that it may depend on the thickness (Haxo et al. 1984; Matrecon 1988; Pierson & Duquennoi 2000). Furthermore, it may be difficult to measure the thickness of geomembrane specimens accurately. Lastly, this coefficient may be confused with the permeability coefficient used for porous media (Darcy law). Therefore, it is advisable to use the permeance, P_G, in mol m^{-2} s^{-1} Pa^{-1} for characterising

the permeation of the geomembranes to gas *G*, since it can be calculated only from f_G and Δp_G as follows:

$$P_G = \frac{P_G''}{t_g} = \frac{f_G}{\Delta p_G} \tag{3.8}$$

3.3 FACTORS AFFECTING FLUID MIGRATION THROUGH GEOMEMBRANE

The fluid migration through geomembrane involves a variety of factors including the solubility of the permeant, temperature, concentration, size and shape of permeant molecules, polymer properties, etc. These factors will be briefly addressed in the following paragraphs.

The relationship between the solubility characteristics of the permeant and the geomembrane play an important role in migration. In general, the more soluble is the permeant in the geomembrane, the higher the probability of permeation (Matrecon 1988). The permeability is also dependent on the similarity of the penetrant and polymer. It seems that polar polymers dissolve polar molecules, whereas non-polar polymers dissolve non-polar molecules (Rowe 1998). Strongly polar permeant molecules like water have low transport rates through polyethylene geomembranes, since the molecules of this polymer are non-polar (Sangam & Rowe 2001a, b). Low diffusion resistance for non-polar and weakly polar hydrocarbons were also reported by Mueller et al. (1998). The work by Durin (1999) on diffusion of organic solvents in geomembranes also showed that the diffusion coefficient depends on solvent polarity.

An increase in temperature provides energy for general increase in polymer chain segmental motion (Rogers 1985). Thus, higher temperatures result in higher rates of diffusion. Park (1986) mentioned that for a wide variety of temperatures the change in gas permeability is mainly due to changes in diffusion coefficient. The relationship between temperature and diffusion, solubility and permeability coefficients has been described by Arrehenius' law. However, research conducted by Durin et al. (1998), to study the influence of temperature on water diffusion of various geomembranes, suggest that the application of Arrehenius' law may be inappropriate to estimate the evolution of diffusion coefficient with temperature.

In regard to concentration dependence, a similar behaviour as the one observed with temperature might be expected, if the solution process is ideal (Rogers 1985). Studies conducted by Park et al. (1995) and Mueller et al. (1998) to estimate the solubility and diffusion coefficients of organic pollutants in HDPE geomembranes, showed that the diffusion process exhibits a significant dependence on the concentration. Their results suggested that the diffusion coefficient was lower for contaminants at low concentrations in aqueous solutions than for pure chemicals. Research by Chul Joo et al. (2001) suggests that the diffusion coefficients increased exponentially as the initial aqueous concentration of organic chemicals increased. In addition, these authors reported that the correspondent partioning coefficients were not significantly affected.

The diffusion coefficient decreases with increasing permeant size, weight, and cross sectional area. The energy of activation for a large molecule is higher than for a small molecule. The shape of the permeant molecules has also been reported to have an effect on permeability. Permeants with linear, flexible and symmetrical molecules have higher mobility than rigid

molecules (Rogers 1985). The migration of permeant through geomembranes is closely related to the polymer properties, namely the degree of crystallinity, density, filler content, etc. Polyethylene exhibits high degree of crystallinity, which is associated with close packing of the molecular chains. The permeability to many liquids, gases and vapours decreases as and when the crystallinity increases. The degree of crystallinity is linked with density. Thus, the geomembrane permeability is expected to decrease with density (Ingold 1994, Durin 1999). Research conducted by Park & Nibras (1993) on mass transport of organic chemicals through various geomembranes showed that low density polyethylene geomembranes had higher partition and diffusion coefficients than high density polyethylene membranes.

Thickness of the geomembrane is another factor that influences the migration process. Results presented by Haxo et al. (1984) and Haxo (1990) show that the methane flow through HDPE geomembranes decreases with increasing thickness. However, the decrease was not inversely proportional to the thickness as expressed by Fick's law. Similar behaviour was reported by August & Tatzky (1984) in a study about the permeability of several geomembranes to organics. Recent research performed by Chul Joo et al. (2001) on organic chemical permeation showed that as the HDPE geomembranes thickness increased from 1.5 mm to 2.5 mm the diffusion coefficients decreased, but the partition coefficients were not affected. This can be explained by the fact that permeability coefficients characterise the whole process of transport from one side to the other side of the geomembrane, and not only the diffusion process through the geomembrane itself.

In conclusion, permeance and permeability coefficients cannot be considered as intrinsic characteristics of the permeation of a given gas through a given geomembrane. Thus, all results must specify experimental conditions such as temperature, concentration, etc.

3.4 EXPERIMENTAL METHODS FOR ASSESSING THE PERMEATION PARAMETERS

A variety of test methods is available for assessing the permeation parameters of geomembranes (e.g. diffusion, solubility, portioning, permeability coefficients), such as permeation/diffusion methods, immersion/sorption tests, pouch tests, etc. Some applications of these methods are briefly presented in the following paragraphs.

Permeation/diffusion methods consist basically in monitoring the migration of a permeant from a fluid on one side (source) of the geomembrane to the fluid on the other side (receptor). One example of the application of this method is the two-compartment diffusion test, in which the source is filled with permeant fluid while the receptor is filled with a fluid of known composition (reference fluid). Only one face of the geomembrane specimen is in contact with a solution containing the permeant and the permeant concentration in the reference fluid must be kept negligible during the test. Migration through the geomembrane is to be monitored as the permeant goes from the source to the receptor over time. This method is suitable for aqueous solutions or leachates (Sangam & Rowe 2001b).

Other examples of permeation/diffusion tests are the manometric and volumetric tests used for determining gas permeability of geomembranes. Both test procedures are covered in ASTM D 1434. Briefly, the specimen is mounted in a cell so as to form a sealed semibarrier between two chambers. One chamber contains the test gas at a specific high pressure, and the other chamber, at a low pressure, receives the permeating gas. In manometric procedure, the migration of gas is indicated by the measurement of the increase in pressure with a manometer on the downstream chamber. In volumetric procedure the lower pressure chamber

is maintained at near atmospheric pressure, whereas higher-pressure chamber has a pressure higher than the atmospheric one. A capillary pipe is used to measure the volume of gas that migrates through the specimen under specific test pressure or concentration gradient. The disadvantage of these tests is that small leaks around the connections and joints might occur.

According to Pelte (1993) permeation/diffusion tests can also be performed for measuring the water flow through the geomembrane only due to a hydraulic pressure difference (without any concentration difference). For such tests, radioactive tracer molecules can be used. Succinctly, a known quantity of radioactive molecules is introduced into the upstream chamber of the test apparatus and the flux is evaluated by measuring the quantity of radioactive molecules reaching the downstream chamber (Eloy-Giorni et al. 1996). The measured flow is very accurate but the disadvantage of this method is that, contrary to other methods, it takes into account the "auto-diffusive" flux which always occurs without any chemical potential difference (molecules moving freely in both directions). In case of small chemical potential difference, this flux may hide the flux that is to be measured.

In accordance with ASTM E 96, another different type of permeation/diffusion test can be carried out to assess the water vapour transmission rate (WTR)[1], water vapour permeance (P_W)[2], and water vapour permeability $\left(\underline{P_G}''\right)$[3]. In this test, a circular specimen is sealed into the mouth of a test dish with either distilled water or a desiccant in it and a controlled relative humidity difference across the geomembrane boundary is maintained. With water in the cup (i.e. 100 % relative humidity) and lower relative humidity at the outside, a weight loss can be monitored, by weighting the dish assembly periodically. With a desiccant in the cup (0% of relative humidity) and a higher relative humidity at the outside, a weight gain is monitored. Permeation coefficients can be estimated by knowing water vapour pressure gradient (estimated from relative humidity difference). This test method is extremely difficult to conduct for thick geomembranes, especially for HDPE since this material presents low WTR. In addition, the least amount of leakage around the test specimen-to-cup seal may influence the test results (Koerner 1998). A procedure similar to that described above can also be used to evaluate the permeability of geomembranes to solvent vapours. In this case, a solvent of interest is placed within the test dish.

Immersion/sorption methods consist in immersing the geomembrane specimen in a container filled with the fluid of interest. Both faces of the specimen are in contact with the permeant, which permeates from both sides and then migrates within the geomembrane. The increase in mass of specimen is monitored until equilibrium, i.e. until mass of geomembrane becomes constant. Based on weight gain, permeation coefficients can be evaluated (Petle 1993). The inconvenient of this method is its duration.

Pouch test method consists in filling a geomembrane pouch with a test permeant and immersing it in a fluid of known composition. This method was used by Haxo (1990) to assess the permeability of geomembranes to water, ions, and to various constituents of a leachate. The author immersed the pouch specimens in deionised water to create a concentration gradient across the geomembrane. This results in the movement by diffusion of

---

[1] WTR is the time rate of water vapour flow normal to its surfaces under steady state conditions through a unit area under the conditions of test.

[2] P_w is the time rate of water vapour transmission through unit area of a flat material induced by unit vapour pressure difference between two specific surfaces, under specified temperature and humidity conditions.

[3] $\underline{P_G}''$ is permeance multiplied by the thickness of the geomembrane.

water, ions and other dissolved components through the pouch walls (Figure 3.1). The initial pouch contents were analysed (composition, pH and electrical conductivity). Weight, pH, and conductivity measurements were periodically done in order to evaluate, respectively, the extent of migration of water into the geomembrane and the extent to which constituents in the adjacent fluid migrate through the geomembrane. At the end of the exposure, the pouch was dismantled, and pouch walls were analysed again. The interpretation of results assumes that diffusion through the geomembrane specimen is slow relatively to that in fluid. Leaks in pouch must be avoided (Haxo & Pierson 1991).

The permeability of the geomembranes to gases can also be assessed by a pouch test. The test procedure is similar to the above mentioned, except that the pouch is filled with gas, at a specific pressure. The permeability coefficient is determined from the pressure drop inside the specimen, monitored during the test (Hurtado-Gimeno 1999).

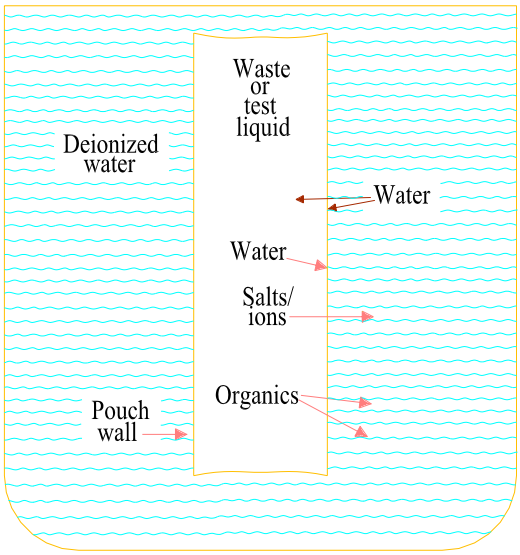

Figure 3.1 - Schematic representation of a pouch assembly showing the movement of constituents during a pouch test (based on Haxo & Pierson 1991)

A new application of the pouch test method for evaluating the permeation coefficients to gas through geomembrane seams is one of the aims of the present work, which will be presented in Chapter 5. It makes also possible to estimate the permeation to water vapour. In this context, existing data regarding the permeability of geomembranes to gases and to water vapour will be presented in the following section.

3.5 PREVIOUS STUDIES ON GEOMEMBRANES PERMEATION TO GAS AND WATER VAPOUR

3.5.1 Haxo et al. (1984) and Haxo (1990)

The permeability of various geomembranes to three gases of interest in landfills (methane, carbon dioxide, and nitrogen) and to water vapour was reported by Haxo et al. (1984) and by Haxo (1990) for a broad range of geomembranes. Permeabilities were determined by the

volumetric method in accordance with ASTM D 1434. Table 3.1 shows the results obtained by these authors on gas permeability to carbon dioxide (CO_2), methane (CH_4), and nitrogen (N_2).

The main findings reported by Haxo et al. (1984) and by Haxo (1990) can be summarised as follows: (1) the permeability of a given geomembrane can vary significantly with the gas; for instance, all geomembranes had a much higher permeability to CO_2 than to CH_4 or to N_2 and a higher permeability to CH_4 than to N_2; (2) permeability of a given generic polymer can differ as a result of compounding variations; (3) higher polymer crystallinity yields lower permeability; (4) permeability of geomembranes to gases increases with temperature.

The permeability of HDPE geomembranes to carbon dioxide shown in Table 3.1 is consistent with the permeability included in ASTM 1434 standard for a polyethylene film: 2.6×10^{-15} mol s^{-1} Pa^{-1} m^{-1}. Permeabilities presented in that standard resulted from an interlaboratory research conducted in ten laboratories for studying test precision.

Table 3.1 - Permeability of geomembranes to different gases at 23ºC (based on Haxo et al. 1984, Haxo 1990)

Polymer	Thickness (mm)	Gas permeability $\left(\underline{P_G}''\right)$ (mol s^{-1} Pa^{-1} m^{-1})		
		CO_2	CH_4	N_2
CSPE	0.82	0.509×10^{-15}	0.904×10^{-16}	1.11×10^{-16}
	0.86	1.83×10^{-15}	5.43×10^{-16}	1.21×10^{-16}
CPE	0.72	0.388×10^{-15}	0.231×10^{-16}	0.0536×10^{-16}
LDPE	0.25	7.87×10^{-15}	17.1×10^{-16}	----
LLDPE	0.46	3.21×10^{-15}	7.54×10^{-16}	----
HDPE	0.61	2.27×10^{-15}	4.29×10^{-16}	----
	0.86	2.05×10^{-15}	4.55×10^{-16}	----
PVC	0.25	9.85×10^{-15}	14.7×10^{-16}	----
	0.49	7.50×10^{-15}	11.1×10^{-16}	2.71×10^{-16}
	0.81	11.7×10^{-15}	11.8×10^{-16}	----

The water vapour transmission rate (*WTR*) and water vapour permeability $\left(\underline{P_W}''\right)$ were also measured by Haxo et al. (1984) in accordance with ASTM E 96. Table 3.2 presents the results. As for HDPE polymer, the measured water vapour flux was 0.109×10^{-7} mol m^{-2} s^{-1} for a 0.8 mm thick geomembrane, and 0.0386×10^{-7} mol m^{-2} s^{-1} for a 2.44 mm thick geomembrane. These fluxes correspond to permeabilities of 0.0627×10^{-13} mol m^{-1} s^{-1} Pa^{-1} and 0.675×10^{-13} mol m^{-1} s^{-1} Pa^{-1}, respectively. Other findings reported by these authors can be summarised as follows: (1) permeability to water vapour varies considerably among the polymer type; (2) increased thickness and increased crystallinity of geomembranes reduce permeability rates; (3) within a given geomembrane, significant variation was obtained, which was attributed to differences in polymer composition.

Table 3.2 - Flux, permeance, and permeability to water vapour for various geomembranes (based on Haxo et al. 1984, Matrecon 1988)

Geomembrane polymer	Thickness (mm)	Flux (WTR) (mol m^{-2} s^{-1})	Permeance (P_W) (mol s^{-1} Pa^{-1} m^{-2})	Permeability $\left(\underline{P_W}''\right)$ (mol s^{-1} Pa^{-1} m^{-1})
HDPE	0.80	0.109×10^{-7}	0.0786×10^{-10}	0.0627×10^{-13}
	2.44	0.0386×10^{-7}	0.0284×10^{-10}	0.0675×10^{-13}
LDPE	0.76	0.367×10^{-7}	0.262×10^{-10}	0.198×10^{-13}
PVC	0.28	28.4×10^{-7}	20.2×10^{-10}	5.64×10^{-13}
	0.52	18.9×10^{-7}	13.4×10^{-10}	6.99×10^{-13}
	0.79	11.9×10^{-7}	8.48×10^{-10}	6.71×10^{-13}
CPE	0.53	4.13×10^{-7}	2.94×10^{-10}	1.56×10^{-13}
	0.79	2.06×10^{-7}	1.47×10^{-10}	1.16×10^{-13}
	0.97	4.13×10^{-7}	2.94×10^{-10}	2.86×10^{-13}
CSPE	0.74	2.14×10^{-7}	1.52×10^{-10}	1.13×10^{-13}
	1.07	1.62×10^{-7}	1.15×10^{-10}	1.23×10^{-13}
EPDM	0.51	1.74×10^{-7}	1.23×10^{-10}	0.632×10^{-13}
	1.70	1.11×10^{-7}	0.786×10^{-10}	1.34×10^{-13}

3.5.2 Lambert (1994)

Lambert (1994) evaluated the permeability of HDPE geomembranes to air and helium, using a manometric cell (Figure 3.2). Geomembrane specimens were assembled inside the cell between two chambers (upstream and downstream chambers). The upstream chamber was filled with the specific gas at constant high pressure, whereas the downstream chamber received the gas. Evolution of gas pressure in the downstream chamber was monitored with a monometer. Gas flux and the correspondent permeability were assessed from the relationship obtained between pressure and time. Air permeability obtained using a 1.7 mm thick HDPE geomembrane was 2×10^{-16} mol s^{-1} Pa^{-1} m^{-1}.

3.5.3 Hurtado-Gimeno (1999)

Hurtado-Gimeno (1999) conducted a series of permeability tests to nitrogen with a 1.5 mm thick HDPE geomembrane using the cell shown in Figure 3.2. Tests were carried out with the upstream chamber filled with the nitrogen gas at constant high pressure, and the downstream chamber filled with water. Evolution of gas pressure in the upstream chamber was monitored with a monometer. Gas flux and the correspondent permeability were assessed from the relationship obtained between pressure and time. Permeability to nitrogen of 10^{-15} mol s^{-1} Pa^{-1} m^{-1} was reported by this author.

Hurtado-Gimeno (1999) also performed gas permeability tests using circular pouch specimens of HDPE and bituminous geomembranes. Each specimen was tested in two different ways to

assess the permeability to nitrogen and to water vapour. For that, specimens were filled with nitrogen and placed either in air (in controlled temperature and humidity box, under a temperature of 27ºC and a relative humidity of 50 %), or they were immersed in water (also at 27ºC). Atmospheric pressure and temperature (air or water) were recorded. Results reported by this author are reviewed in Chapter 5, Section 5.11.

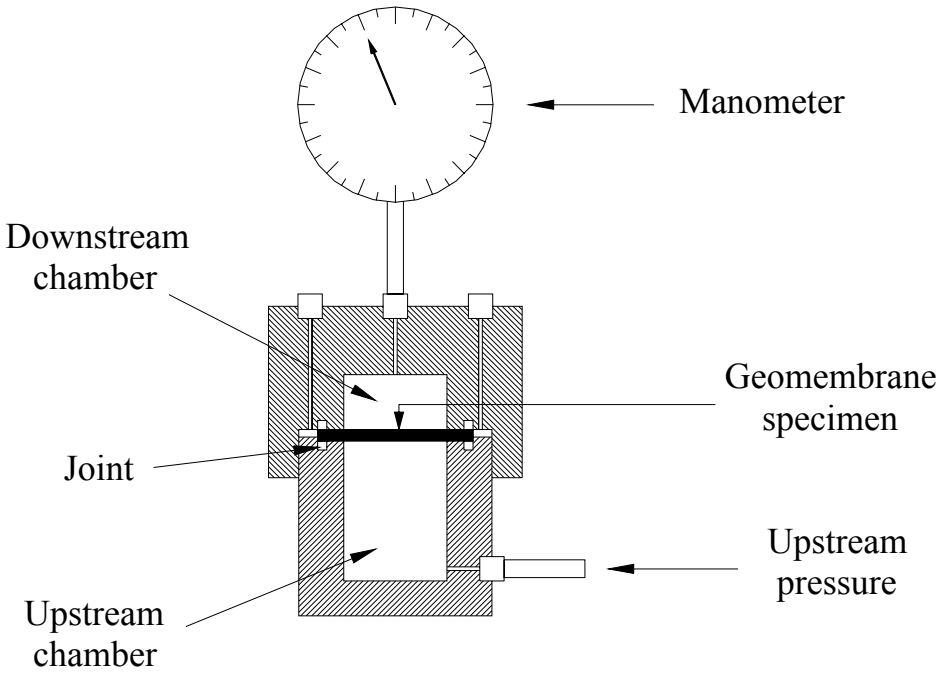

Figure 3.2 – Scheme of the manometric cell designed at University of Grenoble (adapted from Lambert 1994)

3.6 SUMMARY AND CONCLUSIONS

The fundamental equations for evaluating the permeation coefficients of geomembranes have been presented at the beginning of this chapter. Then, the main factors affecting the fluid migration through the geomembranes have been discussed. These factors include, amoung others, solubility of the permeant, temperature, concentration, size and shape of permeant molecules, and polymer properties. Discussion addressed indicated that: (i) the more soluble the permeant, the higher is the permeation rate; (ii) polar molecules have lower permeation rates than non-polar through non-polar polymers such as HDPE; (iii) higher temperatures result in higher permeation rates; (iv) the diffusion coefficient decreases with increasing size, weigh, and cross sectional area of the permeant; and (v) flow decreases with increasing thickness of the geomembranes. Dependence of permeation on the mentioned factors emphasised that the permeation coefficients cannot be considered as intrinsic characteristics of the permeation of a given fluid through a given geomembrane, as well as that the experimental results must specify test conditions.

It could be seen that there are several test methods for assessing the permeation coefficients of geomembranes. Nevertheless, none of them has been used for predicting the permeation coefficients of the geomembrane seams, in spite of their susceptibility, as Chapter 2 shows.

Therefore, a new application of the pouch test method for evaluating the permeation coefficients to gas through geomembrane seams is made in this work, and it will be presented in Chapter 5. That test method makes it possible to estimate the permeation coefficient not only to gas, but also to water vapour. At the end of the present chapter, a summary of the previous studies about gas and water vapour permeation through geomembranes has been presented.

4 ADVECTIVE FLOW THROUGH COMPOSITE LINERS DUE TO GEOMEMBRANE DEFECTS

4.1 INTRODUCTION

Composite liners are commonly used as standard liner systems. The basic premise for using a composite liner in landfills is that the advective contaminant flow (herein simply referred to as flow) through the unavoidable defects in the geomembrane is limited by the presence of a GCL or a CCL.

When there is a defect in geomembrane, the liquid first flows through the defect, then flows laterally to some distance in the interface between the geomembrane and the underlying layer(s), and, finally, flows through the latter(s). This process depends on many factors, such as the hydraulic conductivity of the underlying layer, the transmissivity of the interface between the geomembrane and the underlying layer, the thickness of the liner system, the size of the hole in the geomembrane, and the liquid head on the top of the liner (Giroud 1997).

To evaluate the performance of the composite liners involving GCLs, the hydraulic conductivity value of the GCLs is needed. However, in landfills, GCLs are typically installed at their natural water content, which means that they are not fully saturated. In this circumstance, the saturated hydraulic conductivity may not be representative of the field conditions, being necessary to know the unsaturated hydraulic conductivity.

Direct measurement of the unsaturated hydraulic conductivity is quite complex. Predictive methods are typically used. They are based on the water retention curve (relationship between the volumetric water content and the matric suction) and the saturated hydraulic conductivity, where the water retention curve is commonly represented by the van Genuchten parameters.

This chapter focuses on theoretical aspects related with both the water retention curves and the flow rate through composite liners due to geomembrane defects, aiming to assist the interpretation of the experimental work carried out on these topics, which is presented in Chapter 6.

The chapter begins with background information on water flow through porous media. Then, it discusses the predictive methods for assessing the unsaturated hydraulic conductivity, the methodology to obtain the van Genuchten parameters and the techniques for measuring suction. This topic finishes with a literature review on water retention curves of GCLs.

Regarding the flow rate through composite liners due to geomembrane defects, this chapter discusses the existing analytical solutions and empirical equations to predict the flow. Also, it makes a literature review on experimental studies carried out, both in laboratory and in situ, for measuring flow through composite liners, in which the geomembrane exhibits a defect.

4.2 WATER FLOW THROUGH POROUS MEDIA

4.2.1 Energy states of water in soil

Water processes two types of energy: potential and kinetic. The first is associated with its position and state, with reference to some datum conditions, whereas the second is associated with its motion. In most cases, the velocity of water flow in soils is not significant enough to

make necessary kinetic energy considerations. It is the variation in the total potential energy from one location to another that is responsible for water flow in soils. Thus, it is important to distinguish each potential energy sources (Reddi & Inyang 2000).

The total potential of soil water, ψ, can be expressed as follows (Reddi & Inyang 2000):

$$\psi = \psi_g + \psi_p + \psi_o \tag{4.1}$$

where ψ_g is the gravitational potential; ψ_p is the pressure potential, and ψ_o is the osmotic potential.

The gravitational potential, ψ_g, is the work required to transfer water from the reference elevation to the soil elevation. It is expressed as the product of unit weight of water, γ_w, and the elevation of the water body above a specified datum, h_w:

$$\psi_g = -\gamma_w h_w \tag{4.2}$$

This potential is independent from pressure conditions of the soil as well as of its saturation.

The pressure potential, ψ_p, can be either positive or negative, depending on whether the point in the soil under consideration is at a hydrostatic pressure higher or lower than the atmospheric pressure. In the first case, the point is below a free water surface and is typically termed as piezometric. If it is negative, the energy required to transport a unit volume of water from atmospheric conditions is governed by the capillary principle (Reddi & Inyang 2000), and the potential is generally referred to as capillary or matric potential, ψ_m.

The osmotic potential, ψ_o, is the work required to transfer water from a reference pool of pure water to a pool of soil solution at the same elevation, temperature, etc. (Yong et al. 1992). This potential is relatively low when compared to the others previously mentioned.

The potential is a measure of the energy state of the soil-water. Many terms have been used to describe the energy with which water is held in soils. The term soil-water potential is commonly used in thermodynamics, whereas the term soil-water suction or tension is typically used in geotechnical engineering. Following a geotechnical approach, the term potential will be designated henceforth by suction.

The unit for soil-water suction is called pF unit (pF=$\log_{10}$ height of water column in cm), although it can also be expressed in units of "head" (e.g. meters) or pressure (Fang 1997).

4.2.2 Governing equations for flow

Flow of water takes place in soils due to spatial differences in the energy states. Nevertheless, as pointed out by Reddi & Inyang (2000) the driving mechanism for water movement is the pressure suction (termed matric suction when referring to the unsaturated conditions, as previously mentioned).

The flow of water in porous media may be divided into two particular systems for general consideration: a saturated system where all pore space is filled with water and is participating to flow, and an unsaturated system where both air and water are present and only a limited pore space (saturated pores) will participate to flow of water.

The flow of water through saturated porous media follows Darcy's law, which states that:

$$v = -k \frac{\partial h_w}{\partial x} \tag{4.3}$$

where v is the flow velocity also known as Darcian velocity, k is the hydraulic conductivity, and $\partial h_w / \partial x$ is the hydraulic head gradient in the x direction, commonly designed as i. The hydraulic conductivity is constant for a specific saturated media. The negative sign in Equation (4.3) indicates that water flows towards of a decreasing hydraulic head.

For steady state conditions, the mathematical representation of saturated water flow is derived by combining a three-dimensional form of Darcy's law with the continuity equation:

$$\frac{\partial}{\partial x}\left[k_x \frac{\partial h_w}{\partial x}\right] + \frac{\partial}{\partial y}\left[k_y \frac{\partial h_w}{\partial y}\right] + \frac{\partial}{\partial z}\left[k_z \frac{\partial h_w}{\partial z}\right] = 0 \tag{4.4}$$

where k_x, k_y, and k_z are the hydraulic conductivity values in x, y, and z directions.

Under unsaturated conditions, the value of k is no longer constant being highly dependent on water content and the flow is always transient. Mathematically it can also be expressed by coupling Darcy's law and the continuity equation. This equation, known as Richard's equation, is presented below:

$$\frac{\partial}{\partial x}\left[K(\psi) \frac{\partial h_w}{\partial x}\right] + \frac{\partial}{\partial y}\left[K(\psi) \frac{\partial h_w}{\partial y}\right] + \frac{\partial}{\partial z}\left[K(\psi) \frac{\partial h_w}{\partial z}\right] = \frac{\partial \Theta}{\partial t} \tag{4.5}$$

where $K(\psi)$ is the unsaturated hydraulic conductivity that varies with respect to the matric suction (ψ), h_w is the total hydraulic head, and Θ is the volumetric water content at a given suction. As Equation (4.5) shows, the flow in an unsaturated zone is a function of the volumetric water content and the matric suction. Due to its high nonlinearity, numerical methods are generally used to solve Richard's equation.

4.3 UNSATURATED HYDRAULIC CONDUCTIVITY

4.3.1 Predictive methods

Direct measurement of unsaturated hydraulic conductivity is quite complex. Thus, predictive methods are typically used. Several empirical expressions exist to describe the variation in unsaturated hydraulic conductivity, K, with either ψ or Θ. Some of the expressions commonly used are listed in Table 4.1. From the equations included in this table, van Genuchten closed form equation, based on the hydraulic conductivity model of Mualem (1976), is commonly employed, mainly because a good agreement between measured and predicted hydraulic conductivities has been obtained. However, van Genuchten closed form equation can only be used when the parameters α, m and n are known. As Section 4.3.3 will describe, these parameters can be estimated from the relationship between the volumetric water content and the matric suction.

Table 4.1 – Examples of expressions for assessing unsaturated hydraulic conductivity (Reddi & Inyang 2000)

Function	Source
$K(\psi) = \alpha(b + \psi^n)^{-1}$	Childs & Colls-George (1950)
$K(\psi) = \dfrac{k}{\left[1 + \left(\dfrac{\psi}{\psi_c}\right)^n\right]}$	Gardner (1958)
$K(\Theta) = k\left(\dfrac{\Theta - \Theta_r}{\Theta_s - \Theta_r}\right)^n$	Brooks & Corey (1966)
$K(\psi) = \dfrac{\alpha}{\psi}$	Baver et al. (1972)
$K(\psi) = k\, exp(\alpha\psi)$	Mualem (1976)
$K(\Theta) = \alpha(\Theta)^n$	Marshall & Holmes (1979)
$K = k\dfrac{\left\{1 - (\alpha\psi)^{n-1}\left[1 + (\alpha\psi)^n\right]^{-m}\right\}^2}{\left[1 + (\alpha\psi)^n\right]^{m/2}}$	van Genuchten (1980)

k= saturated hydraulic conductivity; Θ_s= volumetric water content at saturation (equals to porosity); ψ_c= suction for which $K=k/2$; Θ_r= residual water content; and α, b, m and n are fitting parameters.

4.3.2 Water retention curves

The relationship between the volumetric water content and the matric suction is known as water retention curve, soil water characteristic curve, or moisture characteristic curve. Figure 4.1 presents a schematic drawing of these curves for different soils.

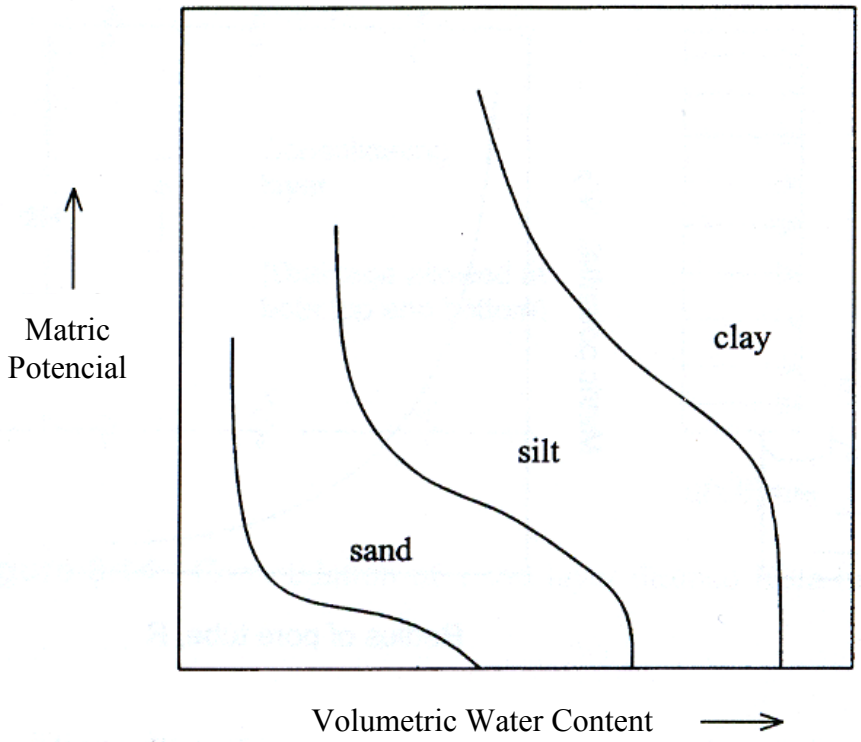

Figure 4.1 - Water retention curves for different soils (Reddi & Inyang 2000)

The variation in these curves highlights the effect that the soil properties have on the water retention curves. Typically, coarse-grained soils contain most of their water in large pores, which can be drained at relatively low suctions. Conversely, fine-grained soils have their water distributed in a range of relatively smaller pores, requiring high suctions to be drained (Castro 1974). For all cases, there is a water content below which water cannot be practically drained (residual water content), and the water retention curve goes asymptotic to the suction axis (Reddi & Inyang 2000). When the soil is fully saturated, the volumetric water content is equivalent to the soil porosity (ratio between the volume of voids and the total volume).

The water retention curves are hysteretic for almost all soils, i.e. the shape of the curve depends on whether the soil is wetting or drying, as Figure 4.2 schematically shows. This means that the volumetric water content at a particular value of suction is lower during wetting than during drying (Castro 1974, Stormont et al. 1997, Reddi & Inyang 2000). This is primarily because the relationship between water content and suction depends on the properties of the air-water interface (Castro 1974, Reddi & Inyang 2000). The retention curve is called a drying or drainage curve when the soil is progressively dried from a saturated state and a wetting or imbibition curve when the soil is wetted from an initially dry state.

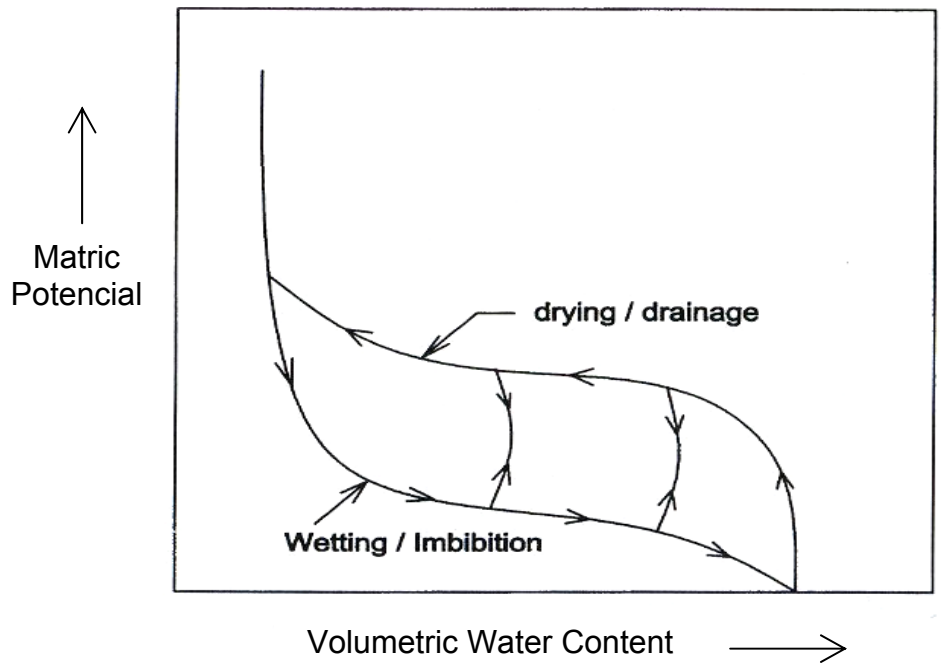

Figure 4.2 – Example of water retention curve during wetting and drying (Reddi & Inyang 2000)

4.3.3 Van Genuchten parameters

In modelling the hydraulic behaviour of unsaturated porous media, water retention curves are often represented by the van Genuchten parameters, which can be estimated by matching a theoretical water retention curve (model) to experimental data on matric suction. The theoretical water retention curve can be obtained from the closed form equation proposed by van Genuchten (1980) to estimate the volumetric water content as a function of the matric suction, mathematically expressed as follows:

$$\Theta = \Theta_r + \frac{\left(\Theta_s - \Theta_r\right)}{\left[1 + \left(\alpha\psi\right)^n\right]^m} \tag{4.6}$$

where Θ = volumetric water content; ψ = matric suction (understood as positive); Θ_r = residual volumetric water content; Θ_s = saturated volumetric water content; and α , m, and n = curve fitting parameters, with $m = 1 - 1/n$.

Equation (4.6) contains four independent parameters (Θ_r, Θ_s, α and n) that can be obtained from a measured water retention curve (experimental data). Of these four parameters, saturated volumetric water content, Θ_s, and residual volumetric water content, Θ_r, can be inferred to from the water retention curve, by extrapolating available water retention curve either towards lower water contents to obtain Θ_r (van Genuchten 1980), or towards the higher water contents to obtain Θ_s. Saturated water content can also be evaluated from the soil

porosity. For clayey soils, Θ_r is often assumed to be equal to zero (Babu et al. 2002). In that case, Equation (4.6) can be simplified as follows:

$$\Theta = \Theta_s \left\{ \frac{1}{\left[1 + (\alpha\psi)^n\right]} \right\}^m \tag{4.7}$$

The remaining parameters α and n, can be obtained using, for example, a least-square curve-fitting technique, or the RETC code (van Genuchten et al. 1991).

Figure 4.3 and Figure 4.4 present the influence of α and n on variation of matric suction. The first figure shows that α has a significant influence on the mobilisation of matric suction. Low matric suction values are obtained for higher values of α over a wide range of saturation. Figure 4.4 demonstrates that n has an influence mainly on the shape of the curve. It is then related with the type of soil.

Since the parameters α and n are obtained by fitting a theoretical water retention curve (model) to experimental data, it follows that experimental measurement of the relationship between the volumetric water content and matric suction is required.

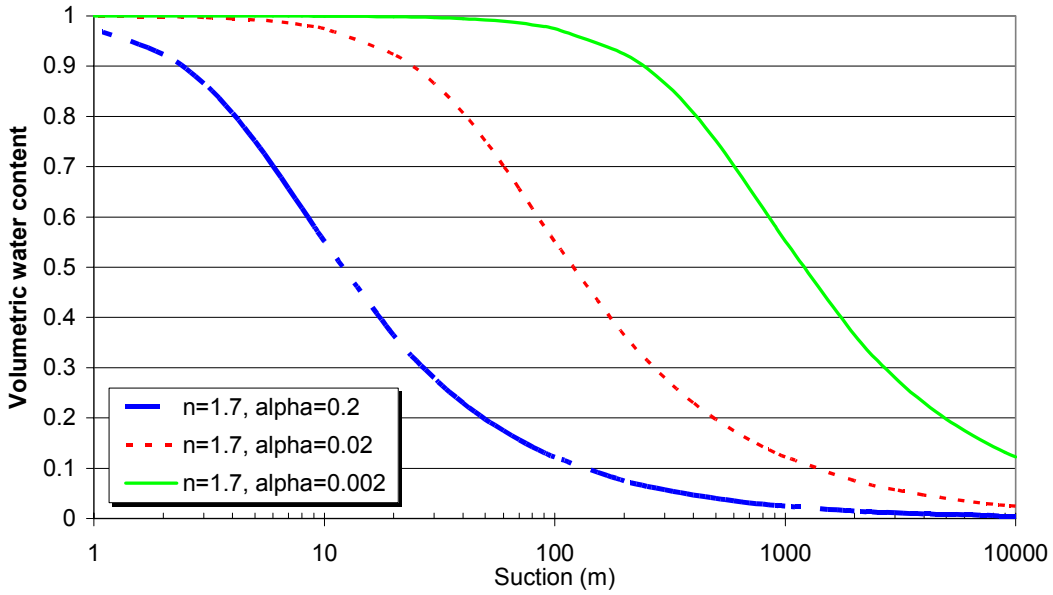

Figure 4.3 – Influence of α on variation of matric suction

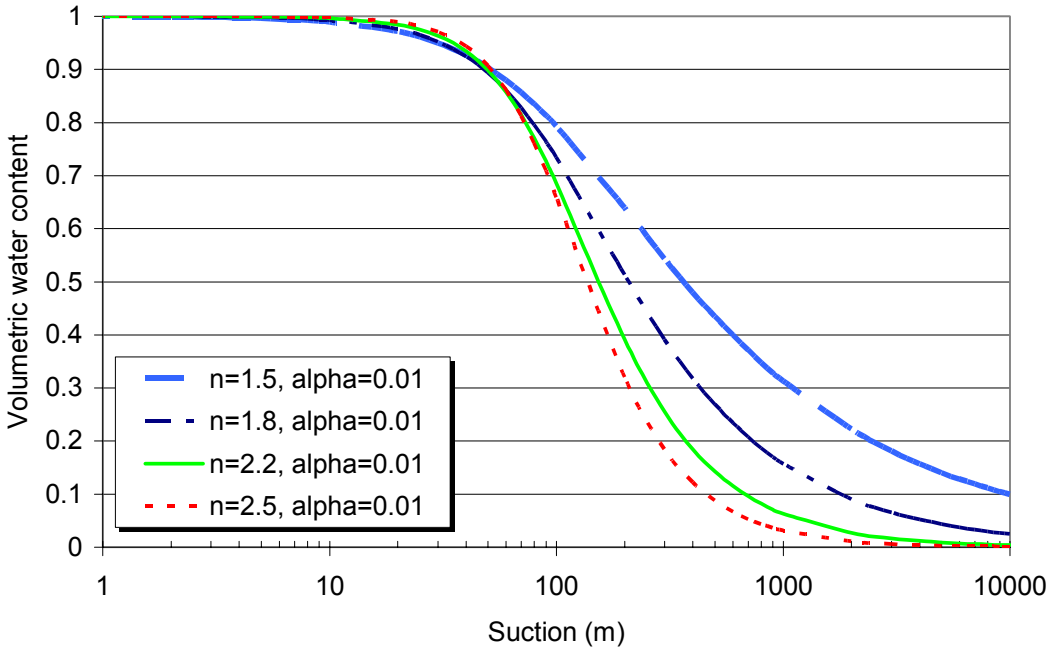

Figure 4.4 – Influence of *n* on variation of matric suction

There are numerous devices capable of measuring soil suction, including thermocouple psychrometers, filter paper, pressure plates, etc. The section below presents a brief description of the main techniques used for assessing the suction.

4.3.4 Techniques for measuring the suction

4.3.4.1 Thermocouple psychrometers

Thermocouple psychrometers can be used to measure the total suction of a soil. They measure the relative humidity either in the air phase of the soil pores or in the region close to the soil (Daniel 1982). There are two basic types of thermocouple psychrometers: wet-loop and Peltier. The second type is generally used in geotechnical engineering. Both operate on basis of temperature difference measurements between a nonevaporating surface and an evaporating surface, differing in the manner by which the evaporating junction is wetted to induce evaporation. Measurements of suction are carried out by suspending the psychrometer in a closed system containing a soil specimen. A controlled temperature environment of $\pm 0.001^{o}C$ is required to measure total suction. Calibration curves relate the psychrometer reading to a corresponding total suction. The range for measurable suction using this method varies from 100 to 8 000 kPa (Daniel 1982; Fredlund & Rahardjo 1993).

4.3.4.2 Tensiometers

Tensiometers are used for the direct measurement of negative pore-water pressure in a soil. However, negative pore-water pressure is numerically equal to the matric suction when the air

contained in the pores is at atmospheric pressure. Tensiometers consist of a high air entry, porous ceramic cup connected to a pressure measuring device through a small bore tube. The tube and the cup are filled with deaired water. The later is inserted into a precored hole until there is a good contact with the soil. When the equilibrium is reached, the water in the tensiometer has the same negative pressure as the pore-water in the soil. The maximum pore-water pressure measurable with tensiometers is 90 kPa due the possibility of cavitation of water in the equipment (Fredlund & Rahardjo 1993).

4.3.4.3 Pressure plate

Pressure plates are also employed for direct measurement of negative pore-water pressure. They are based on the axis-translation approach, which generates matric suction within the soil by applying air pressure to the samples while maintaining water pressure at the atmospheric level. Basically a soil specimen is mounted on top of a saturated high entry porous ceramic disk in an air pressure chamber. The air entry value of the disk must be higher than the matric suction under measure. The water pressure in the compartment below the high entry disk is maintained as close as possible to zero by increasing the air pressure in the chamber. A pressure transducer connected to the water compartment is used as indicator. The difference between the air pressure in the chamber and the measured negative water pressure at equilibrium is taken to be the matric suction of the soil (matric suction is equal to the negative pore-water pressure when the air pressure is atmospheric). The range of measurements is a function of the air entry value of the ceramic disk. The pore-water pressure that can be measured with this technique is limited to 1500 kPa (Fredlund & Rahardjo 1993).

4.3.4.4 Thermal conductivity sensors

Thermal conductivity sensors have been used as indirect methods for assessing the matric suction. They consist of a porous ceramic block containing a temperature sensitive element and a miniature heater. The principle behind this technique is that the thermal conductivity of a soil increases with an increasing water content. The matric suction is inferred from the water content of the porous block. Sensor calibration is required. Typically, the sensors cover a range between 0 kPa and approximately 400 kPa (Fredlund & Rahardjo 1993).

4.3.4.5 Filter paper method

This method is based on the assumption that a filter paper will reach equilibrium with a soil having a specific suction. The filter paper is used as a sensor. Equilibrium can be obtained by either liquid or vapour moisture exchange between the soil and the filter paper. When a dry filter paper is placed in direct contact with the soil, it is assumed that water flows from the soil to the filter paper. In this case, the equilibrium water content of the filter paper corresponds to the matric suction. When a dry filter paper is suspended above a soil specimen, vapour flow of water will occur from the soil to the filter paper until equilibrium is reached. Here, the equilibrium water content of the filter paper corresponds to the total suction of the soil (ASTM D 5298, Fredlund & Rahardjo 1993).

The water content of the filter paper is converted into suction values through a calibration curve. Several authors presented calibration curves for common types of filter paper (e.g. Fawcett & Collis-George 1967, McQueen & Miller 1968, Hamblin 1981, Chandler & Gutierrez 1986). In general, a good agreement is obtained for suction with the different calibration curves reported in literature. Figure 4.5 depicts the calibration curves for total suction.

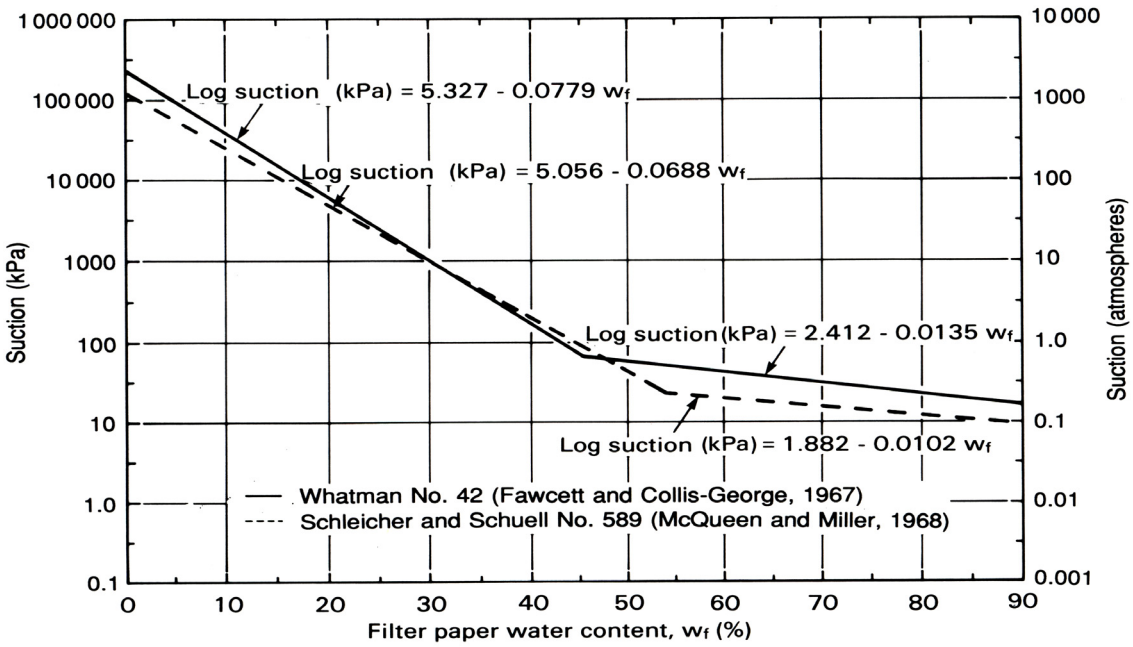

Figure 4.5 – Calibration curves for two types of filter paper (from ASTM D 5298)

Filter paper method was standardised by ASTM for measuring soil suction, giving rise to ASTM D 5298: Standard test method for measurement of soil potential (suction) using filter paper.

The advantage of filter paper method is that it is simple and inexpensive. According to ASTM D 5298 standard, it can also reliably be used with suctions from 10 to 100 000 kPa.

As mentioned, for evaluating the performance of composite liners involving GCLs the hydraulic conductivity of this liner is a necessary parameter. As this material may not be fully saturated in the field, knowledge of the unsaturated hydraulic conductivity is also necessary. It can be estimated from van Genuchten predictive method, based on the water retention curve and on the saturated hydraulic conductivity of the GCLs. The knowledge of the water retention curves requires the measurement of the matric suction and the corresponding volumetric water content. In this work, the filter paper method was adopted to measure the matric suction of the GCLs, as Chapter 6 will present. This method was chosen due to its simplicity, low cost, and its capacity to cover a large range of suctions.

In this context, existing data regarding the water retention curves of the GCLs will be presented in the following section.

4.4 PREVIOUS STUDIES ON WATER RETENTION CURVES OF GCLS

4.4.1 Daniel et al. (1993)

Daniel et al. (1993) measured the relationship between water content and suction in the bentonite component of a geomembrane supported GCL using two methods: thermocouple psychrometer (TM) and vapour equilibrium (VE). With the first method, a piece of GCL, about 175×25 mm^2, was slowly wetted by spraying a known mass of water onto the surface of the bentonite. The moistened GCL was installed in a large tube with the bentonite facing inward. A thermocouple psychrometer was placed in the centre of the test tube. The test tube was then sealed and stored in a heavily insulated container during two weeks, until equilibrium was reached. After that period of time, the GCL specimen was removed and dried to evaluate its water content. The second technique of measurement consisted in placing 25 mm square pieces of GCL samples in sealed vessels that contained salt solutions with known vapour pressures. Test specimens were periodically removed from those samples and oven dried to assess water content. Tested specimens were exposed to controlled vapour pressures for 66 days. Results obtained by Daniel et al. (1993) are summarised in Table 4.2. It can be observed that the measured suction ranged from 0 kPa to 5 200 kPa, whereas the water contents ranged from 17 % (natural water content) to 145 %.

Table 4.2 – Water content and corresponding suctions (modified from Daniel et al. 1993)

Water content (%)	Suction (bars)	Suction (kPa)	Method of measurement
17 (1)	43	4300	TM
18	44	4400	TM
24	49	4900	TM
28	43	4300	TM
29	52	5200	VE
31	25	2500	TM
46	14	1400	TM
54	16	1600	VE
56	8	800	TM
66	7	700	TM
79	6	600	TM
89	5	500	VE
96	4	400	TM
101	1	100	VE
145	0	0	Direct soaking with 14 kPa compressive stress

(1) Natural water content

These authors concluded that, from a practical point of view, if the bentonite side of the GCL was placed against soil with a suction of 1 500 kPa (15 bars that corresponds to the wilting point of typical plants) and the GCL was buried beneath cover soil, the bentonite would absorb water from the soil and would equilibrate at a water content approximately equal to 50 %.

4.4.2 Southen & Rowe (2004)

Southen & Rowe (2004) evaluated the water retention curves of a needlepunched GCL, with the cover geotextile impregnated with bentonite powder (800 g m^{-1}), and a silty sand. For GCL, the methodology adopted consisted in cutting sections of approximately 30×30 cm^2, which were then placed in a water bath and allowed to hydrate for a number of days. Once the sections were suitably hydrated, they were removed from the water bath. Four circular specimens approximately 53 mm in diameter were then cut using a cutting shoe and hydraulic press. The cut specimens were weighed and finally placed in stainless rings for transfer to the pressure plate apparatus for suction measurement (Southen, personal communication). Suction was measured based on the pressure plate technique (see Section 4.3.4.3). Measurements were based on drying. Two sets of tests were performed on GCL samples with different initial water contents and variable sampling tests. Figure 4.6 shows the results obtained by these authors.

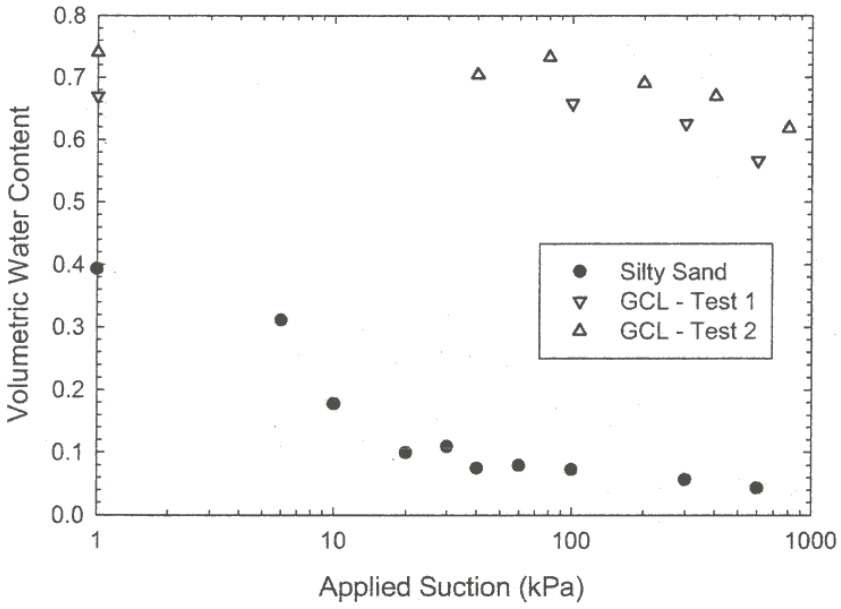

Figure 4.6 – Water retention curve of a needlepunched GCL (from Southen & Rowe 2004)

It can be observed that a good agreement was obtained between the two sets of tests. It appears that the initial water content used and the sampling process had a minor effect on the water retention curves obtained. For test 1, the volumetric water content ranged between 0.56 and 0.67, whereas the corresponding suction ranged from 600 kPa to 1 kPa. For test 2, the volumetric water content varied between 0.62 and 0.76, and the suction between 800 kPa and 1 kPa. It should be noted that the water retention curves depicted in Figure 4.6 are limited to suctions less than 1 000 kPa. This is most likely due to the range of suctions covered by the pressure plate technique (limited to 1 500 kPa, according to Fredlund & Rahardjo 1993). Furthermore, the saturated volumetric water contents (0.67, for test 1 and 0.72, for test 2) were estimated based on measured porosity of the specimens.

Water retention curves are needed to numerically model the unsaturated behaviour of the GCLs, and thus understand the flow through composite liners involving unsaturated GCLs, when there is a defect in a geomembrane. In this respect, there have been several attempts to predict the flow rates by calculations based on fundamental parameters that govern the

problem. Two different approaches have been adopted for determining the flow rate: analytical solutions and empirical equations. Both approaches present advantages and disadvantages. Analytical solutions are rigorous but complex, whereas empirical equations are simple but approximate. The existing solutions for evaluating the flow through composite liners are presented and discussed in the following sections.

4.5 EXISTING SOLUTIONS FOR EVALUATING THE FLOW THROUGH COMPOSITE LINERS

4.5.1 Background

Before discussing the existing solutions for evaluating the flow through composite liners it is important to understand how the liquid flows through a composite liner when there is a defect in the geomembrane. According to Brown et al. (1987), the flow through a composite liner when there is a defect in the geomembrane is as follows: first, the liquid migrates through the geomembrane defect; then it spreads laterally through the interfacial zone between the geomembrane and the underlying layer. This interface flow covers an area called wetted area. Finally, the liquid migrates into and through the soil (Figure 4.7).

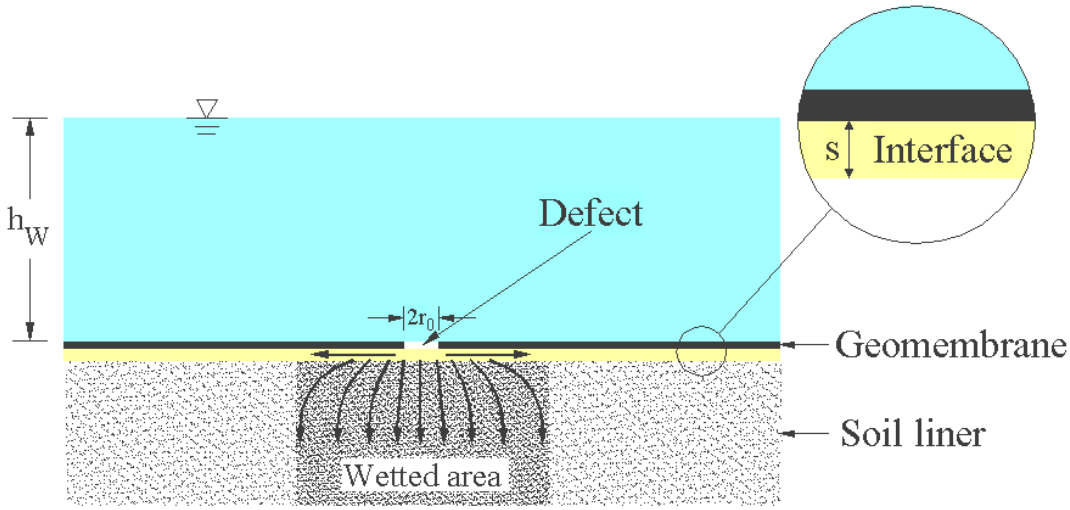

Figure 4.7 – Liquid flow through a composite liner due to a defect in the geomembrane

The liquid flow in the interface is possible only if there is a gap between the geomembrane and the underlying layer. If the geomembrane and the underlying layer are in perfect contact, there is no interfacial gap (Giroud & Bonaparte 1989). The interfacial gap may result from soil particles, rutting and undulations occurring during the construction of the soil liner, or from wrinkles in geomembranes (Rowe 1998).

Observations done during experimental studies involving composite liners made of CCLs and various kinds of geomembranes confirm that the liquid passing through the defect spreads laterally between the geomembrane and the underlying layer (e.g. Fukuoka 1986, Jayawickrama et al. 1988, Touze-Foltz 2001). Thus, herein it is considered that there is a gap,

generally termed as interface, and that the liquid is able to flow laterally between the geomembrane and the underlying soil. Amongst other factors, the amount of fluid flow between the geomembrane and the underlying layer depends on features of the interface.

Experimental data on features of interfaces are scarce. As Sections 4.5.2 and 4.5.3 show, the features of the interface can be defined in two different ways, depending on the approach used for predicting the flow rate through defects in geomembranes: analytical solutions define them in terms of hydraulic transmissivity, whereas empirical equations define them in terms of contact conditions.

4.5.2 Analytical solutions

A number of analytical solutions have been developed to quantify the flow rate through defects in flat or wrinkled geomembranes based on Darcy's law (e.g. Brown et al. 1987, Jayawickrama et al. 1988, Rowe 1998, Touze-Foltz et al. 1999), where the interface between the geomembrane and the underlying layer is of uniform thickness and, consequently, where the hydraulic transmissivity is uniform.

The most commonly used equations were proposed by Rowe (1998) and Touze-Foltz et al. (1999). The first author developed analytical solutions to quantify liquid flow for the case of a circular hole in a flat geomembrane and in a wrinkled geomembrane. Touze-Foltz et al. (1999) extended the solution for a damaged wrinkle for various boundary conditions and to the problem of liquid flow for two, or more, parallel interacting damaged wrinkles. Solutions by Touze-Foltz et al. (1999) were again extended by Touze-Foltz et al. (2001) to take into account the non uniform hydraulic transmissivity at the interface geomembrane/CCL or geomembrane/GCL.

Of particular interest within the scope of the present work are the analytical solutions to quantify liquid flow for the cases of a circular defect in a flat geomembrane, henceforth designated as "axi-symmetric case", and a damaged geomembrane wrinkle or long cuts, tears or defective seams, henceforth designated as "two-dimensional case", developed for a number of specific boundary conditions.

The basic problem configuration follows from Rowe (1998) and Touze-Foltz et al. (1999) and it is depicted in Figure 4.8. It includes a geomembrane resting on a low–permeability layer of thickness H_L and hydraulic conductivity k_L. This layer can be either a CCL or a GCL. From now on, it will be simply designated as "soil liner". The z-axis origin corresponds to the top of the soil liner with upward being positive. The soil liner rests on a more permeable foundation or attenuation layer of thickness H_f and hydraulic conductivity k_f, which, in turn, rests on a highly permeable layer that can be either an aquifer or a secondary collection layer. Accordingly, it can be assumed that the flow through the composite liner is not influenced by the hydraulic conductivity of subgrade layers. It is assumed that the interface can be characterised by a uniform hydraulic transmissivity, θ. The hydraulic transmissivity of this layer can be established either based on experimental data, or on empirical equations as will be discussed in Section 4.5.4. Chapter 6 presents the experimental work carried out to measure the hydraulic transmissivity of the interface between a geomembrane and a GCL.

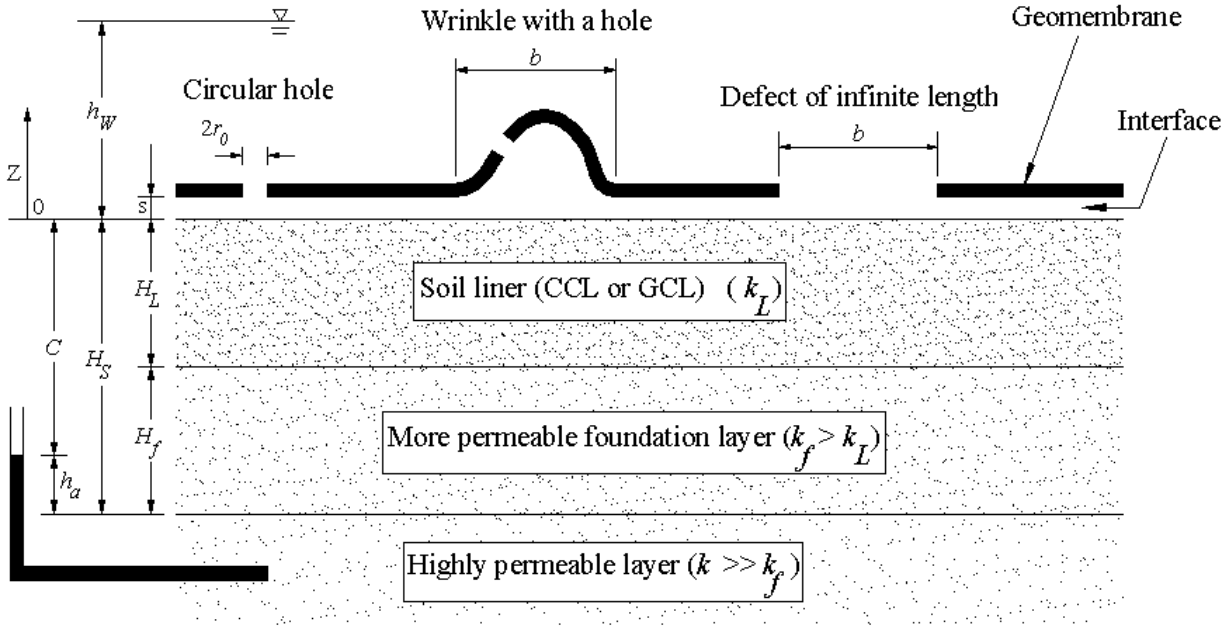

Figure 4.8 – Schematic drawing showing a composite liner with a geomembrane exhibiting different types of defects: circular hole of radius r_0, a damaged wrinkle of width b, and a defect of infinite length and width b (modified from Touze-Foltz et al. 1999)

Furthermore, it is assumed that: (i) liquid flow is under steady-state conditions; (ii) the soil liner and the foundation layer are saturated; (iii) liquid flow through the liner and the foundation layer is vertical (Rowe 1998, Touze-Foltz et al. 1999). According to the continuity of liquid flow, the equivalent hydraulic conductivity, k_s, corresponding to the liner and the foundation layer is given by (Rowe 1998, Touze-Foltz et al. 1999):

$$\frac{H_L + H_f}{k_s} = \frac{H_L}{k_L} + \frac{H_f}{k_f} \tag{4.8}$$

When a hydraulic head, h_w, is applied on the top of the composite liner, the mean hydraulic gradient, i_s, through the liner and foundation is given by (Rowe 1998, Touze-Foltz et al. 1999):

$$i_s = \frac{H_L + H_f + h_w - h_a}{H_L + H_f} = 1 + \frac{h_w - h_a}{H_L + H_f} \tag{4.9}$$

where h_a is the hydraulic head in the highly permeable layer that is not fully saturated, and often assumed to be equal to zero.

4.5.2.1 Solution for the axi-symmetric case

As indicated by Brown et al. (1987), according to the mass conservation equation, the rate of liquid flow entering the hole in the geomembrane, Q, is equal to the sum of the rate of liquid flow infiltrating in the soil, $Q_s(r)$, and the rate of liquid flow spreading laterally in the transmissive layer $Q_r(r)$ at a distance r from the hole. The mass balance is accordingly given by the following equation:

$$Q = Q_s(r) + Q_r(r) \tag{4.10}$$

As Q is not dependant of r, one obtains by derivation on Equation (4.10):

$$\frac{dQ_s(r)}{dr} + \frac{dQ_r(r)}{dr} = 0 \tag{4.11}$$

The rate of liquid flow spreading laterally in the interface, $Q_r(r)$, can be expressed using Darcy's law (Touze-Foltz et al. 1999):

$$Q_r(r) = -2\pi r\theta \frac{dh(r)}{dr} \tag{4.12}$$

And following equation for the annular region comprised between r and $r+dr$ (Touze-Foltz et al. 1999):

$$dQ_r = -2\pi r\theta \left(\frac{1}{r}\frac{dh}{dr} + \frac{d^2h}{dr^2} \right) dr \tag{4.13}$$

For the same annular region comprised between radii r and $r+dr$, the flow rate in the foundation layer (soil or GCL) can be expressed as follows (Touze-Foltz et al. 1999):

$$dQ_s = 2\pi k_s \frac{h(r) + H_s}{H_s} dr \tag{4.14}$$

The principle of conservation of mass applied to the differential element, Equation (4.11) then becomes:

$$2\pi k_s \frac{h(r) + H_s}{H_s} dr - 2\pi r\theta \frac{d^2 h(r)}{dr^2} - 2\pi\theta \frac{dh(r)}{dr} = 0 \qquad (4.15)$$

Equation (4.15) simplifies into equation below, previously given by Giroud and Bonaparte (1989):

$$\frac{1}{r}\frac{dh}{dr} + \frac{d^2 h}{dr^2} = \frac{k_s}{\theta}\left(1 + \frac{h}{H_s}\right) \qquad (4.16)$$

Equation (4.16) can also be re-written as follows (Rowe 1998, Touze-Foltz et al. 1999):

$$\frac{d^2 h}{dr^2} + \frac{1}{r}\frac{dh}{dr} - \beta^2 h = \beta^2 C \qquad (4.17)$$

where the hydraulic head, h, in the transmissive layer is unknown, and β and C can be obtained as follows (Rowe 1998):

$$\beta = \sqrt{\frac{k_s}{(H_L + H_f)\theta}} \qquad (4.18)$$

$$C = H_L + H_f - h_a \qquad (4.19)$$

The solution of the Equation (4.17) allows us to calculate the hydraulic head profile beneath the geomembrane, which is necessary to calculate the rate of liquid flow through the composite liner.

The general solution of Equation (4.17) was given by Brown et al. (1987). It can be written as follows (Touze-Foltz et al. 1999):

$$h(r) = AI_0(\beta r) + BK_0(\beta r) - C \quad \text{for } r_0 \le r \qquad (4.20)$$

where I_0 and K_0 are modified Bessel functions of zero order, and A and B are constants that depend on boundary conditions.

Two boundary conditions are necessary to solve Equation (4.20) and to evaluate A and B. The hydraulic head of liquid entering the circular defect is equal to h_w and provides one boundary condition:

$$h(r_0) = h_w \tag{4.21}$$

The other boundary condition corresponds either to zero flow at $r = R_c$:

$$Q(R_c) = 0 \quad \text{and, in general, } h(R_c) \geq 0 \tag{4.22}$$

or to a specific head, h_s, at $r = R_c$:

$$h(R_c) = h_s \quad \text{and, in general, } Q_r(R_c) \geq 0 \tag{4.23}$$

where R_c is the wetted radius, which can be either the physical radius of a cell in the case of laboratory tests such as the one used to perform the small-scale tests in this work (Chapter 6), or a virtual radius in field conditions, and r is a radial boundary.

Touze-Foltz et al. (1999) have solved Equation (4.20) for these boundary conditions. Also Rowe (1998) has solved Equation (4.20) for the particular case where there is no radial flow at $r = R_c$ and the hydraulic head at $r = R_c$ is zero (i.e. $Q_r(R_c) = 0$ at $r = R_c$ and $h(R_c) = 0$), that is, field contact conditions.

Analytical solutions given for the existence of a flow rate at $r = R_c$ with a hydraulic head equal to zero are of particular interest in the context of the present research. Indeed, they will be used for interpreting the hydraulic transmissivity interface measurements presented in Chapter 6. The analytical solutions given for zero flow at $r = R_c$ with a hydraulic head equal to zero, which corresponds to field contact conditions are also needed for interpreting intermediate and large scale test results.

Regarding the first case, the existence of a flow rate at $r = R_c$ with a hydraulic head equal to zero, i.e. $Q_r(R_c) > 0$ at $r = R_c$ and $h(R_c) = 0$, the following solution was given by Touze-Foltz et al. (1999):

$$h(r) = A_p I_0(\beta r) + B_p K_0(\beta r) - C \qquad \text{for } r_0 \leq r \leq R_c \text{ and } Q_r(R_c) > 0 \tag{4.24}$$

where

$$A_p = -\frac{(h_w + C)K_0(\beta R_c) - (h_s + C)K_0(\beta r_0)}{K_0(\beta r_0)I_0(\beta R_c) - K_0(\beta R_c)I_0(\beta r_0)} \tag{4.25}$$

and

$$B_p = \frac{(h_w + C)I_0(\beta R_c) - (h_s + C)I_0(\beta r_0)}{K_0(\beta r_0)I_0(\beta R_c) - K_0(\beta R_c)I_0(\beta r_0)} \tag{4.26}$$

where K_0 and I_0 are modified Bessel functions of zero order.

The corresponding solutions giving the total flow rate, Q, and the radial flow rate in the interface, $Q_r(R_c)$, are presented below (Touze-Foltz et al. 1999):

$$Q = \pi r_0^2 k_s i_s - 2\pi r_0 \theta\beta\left[A_p I_1(\beta r_0) - B_p K_1(\beta r_0)\right] \tag{4.27}$$

$$Q_r(R_c) = -2\pi\theta\beta R_c\left[A_p I_1(\beta R_c) - B_p K_1(\beta R_c)\right] \tag{4.28}$$

With respect to the second case of interest within the scope of present work, zero flow at $r = R_c$ with a hydraulic head equal to zero, i.e. $Q_r(R_c) = 0$ at $r = R_c$ and $h(R_c) = 0$, the following analytical solution was given by Rowe (1998):

$$h(r) = (h_w + C)\Omega_0 - C(\Omega_1 - 1) \tag{4.29}$$

where

$$\Omega_0 = \frac{K_0(\beta r)I_0(\beta R_c) - K_0(\beta R_c)I_0(\beta r)}{K_0(\beta r_0)I_0(\beta R_c) - K_0(\beta R_c)I_0(\beta r_0)} \tag{4.30}$$

and

$$\Omega_1 = \frac{K_0(\beta r)I_0(\beta r_0) - K_0(\beta r_0)I_0(\beta r)}{K_0(\beta R_c)I_0(\beta r_0) - K_0(\beta r_0)I_0(\beta R_c)} \tag{4.31}$$

where K_0 and I_0 are modified Bessel functions of zero order. According to Rowe (1998), the solution given by Equation (4.29) assumes that the wetted radius, R_c, is known. The value of R_c can be estimated by finding the value of R_c such that:

$$\frac{dh}{dr}(R_c) = 0 \tag{4.32}$$

In other words, R_c can be estimated by solving the following equation:

$$A_Q I_0(\beta R_c) + B_Q K_0(\beta R_c) - H_s = 0 \tag{4.33}$$

where

$$A_Q = \frac{(h_w + C)K_1(\beta R_c)}{K_1(\beta R_c)I_0(\beta r_0) + K_0(\beta r_0)I_1(\beta R_c)} \tag{4.34}$$

and

$$B_Q = \frac{(h_w + C)I_1(\beta R_c)}{K_1(\beta R_c)I_0(\beta r_0) + K_0(\beta r_0)I_1(\beta R_c)} \tag{4.35}$$

where K_1 and I_1 are modified Bessel functions of first order.

The total flow rate, Q, through a composite liner within a zone defined by the wetted radius can be estimated by the following equation (Rowe 1998):

$$Q = \pi r_0^2 k_s i_s - 2\pi r_0 \theta\beta\left[A_Q I_1(\beta r_0) - B_Q K_1(\beta r_0)\right] \tag{4.36}$$

Equations (4.24) to (4.36) can be used with any set of coherent units. The basic SI units are: Q ($m^3\ s^{-1}$), Q_r ($m^3\ s^{-1}$), θ ($m^2\ s^{-1}$), k_s ($m\ s^{-1}$), r_0 (m), h_w (m), β (m^{-1}), A (m), B (m), R_c (m), H_s (m), and C (m).

4.5.2.2 Solution for the two-dimensional case

The two-dimensional case includes both defects of infinite length L_{td} and width b, such as long cuts, tears or defective seams, and damaged wrinkles of length L_{td} and width b. It should be noted that there is no fundamental difference between the two types of two-dimensional defects because it is assumed that the holes in a wrinkle do not control the flow and no assumption is made regarding the height or the shape of the wrinkle. Thus, the two types of two-dimensional defects are defined by a single parameter: their width b (Figure 4.9).

Rather it is assumed that the rate of liquid flow in composite liners is not limited by the defects (defect-limiting case was discussed by Rowe (1998)) and that liquid flow in the transmissive layer is in the x-direction, normal to the longitudinal axis of the wrinkle or the infinite long defect. Flow at both ends of the two-dimensional defects is neglected. Under the assumption of a uniform hydraulic transmissivity, the problem of liquid flow becomes two-dimensional (Touze-Foltz et al. 1999).

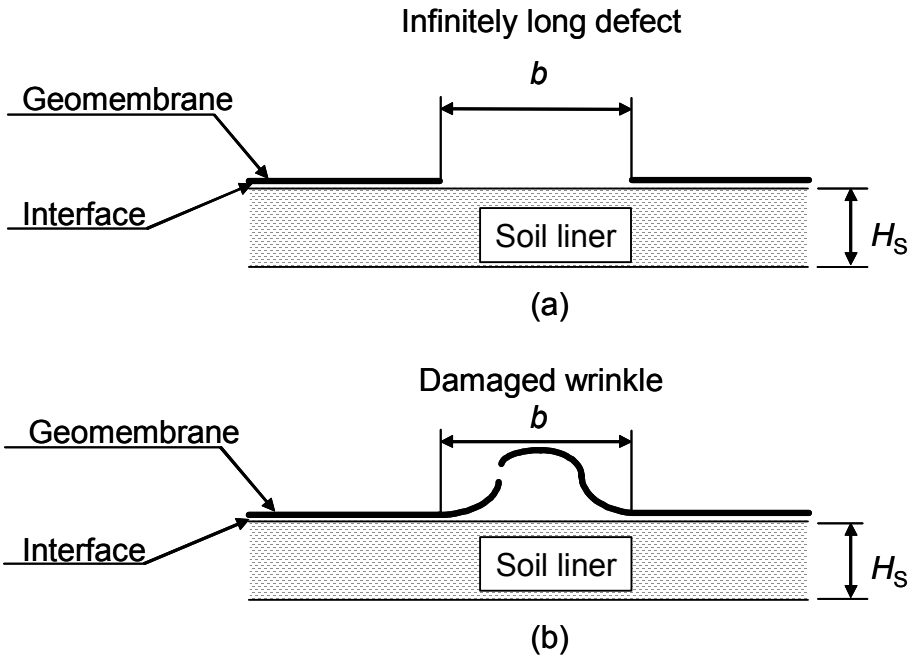

Figure 4.9 – Composite liner including a geomembrane exhibiting: (a) a defect of infinite length and width b; (b) a damaged wrinkle of width b (Touze-Foltz & Giroud 2003)

The head distribution, h, beneath the geomembrane and acting on soil liner is given by the equation presented below (Touze-Foltz et al. 1999):

$$\frac{d^2h}{dx^2} - \beta^2 h = \beta^2 C \tag{4.37}$$

where β and C are given by Equations (4.18) and (4.19), respectively.

The general solution of Equation (4.37) was given by Touze-Foltz et al. (1999):

$$h(x) = E\exp(-\beta x) + F\exp(\beta x) - C \qquad \text{for } b/2 \le x \tag{4.38}$$

where E and F are coefficients with values that depend on boundary conditions.

Two boundary conditions are required to solve Equation (4.38) and to assess coefficients E and F. As for the axi-symmetric case, the hydraulic head of the liquid entering the defect in the geomembrane, h_w, provides one boundary condition:

$$h\left(\frac{b}{2}\right) = h_w \tag{4.39}$$

The other boundary condition is either a zero flow at $x = X_c$:

$$Q_x(X_c) = 0 \quad \text{and} \quad h(X_c) \ge 0 \tag{4.40}$$

or a specific head at $x = X_c$:

$$h(X_c) \ge h_s \quad \text{and} \quad Q_x(X_c) \ge 0 \tag{4.41}$$

where X_c is either the width of a cell in the case of laboratory tests, or the width of the wetted area in the case of field conditions; Q_x is the rate of the liquid flow in the interface in the direction normal to the longitudinal axis of the wrinkle or infinitely long defect; and x is the abscissa.

Solutions for these boundary conditions were given by Touze-Foltz et al. (1999). Particularly important, within the scope of the present work, is the solution for zero flow at $x = X_c$, in which the hydraulic head is equal to zero at boundary X_c (i.e. $Q_x(X_c) = 0$ and $h(X_c) = 0$), which corresponds to field contact conditions and will be used in Chapter 6 for predicting the flow rate through geomembrane defects in the two-dimensional case. This particular case where $X = X_w$ gives the limit of strict validity of both solutions obtained for zero flow and specified head boundary conditions, with (Touze-Foltz et al. 1999):

$$X_w = \frac{1}{\beta}\cosh^{-1}\left(\frac{h_w + C}{C}\right) + \frac{b}{2} \tag{4.42}$$

The hydraulic head in the interface for this case is given by:

$$h(x) = 2C\sinh^2\left[\beta\frac{(X_w - x)}{2}\right] \tag{4.43}$$

and the total flow rate, Q, through the composite liners is obtained from:

$$Q = Lk_s\left[i_s b + 2\frac{(h_w + C)\cosh\left[\beta\left(X_c - \frac{b}{2}\right)\right] - (h_s + C)}{\beta H_s \sinh\left[\beta\left(X_c - \frac{b}{2}\right)\right]}\right] \tag{4.44}$$

or

$$Q = L\,k_s\frac{h_w + H_s}{H_s}\left\{b + 2\sqrt{\frac{\theta H_s}{k_s}}\tanh\left[\cosh^{-1}\left(\frac{h_w + H_s}{H_s}\right)\right]\right\} \tag{4.45}$$

The total flow rate can also be expressed by unit length, Q_L. Equation (4.45) is then written as follows (Touze-Foltz & Giroud 2003):

$$Q_L = k_s\frac{h_w + H_s}{H_s}\left\{b + 2\sqrt{\frac{\theta H_s}{k_s}}\tanh\left[\cosh^{-1}\left(\frac{h_w + H_s}{H_s}\right)\right]\right\} \tag{4.46}$$

Equations (4.38) to (4.46) can be used with any set of coherent units. The basic SI units are: Q ($m^3\ s^{-1}$), Q_L (m^2/s), L (m), k_s ($m\ s^{-1}$), h_w (m), h_s (m), C (m), β (m^{-1}), X_c (m), X_w (m), b (m), and H_s (m).

Equation (4.46) was later on simplified by Giroud & Touze-Foltz (2005), based only in mathematical transformations, and was re-written as follows:

$$Q_L = b\,k_s\left(1 + \frac{h_w}{H_s}\right) + 2\sqrt{k_s\,\theta\,h_w\left(2 + \frac{h_w}{H_s}\right)} \tag{4.47}$$

As highlighted by Giroud & Touze-Foltz (2005), the first term of the right side of Equation (4.47) quantifies the rate of flow into the soil liner (CCL or GCL) located directly under the defect. The second term quantifies the rate of interface flow.

4.5.2.3 Summary of Section 4.5.2

Section 4.5.2 presented some analytical solutions that can be used to predict the flow rate through composite liners due to defects in the geomembrane. These solutions assumed that the soil liner (CCL or GCL) and the foundation layer above the geomembrane are fully saturated, the liquid flow through the soil liner and foundation is vertical, and the interface can be characterised by a uniform transmissivity. Analytical solutions presented included two general cases: axi-symmetric and two-dimensional. The first takes into account a circular hole in a flat geomembrane, whereas the later considers either a defect of infinite length, or a damaged wrinkle.

For the case of a circular hole in a flat geomembrane, emphasis must be put on Equations (4.27) and (4.36), as they will allow the interpretation of the flow rate measurements presented in Chapter 6 in terms of interface transmissivity. A parameter necessary to compute the interface transmissivity is the radius of the wetted area. Therefore, on the one hand, Equation (4.27) will be used for interpreting the results of the tests carried out in small-scale tests, as the wetted radius corresponds to the physical radius of the test cell. On the other hand, Equation (4.36) will be used for interpreting the results of intermediate and large scale tests, given that the radius of the wetted is unknown. In this case, field contact conditions prevail and the radius of the wetted area can be estimated by solving Equation (4.33).

The interpretation of test results, in terms of interface transmissivity, is important because a goal of this study is to develop empirical equations for predicting the flow rate through composite liners involving GCLs. For that, a GCL contact condition has to be defined, which can be done by relating the interface transmissivity to the hydraulic conductivity of the GCLs, as Chapter 6 will show.

For the two-dimensional case, emphasis is put on Equation (4.47) which will be used in Chapter 6 to predict the flow rates through composite liners for both defects of infinite length and damaged wrinkles in field contact conditions. Flow rates computed thanks to analytical the equations will assist in the development of empirical equations for these types of defects.

As could be seen, the analytical solutions are rigorous but complex. Therefore, simple tools are often used, namely empirical equations. Recent advances on empirical equations for predicting the flow rates through composite liners due to defects in geomembrane liners are addressed in the following section.

4.5.3 Empirical equations

4.5.3.1 Contact conditions: qualitative definitions

Before addressing the empirical equations, some comments on contact conditions must be made. Contact conditions express the characteristics of the interface between the geomembrane and the underlying liner. Definition of contact conditions is often done in qualitative terms, such as perfect contact (Giroud & Bonaparte 1989), excellent contact conditions (Giroud & Bonaparte 1989, Touze-Foltz & Giroud 2003), good and poor contact (Giroud 1997), and perfect and imperfect contact (Foose et al. 2001).

Qualitative definitions of the contact conditions relevant for the empirical equations shown in the following section are presented below:

- Poor contact conditions correspond to a geomembrane that has been installed with a certain number of wrinkles, and/or has been placed on a low-permeability soil that has not been adequately compacted and does not appear smooth (Giroud 1997);
- Good contact conditions correspond to a geomembrane that has been installed with as few wrinkles as possible, on top of a low permeability soil layer that has been properly compacted and has a smooth surface. Furthermore, it is assumed that there is sufficient compressive stress to maintain the geomembrane in contact with the low-hydraulic conductivity soil layer (Giroud 1997); and
- Excellent contact conditions correspond to a geomembrane that has been installed with no wrinkles on top of a soil component of a composite liner that consists of a GCL installed on top of, and in close contact with, a low-hydraulic conductivity soil layer that has been adequately compacted and has a very smooth surface. Furthermore, it is assumed that there is sufficient compressive stress to maintain the geomembrane in contact with the GCL (Touze-Foltz & Giroud 2003).

Qualitative definitions of contact conditions are subjective, which may lead to different interpretations of a given field case. To overcome this limitation, Rowe (1998) proposed quantitative definitions for poor and good contact conditions. These quantitative definitions were extended by Touze-Foltz & Giroud (2003), as findings by Touze-Foltz et al. (2002a) showed that for composite liners involving GCLs the flow rate can be significantly less than that calculated considering good contact conditions. Quantitative definitions of contact conditions will be discussed in Section 4.5.4.

4.5.3.2 Existing equations for CCLs

Numerous empirical equations for predicting the flow rate through defects in geomembranes underlain by CCLs have been developed and successively updated. Giroud & Bonaparte (1989) and Giroud et al. (1989) developed the first sets of equations. These equations provide an approximate solution assuming that the hydraulic gradient is close to unity. This assumption may be reasonable for low leachate mounds (design mounds ranging from 0.03 to 0.3 m) and clay liners with thickness of 0.6 to 0.9 m, but are not strictly valid for the levels of leachate mounding that may occur during post-operation, in cases of excessive clogging of a leachate collection system, or a modest leachate mound over a GCL (Rowe 1998). Aware of these limitations, Giroud et al. (1992) extended the approximate solution to consider higher hydraulic heads. They also proposed equations for defects of infinite length. A limitation in these equations was that they required charts to obtain the value of one of the terms of the equation.

Giroud (1997) updated previous empirical equations, providing an entirely analytical means of calculating the flow rate through defects in geomembranes. In addition, he summarised the developed equations in regard of the shapes of the defects, the liquid head above the geomembrane liner, and the contact conditions. Later on, Giroud et al. (1998) developed a new set of equations for calculating: (a) the rate of flow through composite liners due to geomembrane defects; (b) the rate of flow through defects in a geomembrane placed on a semi-permeable medium; and (c) the rate of flow through defects in a geomembrane overlain by a permeable medium and underlain by a highly permeable medium.

Foose et al. (2001) and Touze-Foltz (2001) compared the flow rate through composite liners comprising a geomembrane and a CCL calculated using either empirical equations or analytical solutions. For circular defects, the results obtained using empirical equations developed by Giroud (1997) showed good agreement with the results obtained using analytical solutions developed by Rowe (1998) and Touze-Foltz et al. (1999). Conversely, for defects of infinite length, the results obtained using empirical equations by Giroud et al. (1992) were inconsistent with the results obtained using the analytical solutions. Analysis conducted by Foose et al. (2001) attributed this inconsistency to the fact that the empirical equations for circular defects and defects of infinite length correspond to different values of interface transmissivity even though the same contact conditions are considered. In other words, the interface transmissivity was a function of the type of defect, which should not happen. Based on these findings, these authors proposed new empirical equations for defects of infinite length (Foose et al. 2001) and damaged wrinkles (Touze-Foltz et al. 2002b).

Equations by Touze-Foltz et al. (2002b) were recently updated by Touze-Foltz & Giroud (2003). The latter authors also updated the empirical equations for defects of infinite length developed by Giroud et al. (1992) and proposed a new equation, for circular defects, for excellent contact conditions. An important advance was reached with the new empirical equations developed by Touze-Foltz & Giroud (2003), based on the assumption that the transmissivity is independent from the type of defect. This significant improvement was in part due to the fact that they could define the contact conditions in quantitative terms. Definition of contact conditions in quantitative terms is based on empirical equations as Section 4.5.4 will show.

Table 4.3 summarises the latest empirical equations for assessing the flow rate through composite liners comprising a geomembrane and a low hydraulic conductivity soil (CCL) caused by geomembrane defects. The equations are grouped by type of defect (circular, defect of infinite length and damaged wrinkle) and by contact conditions (excellent, good and poor). These supersede previous equations presented by the same authors.

It should be noted that, except for the equation by Foose et al. (2001), with a validity clearly defined in the second footnote of Table 4.3, empirical equations included in this table can only be used for the following values of the parameters (Touze-Foltz & Giroud 2003):

- Circular defects having radii between 1×10^{-3} and 5.64×10^{-3} m (i.e. a circular defect area of 1 cm^2);
- Defects of infinite length having widths between 2×10^{-3} and 2×10^{-2} m;
- Wrinkle widths ranging from 0.1 to 0.6 m;
- Hydraulic heads ranging from 0.03 to 3 m;
- Hydraulic conductivities of the soil component of the composite liner ranging from 1×10^{-10} to 1×10^{-8} m s^{-1}; and
- Thicknesses of the soil layer component of the composite liner ranging from 0.3 to 5 m.

Table 4.3 – Existing empirical equations for assessing the flow rate through composite liners comprising a geomembrane and a low permeability soil due to geomembrane defects

Defect	Contact conditions	Empirical equations	Reference
Circular defect	Excellent	$Q = 0.096\ h_w^{0.9}\ a^{0.1}\ k_s^{0.74}\left[1+0.1\left(h_w/H_s\right)^{0.95}\right]$	Touze-Foltz & Giroud (2003)
	Good	$Q = 0.21\ h_w^{0.9}\ a^{0.1}\ k_s^{0.74}\left[1+0.1\left(h_w/H_s\right)^{0.95}\right]$	Giroud (1997)
	Poor	$Q = 1.15\ h_w^{0.9}\ a^{0.1}\ k_s^{0.74}\left[1+0.1\left(h_w/H_s\right)^{0.95}\right]$	
Defect of infinite length	Excellent	$Q_L = 0.42\ h_w^{0.45}\ b^{0.004}\ k_s^{0.87}\left[1+0.52\left(h_w/H_s\right)^{0.59}\right]$	Touze-Foltz & Giroud (2003)
	Good	$Q_L = 0.65\ h_w^{0.45}\ b^{0.004}\ k_s^{0.87}\left[1+0.52\left(h_w/H_s\right)^{0.59}\right]$	
	Poor	$Q_L = 1.64\ h_w^{0.45}\ b^{0.004}\ k_s^{0.87}\left[1+0.52\left(h_w/H_s\right)^{0.59}\right]$	
	All (*)	$Q_L = \frac{2}{H_s}\left(\frac{b}{2}+\sqrt{\frac{\theta\ H_s}{k_s}}\right)\left(h_w+H_s\right)k_s$	Foose et al. (2001)
Damaged wrinkle	Excellent	$Q_L = 0.63\ h_w^{0.45}\ b^{0.1}\ k_s^{0.87}\left[1+0.28\left(h_w/H_s\right)^{0.82}\right]$	Touze-Foltz & Giroud (2003)
	Good	$Q_L = 0.89\ h_w^{0.45}\ b^{0.1}\ k_s^{0.87}\left[1+0.28\left(h_w/H_s\right)^{0.82}\right]$	
	Poor	$Q_L = 1.98\ h_w^{0.45}\ b^{0.1}\ k_s^{0.87}\left[1+0.28\left(h_w/H_s\right)^{0.82}\right]$	

Notes:

(i) The symbols as follows are used in this table: Q = flow rate; Q_L = flow rate per unit length; h_w = hydraulic head on top of geomembrane; a = circular defect area; b = width of defect of infinite length or damaged wrinkle; k_s = soil layer hydraulic conductivity; H_s = soil layer thickness; and θ = transmissivity of the interface. These equations must be used with the following units: Q ($m^3\ s^{-1}$), Q_L ($m^2\ s^{-1}$), h_w (m), a (m^2), b (m), k_s ($m\ s^{-1}$), H_s (m), and θ (m^2 s);

(ii) (*) Equation applicable if the ratio between the hydraulic conductivity of the interface and the hydraulic conductivity soil component of the composite liner is higher than 3×10^4.

Based on the ranges of hydraulic conductivity and thickness mentioned above, the equations presented in Table 4.3 are not applicable to the case where the soil component of the composite liner is only a GCL. Nevertheless, they can be used for composite liners that include a CCL overlain by a GCL (Touze-Foltz & Giroud 2003). In this case, the soil

hydraulic conductivity to be used in flow rate calculations is the equivalent hydraulic conductivity determined using the equation below (Touze-Foltz & Giroud 2003):

$$k_s = \frac{H_{GCL} + H_f}{H_{GCL}/k_{GCL} + H_f/k_f} \quad (4.48)$$

where k_s is the equivalent hydraulic conductivity; k_f is the hydraulic conductivity of the foundation layer (CCL); k_{GCL} is the hydraulic conductivity of the GCL; H_f is the thickness of the foundation layer (CCL); and H_{GCL} is the thickness of the GCL.

Accordingly, the equivalent thickness, H_s, is to be used in flow rate calculations (Touze-Foltz & Giroud 2003):

$$H_s = H_{GCL} + H_f \quad (4.49)$$

It should be noted that, except for the equation proposed for Foose et al. (2001) that has a different form, the exponents in the equations are the same for each type of defect. This means that the differences in these equations, which are related with the contact conditions, are expressed by the value of the coefficient at the beginning of the second term of the equations, often designated as quality factor.

4.5.3.3 Existing equations for GCLs

Empirical equations for predicting the flow through composite liners comprising a geomembrane and a GCL are scarce. Foose et al. (2001) analysed the flow through this type of composite liners using numerical models. Flow rates predicted with numerical models were compared to flow rates predicted using the analytical solutions proposed by Rowe (1998). According to Foose et al. (2001), the appropriate tool for calculating flow rates should be selected based on the ratio between the hydraulic conductivity of the interface and the hydraulic conductivity of the GCL liner. Based on these findings, they proposed either new equations, or adjustments on existing analytical solutions (Table 4.4).

Empirical equations for evaluating the flow rate through composite liners involving a geomembrane and a particular type of GCL (geomembrane-supported GCL) can also be found in Gundseal (2001). They are based on equation proposed by Giroud (1997) for circular defects (equation presented in the 3rd row of Table 4.3), and would not be applicable to other types of GCLs, namely the geotextile-supported GCLs (Gundseal 2001). In spite of this important limitation, these equations are presented below, since the present research is focused on the measurement of the flow rate through composite liners comprising a geomembrane and a GCL:

$$Q = 0.01 h_w^{0.9} a^{0.1} k_{GCL}^{0.74} \left[1 + 0.1 \left(\frac{h_w}{H_{GCL}} \right)^{0.95} \right] \tag{4.50}$$

This equation is considered valid for $h_w < 3$ m, and defect diameters between 0.5 and 25 mm (25 mm corresponds to a surface equal to 5×10^{-2} m^2). For higher heads of liquid on top of the geomembrane, up to approximately 30 m, the following equation is proposed (Gundseal 2001) for the flow rate through composite liners having a geomembrane-supported GCL:

$$Q = 0.01 h_w^{0.9375} a^{0.1} k_{GCL}^{0.74} \left[1 + 0.1 \left(\frac{h_w}{H_{GCL}} \right)^{0.95} \right] \tag{4.51}$$

where H_{GCL} is the GCL thickness; a is the area of the defect; and k_{GCL} is the hydraulic conductivity of the GCL. These equations must be used with the following units: Q (m^3 s^{-1}), h_w (m), a (m^2), k_L (m s^{-1}), and H_s (m).

Table 4.4 – Recommended equations for calculating flow rates through composite liners comprising a geomembrane and a GCL (adapted from Foose et al. 2001)

Defect	Interface condition $\left(\log \frac{k_i}{k_{GCL}} \right)$	Recommended equations
Circular defect	> 4	Rowe's (1998) analytical solution (Equation 4.36) or Giroud's (1997) empirical equations (third and fourth lines in Table 4.3)
	< 4	$Q_a = 2.85 Q_R \left[\log \frac{k_i}{k_{GCL}} \right]^{-0.73}$
Defect of infinite length	> 4	$Q_L = \frac{2}{H_{GCL}} \left(\frac{b}{2} + \sqrt{\frac{\theta H_{GCL}}{k_{GCL}}} \right) (h_w + H_{GCL}) k_{GCL}$
	< 4	$Q_a = 2.85 Q_L \left[\log \frac{k_i}{k_{GCL}} \right]^{-0.73}$

The following symbols are used in this table: k_i = hydraulic conductivity of the interface; k_{GCL} = hydraulic conductivity of the GCL; Q_a = adjusted flow rate in a GCL composite liner; Q_R = flow rate predicted using Rowe's (1998) analytical solution (Equation 4.36); Q_L = flow rate per unit length; H_{GCL} = GCL thickness; b = width of defect of infinite length; and θ = transmissivity of the interface.

4.5.3.4 Summary of Section 4.5.3

Section 4.5.3 shows that there are many empirical equations for composite liners comprising a geomembrane and a CCL, which cover different types of defects and characteristics of the interface. In contrast, there are few empirical equations for composite liners involving GCLs. To our knowledge, only Foose et al. (2001) proposed some empirical equations for this type of composite liner, but, even those, are applicable only to defects of infinite length. In addition, for a particular type of composite liner involving geomembrane supported GCLs, an adaptation of the empirical equations proposed by Giroud (1997) for circular holes, is suggested by Gundseal (2001).

Therefore, for composite liners involving GCLs available tools were developed either for a particular type of defect or for a particular type of product. These equations cover only a narrow range of cases. New equations for different types of defects and composite liners including geotextile-supported GCLs are needed. Taking into account this lack of empirical equations, in the present work, an attempt is made to develop this tool, based on the experimental data as Chapter 6 will present.

On the other hand, discussions addressed in Sections 4.5.2 and 4.5.3 highlight that the features of the interface between the geomembrane and the underlying liner are a key issue to predict the flow rate through composite liners due to geomembrane defects. Analytical solutions take them into account through the interface transmissivity, whereas empirical equations consider different types of contact conditions. Interface transmissivity and quantitative definition of the contact conditions are discussed in the following section.

4.5.4 Interface transmissivity for CCL/geomembrane composite liners and quantitative definition of the contact conditions

The transmissivity, θ, of the interface between the geomembrane and an underlying soil liner can be estimated based on Newton's viscosity theory for flow, assuming that the interface can be approximated by two smooth parallel plates (Brown et al. 1987; Giroud & Bonaparte 1989, Rowe 1998, Foose et al. 2001, Touze Foltz & Giroud 2003):

$$\theta = k_i s = \frac{\rho_w g s^3}{12\eta} \tag{4.52}$$

where k_i is the hydraulic conductivity of the interface; s is the interface thickness; ρ_w is the density of water; g is the acceleration due to gravity; and η is the dynamic viscosity of water. Equation (4.52) can be used with any set of coherent units. The basic SI units are: θ ($m^2\ s^{-1}$), k_i ($m\ s^{-1}$), ρ_w ($kg\ m^{-3}$), g ($m\ s^{-2}$), s (m), and η ($kg\ m^{-1}\ s^{-1}$).

Equation (4.52) shows that in order to compute the transmissivity, it is necessary to know the interface thickness. This issue was addressed by Brown et al. (1987), who carried out laboratory tests using various types of geomembranes with defects placed on soil layers having hydraulic conductivities ranging from 1×10^{-9} to 1×10^{-6} m s^{-1}. A theoretical analysis of

their results led Brown et al. (1987) to propose interface thickness values that correspond to soil hydraulic conductivity values ranging from 1×10^{-9} to 1×10^{-6} m s^{-1}.

Corresponding transmissivities can then be calculated using Equation (4.52) and are shown in Table 4.5. It should be noted that the contact conditions in Brown et al.'s (1987) tests could be characterised as excellent (Giroud & Bonaparte 1989), and thus the interface thickness and the interface transmissivity included in Table 4.5 correspond to excellent contact conditions (Rowe 1998, Touze Foltz & Giroud 2003).

Table 4.5 - Interface thickness and transmissivity as a function of soil layer hydraulic conductivity according to experimental data from Brown et al. (1987)

Soil layer hydraulic conductivity (m s^{-1})	Interface thickness (mm)	Interface transmissivity (m^2 s^{-1})
1×10^{-6}	0.15	2.8×10^{-6}
1×10^{-7}	0.08	4.2×10^{-7}
1×10^{-8}	0.04	5.2×10^{-8}
1×10^{-9}	0.02	6.5×10^{-9}

Another important finding reported by Brown et al. (1987) was that the hydraulic conductivity of the soil layer and the interface transmissivity are linked: the smaller the soil particle size, the lower its hydraulic conductivity and roughness of its surface, hence, the thinner the interface.

Following the rationale given by Brown et al. (1987), Rowe (1998) used his analytical solution, Equation (4.36), to back-calculate the transmissivity of the interface between the geomembrane and the soil layer necessary to yield flow rates through the defects corresponding to those obtained from Giroud's (1997) equations for circular defects (equations presented in the 3rd and 4th rows of Table 4.3). Input parameters included: defect radii ranging from 1×10^{-3} to 5.64×10^{-3} m, soil layer thickness values ranging from 0.6 to 1.2 m, soil hydraulic conductivity values ranging from 1×10^{-10} to 1×10^{-8} m s^{-1}, and hydraulic head equal to 0.3 m. Accordingly, Rowe (1998) proposed two empirical relationships between soil hydraulic conductivity and interface transmissivity, for good and poor contact conditions as previously defined in Section 4.5.3.1 of this chapter. Relationships proposed by Rowe (1998) are presented below:

For good contact conditions:

$$\log\theta = 0.07 + 1.036 \log k_s + 0.018 \left(\log k_s\right)^2 \tag{4.53}$$

For poor contact conditions:

$$\log\theta = 1.15 + 1.092 \log k_s + 0.0207 \left(\log k_s\right)^2 \tag{4.54}$$

Equations (4.53) and (4.54) are represented by the solid curves identified as "good" and "poor" in Figure 4.10. This figure shows that the curves for good and poor contact conditions are approximately straight lines, even though they are not linear in a logarithmic scale. It can be also seen that the curves for good and poor contact conditions are approximately parallel.

Based on the analytical solutions developed by Touze-Foltz et al. (1999), Touze-Foltz & Giroud (2003) extended the work by Rowe (1998) and proposed an equation for excellent contact conditions. As an attempt to obtain consistent empirical equations for the three contact conditions, and given that the contact conditions in the Brown et al.'s (1987) tests were characterised as excellent, they assumed that the interface transmissivity for the case of excellent contact conditions is represented by a quasi-straight line parallel to the quasi-straight line representing good contact conditions in Figure 4.10 and passing through the point with transmissivity given in Table 4.5, for a soil hydraulic conductivity of 1×10^{-9} m s^{-1}. Therefore, the following relationship for excellent contact conditions was obtained:

$$\log\theta = -0.321 + 1.036 \log k_s + 0.018 \left(\log k_s\right)^2 \qquad (4.55)$$

where θ is the interface transmissivity, and k_s is the hydraulic conductivity of the soil component of the composite liner. This equation is also represented by a solid curve in Figure 4.10.

Equations (4.53) to (4.55) can only be used with the following units: θ (m^2 s^{-1}) and k_s (m s^{-1}).

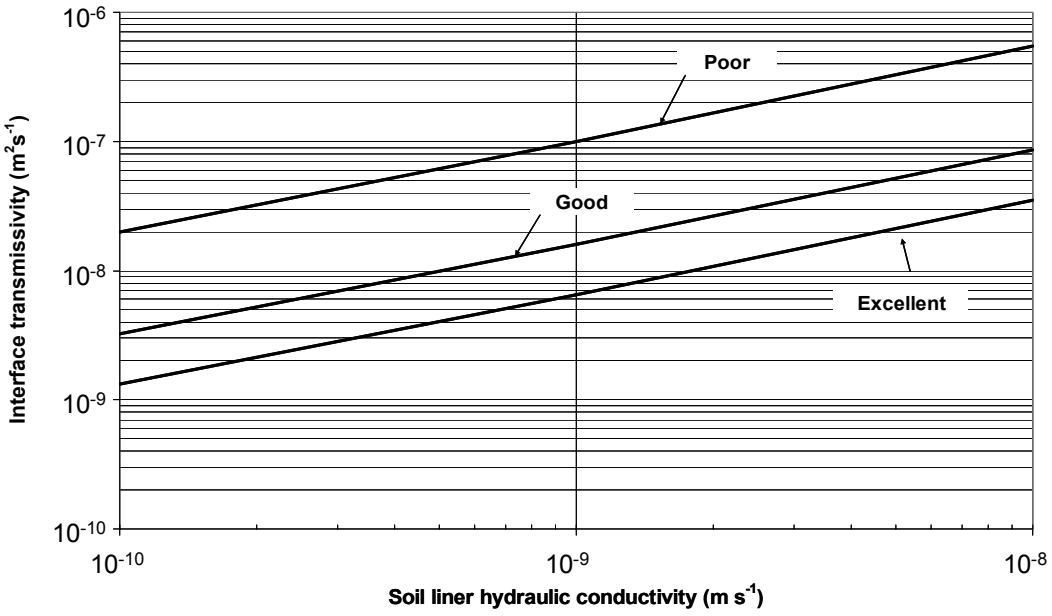

Figure 4.10 – Relationships between interface transmissivity and soil layer hydraulic conductivity for poor, good, and excellent contact conditions (adapted from Touze-Foltz & Giroud 2003)

According to Touze-Foltz & Giroud (2003), a good approximation of Equations (4.53), (4.54), and (4.55) is achieved by the following linear equations that correspond to three parallel straight lines that could hardly be distinguished from the solid curves presented in Figure 4.10:

For excellent contact conditions:

$$\log\theta = -1.7476 + 0.7155 \log k_s \quad (4.56)$$

For good contact conditions:

$$\log\theta = -1.3564 + 0.7155 \log k_s \quad (4.57)$$

For poor contact conditions:

$$\log\theta = -0.5618 + 0.7155 \log k_s \quad (4.58)$$

These equations have to be used with SI units.

Quantitative characterisation of contact conditions is very important to avoid inconsistency such as the interface transmissivity being a function of the type of defect (Touze-Foltz & Giroud 2003). In addition, it is very important to evaluate the flow rate through composite liners due to geomembrane defects using analytical solutions, in which the transmissivity of the interface is integrated.

The addressed issues showed that the hydraulic transmissivity of the interface is a key parameter to calculate the flow rate through composite liners due to defects in geomembranes. Some experimental studies can be found in the literature on this topic. Some of them focused on composite liners involving CCLs (e.g. Fukuoka 1986, Brown et al. 1987, Jayawickrama et al. 1988, Liu 1998, Touze-Foltz 2001, 2002b). Other focused on composite liners involving GCLs, such as Harpur et al. (1993), Estornell & Daniel (1992) and Koerner & Koerner (2002). Within the scope of this study, studies dealing with composite liners involving GCLs will be reviewed in Section 4.6. Furthermore, flow rates from field studies on this type of composite liners are presented and discussed in Section 4.7.

4.6 PREVIOUS LABORATORY STUDIES ON FLOW RATES THROUGH COMPOSITE LINERS INVOLVING GCLS

4.6.1 Estornell & Daniel (1992)

Estornell & Daniel (1992) studied the hydraulic performance of composite liners involving different GCLs and a punctured 1.5 mm thick geomembrane (HDPE). Three GCLs were used: geomembrane-supported, needlepunched, and adhesive bounded. Tests were carried out in steel tanks (2.4 m long, 1.2 m wide, and 0.3 m high). Punctures in geomembrane specimens

comprised two 75 mm diameter holes, three 25 mm diameter holes, and three 0.6 m long slits about 1mm wide. The confining stress varied from 8 to 10 kPa, and a pressure head of 0.3 m was maintained on the products tested. Effluent water passing through the composite liners was collected and weighed to estimate the flow of water (Figure 4.11).

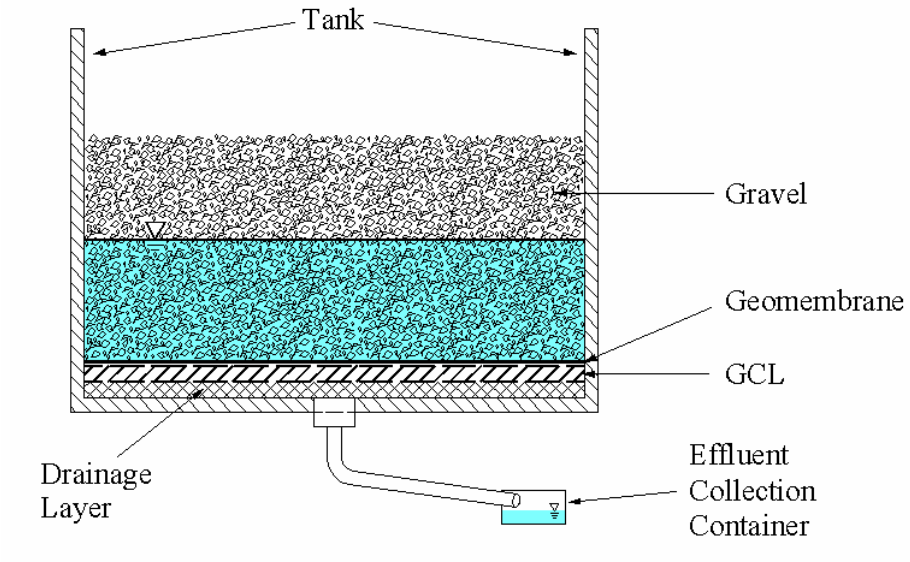

Figure 4.11 – Cross-sectional view of configuration of materials in tank (modified from Estornell & Daniel 1992)

The main results reported by these authors include: (i) no outflow was observed with the geomembrane-supported GCL; water penetrated the bentonite at the holes, but migrated no more than 75 mm from the holes (wetted area) over the five-month testing period; the authors attributed this behaviour to a composite action: the bentonite sealed off the holes in the geomembrane, and the GCL prevented the outflow of water from the punctured geomembrane/GCL composite liner; (ii) outflow could be collected with tests involving geotextile-supported GCLs; when the tests were disassembled (after about three months of permeation), they observed that the bentonite was fully hydrated over the entire area of the specimens, suggesting that water flowed through the holes in the geomembranes, spread laterally through the upper geotextile, and soaked the GCLs. As regards the amount of water collected, no data was reported by these authors.

Estornell & Daniel (1992) concluded that the effectiveness of composite action between a punctured geomembrane and the bentonite in the GCLs depends on whether a geotextile separated the punctured geomembrane from the bentonite. Good performance was observed when the bentonite was in direct contact with the damaged geomembrane, whereas a worse performance was observed when a geotextile separated the bentonite from the geomembrane.

4.6.2 Harpur et al. (1993)

Harpur et al. (1993) carried out tests to measure the liquid flow beneath a geomembrane with a hole placed over a GCL, from which they quantified the transmissivity of the interface. Liquid flow measurements were conducted in two different ways. Constant head tests were

carried out when the radial flow rate, $Q_r(R_c)$, was high. As the radial liquid flow rate decreased, the use of the falling head test became necessary due to its high accuracy at low flow rates. In this case, the total flow rate, Q, was measured.

Tests were conducted on a 0.108 m diameter permeameter (Figure 4.12). Each test was performed under a normal stress of 7 and 70 kPa. Constant head tests were run at 0.3 m head and falling head tests at around 0.325 m. Five different types of GCL were tested under a 1.5 mm thick HDPE geomembrane with a circular hole at its centre, with a 7.6 mm diameter. The various GCLs tested were the following:

- Granular bentonite glued to a lower geomembrane;
- Powdered bentonite sandwiched between a woven slit film and a non-woven needlepunched geotextile;
- Granular bentonite glued between a woven spun laced and a woven geotextile;
- Granular bentonite sandwiched between a woven slit film and a non-woven needlepunched geotextile; and
- Powdered bentonite sandwiched between two non-woven needlepunched geotextiles.

The GCL specimens were tested with no prehydration. The tests were run during a two-week period.

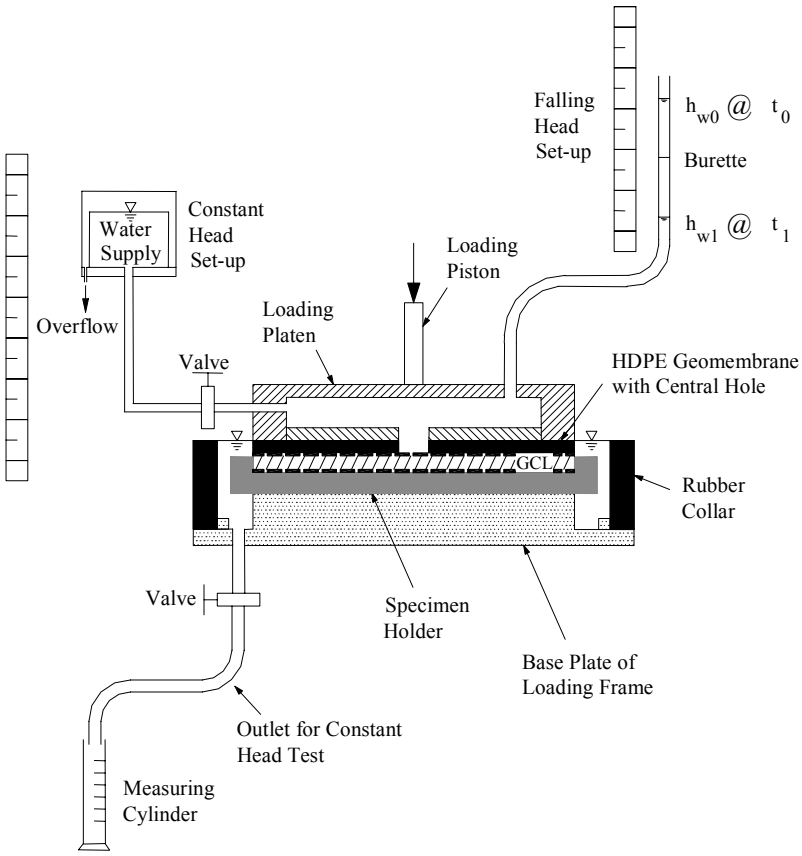

Figure 4.12 – Schematic drawing of the transmissivity apparatus used by Harpur et al. (1993)

Transmissivities determined by Harpur et al. (1993) neglected the flow within the bentonite. Therefore, the term "apparent transmissivity" was adopted by these authors. According to them, the computed transmissivity represents an upper limit to the real transmissivity. The radius of the wetted area that corresponds to the GCL specimen radius may be also overestimated by the assumption that the wetted area corresponds to the whole specimen surface, as underlined by Touze Foltz et al. (2002a). The equations below were used by Harpur et al. (1993) to evaluate the apparent transmissivity:

- For constant head tests:

$$\theta = \frac{Q_r(R_c)\,\ln\left(\frac{R_c}{r_0}\right)}{2\,\pi\,h_w} \tag{4.59}$$

- For falling head tests:

$$\theta = \frac{a_c\,ln\left(\frac{R_c}{r_0}\right)\,ln\left(\frac{h_{w_0}}{h_{w_1}}\right)}{2\,\pi t} \tag{4.60}$$

where a_c is the cross-sectional area of falling head capillary tube; h_{w_0} is the hydraulic head on top of the geomembrane hole at the beginning of a falling head test; h_{w_1} is the hydraulic head on top of the geomembrane hole at the end of a falling head test; and t is the falling head test duration.

Interface transmissivities reported by Harpur el al. (1993) are in the range 6×10^{-12} to 2×10^{-10} $m^2\ s^{-1}$, for the four geotextile-supported GCLs, and 3×10^{-12} $m^2\ s^{-1}$ for geomembrane-supported GCL. Other important findings reported by Harpur et al. (1993) can be summarised as follows: (i) at the initial stages of testing the apparent transmissivity was high in most GCLs, since it is governed by the relatively high transmissivity of the geotextile and the relatively large size air channels in the bentonite during its initial dry state; (ii) at the initial stages of testing, apparent transmissivity was lower under a normal stress of 70 kPa than at a normal stress of 7 kPa. However, with time, this difference was significantly reduced, which was explained, on one hand, by intrusion of the bentonite into the geotextile and extrusion of the bentonite through the geotextile, what obstructs the flow of water, and, on the other hand, by the fact that any air channels within the initially dry bentonite can close because of swelling; (iii) of the two GCLs made of the same upper geotextile (woven slit film geotextile), one comprising granular bentonite and the other powdered bentonite, the latter presented an apparent transmissivity of one order of magnitude lower, indicating a better performance of the powdered bentonite; (iv) the GCL with the upper needlepunched geotextile presented a transmissivity of the same order of magnitude than the other GCLs with a woven geotextile. This was attributed to the fact that the needlepunched geotextile contained a considerable quantity of powdered bentonite in its dry state as a consequence of the needling process. Also, the possible effect of vibrations occurring during transportation and handling of the material influenced the results; and (v) the highest effect of normal stress was observed in the GCL

with a woven spun laced geotextile.

In addition, Harpur et al. (1993) reported that GCLs tested showed significantly lower transmissivities than the one predicted using Newton's viscosity law (Equation (4.52) assuming an interface thickness of 0.02 mm between the geomembrane and an underlying liner. Transmissivity corresponding to this interface thickness is 6.5×10^{-9} m^2 s^{-1} (Table 4.5). Nevertheless, it should be noted that this calculation is based on Giroud & Bonaparte (1989), which, supported on data from Brown et al. (1987), suggested that the transmissivity of a CCL having a hydraulic conductivity of 10^{-9} m s^{-1} can be determined, under excellent contact conditions, by assuming an interface thickness of 0.02 mm. Thus, the hydraulic conductivity and the interface thickness used by Harpur et al. (1993) may not be representative for GCLs.

4.6.3 Koerner & Koerner (2002)

Laboratory tests were carried out by Koerner & Koerner (2002) to evaluate what amount of flow might result from a needle punctured geomembrane over a needlepunched GCL. Flow through a 1.5 mm thick HDPE geomembrane was estimated for four different circular hole scenarios: 3.6 mm in diameter, 1.0 mm in diameter, approximately 0.1 mm diameter (needle diameter), and a 0.1 mm diameter with the needle left in the hole. For comparison purposes, tests were also conducted with a drainage geonet beneath the geomembrane (free drainage).

The tests were performed in a compartmentalised permeameter, partitioned in four sections so that each hole scenario could be tested at the same time. Specimens were tested under a confining stress of 35 kPa, and constant hydraulic heads of 2.5, 7.5, 15, 30 and 60 cm were successively applied. The GCL was allowed to hydrate for 7 days under stress prior to testing (prehydrated specimens). Tests were ended when the three criteria as follows were met: (i) the ratio of rate inflow was between 2.8 and 4.7 litre $hour^{-1}$ for the last three consecutive flow measurements, (ii) no significant upward or downward trend in flow was noted for the last three consecutive flow measurements, and (iii) none of the last three flow values were less than 0.75 times the average flow rate nor higher than 1.25 times the average value. Flow rates were calculated and plotted against hydraulic head. No information is given about the prehydration value.

The results show that the four hole scenarios with the geomembrane over the GCL produced flow rates 4 to 5 orders of magnitude lower than with the geomembrane over the drainage geonet. However, whereas individual differences in the results from the different hole scenarios were logical for the geomembrane/geonet tests, they were not logical for the geomembrane/GCL tests. For the latter, the highest flow rate was obtained for the test carried out with the needle left in the hole in geomembrane. According to Koerner & Koerner (2002), this incongruence indicated that the accuracy limit of the test device was exceeded in this case. Disregarding that particular result, at 30 cm of hydraulic head, flow rates through the remaining holes in geomembrane over the GCL were similar: approximately 3×10^{-11} m^3 s^{-1}. Another observation reported was that, in general, the flow rate gradually increased as the hydraulic head increased.

These authors also compared the measured flow rates to the ones theoretically calculated using the empirical equation proposed by Giroud & Bonaparte (1989). Input parameters for the empirical equation included: a hydraulic conductivity of the GCL equal to 7.0×10^{-12} m s^{-1}, a GCL thickness of 1 cm, and a hydraulic head equal to 30 cm. The theoretically calculated values of flow rate were found to be much less than the measured values. According to the authors this may be due to the fact that the empirical equation does not apply for such small

holes and/or the experimental setup was not sensitive enough to measure such low values. In this regard, it should be noted that Giroud & Bonaparte's (1989) equation was not developed for geomembrane in contact with GCL and for such low hydraulic conductivity of the underlying liner. Therefore, the comparison made might be meaningless.

Issues addressed in Section 4.6 highlight that, even though some experimental studies were conducted on flow rate through composite liners due to geomembrane defects, there are many aspects regarding their performance that remain unstudied. For example, very little is known about the performance of a composite liner when there is a prehydrated GCL under the geomembrane, although it is usually recommended that GCLs be hydrated under a vertical stress after their installation. Also, very little is known about the degree of dependency of the transmissivity on the applied head, or on the applied load above the geomembrane. To deal with these issues, a parametric study on flow rate through composite liners due to a circular hole in the geomembrane was carried out in laboratory. This study will be presented in Chapter 6.

4.7 PREVIOUS FIELD STUDIES ON FLOW RATES THROUGH COMPOSITE LINERS INVOLVING GCLS

Some landfills have been constructed with double composite liner systems, that means with a secondary leachate collection system (SLCS) between the primary and secondary liners (recall Figure 2.3). The SLCS consists either of granular material or a geonet. Monitoring data from SLCS provides a rapid detection system of leaks through the primary liner, as well as it gives operator time for response before contaminants escape from the landfill and migrate into the subsurface. It also may provide insight regarding the effectiveness of the primary liners as emphasised by Rowe (1998).

A certain number of studies on flow rates has been made on landfills with SLCS by measuring the flow in these systems. Nonetheless, the interpretation of the data requires careful consideration of sources of fluid other than flow from the landfill (Gross et al. 1990). According to these authors, fluid may enter the SLCS as: (i) infiltration during construction of the system; (ii) water arising from the compression and consolidation of the clay component of the primary liner under the weight of the waste; (iii) groundwater infiltration from outside the landfill; and (iv) flow through the primary liner due to defects in the geomembrane.

A review of significant published studies on this topic has been done by Rowe (1998). Of particular interest, in the context of the present work, is the study conducted by Bonaparte et al. (1996). These authors compiled flow rate data from 26 double lined cells at six landfills containing geomembrane/GCL composite primary liners. The authors used the data to calculate average and peak SLCS flow rates for three distinct landfill development stages: (i) initial period of operation; (ii) active period of operation; and (iii) post-closure period. Table 4.6 shows the mean values and standard deviation of flow estimated by Bonaparte et al. (1996).

As can be seen, the mean SLCS flow rates are very low during both the active and post-closure period, respectively 0.7 and 0.2 litres per hectare/day (lphd). Peak flow rates are about one order of magnitude higher than the average, even though they are relatively small.

Table 4.6 – Mean flow rates in SLCS for 26 landfill cells with GM/GCL composite primary liners given in litres per hectare/day (lphd) (based on Bonaparte et al. 1996)

SLCS flow rates	Cells	Average flow rate (lphd)		Peak flow rate (lphd)	
		Mean	Standard deviation	Mean	Standard deviation
Initial period	26	36.6	68.5	141.8	259.9
Active operation	19	0.7	1.1	7.7	13.7
Post-closure	4	0.2	-	2.3	-

Recently, Majdi et al. (2002), under USEPA auspices, developed a database that includes information for 187 cells at 54 double lined landfills. Information compiled concerns geomembrane primary liners, and composite liners consisting of geomembrane/CCL, geomembrane/GCL or of geomembrane/GCL/CCL with either sand or geonet secondary leachate collection system. The main findings reported by Majdi et al. (2002) can be summarised as follows:

- For geomembrane primary liners, data gathered from 31 cells gives an average SLCS flow rates ranging from 5 to 2100 lphd during the initial period of operation, from 1 to 1600 lphd during the active period of operation, and from 2 to 330 lphd after closure;
- For geomembrane/GCL composite primary liners, data compiled from 28 cells gives an average monthly SLCS flow rates ranging from about 0 to 290 lphd during the initial period of operation, from 0 to 11 lphd during the active period, and from 0 to 2 lphd after closure; peak monthly SLCS flow rates were typically two to five times the average monthly values; between the initial and active periods of operation, SLCS flow rates decreased one to three orders of magnitude; and
- For geomembrane/CCL and geomembrane/GCL/CCL composite primary liners, the interpretation of results is complex due to the relatively significant contribution of consolidation water in SLCS flow, as well as the breakthrough time (i.e. times of travel) for advective transport through the CCL or GCL/CCL component of the composite liner; the average monthly SLCS flow rates (13 landfill cells) ranged from about 10 to 1400 lphd during the initial period of operation, from 0 to 370 lphd during the active period, and from 5 to 210 lphd after closure.

Additional observations regarding SLCS flow rate data for geomembrane/CCL and geomembrane/GCL/CCL indicate that the consolidation water flow rates are dependent on the thickness and hydraulic conductivity of the CCL, as well as the rate of overlying waste placement. Average monthly rates during the active period may initially be as high as 200 to 400 lphd, with flows attributed primarily to consolidation water (Majdi et al. 2002).

It is important to note that higher flow rates appear to be achieved in landfills with no CQA. For example, Bonaparte & Gross (1990, 1993) reported that 19 % of landfills with CQA had SLCS flow rates of 50 lphd or less and 57 % of landfills had SLCS flow rates of 200 lphd or less, whereas for landfills with no CQA, only 20 % had SLCS flow rates of 200 lphd or less. Higher average flow rates for landfills with no CQA were also indicated by Tedder (1997).

Discussions carried out in Section 4.6 show that the mean flow rates are small during the active and post-closure periods. Nonetheless, reported SLCS flow rates for composite liners comprising a GM and a GCL varied considerably according to the author. Bonaparte et al. (1996) report a mean SLCS flow rate of 0.7 lphd, during the active period and 0.2 lphd, in the post-closure period, whereas Majdi et al. (2002) reports that the flow rate ranged from 0 to 11 lphd, during the active period, and from 0 to 2 lphd in the post-closure period. These results emphasise that there are still many uncertainties about the amount of fluid that can be expected in the SLCS for composite liners involving GCLs, being necessary further research on this topic.

In this study, an attempt is made to add some information about the amount of fluid that can be expected due to geomembrane defects. For that, laboratory tests were carried out in three different scales, and are presented in Chapter 6.

4.8 SUMMARY AND CONCLUSIONS

This chapter discussed the theoretical issues related with the water retention curves and the advective flow through composite liners due to geomembrane defects. It started with a general discussion about water flow through porous media. From that discussion, it could be seen that the hydraulic conductivity is a key factor. Thus, for evaluating the performance of composite liners involving a GCL, it is necessary to know the hydraulic conductivity of the GCLs. As these materials are typically installed with their natural water content, it follows that saturated hydraulic conductivity may not be representative of the field conditions. Experimental evaluation of unsaturated hydraulic conductivity is difficult. Consequently, predictive methods based on water retention curves, typically represented by the van Genuchten parameters, are often used. The van Genuchten parameters can be estimated by matching a theoretic water retention curve to experimental data on matric suction. In this framework, experimental methods for assessing the suction and for estimating the van Genuchten parameters were also described. Issues addressed will support the interpretation of the experimental work presented in Chapter 6 on water retention curves of the GCLs.

Section 4.5 presented a discussion about the analytical and empirical tools for calculating the flow rate through composite liners due to geomembrane defects. In fact, the characteristics of the interface between the geomembrane and the underlying liner are a key parameter for this calculation. Analytical solutions define these characteristics in terms of interface transmissivity, whereas empirical equations define them in terms of contact conditions. For composite liners consisting of a geomembrane and a GCL, it could be seen that the existing empirical equations to predict the flow rate are applicable to infinitely long defects and thus, for other types of defects, the analytical solutions have to be used.

Important limitations of the analytical solutions are that they are complex and that direct measurements of interface transmissivity are scarce. In the present work, an attempt is made to overcome these limitations, through experiments carried out on flow rate through composite liners involving GCLs that are presented in Chapter 6. Results obtained are both intended to improve our knowledge about the interface characteristics and to develop simple tools for predicting the flow rate through different types of defects in geomembranes, namely empirical equations.

This chapter finished with a literature review on flow rate through composite liners comprising a geomembrane and a GCL.

5 EXPERIMENTAL WORK ON GAS PERMEATION THROUGH GEOMEMBRANE SEAMS

5.1 INTRODUCTION

As pointed out in Chapter 2, the successful performance of the geomembrane as a barrier is linked with seams quality: the seam needs to be fluid-tight and have a mechanical strength of the same order of magnitude as the geomembrane panels. In landfills, where HDPE geomembranes are typically used, seams are made by the thermal-hot dual wedge method. From a fluid-tightness point of view, in field, the quality of this type of seams is usually assessed based on the results of the pressurised dual seam test. This method provides only qualitative information about the continuity of the seams, does not provide any information about fluid-tightness, despite the recognised vulnerability of those areas and their importance to ensure the performance of the geomembrane as barriers. Thus, a tool for assessing the quality of the seams by a quantitative measurement would be very useful. In this framework, the present work makes an attempt to provide a test method, the "gas permeation pouch test", for studying the gas-tightness of HDPE geomembrane seams.

Gas permeation pouch tests are carried out at two scales, using pouch specimens consisting of true HDPE geomembrane seams made by the thermal-hot dual wedge method. After the conclusion of the gas permeation pouch tests, the mechanical strength of the seams is also evaluated by performing peel and shear tests. Small-scale tests are performed in laboratory, using pouches prepared with different adjustable parameters of the seaming device (seaming parameters), to investigate a possible correlation between gas permeation test results and mechanical strength of the seams. Another goal of the small-scale tests is to study the suitability of the pressurised dual seam method to assess the quality of the seams. Also, two different gases are used to study the influence of the type of gas. Large-scale tests are performed, both in laboratory and in field conditions, to compare test results and to study the suitability of the gas permeation pouch test to assess the quality of the seams on site.

This chapter presents, first, the gas permeation pouch test principle, second, the basic equations used for estimating the permeation parameters of geomembranes to gas (pouch specimens immersed in air), and to water vapour (pouch specimens immersed in water) in steady conditions (permeance) and in unsteady state conditions (time constant). Third, it describes the experimental work carried out. Finally, it reports and discusses the test results.

5.2 TEST PRINCIPLE

In the gas permeation pouch test, the specimen is pressurised with a gas characterised by an initial pressure, $p_{Gin}(0)$, and is immersed in a fluid, gas or liquid (Figure 5.1). Taking into account that geomembranes are non-porous materials and that the main mechanism of migration through the intact geomembranes is the diffusion, the flux of gas across the geomembrane can be estimated based on the decrease of the pressure inside the pouch, by using the mathematical tools presented in the Chapter 3. Beyond the pressure inside the pouch specimen, other variables necessary to calculate the permeation parameters include the atmospheric pressure, temperature, volume of the pouch specimen, and relative humidity. Except for the volume, these quantities can be directly measured each time (step: δt), using different apparatus, as Section 5.6.2 will show.

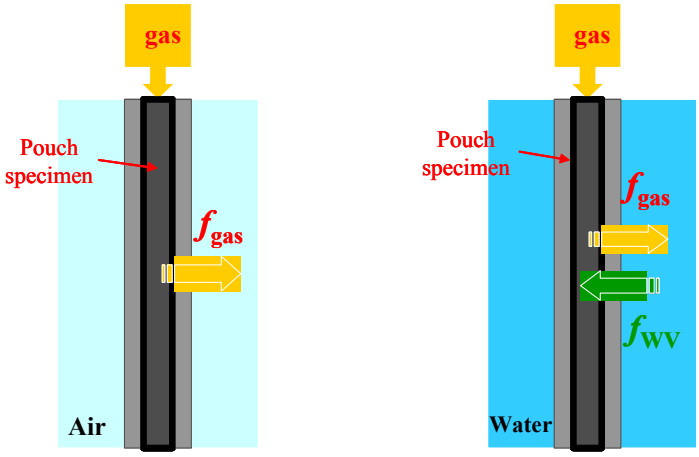

Figure 5.1 - Schematic drawing of the gas permeation pouch tests with the specimen immersed into different medium: air and water

The volume of the specimen at time t can be assessed based on Archimedes' principle. For that, the specimen is immersed in a liquid (e.g. water) and the variations in volume are estimated by monitoring the variation in water level in a capillary pipe during the test. However, in this circumstance, two simultaneous fluxes must be considered: the gas flux from inside to outside the specimen, and the water vapour flux (or other element if the liquid is not water) from outside to inside the specimen.

For evaluating the gas flux from inside to outside the specimen, a complementary test, where the same specimen is immersed in a gas (at a lower pressure than the gas inside the specimen), must be carried out. The gas migrates from inside to outside in response to the partial pressure difference, established due to the difference in gas pressure from inside to outside of the specimen. The flux of gas is estimated based on the pressure drop inside the specimen during the test. By knowing the partial pressure of the gas on both sides of the specimen, the permeability and the permeance coefficients for a specific gas can be estimated using Equations (3.7) and (3.8), respectively.

After determining the flux of gas from inside to outside the specimen, it is possible to estimate the water vapour flux (or other element) and the permeation coefficients to water (or other elements), when the same specimen is immersed in water, assuming that both the volume variations of the specimen and the gas flux from inside to outside (considering the same gas concentration difference) are the same, whenever the specimen is immersed in gas (e.g. air) or in water.

In brief, from an operational point of view, gas permeation pouch test comprises two complementary steps, one with the specimen immersed in air (subsequently designated as test in air) and other with the specimen immersed in water (subsequently designated as test in water).

To estimate the permeation coefficients of geomembrane seam specimens, according to Equations (3.7) and (3.8), it is necessary to know the area of the pouch. However, it can be observed that this area is difficult to estimate accurately. This difficulty derives from non-regular seams, and, mainly, from an irregular specimen shape when it is filled with the gas. In this case, there is no reason here to express the gas mass flux, f_G, as a function of the geomembrane area, and it is suggested that f_G should be considered as the mole flow rate

through the pouch specimen ($\Delta n/\Delta t$) expressed in mol s^{-1} instead of mol m^{-2} s^{-1}, leading to a permeance, P_G, in mol s^{-1} Pa^{-1} instead of mol m^{-2} s^{-1} Pa^{-1}. A consequence of such new definitions of f_G and P_G is that if different seamed specimens are to be compared with this method (different materials, different seam parameters), then the pouch must be made using the same procedure. For instance, pouches made using the thermal hot dual wedge method are then well adapted to the study of seam parameters if the seam length is the same.

In order to compare results of different specimens, the fluxes and permeance can also be defined by unit of seam length.

The test principle above mentioned is used to study the influence of the seaming parameters and the gas type on seams quality.

5.3 ASSESSING THE PERMEATION COEFFICIENTS IN STEADY STATE

5.3.1 Specimens immersed in air

In the gas permeation pouch tests carried out with specimens immersed in air, the flux of gas from inside to outside the specimen, f_G, can be estimated from Equation (5.1). This quantity is named as gas transmission rate, according to the terminology used by ASTM D 1434.

$$f_G = \frac{n_G(t + \Delta t) - n_G(t)}{\Delta t} \tag{5.1}$$

where f_G is expressed in mol s^{-1}, Δt is the interval of time considered in steady state and where $n_G(t)$ must be calculated, step by step, from the ideal gas law:

$$n_G(t) = \frac{p_{Gin}(t)\ V(t)}{R\ T(t)} \tag{5.2}$$

where $p_{Gin}(t)$ is here the absolute pressure (relative pressure + atmospheric pressure) measured inside the pouch at time t (Pa); $V(t)$ is the volume of the specimen at time t (m^3); R is the Universal Gas Constant (8.3143 m^3 Pa mol^{-1} K^{-1}); and $T(t)$ is the absolute temperature at time t (K).

In the case of HDPE geomembranes, the volume variations $V(t)$ with time are slight (see Section 5.6.2.1 for the measurement method): the experimental results obtained in the present research for f_G, either considering the volume constant, or considering the volume variable (1.4×10^{-10} and 1.7×10^{-10} mol s^{-1}, respectively for constant and variable volume), indicate that the volume variations were negligible, considering the measurement errors. Therefore, $V(t)$ is considered here as being constant: $V(t) = V(0)$.

In the case of more flexible geomembranes, $V(t)$ can be estimated after the experiment is conducted with the pouch specimen immersed in water, if the temperature and the difference in pressure are the same (see Section 5.3.2).

Therefore, for the HDPE geomembranes studied here, by combining Equations (5.1) and (5.2), it is possible to calculate the gas flux f_G:

$$f_G = \frac{V(0)}{R\ T(t)} \frac{p_{Gin}(t + \Delta t) - p_{Gin}(t)}{\Delta t} \tag{5.3}$$

The permeance, P_G, can then be calculated from Equation (3.8), where the partial pressure difference between inside and outside the specimen (Δp_G) cannot be considered as a constant, since the gas pressure in the specimen, p_{Gin}, decreases during the entire test. If the variations in partial pressure difference, $d(\Delta p_G)$, are minor during a reasonable number of hours, "pseudo steady state" conditions can be assumed and permeance P_G is evaluated for the mean value $\overline{\Delta p_G}$. On the contrary, if those variations are significant, unsteady state conditions prevail and a different approach needs to be followed as Section 5.4 will describe. From all the tests conducted, the criterion retained to define the "pseudo steady state" is:

$$d(\Delta p_G) < u(\Delta p_G) \text{ during } \Delta t \geq 100 \text{ hours} \tag{5.4}$$

where $u(\Delta p_G)$ represents the uncertainty concerning Δp_G.

In a steady state analysis, the mean gas partial pressure difference $\overline{\Delta p_G}$ can then be deduced from Equation (5.5):

$$\overline{\Delta p_G} = \overline{p_{Gin}} - p_{Gout} \tag{5.5}$$

where $\overline{p_{Gin}}$ is the mean pressure inside the specimen during the interval of time Δt (considered for the calculation of f_G), which can be evaluated through the equation below:

$$\overline{p_{Gin}} = \frac{1}{\Delta t} \int_{\Delta t} p_{Gin}(t)\, dt \tag{5.6}$$

While the gas *G* diffuses from inside to outside the pouch, air molecules also diffuse through the pouch from outside to inside. This flow is smaller than the precedent one because of a smaller partial pressure difference, and experiments showed that it might be considered negligible if gas *G* in the pouch is nitrogen, which is the main constituent of air. But, for other

gases (for example: CO_2), p_{Gin} is a partial pressure which is not measured in the pouch and must be calculated with the same method described in Section 5.3.2 where the pouch is immersed in water.

Finally, in Equation(5.5), p_{Gout} is the gas pressure outside the specimen. This pressure may be the partial pressure of gas *G* in the medium if this medium does not consist of pure gas *G*. It is the case of the gas permeation pouch test described in the present work, where gas *G* is nitrogen or carbon dioxide and the medium is air. In the case of nitrogen, the atmospheric pressure and the humidity must then be recorded during Δt for the calculation of p_{Gout}. This calculation is presented in Appendix A. For the carbon dioxide, p_{Gout} can be considered as zero.

The permeance calculated from $\overline{\Delta p_G}$ is then a mean permeance $\overline{P_G}$:

$$\overline{P_G} = \frac{f_G}{\overline{\Delta p_G}} \tag{5.7}$$

or by unit of seam length (*L*), as follows:

$$\overline{P_{GL}} = \frac{f_G}{\overline{\Delta p_G}\, L} \tag{5.8}$$

5.3.2 Specimens immersed in water

Regarding the tests carried out with the specimen immersed in water, two simultaneous fluxes must be considered. They correspond, respectively, to the migration of gas from inside to outside the specimen (f_G') and to the migration of water (water vapour) from outside to inside the specimen (f_W) as a result of the existing relative humidity difference.

5.3.2.1 Determining f_G'

The gas flux from the inside to the outside of the specimen (f_G') can be calculated from Equation (3.8), by considering the same specimen but taking into account a new pressure difference $\Delta p_G'$, between the two sides of the specimen, different from the Δp_G considered in the previous section. Thus, from the results of the test carried out in air (giving f_G, corresponding to Δp_G):

$$f_G' = f_G \frac{\Delta p_G'}{\Delta p_G} \tag{5.9}$$

If the concentration of gas *G* in the medium outside the specimen (which is initially pure liquid *W*) can be considered as negligible (generally the case when the fluid volume is much higher than the specimen volume), $\Delta p_G'$ can be assimilated to the partial pressure p_{Gin} of gas *G* in the specimen. Appendix B presents its calculation at each time *t*.

5.3.2.2 Determining f_W

After calculating f_G', it is possible to calculate $n_G(t)$, step by step, from the definition of f_G, (Equation (5.1)):

$$n_G(t) = n_G(t - \delta t) - f_G' \, \delta t \tag{5.10}$$

As the specimen contains $n_{G+W}(t)$ moles of elements *G* and *W* at time $t > 0$, the application of the ideal gas law gives:

$$n_{G+W}(t) = \frac{p_{G+W}(t) \; V(t)}{R \; T(t)} \tag{5.11}$$

where $p_{G+W}(t)$, $V(t)$ and $T(t)$ are, respectively, the absolute total pressure in the specimen (relative + atmospheric), the specimen inner volume and the absolute temperature, measured at time *t*.

By combining Equations (5.10) and (5.11), it is then possible to calculate, also step by step, the mole quantity $n_W(t)$ of element *W* in the specimen:

$$n_W(t) = n_{G+W}(t) - n_G(t) = \left[\frac{p_{G+W}(t) \; V(t)}{R \; T(t)} \right] - \left[n_G(t - \delta t) - f_G' \; \times \delta t \right] \tag{5.12}$$

where $V(t)$ can be considered as a constant, as mentioned in Section 5.3.1, in the case of inflexible geomembranes.

If the function $n_W(t)$ is linear during an acceptable time interval Δt (corresponding to the achievement of pseudo steady state), it will be possible to deduce the flux f_W in the same way as f_G, was deduced from Equation (5.1) in Section 5.3.1.

5.3.2.3 Determining water permeance P_W

The mean water permeance, $\overline{P_W}$, can then be obtained from f_W as follows:

$$\overline{P_W} = \frac{f_W}{\Delta p_W} = \frac{f_W}{p_{Wout} - \overline{p_W}} \tag{5.13}$$

where Δp_W is the water partial pressure difference, p_{Wout} is the pressure of liquid outside the specimen (which depends on the mean height of liquid above the specimen and on the atmospheric pressure) and $\overline{p_W}$ is the mean partial pressure of the element W in the specimen during Δt. This pressure can be obtained from the mean absolute pressure in the specimen $\left(\overline{p_{G+W}}\right)$ and from the mean partial pressure $\left(\overline{p_{G\,in}}\right)$:

$$\overline{p_W} = \overline{p_{G+W}} - \overline{p_{Gin}} \tag{5.14}$$

Mean pressures are defined as $\overline{p_{Gin}}$ in Equation (5.6) from $p_{G+W}(t)$, which is measured at each time t, and from $p_{Gin}(t)$, which is calculated at each time from Equation B.1 (Appendix B).

As for permeance to gas, permeance to water vapour can also be defined by unit of seam length (L), as follows:

$$\overline{P_{WL}} = \frac{f_W}{\Delta p_W\, L} \tag{5.15}$$

5.4 STUDY IN UNSTEADY STATE

As mentioned in Section 5.3.1, sometimes, the pseudo steady state conditions cannot be assumed since the partial pressure difference between the inside and outside of the specimen do not fulfil the criteria defined by Equation (5.4). This may occur in the case of large-scale tests, as will be explained later in Section 5.9.2.1, or in the case of poor seams, where the pressure inside the specimen decreases very quickly.

Under unsteady state conditions, considering an infinitesimal interval of time dt, Equation (5.1) can be written as follows, if volume V and temperature T are supposed to be constant:

$$f_G = -\frac{dn}{dt} = -\frac{V}{RT}\frac{dp_{Gin}(t)}{dt} \tag{5.16}$$

f_G can also be expressed as a function of permeance P_G from Equation (3.8), where the partial pressure of gas *G* outside the pouch p_{Gout} is supposed to be constant:

$$f_G = P_G \left[p_{Gin}(t) - p_{Gout}\right] \tag{5.17}$$

Combining Equations (5.16) and (5.17), the following differential equation is obtained:

$$\frac{dp_{Gin}(t)}{dt} + \varepsilon\, p_{Gin}(t) = \varepsilon\, p_{Gout} \qquad \text{where} \quad \varepsilon = \frac{R\,T\,P_G}{V} \tag{5.18}$$

The solution of Equation (5.18) can be written under the form below:

$$p_{Gin}(t) - p_{Gout} = \left[p_{Gin}(0) - p_{Gout}\right] e^{\frac{-t}{\tau}} \tag{5.19}$$

Where $p_{Gin}(0)$ is the absolute initial pressure of the gas inside the specimen, $p_{Gin}(\infty)$ is the final value of $p_{Gin}(t)$, which tends towards absolute pressure outside the specimen: p_{Gout}. Quantity τ is a constant with the dimension of time and expressed in hours if time *t* is also expressed in hours, herein termed as time constant and defined as follows:

$$\tau = \frac{1}{\varepsilon} = \frac{V}{R\,T\,P_G} \tag{5.20}$$

From the observation of the evolution of $p_{Gin}(t)$ during the testing time (see Section 5.9), it is possible to show that, after a delay time t_0, Equation (5.19) expresses the decrease in pressure in pouch the specimen with reasonable accuracy.

The time constant τ characterises the seam quality, from a permeation point of view, as well as the permeance P_G. In the case of a good seam, a long time is necessary to achieve the final steady state (corresponding to atmospheric pressure inside the pouch), leading to a high time constant value. On the other hand, this final steady state would rapidly be achieved in the case of a poor seam, corresponding to a small time constant value.

Quantity τ can be graphically determined after a few days of test: it corresponds to the inverse of the slope of the linear function *ln Z(t)*, defined in Equation (5.22), derived from Equation (5.19) for $t \geq t_0$:

$$ln\, Z(t) = \frac{-t}{\tau} \tag{5.21}$$

where

$$Z(t) = \left[\frac{p_{Gin}(t) - p_{Gout}}{p_{Gin}(0) - p_{Gout}} \right] \tag{5.22}$$

Permeance P_G can de deduced from Equation (5.20) if the inner volume V of the pouch is known.

The challenge is to turn this test into a useful tool to assess the seam quality on a regular basis, in situ, as part of the construction/quality assurance programme. In such a case, the volume V cannot be measured and the results have then to be expressed in terms of τ and not in terms of P_G.

The experimental work carried out is described and discussed in the following sections. As mentioned in the introduction, it comprised two scale gas permeation pouch tests and mechanical tests. Small-scale tests were carried out in laboratory to investigate a possible correlation between gas permeation test results and mechanical tests results, as well as to study the suitability of the pressurised dual seam method, usually used on site to assess the quality of the seams, within the framework of the quality construction/quality assurance activities. Also, two different gases were used to study the influence of the type of gas. Large-scale tests were performed, both in laboratory and in field conditions (outdoors), in order to compare the test results and to study the suitability of this test to assess the quality of the seams in situ.

5.5 SPECIMENS

The experimental work was carried out using a 2.0 mm thick HDPE geomembrane. Specimens consisted of a true seam made using the double wedge thermal seaming method (Figure 5.2). The pouch inner volume corresponds to the air channel that results between the double seams. On one extremity of the pouch, the two parallel seams are sealed by fusion. The other extremity is connected to the HDPE gas pipe. The connection between the pipe and the pouch and between the two parallel seams is achieved here by specific glue for polyolefin material: fusion must be avoided due to the risks of pipe connection damage and of polyethylene flow into the pouch.

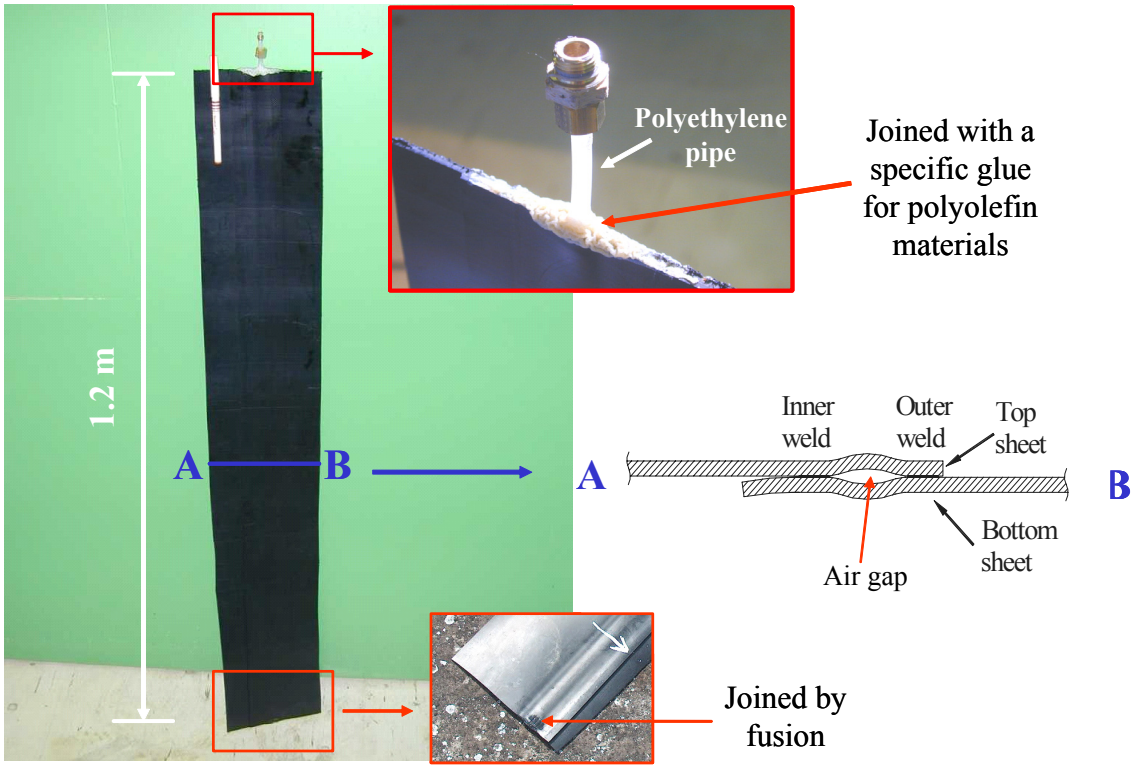

Figure 5.2 - Example of a pouch specimen for small-scale tests

The small-scale specimens were made with different adjustable parameters of the seaming device, namely velocities, temperatures and forces, aiming to study the influence of those parameters on seams quality. Table 5.1 presents the characteristics of the specimens tested in this study.

Table 5.1 - Seaming parameters of the specimens

SEAMING PARAMETERS	SPECIMENS							
	Small-scale							Large-scale
	S-9	S-10	S-11	S-12	S-13	S-14	S-15	S-LS-lab S-LS-exp
Velocity (m min^{-1})	2.5	2.5	2.5	1.8	1.8	1.5	2.5	2.5
Temperature (° C)	280	355	355	355	280	280	355	355
Force (N)	200	200	300	300	300	400	400	400

For small-scale tests, the length of the specimens (S-9 to S-15) was about 1.2 m. For large-scale tests, two different lengths were used: 10 m for the test carried out in laboratory (S-LS-lab), and 5 m for the test conducted with the specimen outdoors, exposed to weather conditions (S-LS-exp).

5.6 SMALL-SCALE TESTS

5.6.1 Apparatus

Small-scale tests were carried in laboratory using the experimental assembly presented in Figure 5.3. Tests were conducted at Lirigm, in France, except the test carried out using S-15, which was tested at LNEC, in Portugal, as Section 5.7 will describe. Test apparatus consisted of a permeation cell, a gas bottle, and measuring devices connected to a data acquisition system.

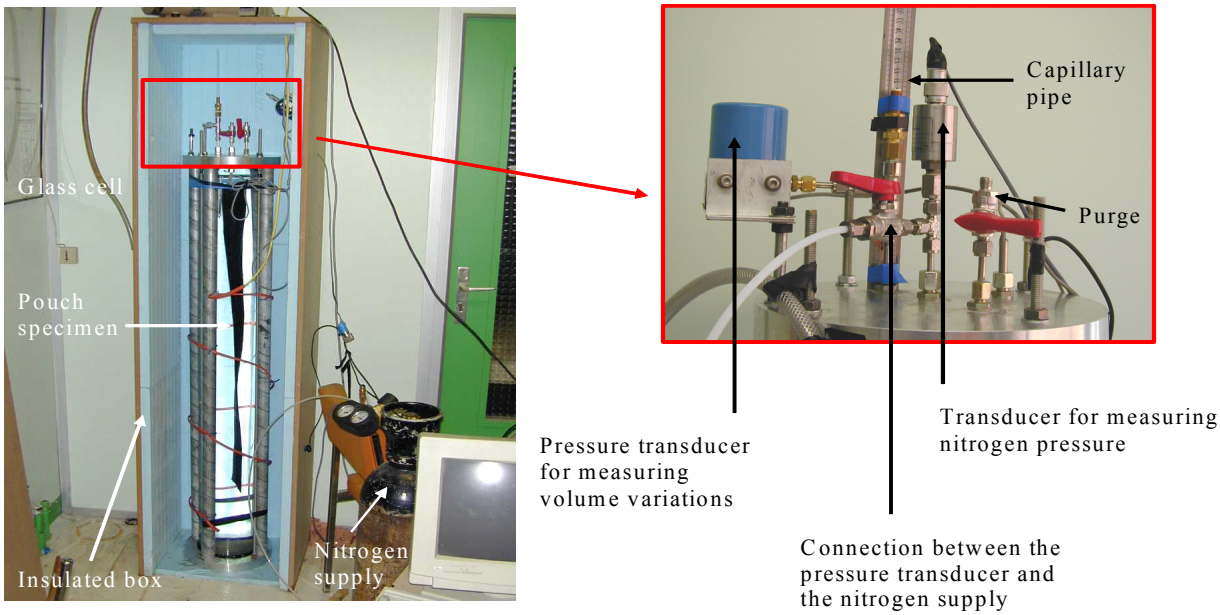

Figure 5.3 - General view of the apparatus

The permeation cell was designed to allow the immersion of each specimen either in air or in water. It consists of two circular stainless steel plates (top and base) and a glass pipe (1.5 m long, inside diameter of 0.186 m) including an agitator for homogenising the water temperature when filled with water. To the top plate are connected the measuring devices used for monitoring the test conditions. These measuring devices include: (i) a pressure transducer for measuring the gas pressure inside the specimen; (ii) sensors for characterising the ambient air temperature (maintained at 27.0 ± 0.1°C thanks to a regulation device), the atmospheric pressure, and the relative humidity. For the tests carried out with the specimen immersed in water, the additional devices as follows were used: (iii) a water temperature sensor; and (iv) a capillary pipe (0.026 m long glass pipe with a 0.00564 m inside diameter) connected to a pressure transducer, for measuring the volume variations of the pouch (transducer readings were converted into height of water in the capillary pipe and were then multiplied by the area of the pipe to obtain the volume change at each time).

5.6.2 Procedure

5.6.2.1 Test in water

After the pouch is inserted into the glass cell, which is filled with de-aired water (by means of a vacuum pump), the water level in the capillary pipe is adjusted and connected to the pressure transducer. All measuring devices are then connected, the ambient air temperature regulation device is activated and finally the pouch is pressurised with gas, at a specific pressure. Data are recorded by running a computer application especially developed for these tests.

5.6.2.2 Test in air

The water temperature sensor and the pressure transducer connected to the capillary pipe are replaced by air humidity and air temperature sensors. The test is then initialised with the same procedure as for the test carried out in water.

5.6.2.3 Initial volume, type of gas, and pressure of gas in the specimens

Before conducting any test, the initial inner volume $V(0)$ of the pressurised pouch must be determined. It was estimated indirectly by adding the volume of the pouch without pressure ($V_{prel=0}$) and the volume variation due to the pressurisation of the specimen ($dV_{p=150\ kPa}$). The volume of the pouch without pressure was determined from the weight difference between the specimen full of water and dry. The volume variation due to the pressurisation of the specimen was calculated by measuring the increase in water height in a capillary pipe connected to the cell before and after pressurisation. The time interval to do these measurements was short (a couple of minutes) to avoid variations in water height due to potential variations of temperature.

Small-scale tests were carried out using nitrogen gas. Specimen S-14 was also tested using carbon dioxide in order to study the influence of the type of gas on seam permeation coefficients. Nitrogen was chosen because it is the main constituent of the air, which is used to perform field pressure tests on seams. Carbon dioxide was chosen because it is present in landfills.

Relative pressures of 150 kPa (corresponding to an absolute pressure of approximately 250 kPa) have been used to pressurise all pouch specimens. This value was selected for having a pressure of the same order of magnitude as the one usually used in field tests.

5.7 LARGE-SCALE TESTS

The large-scale permeation testing assembly (Figure 5.4) consists of a gas bottle, an absolute pressure transducer for measuring the gas pressure inside the specimen and a data acquisition system. Air temperature, relative humidity and atmospheric pressure were also measured using a sensor (Rotronic BM 90), which is also shown in the figure.

Figure 5.4 - Large-scale test assembly

Tests were carried out with specimens in air, using nitrogen gas. Like in small-scale tests, the specimen was pressurised with nitrogen at 150 kPa (relative pressure) by introducing gas into the gap between the two parallel welds. Gas drop inside the specimen was monitored during the test.

The initial inner volume of the pressurised pouches was estimated from the mean value by unit of length obtained in small-scale tests.

Two large-scale tests were performed at LNEC, under different test conditions. The specimen S-LS-lab was tested in a conditioned laboratory, at a temperature of 20 ± 2ºC and a relative humidity of 65 ± 5%. This means, at different conditioning conditions than the ones used in small-scale tests conducted in gas permeation cell at Lirigm (27 ± 0.1ºC, 50 ± 5% relative humidity). Thus, in order to compare the results, a sub-specimen (S-15) was cut from the large-scale specimen and it was tested in the same test conditions as the ones of the large-scale test.

A second large-scale test was carried out with the same apparatus but with the specimen S-LS-exp placed outdoors, on top of the laboratory building roof, without controlled temperature and humidity. The aims of this test were to simulate the field conditions and to identify the shortcomings of performing gas permeation pouch tests on site.

5.8 MECHANICAL TESTS

Mechanical properties of the specimens were assessed after completion of the gas permeation pouch tests, by conducting shear and peel test. The aim of these tests was to study a possible correlation between the gas permeation coefficients and the mechanical strength of the seams.

The tests were conducted in laboratory using a field tensiometer available at LNEC (Figure 5.5). It contains a memory card where it is possible to record the results of elongation (%), force (N), and testing velocity (mm min^{-1}) during the tests. It can also display the values of force and elongation at yield and break. Grip separation can range from 0 mm to 300 mm. Testing velocities are also adjustable, ranging from 10 to 300 mm min^{-1}.

Figure 5.5 - Tensiometer used for performing the mechanical seam tests

Shear and peel strength tests (Figure 5.6) were performed based on ASTM D 4437. From each gas permeation test specimen (S-9 to S-14, and S-LS/S-15), ten test strip-specimens were cut using a 25 mm wide die. The initial grip separation was 24.4 mm in peel mode and 101.2 mm in shear mode. Testing velocity was 51 mm min^{-1}. Peel test was performed on both seams of each specimen. Shear strength, peel strength, and type of failure, in the peel test, were recorded.

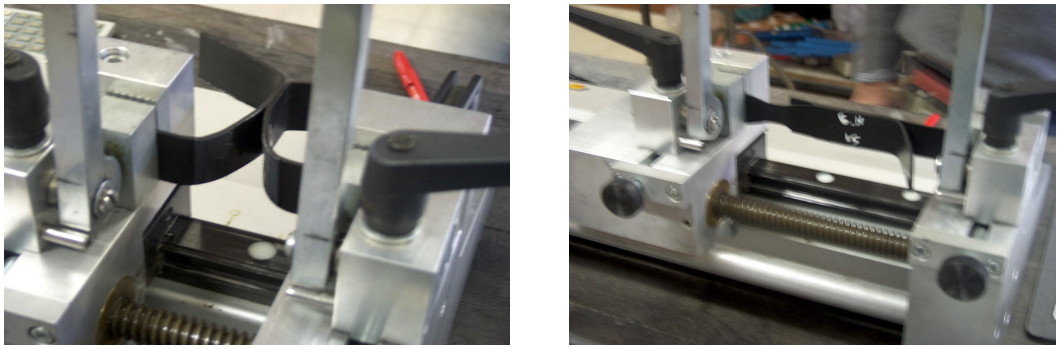

(a) Peel test (b) Shear test

Figure 5.6 - Mechanical tests in progress

Shear and peel test results were then evaluated based on the criterion presented in USEPA report (Daniel & Koerner 1993). Recalling Section 2.3.1.2.3, the seam shear strength must be higher than 95% of the yield strength of the unseamed geomembrane, and the seam peel strength must be higher than 62% of the yield strength of the unseamed geomembrane. To assist in the interpretation of the results, the yield strength of the unseamed geomembrane was determined based on ASTM D 638. A mean 18.6 MPa tensile stress at yield was obtained. Since the nominal thickness of the unseamed geomembrane sheet is usually used for the comparison value, i.e. the tensile stress at yield of the unseamed geomembrane is multiplied by the thickness and the results are presented accordingly in kN m^{-1}, the thickness was also

estimated. This property was evaluated based on ASTM D 5199. A mean value of 2.0 mm was obtained.

Considering the tensile stress at yield obtained for the unseamed geomembrane (18 MPa) and the nominal thickness of the geomembrane, acceptable seams, from a mechanical point of view, would have a peel strength ≥ 23 kN m^{-1} and a shear strength ≥ 35 kN m^{-1}.

In addition, the location of the failure and separation in peel were also analysed, considering the cases presented in Figure 5.7. In types (a) and (b), the failure occurs outside the seam, which is typically called film tearing bond (FTB), and there is no peel separation. In the types (c) to (g), peel separation occurs in variable percentage regarding the seam area.

Location of failure		Failure description
	(a)	Failure in sheeting. Failure can be on either top or bottom sheet. There is no peel separation.
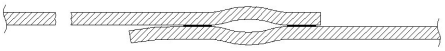	(b)	
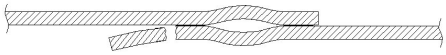	(c)	Failure at outer edge of seam. Failure can be on either top or bottom sheet. Some peel separation is observed.
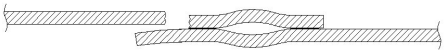	(d)	
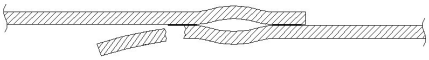	(e)	Failure in inner weld after some adhesion failure. Failure can be on either top or bottom sheet. Considerable peel separation is observed.
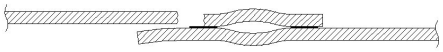	(f)	
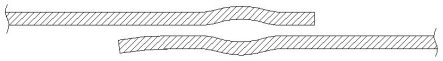	(g)	Adhesion failure.

Figure 5.7 - Location of the failure in peel test (based on NSF 54 1993)

Results obtained in these tests are presented in sections below. Sections 5.9.1 and 5.9.2 are respectively dedicated to small and large tests. Section 5.9.3 compares the different results, after uncertainty calculations. Finally, Section 5.9.4 is devoted to the mechanical tests. The results are then discussed in Section 5.10.

5.9 RESULTS

5.9.1 Small-scale tests

5.9.1.1 Evolution of gas pressure inside the specimens

Figure 5.8 shows the drop in the absolute pressure of nitrogen over time, for specimen S-14. Only specimen S-14 is presented in interest of brevity. Similar results were obtained with the other specimens and they are presented in Appendix C.

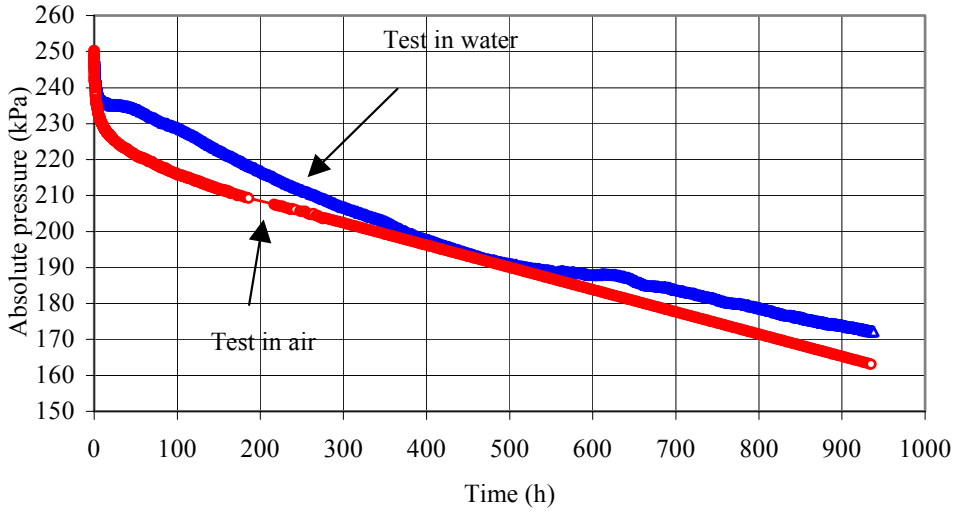

Figure 5.8 - Decrease in the absolute pressure of nitrogen for S-14 during the test in air and in water

As can be observed in Figure 5.8, the results obtained with tests carried out in air and water present a similar trend. The absolute pressure of nitrogen decreased with time in both tests. It dropped 87 kPa (58 %) for the test in air, and 77 kPa (51 %) for the test in water.

5.9.1.2 Fluxes and permeances

The number of moles of nitrogen, $n_{N2}(t)$, permeating through the specimen S-14 (air test) during a pressure interval where a pseudo steady state could be assumed was estimated from Equation (5.2). It is plotted versus time in Figure 5.9 (results obtained with the other specimens are presented in Appendix C). The nitrogen flux (f_{N2}) was then calculated from the slope of this line. For comparison purposes, f_{N2} was evaluated considering the same pressure interval, approximately 220-208 kPa, whenever the pseudo steady state was achieved (results in Table 5.2).

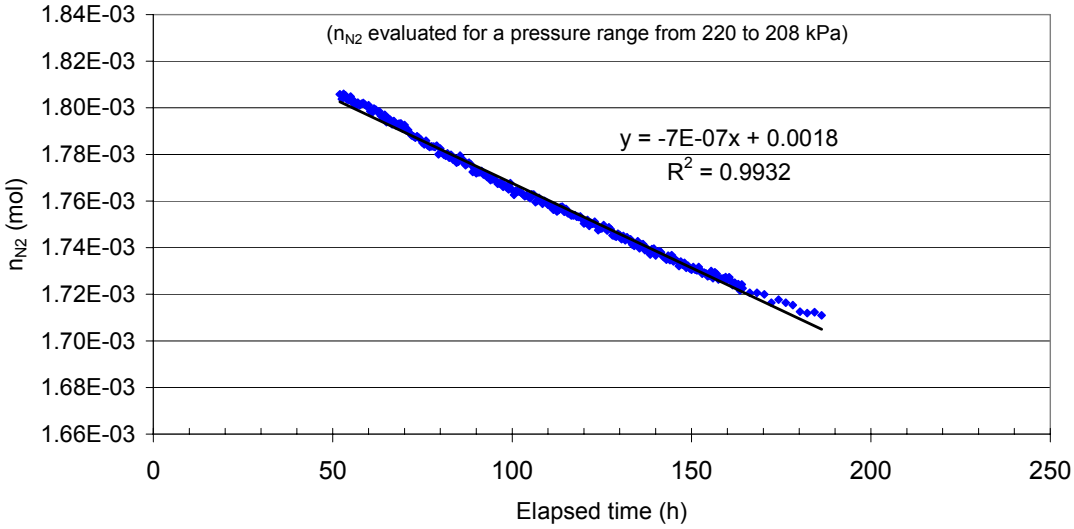

Figure 5.9 - Nitrogen quantity permeating through the S-14 in test carried out with the specimen in air

As regards the test conducted with the specimens immersed in water, to calculate the different quantities defined in Section 5.3.2, it is necessary to be sure that the nitrogen moles passing through the geomembrane do not concentrate in the water layer adjacent to the pouch, which would affect the value of the partial pressure outside the specimen. Agitating the water (for temperature homogenisation purposes) minimises this risk. Furthermore, nitrogen diffuses easily in water. Its diffusion coefficient is 2.6×10^{-9} m^2 s^{-1} (Reid et al. 1987), with a solubility coefficient of Bunsen equal to 0.01557 (Air Liquide 2002). The latter coefficient gives the volume of nitrogen that can be dissolved in the unit volume of water. In the experiments conducted for this study, the number of nitrogen molecules that reach the water by crossing the geomembrane and the number of nitrogen molecules that can be dissolved in water are of the same order of magnitude. Therefore, no nitrogen bubbles were observed, or could have been observed, in the water.

The number of moles of nitrogen that migrated from inside to outside and the number of moles of water vapour that migrated from outside to inside of the specimen due to the humidity difference, was estimated using Equations (5.10) and (5.12), respectively. Results showed that the water vapour flux towards the inside of the specimen was small compared with the nitrogen flux: the water vapour flux was even non-measurable at the beginning of the test (approximately 600 hours). After that time until the end of the test, the flux of water vapour was two orders of magnitude less than the flux of nitrogen. These results might be attributed to the relatively low water vapour pressure difference (mean partial pressure difference around 80 kPa), requiring long testing times before the permeation starts. The hydrophobic features of the HDPE geomembranes may also raise difficulties in the water vapour migration process.

Based on these results, for testing times used in the present work, the water vapour flux across the specimens was considered negligible, and it was not taken into account in subsequent tests. For that reason, the results presented below will not include the f_W and P_W. Besides, by taking into account that the main goal of the test in water was to measure the volume of the specimen at each time, which was considered constant for practical purposes, since negligible variations of volume were observed after the pseudo steady state achievement, the test in water became worthless for flux measurements carried out with nitrogen gas. Nevertheless,

test in water was important for carbon dioxide. Although it is possible to calculate the permeance of carbon dioxide from test in air, by considering simultaneously the flux of carbon dioxide from inside to outside and the flux of nitrogen (main constituent of air) from outside to inside the specimen, i.e. by adopting a procedure identical to the one used to calculate the flux and permeance to water vapour, more accurate flux and permeance to carbon dioxide are obtained from the test in water. In fact, for the testing times used in this study, it could be seen that the flux of water from the outside to the inside of the specimen is insignificant and therefore can be disregarded.

Table 5.2 presents the nitrogen and the carbon dioxide fluxes, as well as the correspondent permeances by unit of length. Gas fluxes were estimated from the slope of $\Delta n/\Delta t$, with Δn estimated from Equation (5.2) during an absolute pressure interval ranging from approximately 220 to 208 kPa. This pressure interval was chosen because it could be observed that the pseudo steady state conditions could be assumed for all tested specimens. Permeances were calculated from Equation (5.8). The mean partial pressures (estimated from Equation (5.5)) are also included in Table 5.2.

As refers to nitrogen gas, it can be seen from Table 5.2 that small differences were obtained in different pouch specimens, either to fluxes, or to permeances. Values of f_{N2L} ranged from 1.1×10^{-10} to 1.7×10^{-10} mol m^{-1} s^{-1}, and P_{N2L} ranged from 9.7×10^{-16} to 1.0×10^{-15} mol m^{-1} s^{-1} Pa^{-1}. Specimens S-10 and S-13 failed, the first one a couple of hours after being pressurised and, the second one, after 140 hours.

Concerning the carbon dioxide, a flux of $f_{CO2L}=1.2\times10^{-9}$ mol m^{-1} s^{-1}, and a correspondent permeance of $P_{CO2L} = 5.9\times10^{-15}$ mol m^{-1} s^{-1} Pa^{-1} were obtained.

Table 5.2 – Gas fluxes and permeances for tested specimens

Specimens			S-9	S-10	S-11	S-12	S-13	S-14	S-15
Seam parameters	Velocity (m min^{-1})		2.5	2.5	2.5	1.8	1.8	1.5	2.5
	Temperature (ºC)		280	355	355	355	280	280	355
	Roller pressure (kN m^{-2})		200	200	300	300	300	400	400
Specimen features	Length (L) (m)		1.17	1.2	1.18	1.19	1.30	1.14	1.29
	Initial volume (V_0) (m^3)		2.7×10^{-5}	-	2.3×10^{-5}	1.7×10^{-5}	2.1×10^{-5}	2.0×10^{-5}	2.4×10^{-5}
Test results (air test)	Δp_G (kPa)	N_2	122	Failed	136	139	Failed	140	136
		CO_2	-	-	-	-	-	208	-
	Gas flux per unit length (mol m^{-1} s^{-1})	N_2	1.2×10^{-10}	Failed	1.4×10^{-10}	1.4×10^{-10}	Failed	1.7×10^{-10}	1.1×10^{-10}
		CO_2	-	-	-	-	-	1.2×10^{-9}	-
	Gas permeance per unit length (mol m^{-1} s^{-1} Pa^{-1})	N_2	9.7×10^{-16}	Failed	1.0×10^{-15}	1.0×10^{-15}	Failed	1.2×10^{-15}	0.8×10^{-15}
		CO_2	-	-	-	-	-	5.9×10^{-15}	-

5.9.1.3 Time constant

The approach outlined in Section 5.4 can be used to evaluate the time constant from $p_{Gin}(t)$ in unsteady state conditions. For nitrogen, the time constant was evaluated from the air test, whereas for carbon dioxide it was assessed from water test, for the same reason as for permeance (see Section 5.9.1.2). Figure 5.10 shows an example of the relationship between *ln Z* and time for specimen S-12.

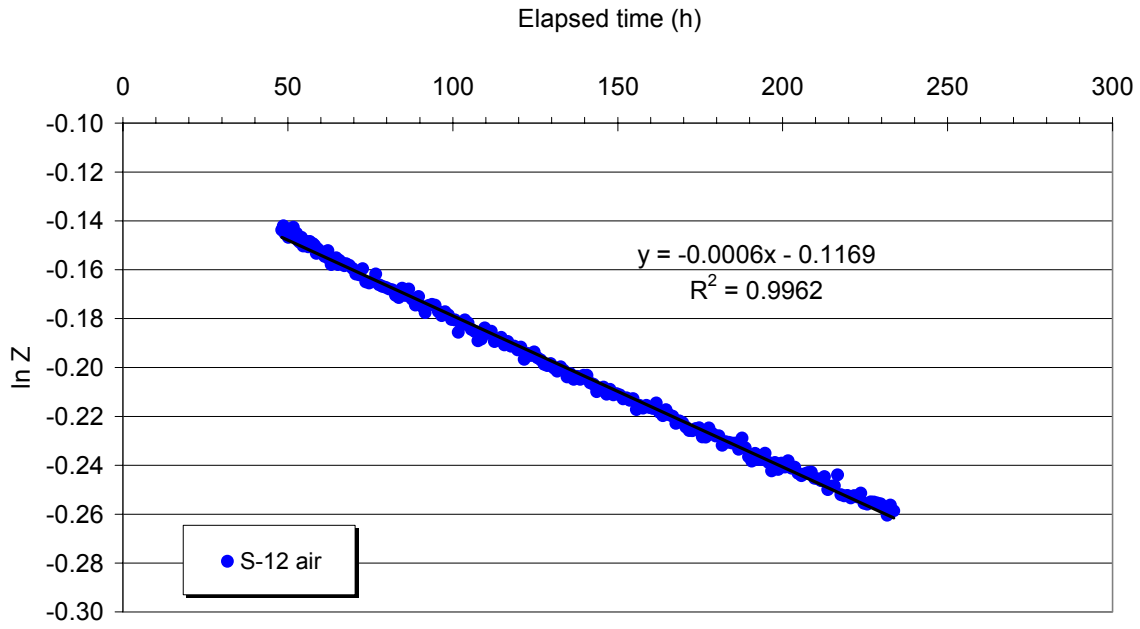

Figure 5.10 – Relationship between *ln Z* and time for S-12

Table 5.3 shows the results obtained for the different specimens. It also includes the delay time t_0 after which Equation (5.19) properly modelled the experimental data, $p_{Gin}(t)$, and for calculating τ. As can be seen, τ ranged from approximately 1700 to 2500 hours for specimens that were able to keep the pressure without failure, whereas a much lower value was obtained (τ around 160 hours) for the specimen that failed (S-13). This result suggests that this coefficient might be useful to identify poor seams.

Furthermore, it could be observed that the time after which Equation (5.19) was suitable to express the behaviour of the specimens changed with the gas. In general, for nitrogen, that equation properly models the behaviour of the specimens after approximately 48 hours, whereas for carbon dioxide longer testing times are necessary (140 hours).

Table 5.3 - Results of time constant for the tested specimens

Specimens			S-9	S-10	S-11	S-12	S-13	S-14	S-15
Seam parameters	Velocity (m min^{-1})		2.5	2.5	2.5	1.8	1.8	1.5	2.5
	Temperature (ºC)		280	355	355	355	280	280	355
	Roller pressure (kN m^{-2})		200	200	300	300	300	400	400
Test results (air test)	Delay time, t_0 (hours)	N_2	~ 48	Failed	~ 48	48	48	48	~ 48
		CO_2	-	-	-	-	-	140	-
	Time constant, τ (hours)	N_2	2500	Failed	2500	1667	159	1667	2500
		CO_2	-	-	-	-	-	1000	-

Note: ~ = approximately

5.9.2 Large-scale tests

5.9.2.1 Evolution of gas pressure inside the specimen

Figure 5.11 shows the evolution of the absolute pressure during the large-scale test carried out with specimen in laboratory (S-LS-lab). This test lasted for approximately 193 days (4637 hours). The mean atmospheric pressure recorded during that period was 101 kPa. As can be observed, in six months, the relative nitrogen pressure inside the specimen decreased 136 kPa (95 % of the initial value), corresponding to a drop of 44 % in absolute pressure.

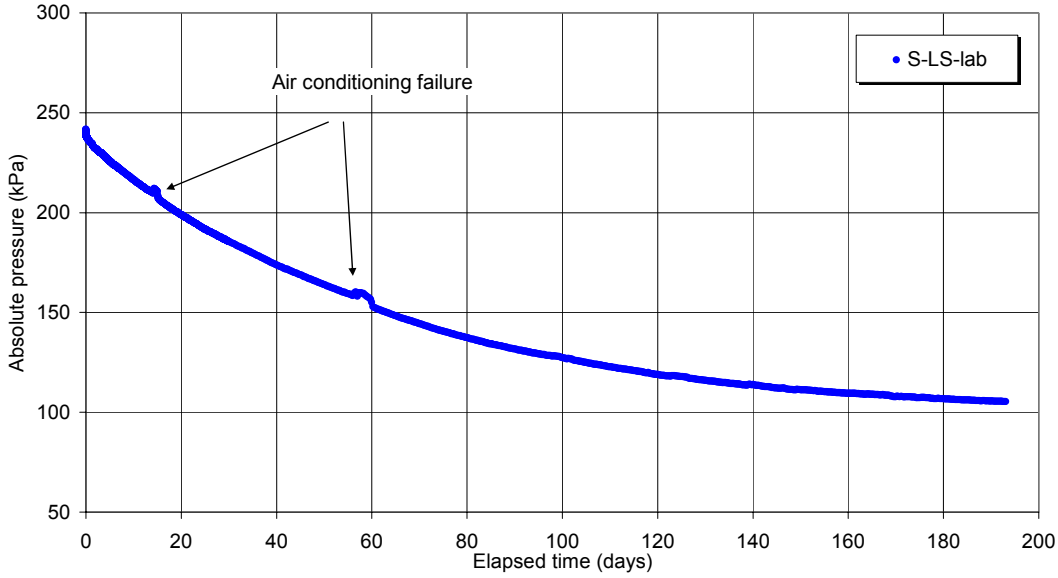

Figure 5.11 - Decrease in the absolute pressure of nitrogen during the large-scale test conducted in laboratory

This test is long enough to observe that the pressure inside the pouch tends toward atmospheric pressure and not toward the nitrogen partial pressure in ambient air. This is due to oxygen and hydrogen which diffuse from outside to inside the pouch, while nitrogen is diffusing from inside to outside the pouch, leading to a pressure balance on both sides of the geomembrane at an infinite time. It shows that an error is made when calculating τ from Equations (5.21) and (5.22) assuming that $p_{Gin}(\infty)$ is equal to p_{N2out} and not p_{atm}. Section 5.9.2.2 will show that this error is compatible with the uncertainty range and that the comparison of the permeance P_{N2}, calculated from τ (Equation (5.20)) and from "pseudo steady state" analysis shows a good agreement.

Regarding the large-scale test conducted with the specimen exposed outdoors (Figure 5.12), a leak was observed at 309 hours (approximately 13 days), and thus the test was disassembled.

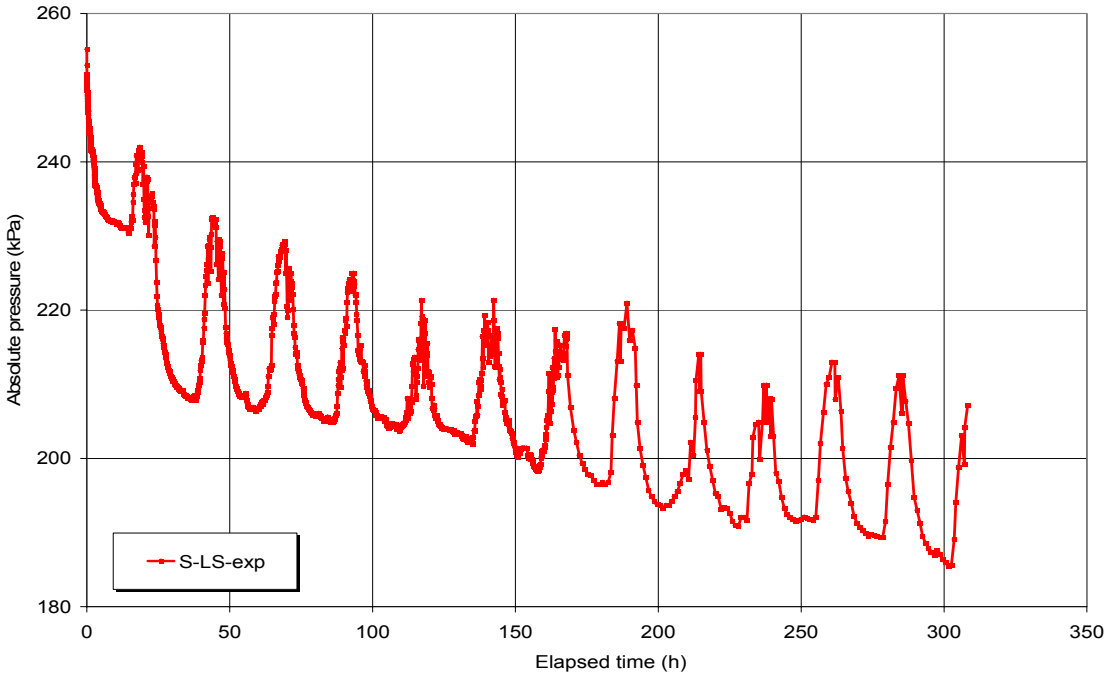

Figure 5.12 - Decrease in the absolute pressure of nitrogen during the large-scale test conducted with the specimen exposed

It can be observed that in large-scale tests the pseudo steady state could not truly be assumed as in small-scale tests. Actually, the nitrogen pressure difference between the inside and the outside of the specimen could not be considered as constant for an acceptable time interval (criteria defined by Equation (5.4) not fulfilled). Thus, results of these tests are going to be analysed based on time constant determination in the subsequent section.

5.9.2.2 Time constant

The first step for assessing the time constant parameter, τ, consisted in evaluating *ln Z*, using Equation (5.21). Results obtained with two large-scale tests undertaken were plotted versus time in Figure 5.13, for the same testing times. Regarding specimen exposed at environmental conditions (S-LS-exp), for minimising the effects of temperature on pressure (in agreement

with ideal gas law), only the values of pressure registered at the same temperature each day were used to estimate τ. The time constant was then calculated from the inverse of the slope of the lines depicted in Figure 5.13. The values obtained were:

S-LS-exp: τ_{N2} = 1700 hours;

S-LS-lab: τ_{N2} = 2000 hours.

It should be noted that the time constant could be calculated from the exposed specimen even if important variations in pressure occur each day due to temperature variations between day and night. However, if such test has to be conducted in situ under any weather conditions, it is suggested to measure ambient temperature every hour and to register pressure inside the pouch, whenever ambient temperature is within an acceptable range.

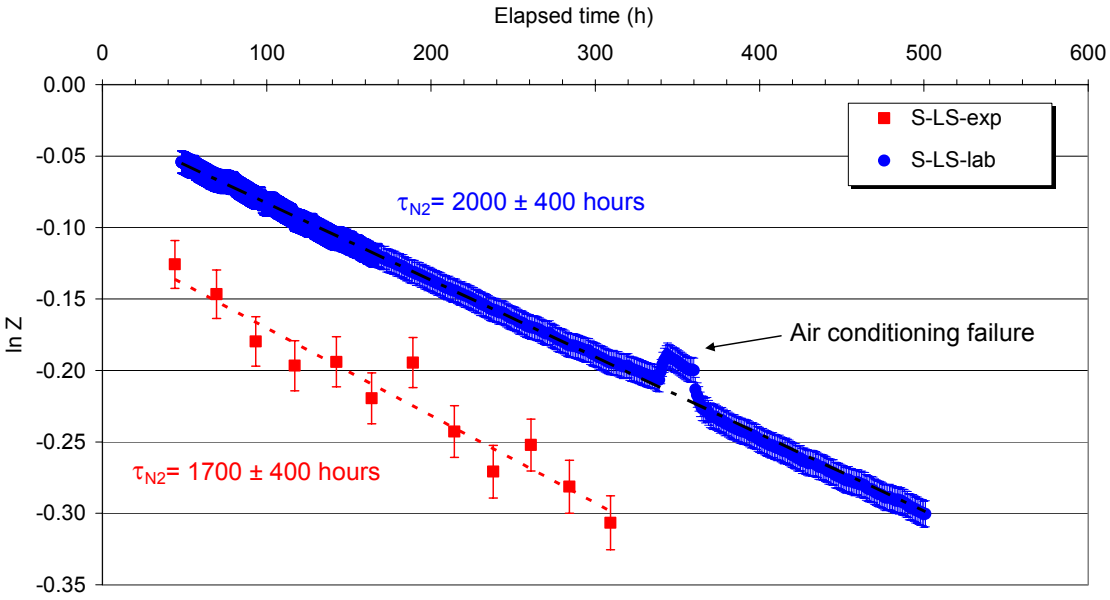

Figure 5.13 - Relationship between *ln Z* and time for large-scale tests carried out in laboratory (S-LS-lab) and exposed (S-LS-exp)

Even though the pseudo steady state conditions could not be achieved, for comparison purposes, both the nitrogen flux and the corresponding permeance were estimated for S-LS-lab, considering the same pressure interval as for small-scale tests (approximately 220-208 kPa) and assuming that the volume was constant during the test. This was not done for specimen S-LS-exp because, in this case, the volume varies with temperature, and the volume variations of the specimen during the test were not monitored as the test was carried out in air.

The number of moles of nitrogen permeated through the specimen S-LS-lab was calculated from $p_{N2}(t)$ using Equation (5.2). The result is plotted versus time in Figure 5.14. The f_{N2} was then calculated from the slope of this line. This coefficient, per unit of length, was $f_{N2L} = 1.7\times10^{-9}$ mol m^{-1} s^{-1}. The corresponding nitrogen permeance, per unit of length, was $P_{N2L}=1.2\times10^{-15}$ mol m^{-1} s^{-1} Pa^{-1}, estimated for a mean partial pressure of 137 kPa.

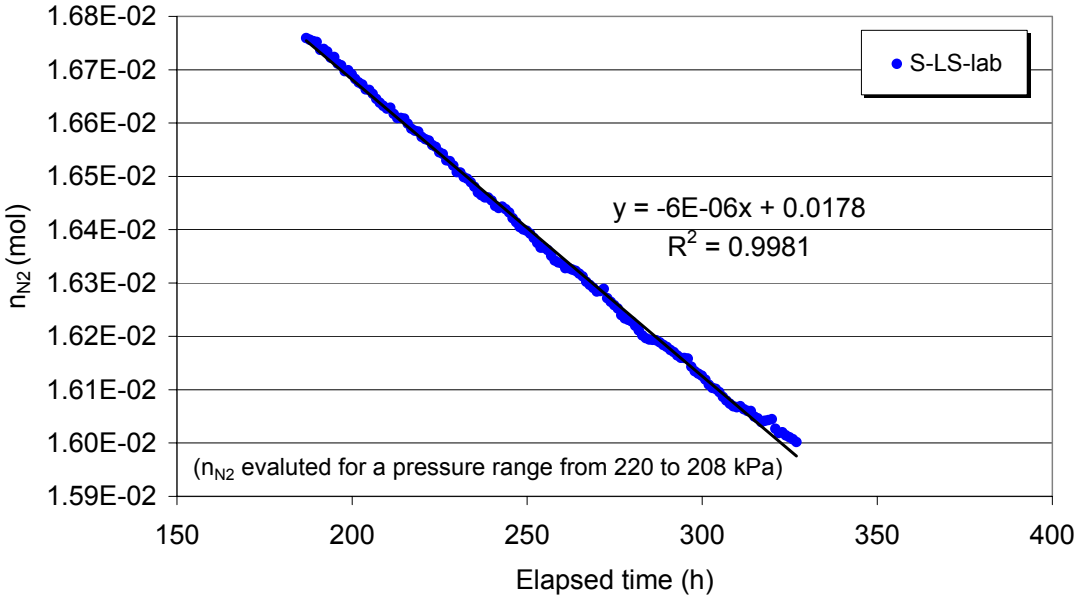

Figure 5.14 - Number of moles of nitrogen permeated through the specimen S-LS-lab

Although with a higher uncertainty, for S-LS-lab, the permeance P_{N2} was also calculated based on Equation (5.20). The results obtained using these two approaches were identical, suggesting that:

- this parameter can be estimated with a reasonable accuracy both under pseudo steady state and under unsteady state conditions;
- the error called up in Section 5.9.2.1 about $p_{Gin}(\infty)$ has an insignificant influence on τ calculation.

However, taking into account that in situ "pseudo steady state" conditions are generally not achieved and that the pouch volume V (necessary to deduce permeance P_G from τ) cannot be estimated in field, it is suggested hereafter, to consider the time constant as the measured parameter obtained from unsteady state conditions and the permeance as the measured parameter obtained from "pseudo steady state" conditions.

Before comparing the test results, the uncertainties associated to experimental measurements need to be estimated, which is presented in the following section.

5.9.3 Uncertainties and comparisons between test results

The uncertainties associated with the permeance were evaluated according to Appendix D, for small and large scale test (specimen S-LS-lab). The results obtained are shown in Figure 5.15. It can be seen that, for the different specimens, the uncertainties associated to nitrogen are similar and they are higher than the permeance variations. Based on these results, the

permeance to nitrogen can be considered similar for all tested specimens, including large-scale test, where pseudo steady state criterion was not fulfilled.

The uncertainty associated to carbon dioxide was higher than for nitrogen, because the flux of carbon dioxide, from which permeance is estimated, was assessed considering a smaller time interval (few hours) than the fluxes of nitrogen (few days). Smaller uncertainty would be obtained for carbon dioxide if a larger time interval were considered. This was not the case because it would make it impossible to estimate the gas flux using the same pressure interval considered for the other tests (approximately 220-208 kPa). By taking into account the uncertainty obtained in this case, the differences obtained between permeance corresponding to nitrogen and carbon dioxide are meaningful.

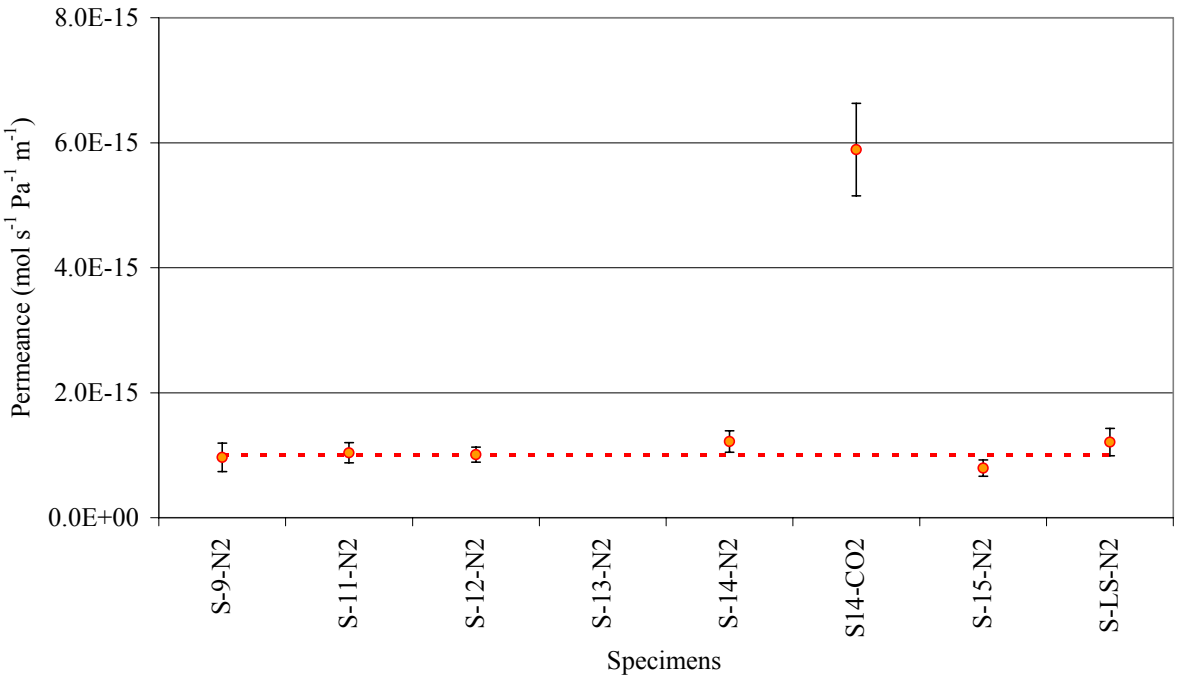

Figure 5.15 – Uncertainties associated to the evaluation of permeance

The uncertainty associated with the time constant (Appendix D) was also estimated for small and large scale tests, and the results obtained are depicted in Figure 5.16. The uncertainty was generally less than 500 hours, except for S-9 where a higher value was obtained. The high uncertainty associated with specimen S-9 is due to the fact that this test was finished too early. It should be noted that, in this test, the drop in pressure was very small compared to the other tests.

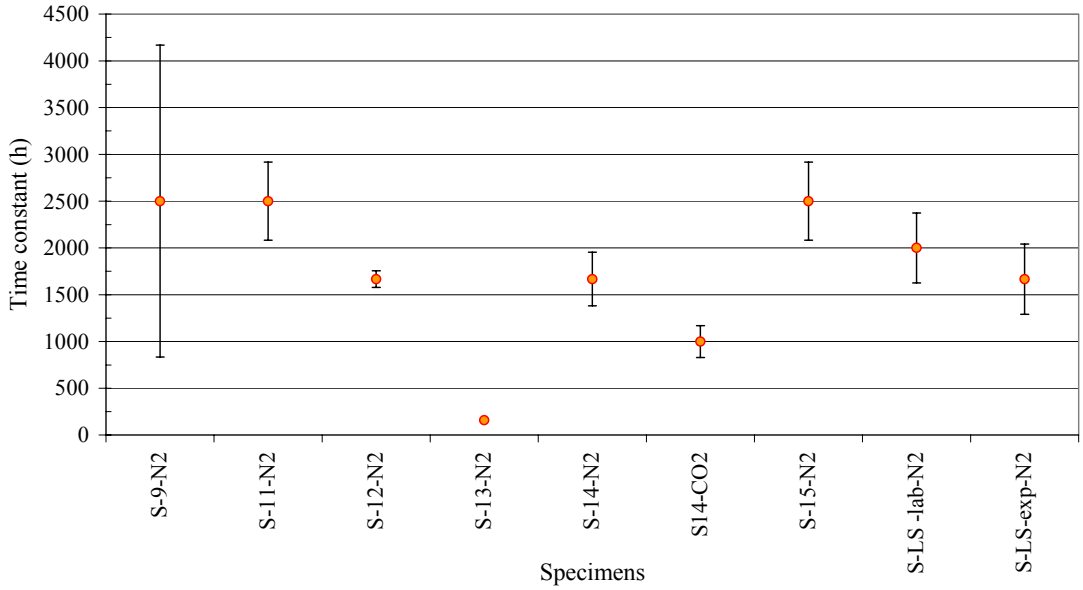

Figure 5.16 – Uncertainties associated to the evaluation of time constant parameter

Comparison between Figure 5.15 and Figure 5.16 clearly shows that it is easier to differentiate a test result by permeance measurement than by time constant measurement: differences between carbon dioxide flux (specimen S-14) and nitrogen flux (other specimens) are clearer on Figure 5.15 than on Figure 5.16. In addition, by taking into account uncertainties, all results are in agreement, which suggests that it is possible to characterise on site the gas permeability of seams by means of the time constant.

5.9.4 Mechanical tests

Table 5.4 summarises the results obtained from the mechanical tests. The first aspect examined was to check if the seams of the pouch specimens met the acceptance criterion suggested by USEPA (Daniel & Koerner 1993), i.e. a peel strength > 23 kN m^{-1} and a shear strength > 35 kN m^{-1} (see Section 5.8). It could be observed that, in the peel test, only specimens S-12 and the S-LS/S-15 met the acceptance criterion, whereas in the shear test all specimens met it. The results of shear strength showed no significant variation for the different specimens: 2.6 kN m^{-1}. Unlikely, the peel strength showed a large variation for the different specimens: 23.7 kN m^{-1}, for inner weld and 21.7 kN m^{-1}, for outer weld. These results can be explained by the fact that whereas the peel strength concerns seam adhesion, the shear strength concerns the geomembrane sheets (failure always occurs in the sheet adjacent to the weld).

Then, the location of the failure and the separation, in the peel test, were analysed according to Figure 5.7. It could be observed that peel separation always occurred. Nevertheless, in specimens S-12 and S-LS/S-15 the percentage of separation through the seam varied, ranging from 10 %, in failures type (c) and (d), to 100 %, in failures type (g). The analysis done seems to confirm that, except for specimens S-9 and S-LS/S-15, the adhesion of the seams in pouch tests was poor.

Table 5.4 - Results of the peel and shear tests

Specimens			S-9	S-10 [(1)]	S-11	S-12	S-13 [(2)]	S-14	S-LS/S-15
Peel	Mean peel strength (kN m^{-1})	inner weld	12.1	9.5	12.7	25.9	3.6	4.5	27.3
		outer weld	8.3	6.1	11.4	24.3	3.2	9.8	22.9
	Location of failure in each of the five peel specimens (according to Figure 5.7)	inner weld	g	g	g, g, g, e, g	c, g, g, c, f	g	g	c
		outer weld	g	g	g	d, d, f, d, f	g	g	e, g, c, c, e
Shear	Mean shear strength (kN m^{-1})		36.9	37.1	37.6	38.1	37.6	38.5	39.5
Acceptance criteria from USEPA (Daniel & Koerner 1993)			Fail	Fail	Fail	Pass	Fail	Fail	Pass

[(1)] Gas permeation pouch test failed a couple of hours after being pressurised.

[(2)] Gas permeation pouch test failed before reach the pseudo steady state.

5.10 DISCUSSION

5.10.1 Correlation between gas permeation pouch test results and mechanical test results

Within the framework of the quality construction/quality assurance (QC/QA) activities, during the installation of geomembrane lining systems, HDPE seams are usually destructively tested through shear and peel tests according to the project specifications (generally every 150 to 500 linear meters) and non-destructively tested by pressurised dual seam method (100 % of the seams length). Destructive tests require repairs, more seams to do (patches), and need to be re-tested. These operations are time consuming and expensive. In this context, searching for a correlation between mechanical and permeation coefficients could be very helpful and could reduce significantly the number of destructive tests.

The relationship between the gas permeation and the mechanical strength of the pouch specimens, consisting of a true seam made using the double-wedge thermal seaming method, was analysed based on the results of gas permeation pouch tests and seam peel tests (small-scale tests). The results of the seam shear tests were not included in this analysis because, in tested specimens, the shear failure always occurred in the sheet adjacent to the weld. Thus, strength values obtained in this tests concern mainly unseamed geomembrane sheets. This explains why the shear strength was similar in the different specimens, conversely to peel strength that refers to seam adhesion. This approach is in agreement with the recommendations repeatedly made by Peggs (e.g. 1994a, 1996b). According to this author, shear strength does not provide useful information about seam bond.

When comparing the results of gas permeation pouch tests to mechanical tests, it can be seen that the poorest seam (specimen S-13), from a mechanical point of view, is also the poorest one, from a gas permeation point of view. Specimen S-13 presented the lowest peel strength and it failed during the gas permeation pouch test. This trend is also confirmed by the time

constant parameter, where a very low value was attained for S-13 (159 hours) compared with the other specimens (mean value about 2000 hours). These results suggest that the gas permeation pouch test is able to identify the poorest seams.

On the other hand, it is more difficult to find a correlation between mechanical tests and permeation tests for the good specimens: specimens S-12 and S-15 seem clearly to be the best from a mechanical point of view. It is confirmed by the permeance test for specimen S-15, which shows a permeance 20% less than the average permeance obtained for nitrogen flux and a time constant 20% higher than the average one obtained for nitrogen flux. Nevertheless, specimen S-12 shows a permeance similar to the average one and a time constant 15% less than the average one. Therefore, it is only possible to conclude that mechanical tests are more selective than permeation tests.

Results also show that peel tests can easily express the seam differences (seaming parameters) unlike gas permeation pouch tests. Destructive tests are the best approach to evaluate seams quality. Furthermore, peel test is also important because it can provide useful information on the probable durability of the geomembrane adjacent to the seams. According to Peggs (1994a, b; 1996b) the durability can be compromised if the peel specimen fails in a brittle manner (loss of ductility). Brittle failures might be due mainly to overheating or by excessive grinding during the seaming process. Overheating increases the susceptibility of the geomembrane to stress cracking by consuming protective oxidants, increasing oxidation, and crystallinity. Besides, it can cause stress concentrating notch geometries on the bottom of the geomembrane. In addition, when a HDPE geomembrane seam is not adequately bonded and separates in a peel test, crazes (precursors of stress cracks) may be induced on the separated surfaces (Peggs 1996b). Therefore, peel separation and adjacent geomembrane ductility are important issues to study bond efficiency and stress cracking. Thus, peel test is an indispensable tool to analyse the long-term performance of geomembranes.

To sum up, it can be concluded that a seam validated by a peel test is also a good seam from a permeation point of view, with a proven safety margin. This is an important conclusion, which highlights peel test significance.

5.10.2 Studying seaming parameters

Gas permeation pouch tests do not allow any optimisation of seaming parameters since resulting differences between specimens cannot be correlated to seam parameters. But this conclusion can also be applied to mechanical tests: specimen S-10, which failed during the permeation test, produced similar results compared to specimen S-14, which gave good results during the permeation test. Fortunately, peel test results obtained on specimens S-10 and S-14 would have led to their rejection in field.

Furthermore, there is no obvious correlation between the seaming parameter values of specimen S-10 and S-13 and the fact that they both failed during the permeation test. Actually, on the one hand, the range of seaming parameters values is probably not large enough to observe tangible variations in test results and, on the other hand, choosing the seaming parameters out of this range leads to the risk of failure during the permeation test.

Therefore, it can be concluded that unlikely gas permeation pouch tests, mechanical tests make it possible to define an acceptable range of seaming parameters, but without giving the possibility of optimising them.

In addition, it must be pointed out that if we consider nitrogen flux, and by taking into account uncertainties, permeance results are similar whatever the specimen considered, whereas differences up to 30 % are observed on the same specimens when comparing time constant results. Such differences cannot be directly attributed to the different seaming parameters that characterise the specimen: as mentioned before, except for poor seams, it is difficult to establish a correlation between mechanical tests results and permeation tests results. Thus, one must be very careful in interpreting time constant variations from one specimen to another. Actually, they may be due to the seam quality but also to the non-perfect reproducibility of the unsteady state. It must be reminded that the permeance was calculated for each test from a similar pseudo steady state corresponding to similar experimental conditions, which may help in obtaining more homogeneous values of permeance when compared to time constant values.

5.10.3 Influence of the type of gas

The influence of the type of gas was studied by carrying out two tests under the same test conditions, using either nitrogen or carbon dioxide. Specimen S-14 was randomly selected to perform this study. It could be observed that the flux of nitrogen was about one order of magnitude less than the flux of carbon dioxide, leading to a permeance to nitrogen five times less than the permeance to carbon dioxide (see Figure 5.15) and a time constant with nitrogen that is 40 % higher than the time constant with carbon dioxide (see Figure 5.16). Such results are significant when uncertainties are taken into account, and are consistent with the findings reported by Haxo et al. (1984) to different gases.

5.10.4 Suitability of the pressurised dual seam method for assessing seams quality on site

As mentioned in Chapter 2, in field, HDPE seams are typically non-destructively tested by the pressurised dual seam method to evaluate their quality. In that method, the existing gap between both seams is pressurized by air injection. The seam is considered acceptable if no air pressure drop occurs during a specified time interval (3 to 5 minutes for an initial air pressure ranging from 200 to 300 kPa). This qualitative test does not provide any information about the long-term fluid-tightness of the seam. The suitability of the pressurised dual seam method has never been verified in laboratory. To address this issue, results obtained from gas permeation pouch test with specimen S-13 are analysed.

Specimen S-13 was able to keep itself pressurised with nitrogen during about 140 hours, which means that, on site, this seam would never be rejected with the traditional control even though it should not be allowed to remain in service. It can be argued that this seam would be rejected because it presents low mechanical strength, but the fact is that destructive tests do not cover 100 % of the seams. The results obtained with specimen S-13 suggest that the pressurised dual seam method might not be suitable for evaluating the long-term quality of the seams, and it highlights the need to improve the tools currently used for that purpose.

In this respect, it is interesting to observe that the time constant obtained for this specimen was very low: 159 hours, whilst for the specimen that did not fail the mean value of τ was 2000 ± 500 hours. This observation is very important for QC/QA purposes since it seems that by identifying seams with low time constant, seams with poor peel strength are also detected. Therefore, it appears that the time constant can be a useful tool to identify the poorest seams.

Based on the above mentioned observations, a question arises: is it possible to conduct gas permeation tests in situ and estimate time constant in a testing time compatible with the QC/QA activities? This issue will be addressed in section below.

5.10.5 Designing a gas permeation pouch test on site

To design a test adaptable in situ, it is necessary:

- to know if results obtained on small-scale specimens are in agreement with results obtained on large-scale specimens: it is necessary to compare the in situ results with reference values of τ, which are obtained from laboratory tests conducted on smaller specimens;
- to define the minimum time required to determine the time constant.

Concerning the first point, looking at Figure 5.16 and Table 5.3, it can be seen that, for the large-scale specimen (S-LS-lab) and the small-scale (specimen S-15, tested in the same conditions of temperature and relative humidity as specimen S-LS-lab), the difference obtained on time constant was lower than the uncertainties associated to these test results, and within the same range as the differences observed for all small-scale specimens tested with nitrogen, that is about 20 %, as already analysed in Section 5.10.1. It also can be observed that the two large-scale specimens present a similar time constant taking into account the uncertainties (difference about 15 %).

Regarding the minimum time required for this test, time constant was calculated in the case of the large-scale specimen tested exposed to weather conditions, when considering different time intervals after the two days delay time (t_0). Figure 5.17 shows that a minimum time interval of 4 days is necessary to obtain a time constant compatible with the one calculated at the end of the test (that is within the uncertainty range). It means that the minimum duration of the test in situ, to take into account the 2 day delay time, is about 6 days.

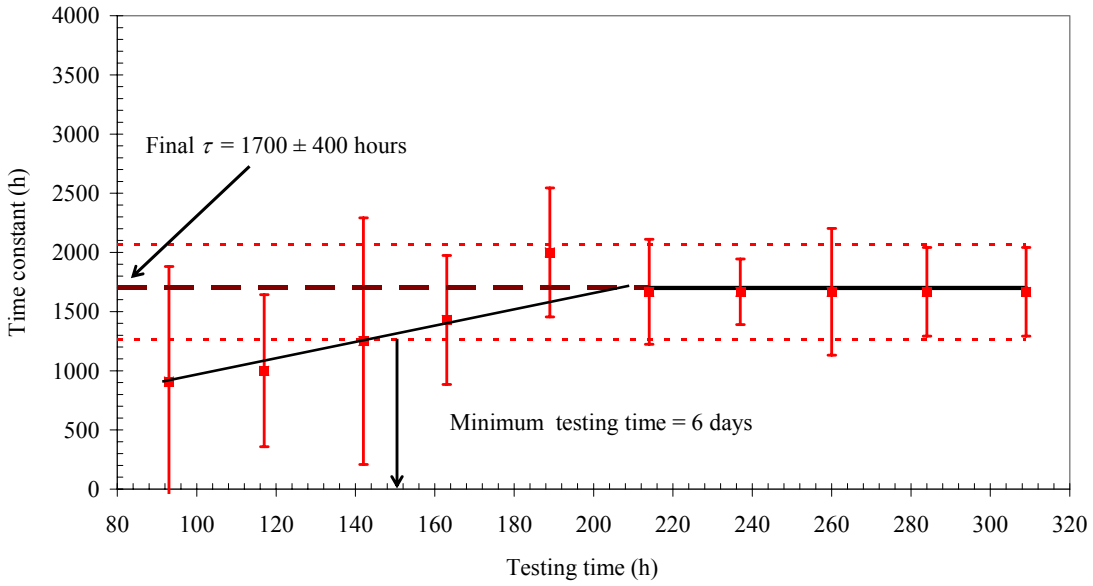

Figure 5.17 – Time constant values calculated for different testing time intervals (S-LS-exp with time interval all considered from t_0 = 44 hours)

These results tend to confirm that the gas permeation pouch test can be used in situ to assess the quality of double hot wedge seams if a week-long test is acceptable. Concerning this testing time, which may look too long, it must be mentioned that the pressure measurement can be automatically and simultaneously recorded in several seams. Furthermore, it should be reminded that the gas permeation pouch test is a non-destructive test, therefore additional repairs and re-tests are only necessary in case of rejected seams.

5.10.6 The limits of the gas permeation pouch test

5.10.6.1 Gas pressure inside the pouch

If the gas pressure inside the pouch is too high, the resulting tensile stress in the geomembrane near the seam and at weak places (e.g. connections, seam joins) may be too high and the gas permeation pouch test becomes a mechanical test. The tests conducted on pouches showed that with a relative gas pressure in the pouch of 150 kPa, the pouches made by thermal hot dual wedge method did not present any damage. It should be noted that 150 kPa is less than the usual relative air pressure used in field to control the seams made by the thermal hot dual wedge method. Experience from field tests shows that those pressures do not affect the mechanical properties of the seams. Furthermore, any damage due to a too high pressure in the pouch can be easily detected by a quite different pressure decrease with time from the one corresponding to a non damaged pouch.

5.10.6.2 Connections and geomembrane thickness

The connection of the gas pipe to the pouch is a potential weak point and must be carefully done using specific connections and specific types of glue (Figure 5.2). Any resulting damage can be easily detected by a quick pressure drop inside the specimen.

Nevertheless, such connections require a minimum value of the geomembrane thickness to be effective. For a membrane thickness that is less than 0.5 mm (which is strictly not recommended in landfill applications), the connections used in the experiments described in this paper may be ineffective. For testing thin geomembranes (films), this connection problem should be solved and the pouch should probably be tested under lower gas pressure. Furthermore, as mentioned in Chapter 3, the geomembrane thickness is difficult to be measured with the required accuracy resulting in the use of permeance instead of permeability. For example, the thickness variation of geomembranes from blown film line is $\pm$ 0.2 mm.

5.10.6.3 Geomembrane flexibility

Only HDPE geomembranes, which are relatively inflexible, were used in the gas permeation pouch tests reported here. Therefore, all specimens showed a negligible volume variation during the test. Thus, it was possible to assess the gas permeation coefficients based only on test in air. For more flexible geomembranes, both tests (in air and in water) are required, since the volume variation of the pouch is determined from the level of water (Section 5.3.2).

5.10.6.4 Variation in temperature

For flexible geomembranes, for which it is necessary to carry out tests with specimens immersed in water to know the volume of the specimen at each time, the relation between the variations in temperature and in volume must be taken into account for calculating the flux and, consequently, the permeance. Even when the tests are conducted in conditioned laboratories or in isolating boxes, the temperature may change during the testing time. Therefore, the volume, measured from the variation of level in a capillary pipe (Section 5.6.1) must be corrected by removing the effect of the dilatation of water. For instance, in the apparatus used in the present work, a variation of 0.5ºC during the test would cause an increase in height of water in the capillary pipe of approximately 18 cm. This clearly shows the need to perform the correction.

On site, the variation in the temperature can also affect the time constant, since variations in temperature are linked with variations in volume and in pressure and are in agreement with the ideal gas law. In this case, for calculation purposes, it is suggested to consider the values of pressure registered at similar temperatures. In this way, the volume can be considered constant, and the measured variations in pressure during time are caused by a drop in pressure as a result of gas flux from inside the specimen to outside. Consequently, monitoring the ambient temperature during testing time must be done in the field.

5.10.6.5 Measuring devices

The uncertainty calculations carried out in this study underlined the necessity of using calibrated devices. The calibration is important to identify the components of the uncertainty. The absence of calibration makes it difficult to correct measurements, as well as to identify the quantities that have a significant impact on test results.

Generally, in the present work, when there was no calibration, the assumptions done were based on experience.

5.10.6.6 Comparisons with literature

A shortcoming of the above mentioned gas permeation pouch tests is that no comparisons with other experimental results can be done because, for that, normalised data must be used (i.e. by unit of area). However, as previously mentioned, an accurate measurement of the area of the pouches used in the present work was impossible. Besides, it should be pointed out that the tests were designed to study the geomembrane seams. A way to confirm the obtained results would be to test other pouch specimens where the percentage of the seamed area would be negligible compared to a non seamed area, in order to assess the permeation coefficients of the geomembrane materials. Actually, for them, there are some experimental results available as the following section illustrates.

5.11 REVISING THE WORK OF HURTADO-GIMENO (1999)

By taking into account the shortcoming mentioned above, data reported by Hurtado-Gimeno (1999) - see Section 3.5.3 - were recalculated according to the procedure presented in Section 5.3. The work of Hurtado-Gimeno (1999) is focused on the permeability of HDPE geomembranes to gas by using circular pouches, where the seamed area (seals) was negligible compared with the non-seamed geomembrane.

The pouch specimens used consisted of two overlapped circular sheets joined by the thermal-hot dual wedge seaming method (diameter of 0.6 m, area of 0.635 m^2, and initial inner volume of 0.04296 m^3). Tests were performed either immersing the specimens in air, or in water, under a temperature of 27ºC.

Figure 5.18 shows the results obtained for the test carried out with the specimen in air during 40 days. The relative nitrogen pressure inside the specimen decreased 6 kPa (17 % less than the initial value), corresponding to a decrease of 5 % in absolute pressure.

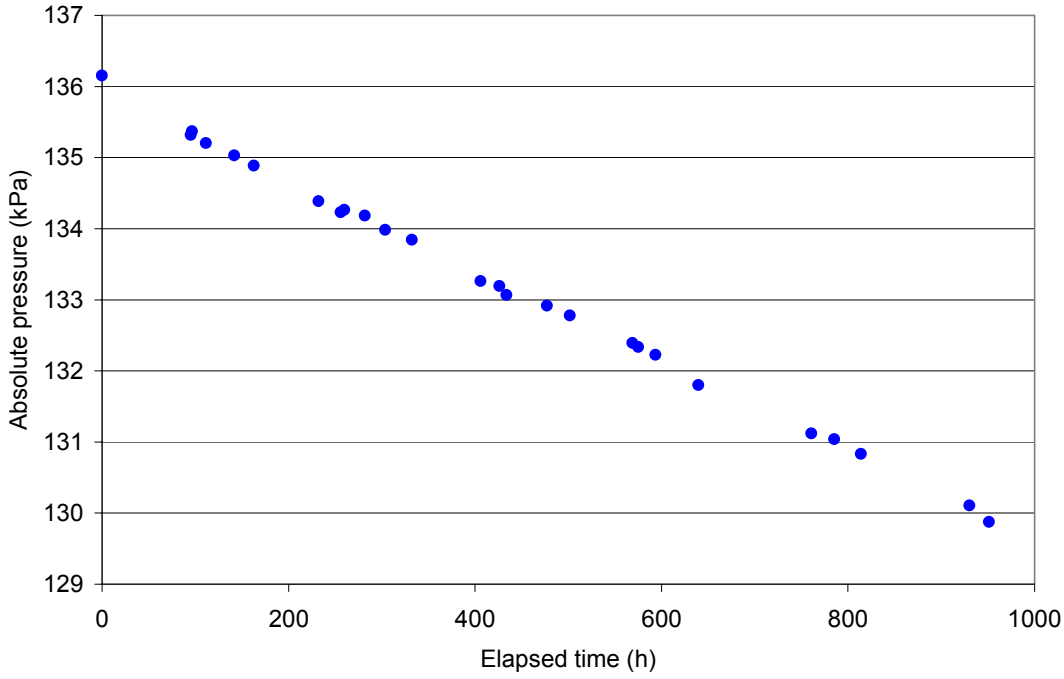

Figure 5.18 - Decrease in the absolute pressure of nitrogen inside the specimen during the test in air (data from Hurtado-Gimeno 1999)

For the test carried out with the pouch in air, the number of nitrogen moles $n_G(t)$ that migrated through the specimen was calculated from $p_G(t)$, using Equation (5.2). The result is plotted versus time in Figure 5.19. This figure also shows that the function $n_{N2}(t)$ is rapidly linear, which corresponds to a rapid steady state achievement.

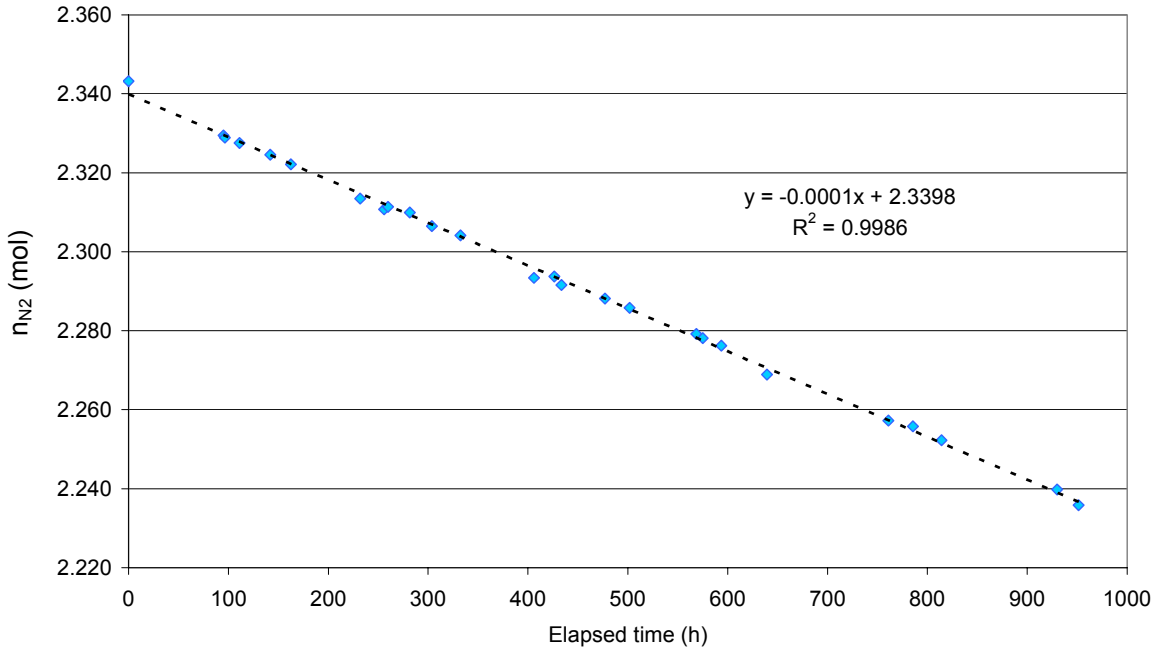

Figure 5.19 - Quantity of nitrogen permeating through the circular pouch specimen (data from Hurtado-Gimeno 1999)

The nitrogen flux was calculated from the slope of that line. This flux, by unit of area, was: $f_{N2} = 4.2\times10^{-8}$ mol s^{-1} m^{-2}.

The nitrogen permeance (by unit of area) was then determined based on Equation (5.7), for a mean partial pressure difference of 55 kPa:

$\overline{P_{N2}} = 7.6\times10^{-13}$ mol s^{-1} Pa^{-1} m^{-2}.

It is interesting to compare these results with results obtained by other authors. Nevertheless, due to the different specimen shapes tested, the comparison must be done in terms of the coefficient of permeability, despite all the disadvantages reported in Section 3.2 as regards the characterisation of geomembrane permeability by this coefficient. The permeability to nitrogen obtained for the 1.5 mm thick HDPE geomembrane was:

$\underline{P_{N2}}'' = 1.1\times10^{-15}$ mol s^{-1} Pa^{-1} m^{-1}.

It must be pointed out that even though $\underline{P_{N2}}''$ is here expressed in the same unit as the permeance per unit of seam length (Equation (5.8)), these two quantities are quite different and cannot be compared.

This result is compared in Table 5.5 with earlier findings reported by Park (1986) and by the Encyclopedia of Polymer Science and Technology (1964), for films of HDPE polymer. It is

also compared with test results obtained with unseamed circular specimens of HDPE geomembranes tested with air (Lambert 1994) and with nitrogen (Hurtado-Gimeno 1999), as described in Sections 3.5.2 and 3.53, respectively. Considering that the coefficient of permeability depends on the thickness, the test conditions, the gas specimen, the temperature, and the polyethylene quality, the order of magnitude of the coefficient of permeability to nitrogen can be considered consistent with the values presented in literature.

Table 5.5 - Comparison of the order of magnitude of HDPE geomembrane permeability coefficients to gas

Reference	Gas permeability, $\underline{P_G}''$ (mol m^{-1} s^{-1} Pa^{-1})	
	Nitrogen	Air
Park (1986)	0.8×10^{-15}	-
Encyclopedia of Polymer Science and Technology (1964)	0.4×10^{-15}	-
Lambert (1994)	-	0.2×10^{-15}
Hurtado-Gimeno (1999), manometric cell (see Section 3.5.3)	10^{-15}	
Present work (data from Hurtado-Gimeno 1999, circular pouch specimens)	1.1×10^{-15}	-

As regards to the data obtained from the tests carried out with the pouch specimen immersed in water, it could be observed that the absolute pressure inside the specimen decreased by roughly 3 % during the first 30 days of the test, increasing later on to reach a value of the same order of magnitude as the initial pressure (Figure 5.20). These results differ from the results obtained in the present work, in which the pressures only dropped during the tests. Nevertheless, the results obtained by Hurtado-Gimeno (1999) are not surprising. In fact, they are in agreement with the hypothesis considered in Section 5.3. According to that hypothesis, two flows occur simultaneously through the specimen: the nitrogen flow from the inside to the outside, leading to a decrease in absolute pressure, and the water flow from the outside to the inside, leading to an increase in absolute pressure. This result shows that water flow, in the case of large circular specimens, is much higher than in the case of double seamed specimens, where, as mentioned in Section 5.9.1.2, it was negligible compared to nitrogen flux.

The differences in pressure results between the pouch specimens used for studying the seams and the large circular specimens used by Hurtado-Gimeno (1999) for studying geomembrane permeability might be attributed to differences in pouch specimens and test conditions.

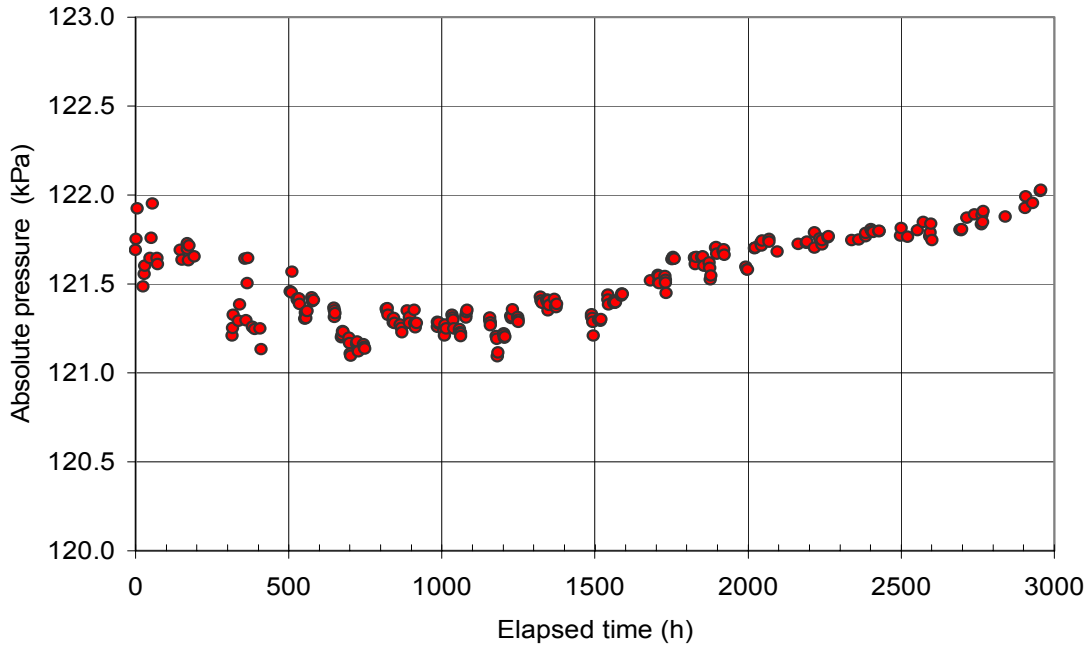

Figure 5.20 – Decrease in the absolute pressure of nitrogen inside the specimen during the test in water (data from Hurtado-Gimeno 1999)

The number of moles of nitrogen (n_{N2}) and of water (n_W) permeating through the specimen was then estimated by Equations (5.2) and (5.12), respectively. Figure 5.21 shows the results of these calculations. In the same figure, the number of moles of nitrogen and water is plotted against time.

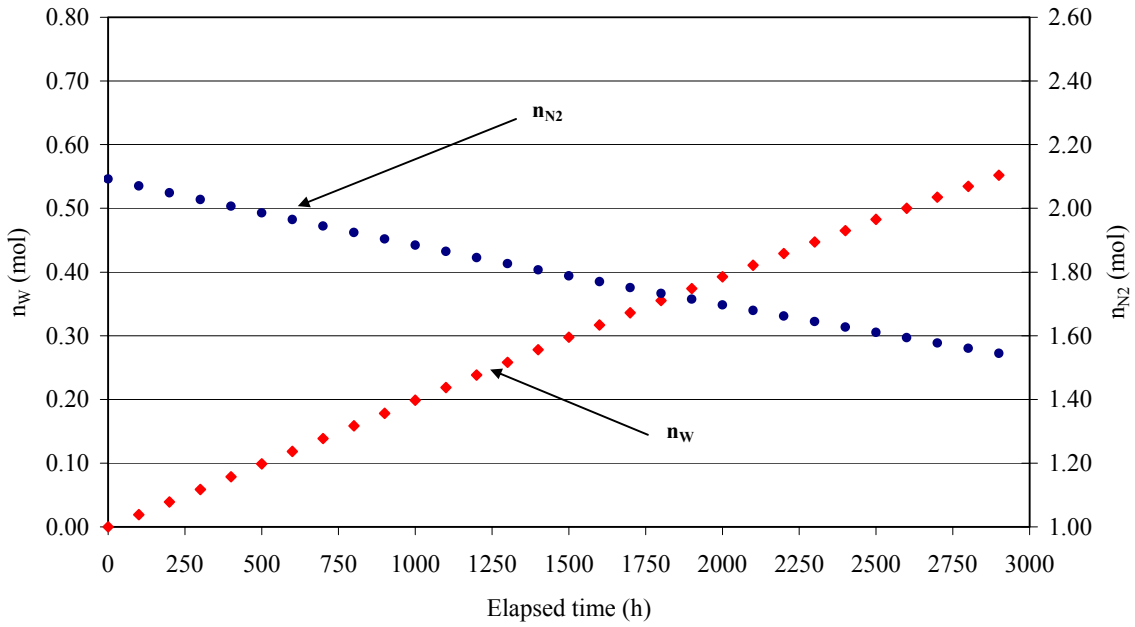

Figure 5.21 - Number of moles of n_{N2} and n_W permeated through the specimen during the tests carried out with the specimen immersed in water (data from Hurtado-Gimeno 1999)

It is interesting to observe that n_W presents a linear variation with time. It confirms that the steady state was achieved in the same way as in the test carried out in air, but over a longer period of time. The water vapour flux, f_W, was calculated from the slope of that line. This flux, by unit of area, was:

$f_W = 8.0\times10^{-8}$ mol s^{-1} m^{-2}.

The water permeance (by unit of area) was then determined based on Equation (5.13), for a mean partial pressure difference of 84 kPa:

$\overline{P_W} = 9.5\times10^{-13}$ mol s^{-1} Pa^{-1} m^{-2}.

Similarly to the results for nitrogen permeability, the results obtained for HDPE geomembrane permeability to water vapour are compared in Table 5.6 (using the coefficient $\underline{P_W''}$) with other results reported in literature (Haxo et al. 1984, Haxo 1990, Rogers 1985) and show an acceptable agreement with nitrogen permeability results.

Table 5.6 - Comparison of the order of magnitude of HDPE geomembrane permeability coefficients to water vapour

Reference	Water vapour permeability, $\underline{P_W''}$ (mol m^{-1} s^{-1} Pa^{-1})
Haxo et al. (1984), Haxo (1990)	7×10^{-15}
Rogers (1985)	8×10^{-15}
Present work (data from Hurtado-Gimeno 1999)	1.4×10^{-15}

The revision of Hurtado-Gimeno (1999) work showed permeability results consistent with values reported in the literature for nitrogen and for water vapour. Based on the comparisons done, it was concluded that the methodology outlined in the present work for the exploration of results might be considered suitable. Compared with other permeability tests with special seals, often presenting leaking problems, sometimes corresponding to a flow of the same order of magnitude as the flow that is to be estimated, as pointed out by Park (1986) and by Koerner & Allen (1997), the advantages of this test can be summarised as follows: first, it can be easily performed in any laboratory, and second, it has no specific seals (pouches are made by means of welding techniques used in situ).

5.12 SUMMARY AND CONCLUSIONS

This chapter presented the experimental work carried out to determine the gas permeation coefficients and the time constant of pouch specimens consisting of true HDPE seams made by the thermal-hot dual wedge method, as well as the mechanical strength of the correspondent seams. Gas permeation coefficient is evaluated if a pseudo steady state can be achieved, whereas time constant is evaluated under unsteady state conditions.

Gas permeation pouch tests were conducted in two scales, according to the same test principle. Small-scale tests were carried out in laboratory to investigate a possible correlation between gas permeation test results and mechanical strength of the seams (assessed by performing peel and shear tests), as well as to study the suitability of the pressurised dual seam method typically used in situ to assess seams quality. In addition, two different gases (nitrogen and carbon dioxide) were used to study the influence of the type of gas. Large-scale tests were performed, in laboratory and in field conditions (outdoors), in order to compare test results and to study the suitability of this test to assess the quality of the seams in situ.

The comparison between the results of permeation tests and mechanical tests showed that the poorest seam, from a mechanical point of view, is also the poorest, from a gas permeation point of view, which validates mechanical test results. This trend is also confirmed by the time constant, as a very low value was obtained for the poorest seam. Thus, it appears that gas permeation pouch test is able to identify poor seams. The results also suggest that mechanical tests, particularly the peel test, are more severe and more adequate to test seam durability.

It could be observed that one specimen with a poor seam was able to keep itself pressurised for approximately 150 hours. This seam would be accepted in field by the acceptance criteria typically based on the pressurised dual seam method (field tests only last a few minutes). This result suggests that pressurised dual seam method might not be suitable for evaluating the quality of the seams in the long term and highlights the need to improve the tools currently used in the field.

The results of small-scale tests also showed that the gas flux and the corresponding permeances varied with the penetrant molecules. Gas flux was approximately one order of magnitude higher for carbon dioxide than for nitrogen and as for the permeance, half an order of magnitude of difference was found. Regarding the time constant parameters, a lower value was obtained for carbon dioxide than for nitrogen, suggesting that this parameter also varies with the gas used.

The results of the large-scale test carried out with the specimen outdoors showed that it is possible to assess the quality of double hot-wedge seams, from a non-destructive test conducted in situ by determining the time constant. It seems that the time constant measurement might be an alternative tool to detect very poor seams. The values of this parameter measured in situ during a week, or less in case of very poor seams, may be compared with the ones of the reference seam (gas permeation pouch tests may be determined in laboratory on smaller specimens).

Compared to peel tests, the disadvantage of the gas permeation pouch test is its duration, but the advantages are as follows: (i) the test is non-destructive; (ii) the information about the seam quality obtained by this procedure is as relevant as the results from peel tests, contrary to many other non destructive tests, and (iii) it concerns the whole seam. Such a test cannot replace destructive tests, namely the peel tests, which have proven here to be the most adequate to calibrate seam parameters. However, it can be used for a better and easy non-destructive control of thermal-hot dual wedge seams.

The work reported here attempted to show the principle, feasibility and interest of the gas permeation pouch test. Other in situ tests, on different materials, under different conditions are now necessary to validate it.

6 EXPERIMENTAL WORK ON ADVECTIVE FLOW RATES THROUGH COMPOSITE LINERS DUE TO GEOMEMBRANE DEFECTS

6.1 INTRODUCTION

Modern landfills are generally designed to protect the environment against contaminants by using a composite liner. Unfortunately, despite all precautions regarding manufacturing, transportation, handling, storage and installation, defects in the geomembrane are unavoidable. As shown in Chapter 2, defects varying in density from 0.7 to 15.3 per hectare and in size from pinholes having a diameter less than one millimetre to defective seams or tears that are more than one meter long may be encountered in landfills.

As discussed in Chapter 4, to evaluate the performance of composite liners involving GCLs when there is a defect in the geomembrane, it is necessary to know the hydraulic conductivity of the GCLs. In landfill bottom liners GCLs are commonly installed at their natural water content. Therefore, they may not be fully saturated, at least on the short term. It follows that the knowledge of the unsaturated hydraulic conductivity is required. It can be estimated through predictive methods based on water retention curves. The literature review carried out in Section 4.4 showed that the water retention curves for GCLs are scarce. In this context, one purpose of the present study was, first, to examine the suitability of the filter paper method for evaluating the suction of the GCLs and, second, to determine the water retention curves of the GCLs.

On the other hand, discussions on flow rates through composite liners due to geomembrane defects, addressed in Section 4.6, showed that very little is known about the performance of composite liners when there is a prehydrated GCL under the geomembrane, despite the typical recommendation that they should be hydrated under a vertical stress, after installation, in order to reach a better performance. A minimum prehydration of 100 % is, for example, suggested by the *Comité Français des Géosynthétiques* (1998). Furthermore, the influence of the load of waste and of the height of leachate above the geomembrane remains unstudied from an experimental point of view. Thus, another goal of this research is to study the influence of prehydration of the GCLs, of confining stress (load of waste), and of hydraulic head (leachate above the geomembrane) on flow rates through composite liners due to defects in the geomembrane.

This chapter describes the experimental works carried out. Section 6.2 presents the materials used, namely soils, GCLs and geomembrane. Section 6.3 is devoted to the water retention curves of the GCLs. First, it describes the preparation of specimens, equipment, test procedures and, then, presents and discusses the results obtained. Section 6.4 is dedicated to the flow rate through composite liners. It begins with the preparation of the materials. Next, it describes the equipment and the test procedures. Composite liners comprising a geomembrane, with a circular hole, over a GCL over a CCL, were simulated in tests at three scales, and the flow rate at the interface between the geomembrane and the GCL was measured. Materials in composite liners were the same as the ones used at a landfill bottom liner in Portugal. In small-scale tests, two additional GCLs were used over the soil. Small-scale tests were carried out to examine the influence of the parameters above mentioned. Intermediate and large-scale tests were intended to complement the small-scale tests and to check the feasibility of an extrapolation of the results obtained on small-scale tests to field conditions. Section 6.4 presents and discusses the results obtained. Section 6.5 proposes some new empirical equations for predicting the flow rate through composite liners

consisting of a geomembrane over a GCL over a CCL, and fulfilling the last objective of the present work. Finally, Section 6.6 summarises the main conclusions obtained in this study.

6.2 MATERIALS TESTED

6.2.1 Geomembrane

A smooth HDPE geomembrane 2 mm thick was used in the experimental work carried out on flow rate through composite liners due to geomembrane defects.

6.2.2 Geosynthetic Clay Liners

Four GCLs were used in the experimental work conducted, here termed as GCL-1, GCL-2, GCL-3 and GCL-4. The first GCL was supplied from a landfill located west of Portugal. Since there was not enough product to carry out the intermediate and large-scale tests, additional product was requested directly to the manufacturer. The same product could not be obtained. A powdered product, identical to the first one, was sent. It was designated as GCL-2.

GCL-3 came from a different manufacturer. It was selected because it is often used in Portuguese landfills.

GCL-4 is a geomembrane supported GCL and was only used on tests conducted to study the suitability of the filter paper method to measure the suction of GCLs. The main characteristics of tested products are summarised in Table 6.1, together with the generic symbols used to identify the products. This table also includes the values of the hydraulic conductivity measured based on ASTM D 5887, under two normal stresses, 50 kPa and 200 kPa, to assist in interpretation of the test results on the Section 6.4.5.9.

6.2.3 Soil

The soil used in the experimental work came from a landfill located west of Portugal. The landfill, nearly quadrangular in shape, divided in 5 cells, involves about 140 000 m^2 of land. It was designed for disposal of approximately 3×10^6 m^3 of MSW in a period of 14 years (Pardo de Santayana & Barroso 2002). The local geological conditions consist of continental deposits of sedimentary Jurassic and Cretaceous formations, comprising different levels of clay, marls, silt-clayey sands and sandstones. Clayey levels (clay and marls) are predominant in Jurassic formations. The Cretaceous formations outcrop at the southern portion of the landfill, consisting of intercalations of clayey soils, sandy silts and sandstones. The cells were excavated with their bottoms at different elevations to achieve the clayey Jurassic formations (Pardo de Santayana & Lopes 2003).

Although all the soil used in the small, intermediate, and large-scale tests came from the same site, the soil for the small-scale tests was sampled in a first phase (approximately 100 kg) and the soil for intermediate and large-scale tests (approximately 4500 kg) was sampled in a second phase. With the progress of the landfill construction, the place where the first

sampling took place was already under the bottom liner when the second sampling occurred and the soil came from a different location. Due to the heterogeneity in the geological formations both soils were different from a geotechnical point of view, being here termed S-1 and S-2, respectively. Soil S-1 was used in the small scale tests carried out with GCL-1, and soil S-2 was used in all other tests. Table 6.2 summarises the relevant characteristics of these soils for the preparation of the composite liner and for interpretation of tests results.

Table 6.1 - Characteristics of GCLs used according to the manufacturers

Specimens			GCL-1	GCL-2	GCL-3	GCL-4
Bentonite layer	Type of bentonite		Natural, Na^+, granular	Natural, Na^+, powdered	Na^+, granular	Natural, Na^+
	Mass per unit area (g m^{-2})		4 670	4 670	5 000	4 900
Cover material (GTX or GM)	Mass per unit area (g m^{-2})		220	220	200	-
	Type		GTX, PP, NW, needle punched	GTX, PP, NW, needle punched	GTX, PP, NW, needle punched	-
Carrier material (GTX or GM)	Mass per unit area (g m^{-2})		110	110	125	-
	Type		GTX, PP, W	GTX, PP, W	GTX, PP, W	HDPE GM (0.5 mm)
GCL	Mass per unit area (g m^{-2})		5 000	5 000	5 300	-
	Type		Needle punched	Needle punched	Adhesive bond plus semi-needle punched	Adhesive bond
	Dry thickness (mm)		6	6	7	--
	Hydraulic conductivity (m s^{-1})	--	$\leq 5 \times 10^{-11}$	$\leq 5 \times 10^{-11}$	$\leq 5 \times 10^{-11}$	--
		50 kPa (ASTM D 5887)	3.7×10^{-11}	3.7×10^{-11}	3.6×10^{-11}	--
		200 kPa (ASTM D 5887)	1.1×10^{-11}	--	1.2×10^{-11}	--

Notes: GTX=geotextile, GM=geomembrane, PP=polypropylene, NW=non-woven; W=woven, Na^+=sodium.

Table 6.2 – Characteristics of soils used

Specimen	Percent fines (%)	Percent clay (%)	Atterberg limits			Proctor modified		k (m s^{-1})
			LL (%)	PL (%)	PI (%)	ω_{opt} (%)	$(\gamma_d)_{max}$ (kN m^{-3})	
S-1	73.6	40.5	54.2	23.7	30.5	13.6	19.1	8×10^{-11}
S-2	37.7	17.0	33.1	19.7	13.4	8.1	21.3	3×10^{-10}

Notes: Percent fines=percent passing the USA No 200 sieve (openings of 75 μm); Percent clay=percent finer than 0.002 mm; LL=Liquid Limit; PL=Plastic limit; PI=Plasticity Index; ω_{opt}=optimum water content; $(\gamma_d)_{max}$=maximum dry unit weight; k=hydraulic conductivity of the soil.

6.3 WATER RETENTION CURVES

6.3.1 Preparation of specimens, equipment and test procedures

Water retention curves, typically represented by the van Genuchten parameters, are necessary in modelling the hydraulic behaviour of unsaturated materials, which is the case of a GCL during a certain period of time after its installation in situ, at its natural water content.

To determine the water retention curve of GCLs, matric suction and volumetric water content were measured experimentally. Matric suction of GCLs was evaluated based on ASTM D 5298: *Standard test method for measurement of soil potential (suction) using filter paper*. This test method is a standard for soils, and thus, the suitability of this method to measure the suction of GCLs was first addressed (see Section 6.3.2).

A full description of the methodology adopted in the present work is outlined in Appendix E. Briefly, prior to suction measurements, GCL specimens were prehydrated covering a range of moisture contents. Two techniques were used to prehydrate the specimens. The first one consisted in spraying a known mass of water onto the surface of the specimens. It was used to prehydrate the GCLs with water contents under 45 %. For GCLs specimens with higher water contents, the specimens were immersed in water during the time necessary to achieve the specified water content. The immersion time depends on the mass of each specimen. Therefore, it was necessary to weigh the specimens at regular intervals until the correspondent wet mass was reached.

Two prehydrated GCL specimens, to the same water content, were wrapped together with a laboratory plastic film (e.g. PARAFILM® M), and placed in isolated boxes during seven days, for water content homogenisation purposes. Homogenisation took place without confining stress. At the end of the homogenisation period, it was assumed that the two GCL specimens had identical suction.

Three stacked pieces of dried filter paper (Whatman®No. 42) were then placed between the two GCL specimens. The outer filter papers were slightly larger in diameter than the centre filter paper, in order to prevent the centre filter paper contamination by bentonite. The filter paper was initially oven dried (105ºC) either for about 16 hours, or overnight, then stored in a desiccant container for cooling. Prepared GCL specimens were again wrapped together with a laboratory plastic film and sealed in an airtight container, for seven days, in order to

equilibrate suctions with the filter paper. Once again, the homogenisation took place without confining stress. After that equilibration period, the filter papers were removed from the GCL specimens (Figure 6.1), and the water content of the centre filter paper was measured.

Figure 6.1 – Removing the filter paper

Water content of the filter paper (ω_f) was estimated by the expression below:

$$\omega_f = \frac{M_w}{M_f} \times 100 \tag{6.1}$$

where M_w is the mass of water in the filter paper (g), and M_f is the mass of dry filter paper (g).

The matric suction of the GCL specimen was estimated from the calibration curve of filter paper presented in ASTM D 5298 standard (see Figure 4.5), by using the measured equilibrium water content of the filter paper.

It should be pointed out that the calibration curves included in ASTM D 5298 standard are applicable to the total suction. However, as can easily be demonstrated, based on the discussion addressed in Section 4.2, the GCLs present a low thickness and therefore the total and matric suction can be considered as equal. Thus, those calibration curves can be used for assessing the matric suction, from now on just called suction.

For the filter paper used in the present work (Whatman®No. 42), the expressions below were then used to calculate the suction, ψ (ASTM D 5298):

$$\psi = 10^{5.327-0.0779\omega_f} \quad \text{for } \omega_f < 45.3\ \%$$

or

$$\psi = 10^{2.412-0.0135\omega_f} \quad \text{for } \omega_f > 45.3\ \% \tag{6.2}$$

The volumetric water content, Θ, was evaluated using the expression below:

$$\Theta = \omega \frac{\gamma_d}{\rho_w} \tag{6.3}$$

where ω is the gravimetric water content of the GCL; ρ_w is the density of water; and γ_d is the dry density of the GCL, i.e. the ratio of the mass of the GCL specimen to the total volume of the GCL specimen. The total volume is equal to the area multiplied by the thickness of the specimen.

The area was considered as constant, despite the methodology used for cutting the specimen. Indeed, they were cut with scissors after wetting of their perimeter. Wetting minimises the loss of bentonite at the specimen boundary during the cutting operation. Circular specimens having a 10 cm diameter were used.

The thickness of GCLs was measured based on EN 964 standard (see Figure 6.2).

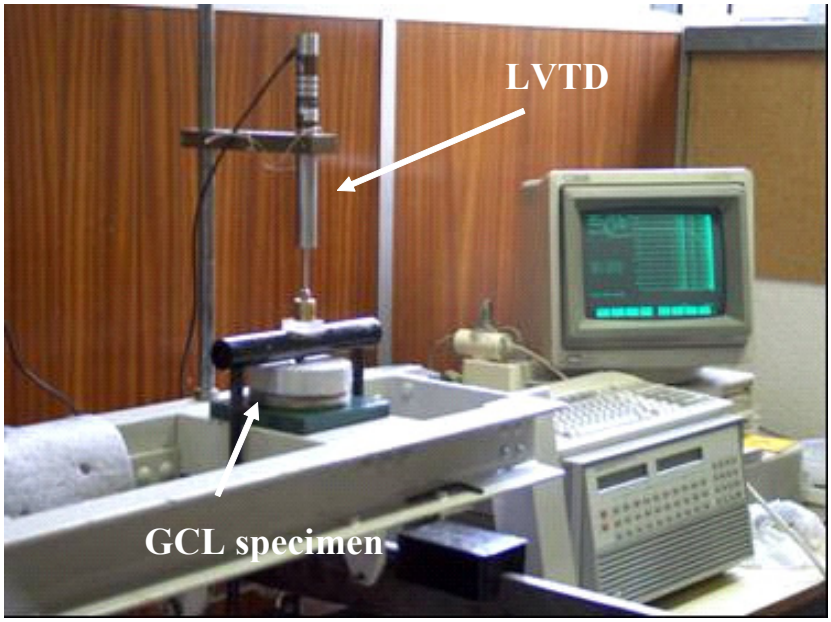

Figure 6.2 – Devices used to measure the thickness of the GCL specimens

6.3.2 Studies on the suitability of the filter paper method to measure the suction of the GCLs

6.3.2.1 Comparison with the results obtained by Daniel et al. (1993)

The suitability of the filter paper method to measure the suction of the GCLs was analysed by comparison with the results obtained by Daniel et al. (1993) and presented in Section 4.4.1. In that framework, a geomembrane supported GCL similar to the one used by Daniel et al. (1993), was used in this study, i.e. GCL-4 (recall Table 6.1). The first step consisted of

prehydrating the GCL specimens, covering the range of moisture contents reported by Daniel et al. (1993). Water contents selected for prehydrating the specimens included: 17%, 28%, 46%, 56%, 66 %, 79%, 89%, 96%, 101% and 145%. Then, the suctions were measured based on the filter paper method.

The suctions obtained in this study are plotted together with the suctions reported by Daniel et al. (1993) against gravimetric water content of the GCL in Figure 6.3. As can be seen, although some scatter can be observed for the suction corresponding to lower water contents, the results obtained in the present study are consistent with the results obtained by Daniel et al. (1993). This suggests that the filter paper method can successfully be used to measure the suction of GCLs.

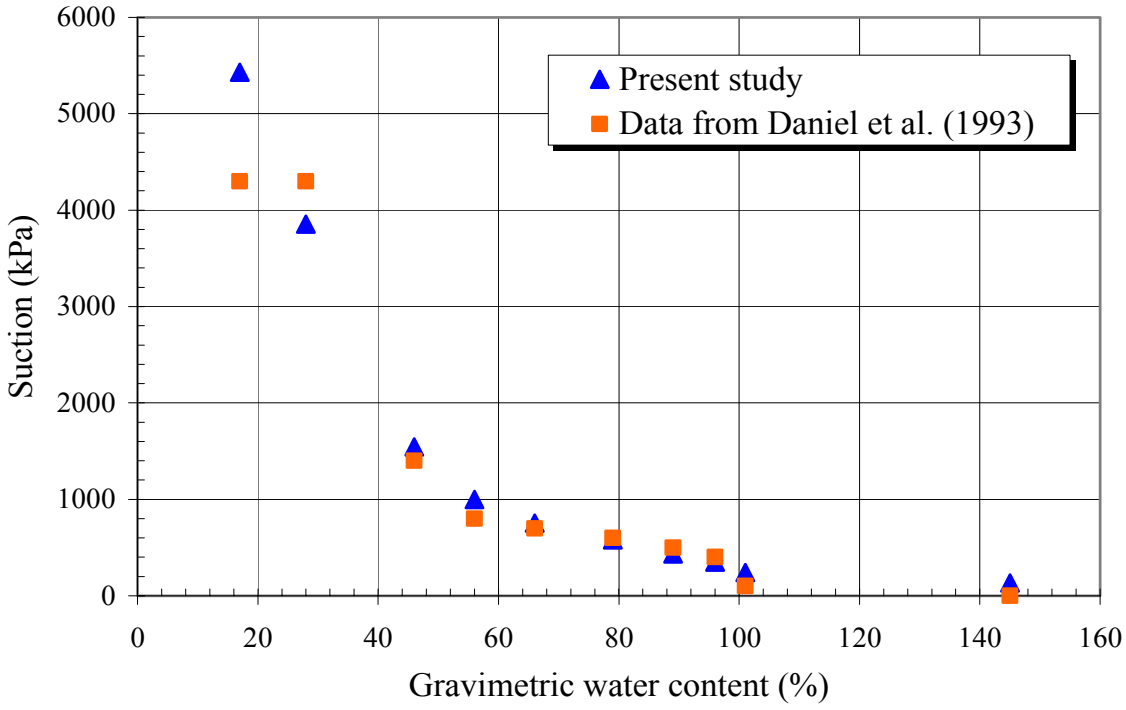

Figure 6.3 – Comparison with the results obtained by Daniel et al. (1993)

6.3.2.2 Influence of the position of GCL

As the GCLs used in this study are mainly geotextile-supported products (see Table 6.1), with different geotextiles in the upper and lower layer, an important issue is to know if the position of the GCL affects the final results of the suction. In other words, will the filter paper be suitable to measure the suction of the whole GCL, or will it mainly measure the suction of the geotextile with which it is in contact?

To answer this question, a second study was carried out. It consisted of measuring the suction with the filter paper facing the GCLs in three different positions: nonwoven/nonwoven (NW/NW), woven/nonwoven (W/NW), and woven/woven (W/W). Three values of water contents were selected to prehydrate the GCLs specimens. This study was carried out both with GCL-1 and GCL-3.

Figure 6.4 depicts the results obtained for GCL-1. Similar results, not included in the graph, for the sake of brevity, were obtained for GCL-3. It can be seen that, despite some scatter on suction corresponding to the lowest and highest water content, results show a close agreement regardless of the type of geotextile that faced the filter paper. The scatter obtained for the lowest and highest suction measurements may be related with some experimental difficulties found with this method for the water contents of the GCLs in this range, as discussed in Section 6.3.4.2.

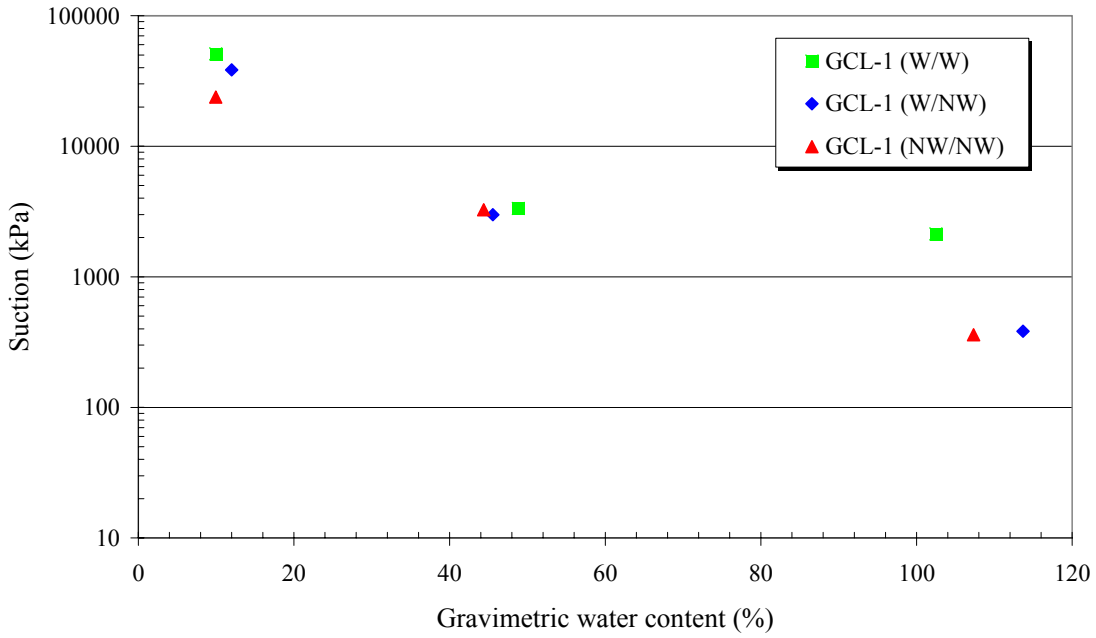

Figure 6.4 – Suctions obtained with filter paper facing the GCL in three different options

Thus, it seems that the position of the GCL does not influence suction measurement for a water content that is intermediate. This point should be validated for other water contents that do not correspond to the limits of validity of the test method.

Another approach to answer the question addressed at the beginning of this section consists of comparing the water retention curves of the GCLs with the water retention curves of geotextiles. In this framework, Figure 6.5 shows the results obtained by Cartaud et al. (2005) for three polypropylene geotextiles (GA, GB, and GC). GA is a needlepunched geotextile with a mass per unit area equal to 300 g m^{-1}, GB is also a needlepunched product with a mass per unit area equal to 330 g m^{-1}; and GC is a thin nonwoven thermal-bonded geotextile with a mass per unit area equal to 130 g m^{-1}. Suction measurements correspond to a wetting phase, i.e. imbibition of the geotextiles.

The water curves obtained by Cartaud et al. (2005) significantly differ from the ones obtained in the present work for GCLs presented in the next section. Suction for GCLs ranged from about 1 to 2800 m, whereas for geotextiles they ranged from 0 to 0.25 m. Suctions in the same range were also reported by Iryo & Rowe (2004) for geotextiles. These comparisons indicate that the suctions measured in the present work regard, with no doubt, the whole GCL and not only the geotextile in contact with the filter paper.

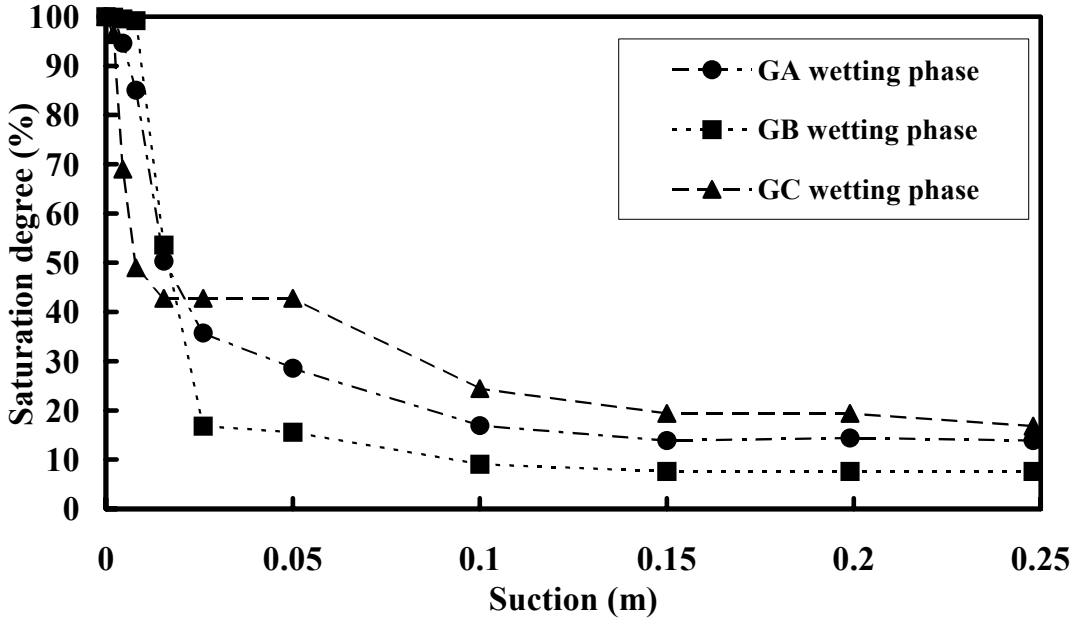

Figure 6.5 – Water retention curve for three geotextiles (Cartaud et al. 2005)

Based on the results obtained in studies carried out, it was assumed that the filter paper method can successfully be used to measure the suction of the GCLs. Accordingly, this method was used to estimate the suctions of GCL-1, GCL-2 and GCL-3. To ensure a good contact between the GCL specimens and the filter paper, the later was placed between the two nonwoven geotextiles, as observations made during the tests disassembly suggest that the best contact is achieved in this case.

6.3.3 Water retention curves obtained for GCL-1, GCL-2 and GCL-3

Water retention curves of GCLs were obtained based on measured suctions and on corresponding volumetric water contents. Water retention curves for GCL-1, GCL-2 and GCL-3 (see Table 6.1) are shown in the figures below, which include the van Genuchten parameters α and n obtained by fitting a theoretic water retention curve to the experimental data, assuming that the residual water content was negligible ($\Theta_r = 0$), according to the discussion addressed in Section 4.3.3.

Figure 6.6 presents the water retention curve of GCL-1. It can be seen that the volumetric water content varied from 0.07 to 0.7, whereas the correspondent suction ranged from 2379 m to 18.9 m (23790 kPa to 189 kPa). The best fitting curves to the experimental data resulted in the following van Genuchten parameters: $\alpha = 0.018$ m^{-1} and $n = 1.50$.

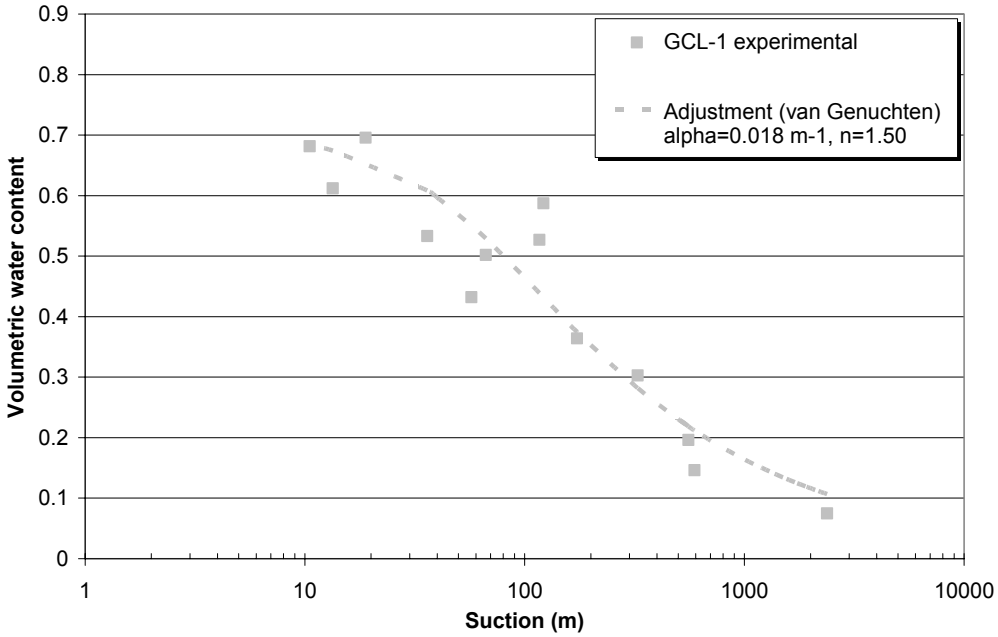

Figure 6.6 – Water retention curve for GCL-1

Figure 6.7 presents the water retention curve obtained for GCL-2. It can be observed that the volumetric water content increased from 0.12 to 0.76 when the suction decreased from 1 443 m to 1.2 m (14 430 kPa to 12 kPa). The best fitting curve to the experimental data resulted in the van Genuchten parameters as follows: $\alpha = 0.032 m^{-1}$ and $n = 1.47$.

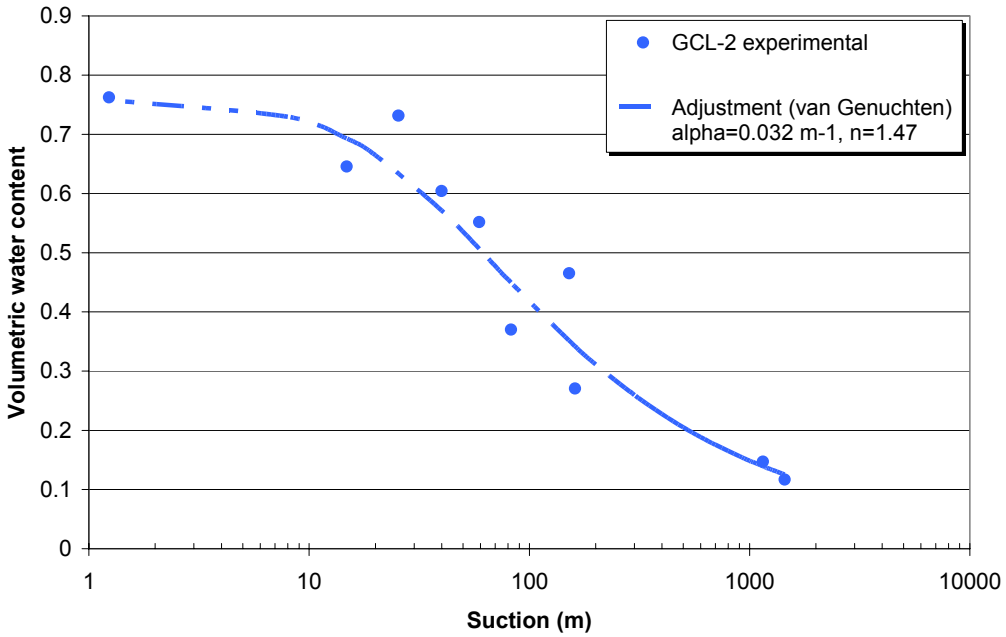

Figure 6.7 – Water retention curve for GCL-2

Figure 6.8 depicts the results of the suction versus volumetric water content for GCL-3. The volumetric water content increased from 0.09 to 0.69, when the suction decreased from 2 821 m to 6.9 m (28 210 kPa to 69 kPa). The values of α = 0.015 m^{-1} and n = 1.67 matched the experimental results.

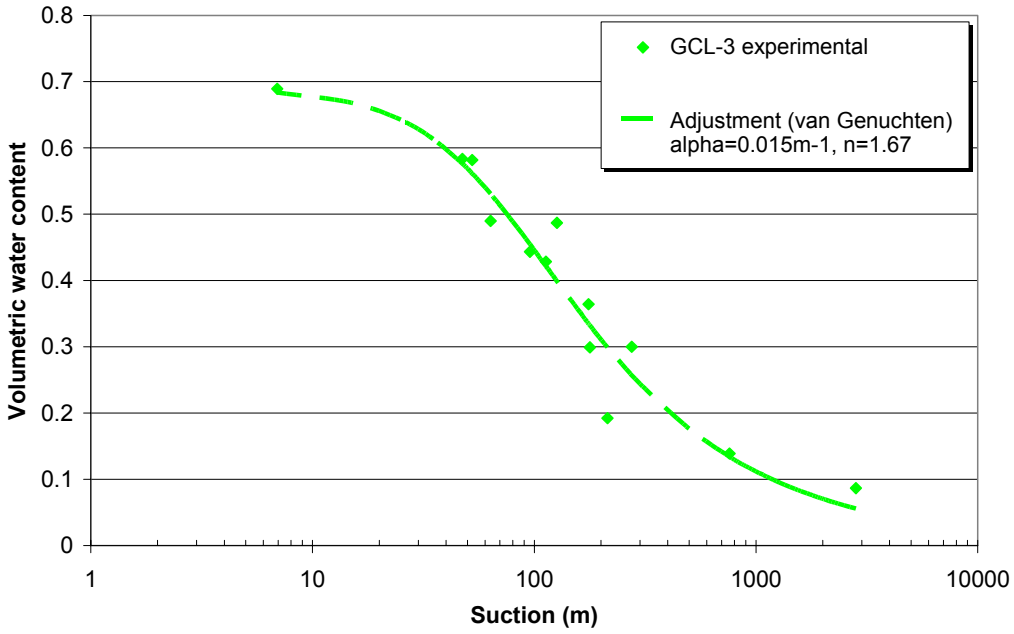

Figure 6.8 – Water retention curve for GCL-3

6.3.4 Discussion

6.3.4.1 Comparisons of van Genuchten parameters and water retention curves

Table 6.3 summarises the van Genuchten parameters and the saturated volumetric water contents that were obtained in this study. It also includes some values of α and n that have been used in numerical simulations carried out in the topic of GCLs desiccation by several authors (e.g. Babu et al. 2002, Southen & Rowe 2002, Southen et al. 2004). Results obtained by Southen & Rowe (2004) were not included in this table because the range of suctions reported by these authors is relatively small to estimate the van Genuchten parameters.

It can be observed that the values of α are quite similar for GCL-1, GCL-2 and GCL-3. It varies between 0.015 and 0.032 m^{-1}. As regards n, it varied between 1.47 and 1.67. Reasonable agreement can be observed between the van Genuchten parameters obtained from the experimental work carried out and data reported in the literature. Consistent results can also be observed between the Θ_s measured and data reported in literature, except for Θ_s found by Southen et al. (2004), which is higher. However, this higher value of Θ_s was based on the initial value of porosity measured with a high uncertainty. In fact, if it were estimated based on water retention curve, this value should have been 0.76 rather than 0.85 (Southen, personal communication).

Table 6.3 – Van Genuchten parameters obtained in the present work and reported in literature

	α (m^{-1})	n	Θ_s
GCL-1	0.018	1.50	0.70
GCL-2	0.032	1.47	0.76
GCL-3	0.015	1.67	0.69
Babu et al. (2002)	0.010	1.85	0.74
Southen & Rowe (2002)	0.015	1.30	0.76
Southen et al. (2004)	0.030	1.50	0.85

Figure 6.9 compares the water retention curves of GCLs obtained in this study and shows water retention curves estimated using van Genuchten parameters reported in the literature (values included in Table 6.3). As can be seen, similar volumetric water content versus suction relationship was obtained for GCL-1, GCL-2 and GCL-3. This suggests that the type of bentonite has no significant influence on the water retention curve of the GCLs, as the only difference between the GCL-1 and the GCL-2 is the nature of the bentonite (granular vs powdered).

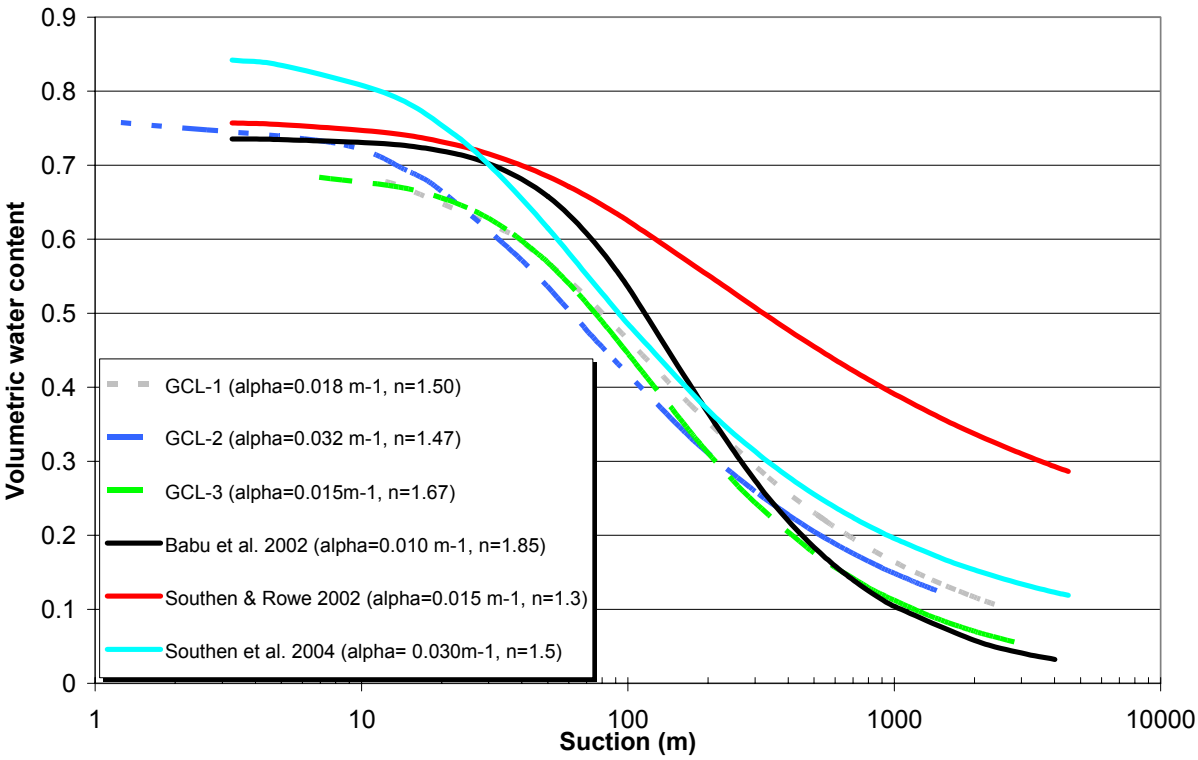

Figure 6.9 – Comparisons between the van Genuchten parameters obtained in the present work and reported in the literature

As regards the GCL modelled by Southen & Rowe (2002), it can be observed that for values of suction less than 40 m the curve is identical to the ones obtained for the other GCLs, deviating for high values of suction. The deviation observed can be attributed to an overestimation of *n*. A good agreement can be obtained using *n* equal to 1.5 instead of 1.3. The overestimation of *n* was due to the fact that, for those tests, these authors were using the

pressure plate method to measure the suction, which only permitted suction measurements for high volumetric water contents (Southen, personal communication). Therefore, to estimate the van Genucthen parameters by fitting a model curve to experimental data, they did not possess the experimental data to cover the whole range of suctions. In contrast, a good agreement can be observed between the data from the present study and the parameters reported by Southen et al. (2004), obtained through a series of laboratory tests using pressure plates and membrane extractors.

6.3.4.2 Difficulties found in water retention curves estimation

As regards suction measurements, some scatter could be observed for low gravimetric water contents (8-15%) of the GCLs. This scatter might be related to the fact that, for these gravimetric water contents, the measured water content of the filter paper was close to the lower values for which the calibration curve can reliably be used (often less than 5%). In some cases, the suctions obtained were less than the limit of validity of the filter paper method (100 000 kPa or 10 000 m) and were not taken into account in the analysis done. In addition, in some filter papers, fungal growth was observed (Figure 6.10). This occurred mainly in protective filter papers and for gravimetric water contents of the GCLs higher than 125 %. When the fungi were observed on the central filter paper used to evaluate the suction of the GCL, the suction was, generally, less than the low limit of validity of the filter paper method (10 kPa or 1 m). These results suggest that the fungi may affect the suction measurements. Suctions estimated from centre filter papers with fungi were not considered in final results.

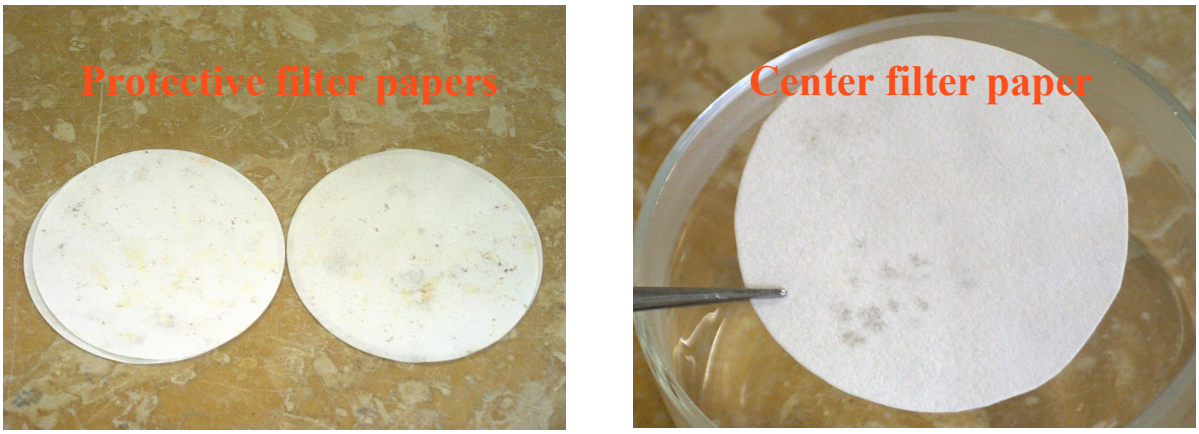

Figure 6.10 – Example of a filter paper with fungi

Difficulties were also encountered to determine the volumetric water content of GCLs. These difficulties came from the measurement of specimen area. The GCL specimens were cut with scissors and thus their final shape was irregular. As a result, estimated values of the area were note very accurate, which caused scatter on experimental measurements of suction. To avoid this problem, it is recommended to cut the specimens using a cutting shoe and a mechanical press.

6.3.5 Summary of Section 6.3

Section 6.3 focused on the experimental work carried out on water retention curves of the GCLs. Water retention curves characterise the relationship between the volumetric water content and suction. Its knowledge, typically represented by the van Genuchten parameters (Θ_r, Θ_s, α and n), is necessary in modelling the hydraulic behaviour of unsaturated materials.

Within the scope of the present work, the first aspect analysed was the suitability of the filter paper method to assess the suction of GCLs. This issue was addressed under two axes: comparison with previous works and influence of the position of the GCL. Results from filter paper agree fairly closely with the results reported in literature. On the other hand, it could be observed that the position of the GCLs does not affect the suction, suggesting that the measured suction regards the whole GCL and not the geotextiles in contact with the filter paper. These results indicate that the filter paper is suitable to measure the suction of GCLs. The first goal of this experimental work was successfully achieved.

The filter paper method was then used to measure the suction of three GCLs, two needlepunched containing either granular or powdered bentonite and one adhesive bonded plus semi-needle punched. Volumetric water content was also assessed experimentally from the gravimetric water content and the total volume of the GCL specimens. Water retention curves for GCLs could thus be determined. Finally, the van Genuchten parameters were estimated by fitting a water retention model to experimental data. For tested GCLs, a good agreement was found between the water retention curves.

Suctions obtained in this study are consistent with the ones obtained by Southen & Rowe (2004), for the range of suctions that could be compared.

As the retention curves were estimated with GCLs without stress, which is not representative of field conditions, this study has to be seen as a starting point. Suction measurements under stress are needed to obtain the van Genuchten parameters representative of field conditions and properly model the flow rate under unsaturated conditions. In fact, as it was possible to prove that the filter paper method can be used for GCL, suction measurements with this technique are in progress, and numerical modelling, involving unsaturated GCLs, is expected for a near future.

Next section is devoted to the experimental work carried out on measurement of flow rate through composite liners due to geomembrane defects. The results obtained will be used to study the influence of prehydration of the GCLs, confining stress, and hydraulic head on advective flow rate through composite liners, as well as to compare different scale test results and check the feasibility of an extrapolation of results obtained on small-scale tests to field conditions.

6.4 FLOW RATE THROUGH COMPOSITE LINERS

6.4.1 Preparation of materials

6.4.1.1 Geosynthetic Clay Liners

6.4.1.1.1 Small-scale tests

In small-scale tests, two different types of specimens, both circular with 20 cm diameter, were used: non-prehydrated (water content as supplied) and prehydrated to an initial water content close to 100%.

Concerning non-prehydrated specimens, they were cut with scissors after wetting their perimeter. This procedure minimises the loss of bentonite at the specimen boundary during cutting operation and the placement of the GCL inside the test cell.

As regards prehydrated specimens, first oversized specimens were immersed in tap water during the time necessary for them to reach a water content of 100 %. Once the process of immersion was completed, the specimens were placed in a watertight plastic bag, under the same normal stress than that used in flow rare measurements, during one week, for moisture content homogenisation purposes. The GCLs were kept under a normal stress because it was found that the uniformity of moisture distribution is better when the specimen is under load (Touze-Foltz et al. 2002a, Bouazza et al. 2002b). After the moisture content homogenisation period, the GCLs were carefully cut with scissors and installed in the test cell.

6.4.1.1.2 Intermediate and large scale tests

In intermediate and large scale tests only non-prehydrated specimens were used. They were cut with scissors after their perimeter was wet. The specimen for intermediate-scale test had a 1 m diameter, whereas for the large-scale test it was a square 2.2 m wide.

6.4.1.2 Soil

6.4.1.2.1 Small-scale tests

In small-scale tests the soil was moistened to a water content about 2 to 4 % above the optimum water content determined based on a Proctor test. This value of moisture content was adopted based on the USEPA recommendations (see Section 2.3.3). The soil was then placed in the cell for compaction purposes.

6.4.1.2.2 Intermediate and large-scale tests

In intermediate and large-scale tests the soil was compacted at its natural water content, as it came from the site already at a water content 5 to 6 % above the Proctor optimum. This value exceeds the value used in small scale tests, but the moisture content could not be lowered due

to the large amount of soil involved in these tests (about 430 kg, in the intermediate scale test and about 2700 kg, in the large-scale test).

6.4.1.3 Geomembrane

Geomembrane specimens were prepared with a 3 mm diameter hole at their centre, regardless of the scale of tests performed. This size took into account that, on the one hand, the majority of the holes in landfills appears to be smaller than 10 cm^2 (as shown in Chapter 2), and, on the other hand, that the dimensions of our laboratory model were small and that we wanted to avoid boundary effects as far as possible.

6.4.2 Equipment and test procedures

6.4.2.1 Small-scale tests

The small-scale tests were carried out in a circular Plexiglas cell specially designed to measure the flow rate through composite liners. The cell consists of four parts: (i) a bottom plate supporting the compacted soil layer; (ii) a base cylinder with an inside diameter of 0.2 m and 0.08 m high, for accommodating the compacted soil and GCL specimen; (iii) a granular cover plate to simulate the presence of a granular drainage layer; and (iv) an upper part being 6 cm high that accommodates the granular cover plate.

First, about 4.5 kg of soil was placed inside the base cylinder, in two lifts approximately 21 mm thick. Lifts were compacted using a hand packer. The excess soil material was carefully cut to yield a smooth surface. The GCL specimen is placed on top of the soil, usually with the non-woven geotextile on top, and, above it, the geomembrane with a circular hole at its centre is placed. Then, the granular cover plate is placed above the geomembrane. Afterwards, the base and upper parts of the cell are held together with retaining threaded rods. The cell is then installed in a mechanical press that applies the confining stress. Finally, the top cell is connected to a water supply reservoir, mounted on a vertical sliding rail. This reservoir feeds the test during the first hours when the water flow through the composite liner is significant. As the water flow decreases throughout the test, the water reservoir is replaced by a Mariotte bottle, more accurate at low flows. Both the water reservoir and the Mariotte bottle can be set for a specified hydraulic head that is kept constant during the entire test (constant head tests). Figure 6.11 summarises the test procedure and Figure 6.12 shows the correspondent scheme of a small-scale test.

The small scale tests were carried out to study the relative importance of some parameters that govern the flow rate through composite liners due to defects in the geomembrane, namely the pre-hydration of GCLs, the confining stress over the geomembrane liner and the hydraulic head applied on top of the geomembrane. These issues were analysed based on the results obtained in tests carried out with GCL-1 and GCL-3. Other goals of the small-scale tests were to study the repeatability of the test procedure, to examine the influence of the type of geotextile in contact with the geomembrane (nonwoven or woven) and to study the influence of the nature of bentonite (powdered or granular) on flow rate through composite liners. These issues were studied based on the results obtained in tests conducted with GCL-2. Tests

carried out with this latter product are also used to assist in interpretation of the intermediate and large-scale tests.

Figure 6.11 – Summary of small-scale test procedure

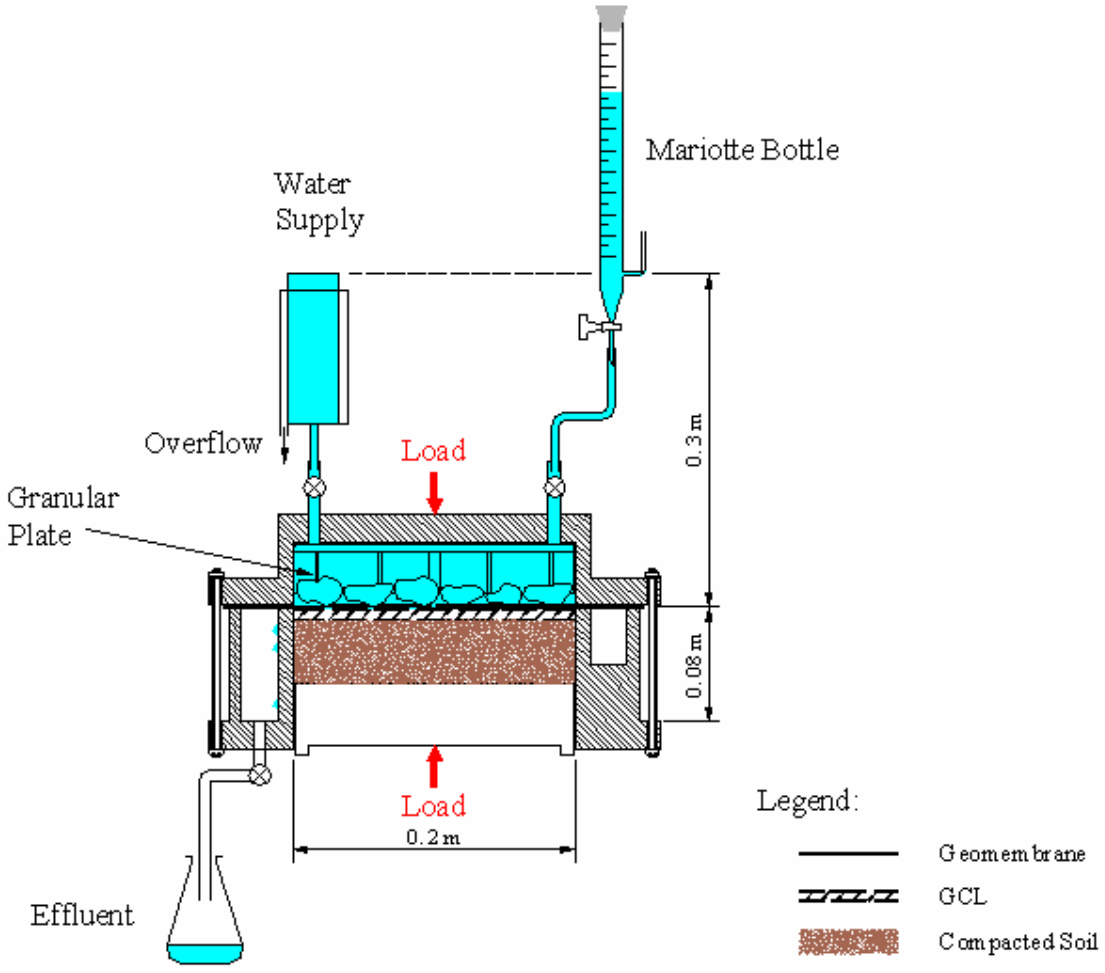

Figure 6.12 - Scheme of the small-scale tests

The tests were conducted using either non-prehydrated GCL or prehydrated to a water content equal to 100 %. These conditions were chosen to represent two possible approaches used during GCL installation. The non-prehydration represents the field conditions, for example, in landfills, where GCL is installed at its natural water content on a foundation layer, whereas prehydration to a water content of 100% represents the recommendation of the *Comité Français des Geosynthétiques* (1998).

Three different normal stresses were applied: 25, 50 and 200kPa. The first stress was chosen to allow a comparison with the results obtained in the large-scale test, which for experimental reasons could not be higher as will be seen in Section 6.4.2.3. The second and third confining stresses represent approximately two stress levels that may be exerted on a bottom liner in a landfill. They would correspond approximately to 5 m and 20 m of cover waste.

Two hydraulic heads were applied on top of the composite liner: 0.3 m and 1.2 m. The first choice represents the maximum allowable leachate head above the geomembrane in most landfill regulations, whereas the second one can represent the case when the leachate head in a landfill is higher due to, for example, inappropriate operation of the leachate collection system.

Each test was run for a minimum period of 400 hours (17 days).

The flow rate was calculated in two different ways. When the radial flow rate at the downstream side of the interface (effluent) was high enough to be measured by weighing, the flow rate, $Q_r(R_c)$, was obtained by dividing the volume of effluent collected by the collecting time. When very low or no flow rates could be measured in this way, the total flow rate, Q, was estimated by dividing the variation of volume in the Mariotte bottle by the corresponding time interval. In order to reduce the scatter on flow measurements, the total flow rate was generally re-calculated on a 24 hours basis.

6.4.2.2 Intermediate-scale tests

An intermediate-scale test was carried out to compare test results and to check the feasibility of an extrapolation of results obtained on small-scale tests to field conditions. It was performed in complement to the large-scale test at a higher confining stress, since that by experimental reasons, the large-scale tests had to be carried out at a low confining stress as will be seen in the next section. Therefore, the intermediate-scale test is more representative of the field conditions, as the load applied by waste over the lining system may reach more than 200 kPa. This test was carried out at Cemagref, in France, and lasted 6.5 months.

The test was conducted in a large circular stainless steel cell. The inner diameter of the cell is 1 m and corresponds to the GCL specimen diameter. It consists of three parts (Figure 6.13): (i) a bottom part with a round base plate fixed onto the beam of a hydraulic press that applies the confining stress; (ii) an intermediate cylinder, 1 m diameter and 0.3 m high, fixed onto the base plate, for accommodating the simulated composite liner; and (iii) an upper cylinder, 25 cm high, for accommodating the granular layer that simulates the drainage layer in a bottom liner of a landfill.

Figure 6.13 – Photograph of the cell for intermediate-scale test

Test assembly comprised several steps, which are briefly described in subsequently. First, a Pollyanna film and geotextile were placed at the bottom part of the cell to protect the base

plate of the cell and ensure drainage of potential effluents. Second, the soil was carefully compacted in 4 lifts. The total thickness of the compacted soil layer was 27 cm. The mean moisture content of the soil was 13.2 %. Third, a non-prehydrated GCL specimen at a water content equal to 9.5 % was placed above the soil, with the non-woven geotextile on top. Fourth, an HDPE geomembrane 2 mm thick, having a 3 mm diameter circular hole at its centre, was installed above the GCL. A special "Y" connection was glued over the hole of the geomembrane. Two pipes were then inserted in this connection, one connected to the water supply (Mariottle bottle) and the other used as purge. Fifth, a geotextile 828 g m^{-2} was placed above to protect the geomembrane against puncturing. Sixth, 25 cm of gravel 25/35 mm was added on top of the geotextile. This layer was added to simulate the drainage layer in a landfill. Then, a stainless steel plate was placed above the gravel layer. Once this operation was concluded, a normal stress of 50 kPa was applied through a mechanical press. Finally, the water supply was activated and the test started. The test was carried out with a hydraulic head of 0.3 m. Flow rates were measured thanks to a Mariotte bottle. Figures 6.14 summarises the test procedure and Figure 6.15 is a scheme of the test.

Figure 6.14 – Summary of intermediate-scale test procedure

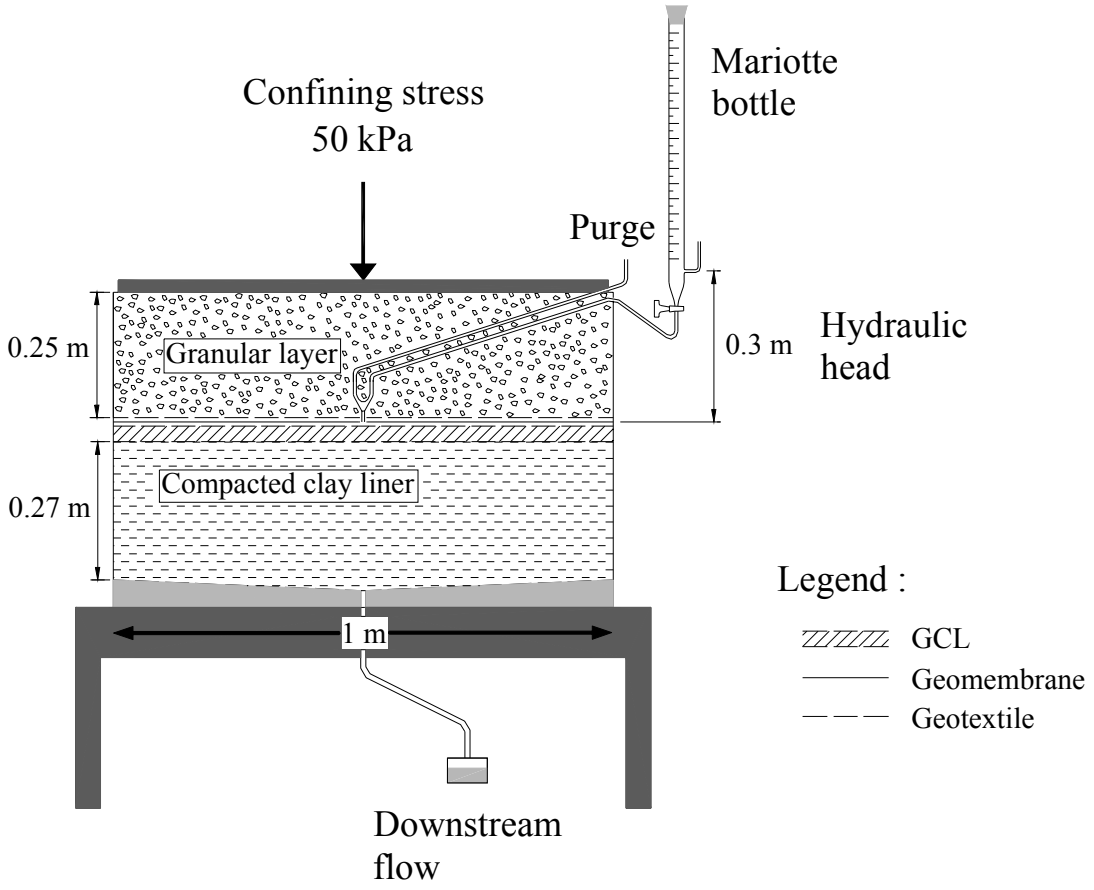

Figure 6.15 – Scheme of the intermediate-scale test

6.4.2.3 Large-scale test

A large-scale test was also carried out to compare test results and to check the feasibility of an extrapolation of results obtained on small-scale tests to field conditions. This test was run at LNEC, in Portugal, where a facility was available (Figure 6.16). It consists of a square box located below ground level, 0.9 m deep, with an area of 4.84 m^2 (2.2 m x 2.2 m). Despite the fact that by operational reasons, a confining stress equal to 25 kPa was used in this test, it represents better the field conditions, due to its dimensions, than the small and intermediate-scale tests. The test lasted 6 months. The same soil and geosynthetics as those used in the intermediate-scale test were used.

The test assembly was similar to that of the intermediate-scale test, as can be seen in photographs included in Figure 6.17. There are two differences. First, the large-scale test included one supplementary gravel layer at the bottom of the test facility. The purpose of this 10 cm thick gravel layer was to hold any potentially water that could migrate towards the bottom of the composite liner due to consolidation of the soil, as due to the features of the test facility it was impossible to collect the water through a container at the base of the facility. Measurements carried out on a weekly basis through a piezometric probe indicated that no water reached that gravel layer. Observations made after the test disassembly confirm the absence of water in the bottom granular layer.

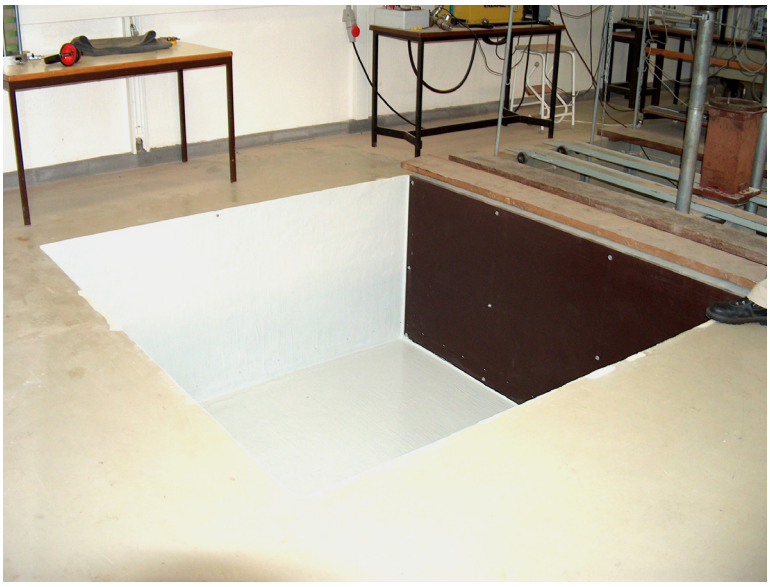

Figure 6.16 – Test facility that accommodated the large-scale test

Second, the normal stress was applied in a different way than in the intermediate scale test. Indeed, as there was no mechanical press to apply the normal stress, this was achieved by dead-weights, namely with concrete cubes (8 kg each), manually placed above the composite liner. As can be anticipated, for such a large area (4.84 m^2), it was necessary to use a huge amount of cubes to obtain a 50 kPa normal stress. Furthermore, the room was not high enough to reach a level of concrete blocks corresponding to this normal stress, and it would have been too much time consuming. Thus, the applied normal stress was limited to 25 kPa. It should be noted that even for such a small confining stress, about 12 tones were necessary, which means about 1500 concrete cubes.

From the bottom to the top, the test comprises the layers as follows (Figure 6.18):

- A geotextile 256 g m^{-2} to protect the base of the facility;
- 10 cm of gravel 25/35 mm to hold the potential water that could migrate from the soil due to its consolidation under the confining stress applied;
- A geotextile 642 g m^{-2} to separate the materials and to simplify the compaction of the cover soil;
- 27 cm of compacted soil at a moisture content equal to 13.9 %; the soil was compacted in 3 lifts 9 cm thick each;
- GCL-2, non-hydrated at a water content of 11.4 %, installed with the nonwoven geotextile on top;
- An HDPE geomembrane 2.0 mm thick, having a 3 mm diameter circular hole at its centre;
- A geotextile 828 g m^{-2} to protect the geomembrane against puncturing;
- A 22 cm thick layer of gravel 25/35 mm to simulate the drainage layer in a landfill; and
- Layers of concrete cubes (12084 kg) to apply a final confining stress over the geomembrane of 25 kPa.

Once again, this test was carried out with a hydraulic head equal to 0.3 m and the flow rates were measured thanks to a Mariotte bottle.

Figure 6.17 – Summary of large-scale test procedure

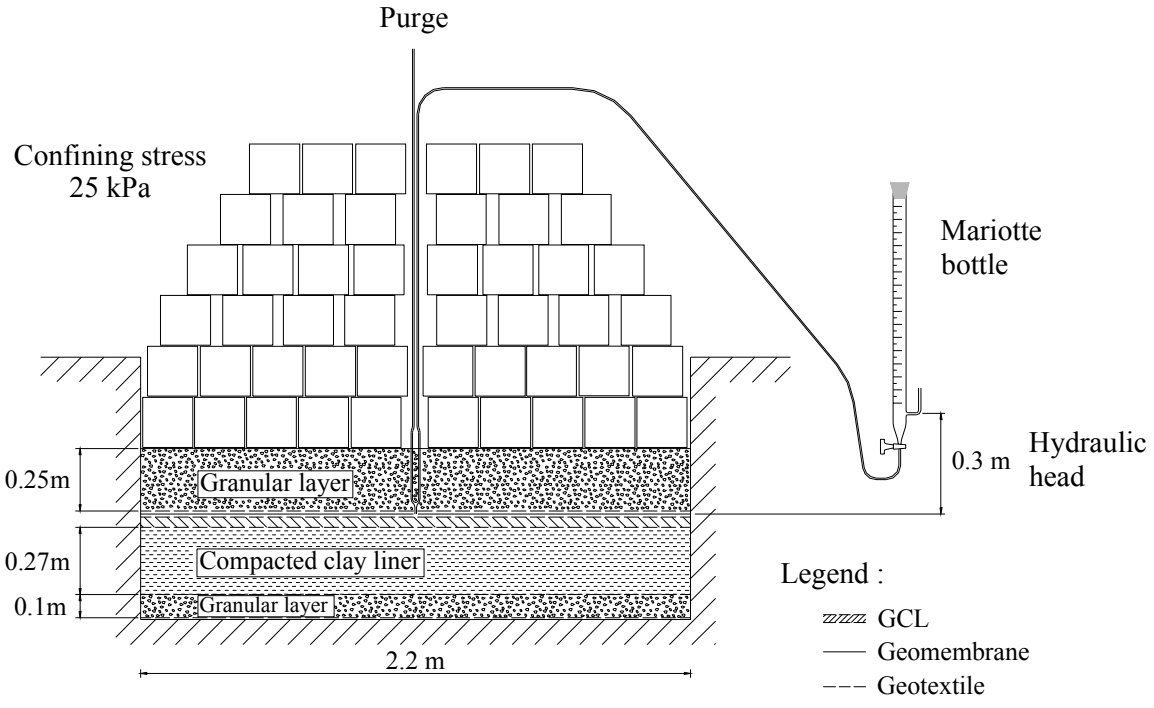

Figure 6.18 – Scheme of the large-scale test

6.4.3 Summary of the tests performed

Table 6.4 lists the tests carried out on flow rate through composite liners due to geomembrane defects as well as the test conditions used.

Table 6.4 – Summary of the tests carried out on flow rate through composite liners

Test No	Soil	GCL specimen	GCL status	Initial water content (%)	Final water content (%)	Normal stress (kPa)	Hydraulic head (m)
1	S-1	GCL-1	n-ph	10.1	131.8	50	0.3
2	S-1	GCL-1	n-ph	13.4	104.9	50	1.2
3	S-1	GCL-1	n-ph	11.1	99.0	200	0.3
4	S-1	GCL-1	n-ph	10.7	88.1	200	1.2
5	S-1	GCL-1	ph	86.6	150.1	50	0.3
6	S-1	GCL-1	ph	113.8	163.8	50	1.2
7	S-1	GCL-1	ph	89.6	96.3	200	0.3
8	S-1	GCL-1	ph	100.1	98.8	200	1.2
9	S-2	GCL-2	n-ph	11.3	110.4	50	0.3
10	S-2	GCL-2 (inverted)	n-ph	11.3	108.2	50	0.3
11	S-2	GCL-2	n-ph	10.3	122.7	25	0.3
11bis	S-2	GCL-2	n-ph	10.0	117.9	25	0.3
12	S-2	GCL-3	n-ph	11.3	152.2	50	0.3
13	S-2	GCL-3	n-ph	10.7	136.0	50	1.2
14	S-2	GCL-3	n-ph	10.2	107.8	200	0.3
15	S-2	GCL-3	n-ph	10.5	98.7	200	1.2
16	S-2	GCL-3	ph	100.8	155.9	50	0.3
17	S-2	GCL-3	ph	101.3	166.3	50	1.2
18	S-2	GCL-3	ph	84.0	98.2	200	0.3
19	S-2	GCL-3	ph	98.8	103.5	200	1.2
IST	S-2	GCL-2	n-ph	9.5	76.7	50	0.3
LST	S-2	GCL-2	n-ph	11.4	83.5	25	0.3

Notes: n-ph=non-prehydrated (water content as supplied); ph=prehydrated (moistened to about 100%); IST=Intermediate-scale test; LST=Large-scale test.

Tests 1 to 8 were performed with GCL-1, either using non-prehydrated specimens (test 1 to test 4), or using prehydrated specimens (test 5 to test 8). Test 9 was carried out in the same test conditions as the intermediate-scale test, with GCL-2, under non-prehydrated conditions. Test 10 was conducted in the same test conditions as test 9, but with GCL-2 inverted, i.e. with woven geotextile in contact with the geomembrane. They were conducted using

non-prehydrated specimens. Test 11 and test 11bis were performed under the same test conditions to study the repeatability of the test procedure. They were conducted using non-prehydrated specimens of GCL-2, in the same test conditions as the large-scale test. Tests 12 to 19 were performed with GCL-3, either using non-prehydrated specimens (test 12 to test 15), or using prehydrated specimens (test 16 to test 19). Non-prehydrated specimens were tested at their natural water content. Prehydrated specimens were moistened to approximately 100 %. Intermediate (IST) and large-scale tests (LST) were conducted using only non-prehydrated GCLs.

Next section is dedicated to the results. They are presented in terms of the evolution of the flow rate with time, final flow rates, radius of the wetted area, interface transmissivities and soil water contents. The results obtained are then discussed and compared in Section 6.4.5.

6.4.4 Results

6.4.4.1 Small-scale tests

6.4.4.1.1 Flow rates

Figures 6.19 to 6.21 present the evolution of flow rate for GCL-2, GCL-1 and GCL-3, respectively. Values of flow rates contain the error bars corresponding to the uncertainty calculated according to Appendix D. It should be noted that for some small values, the uncertainty value was higher than the flow rate value. In these cases, it was impossible to plot the corresponding error bars. To emphasise the big uncertainty associated to those measurements, a dashed line was drawn between the value of flow rate and the x-axis.

As can be observed, flow rate decreases with time until a steady state is reached. For comparison purposes, for GCL-1 and GCL-3, the time-scale of the graphs is truncated at 400 hours. For GCL-2, this procedure was not adopted, since for tests carried out both with woven geotextile facing the geomembrane and with a confining stress of 25 kPa, a longer time was necessary to reach the steady state. In addition, it can be seen that the uncertainty associated to flow rate measurements, in general, decreases as the confining stress used in tests decreases. Furthermore, it is higher for GCL-3 than for GCL-1. This is related with the Mariotte bottles used for performing the flow rate measurements. A lower uncertainty would be obtained if a Mariotte bottle with a higher resolution could be used.

The evolution of the flow rates in test 11 and 11bis is similar by taking into account the uncertainties associated to these measurements. This indicates a good repeatability of the test procedure.

By comparing the evolution of tests 9 and 10, conducted either with the non-woven geotextile in contact with the geomembrane (test 9) or with the woven geotextile (test 10), it can be seen that they presented a distinct behaviour during the initial and intermediate phase of testing, but similar final flow rates.

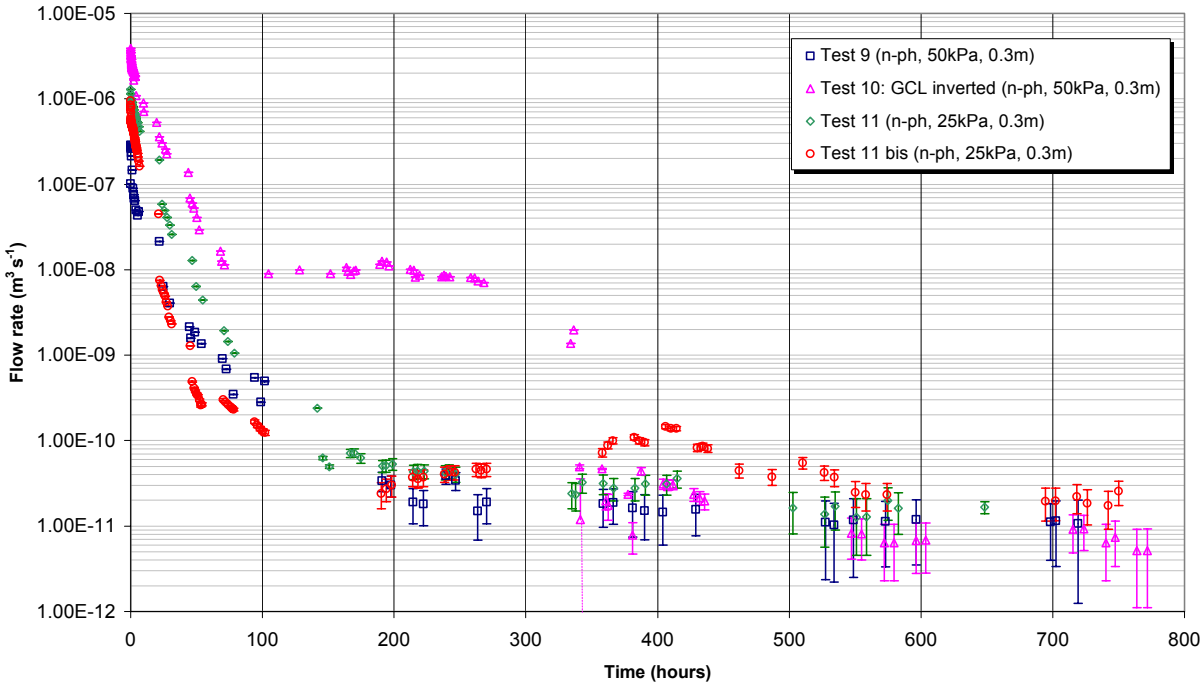

Figure 6.19 – Comparison of test results for GCL-2 in terms of flow rate

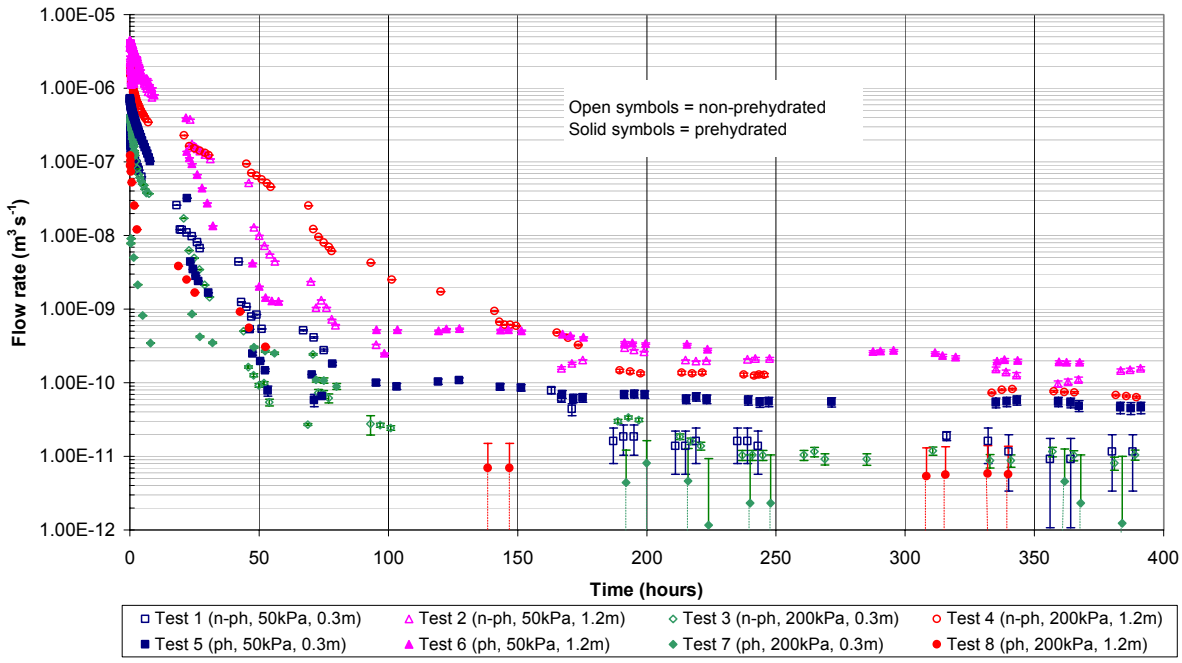

Figure 6.20 – Comparison of test results for GCL-1 in terms of flow rate

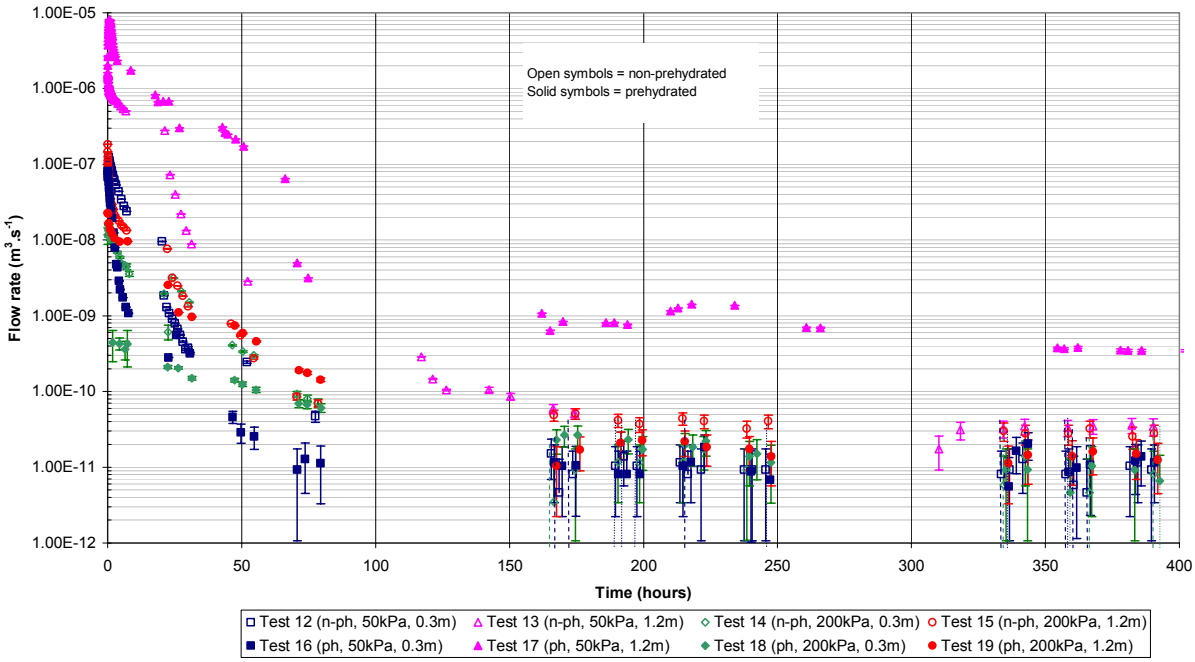

Figure 6.21 – Comparison of test results for GCL-3 in terms of flow rate

For GCL-1 and GCL-3 comparisons done in accordance with the research objectives tend to show that it is difficult to establish general trends expressing the influence of the prehydration, the confining stress, and the hydraulic head, particularly for GCL-3 due to the high uncertainties obtained in this case. Nevertheless, it seems that, as for the effect on the flow rate, it is important to take into account both the initial water content of specimens (non-prehydrated vs prehydrated) and the confining stress. Clearly, the increase in the confining stress affects differently non-prehydrated and prehydrated specimens. For the latter, the final flow rates were about one order of magnitude higher in tests conducted under a confining stress of 50 kPa than in tests carried out at 200 kPa. In contrast, for non-prehydrated GCLs, similar flow rates were obtained for both confining stresses. Also, results seem to indicate that the flow rate increases as the hydraulic head increases.

The observations made in terms of evolution of flow rates are in agreement with the observations made in terms of final flow rates, obtained in steady state conditions as the mean value of at least the last three consecutive flow measurements over a minimum time period of 36 hours.

Final flow rates are summarised in Tables 6.5. In overall terms, values obtained ranged from 2.9×10^{-12} to 3.6×10^{-10} m^3 s^{-1}. Looking these results in terms of ratios, it can be seen that the ratio between the final flow rates obtained in tests carried out with non-prehydrated specimens to that of the tests carried out with prehydrated specimens ranged from 0.1 to 0.7, for tests conducted at 50 kPa, and from 1.3 to 13.2, for tests carried out at 200 kPa. This suggests that prehydration has a small effect on final flow rates when low confining stresses are applied, whereas it may have a significant effect when high confining stresses are used. This finding seems to be confirmed by the ratios between the final flow rates obtained in tests carried out under a confining stress of 50 kPa to that of the tests carried out under a confining stress of 200 kPa. They ranged from 1.1 to 1.9, for tests conducted using non-prehydrated

specimens and from 1.8 to 31.8, for tests carried out using prehydrated specimens. These results tend to confirm that, as for the effect on the flow rate, it is important to take into account the relationship between the initial water content of GCLs and the confining stress. Finally, the ratio between the final flow rates obtained in tests performed with a hydraulic head of 1.2 m to that of the tests carried out with a hydraulic head of 0.3 m ranged from 3.4 to 12.7, for tests conducted using non-prehydrated specimens and from 1.8 to 29.5, for tests carried out using prehydrated specimens. This indicates that the final flow rate is higher for tests conducted with a high hydraulic head than for tests conducted with a low hydraulic head.

Table 6.5 – Summary of the tests carried out on flow rate through composite liners

Test No	Soil	GCL specimen	GCL status	Normal stress (kPa)	Hydraulic head (m)	Final flow rate ($m^3 s^{-1}$)
1	S-1	GCL-1	n-ph	50	0.3	1.0×10^{-11}
2	S-1	GCL-1	n-ph	50	1.2	1.3×10^{-10}
3	S-1	GCL-1	n-ph	200	0.3	1.0×10^{-11}
4	S-1	GCL-1	n-ph	200	1.2	7.0×10^{-11}
5	S-1	GCL-1	ph	50	0.3	5.0×10^{-11}
6	S-1	GCL-1	ph	50	1.2	1.7×10^{-10}
7	S-1	GCL-1	ph	200	0.3	2.9×10^{-12}
8	S-1	GCL-1	ph	200	1.2	5.3×10^{-12}
9	S-2	GCL-2	n-ph	50	0.3	1.1×10^{-11}
10	S-2	GCL-2 (inverted)	n-ph	50	0.3	5.6×10^{-12}
11	S-2	GCL-2	n-ph	25	0.3	1.5×10^{-11}
11bis	S-2	GCL-2	n-ph	25	0.3	2.4×10^{-11}
12	S-2	GCL-3	n-ph	50	0.3	8.7×10^{-12}
13	S-2	GCL-3	n-ph	50	1.2	3.5×10^{-11}
14	S-2	GCL-3	n-ph	200	0.3	8.5×10^{-12}
15	S-2	GCL-3	n-ph	200	1.2	2.9×10^{-11}
16	S-2	GCL-3	ph	50	0.3	1.2×10^{-11}
17	S-2	GCL-3	ph	50	1.2	3.6×10^{-10}
18	S-2	GCL-3	ph	200	0.3	6.6×10^{-12}
19	S-2	GCL-3	ph	200	1.2	1.4×10^{-11}

Notes: n-ph=non-prehydrated; ph=prehydrated (moistened to about 100%)

Final flow rates together with the radius of the wetted areas (presented in the next section) are used to determine the interface transmissivity, which will be used to interpret the results in Section 6.4.5.

6.4.4.1.2 Wetted area

In all small-scale tests, the radius of the wetted area was considered to be equal to the physical radius of the tests cell as a flow could always be observed at the downstream side of the cell, although in some tests this flow consisted just of some drops of water and could not be measured.

It could be observed that the effluent flow was not regularly coming out of the interface, but that there were some preferential flow paths all along the GCL specimen. To visualise the flow patterns in the interface, a blue dye (Comassie Blue) was injected in the influent flow in tests 9 and 10 (Figure 6.22). Results obtained tend to show the non-uniformity of the flow in the interface, regardless of the type of geotextile in contact with the geomembrane. Although at first glance the blue dye seems to involve a small area in the test 10 carried out with the woven geotextile in contact with the geomembrane (right side of the Figure 6.22), a closer look at the upper surface of the specimen shows some water pathways involving the entire area GCL area.

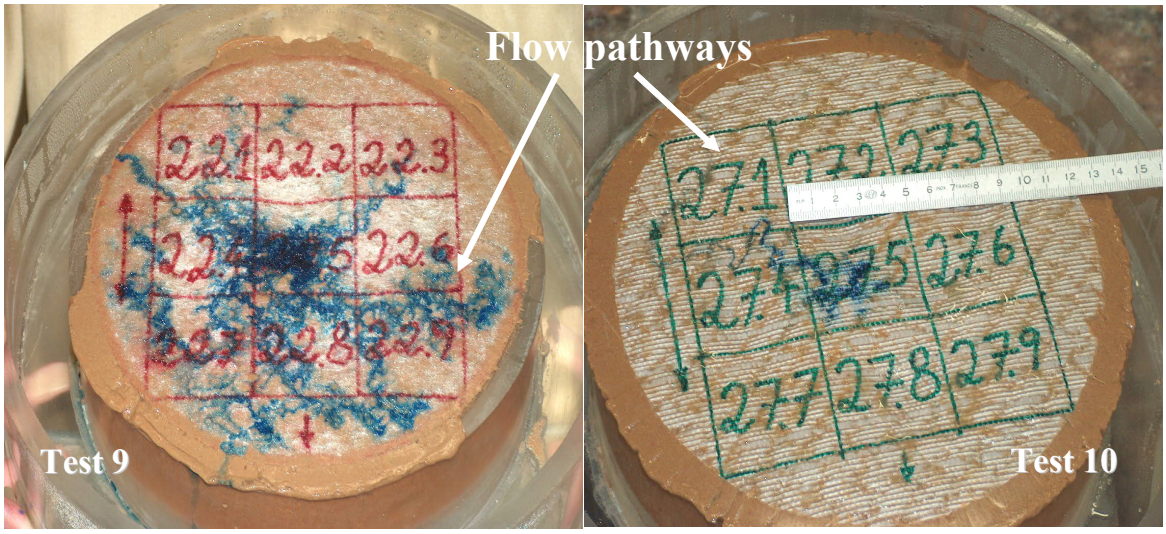

Figure 6.22 – View of the wetted area observed at the end of tests 9 and 10 carried out either with nonwoven geotextile facing the geomembrane or with woven geotextile facing the geomembrane

On the other hand, when the tests were disassembled, it could be observed that the geomembrane surface in contact with the GCL was not uniformly wet, as can be seen in the example depicted in Figure 6.23, confirming the non-uniformity of the flow in the interface.

Figure 6.23 – Example of the geomembrane lower surface in contact with the GCL at the end of test 9

These results tend to show the limitations of the modelling approaches presented in Chapter 4, which are based on the assumption that the flow in the interface is axi-symmetric and that the wetted area is circular. In addition, they indicate that the conceptualisation of a transmissive layer between the geomembrane and the GCL liner of uniform thickness may not be realistic, which highlights the need to improve the tools available for predicting the flow rate through composite liners.

Despite the limitations addressed, a radius of the wetted area equal to the physical radius of the test cell (i.e. 0.1 m) was assumed in order to interpret the results in terms of interface transmissivity.

6.4.4.1.3 Transmissivity

As discussed in Chapter 4, for laboratory tests, the transmissivity of the interface can be evaluated in two different ways: either based on Equations by Harpur et al. (1993), neglecting the flow within the bentonite and assuming that the flow at the interface is axi-symmetric, or based on Equations by Touze-Foltz et al. (1999) or by Rowe (1998), assuming that the GCL, the underlying soil and the interface are fully saturated, as well as that the flow at the interface is axi-symmetric. Following the terminology adopted by Harpur et al. (1993), the first one is termed as apparent transmissivity, whereas the latter is herein termed as effective transmissivity. Equation (4.60) by Harpur et al. (1993) and Equation (4.27) by Touze–Foltz et al. (1999) are respectively used to evaluate the apparent and effective transmissivity in small-scale tests.

This approach can not be followed for the intermediate and large-scale tests presented in Sections 6.4.4.2 and 6.4.4.3, since Equation (4.60) by Harpur et al. (1993) was developed for the case of laboratory tests where the value of R_c is known. Thus, for the intermediate and large-scale tests, an analytical solution has to be used, namely the solution that corresponds to zero flow at R_c with a hydraulic head equal to zero, i.e. field conditions.

Table 6.6 summarises the results obtained sorted by GCL status (non-prehydrated and prehydrated). First, it can be seen that identical values for interface transmissivity were found in small-scale tests, regardless of the approach followed for evaluating this parameter (apparent or effective transmissivity). This suggests that the infiltration of water in the GCL is negligible. It also suggests that both tools may be appropriate to evaluate the transmissivity, in the case of laboratory tests. Despite this finding, considering that for the intermediate and large-scale tests the apparent transmissivity cannot be calculated because the radius of the wetted area, R_c, is unknown, for the sake of the coherence, the analysis undertaken henceforth is made in terms of effective transmissivity, hereafter termed simply as transmissivity.

In the view of the research goals, Tables 6.7 and 6.8 presents the tests results sorted by confining stress and the hydraulic head, respectively.

Table 6.6 – Summary of the test results in terms of effective and apparent transmissivity sorted by GCL status

GCLs	Test conditions		Effective transmissivity (m^2 s^{-1})		Apparent transmissivity (m^2 s^{-1})	
	Normal stress (kPa)	Hydraulic head (m)	Non-prehydrated	Prehydrated	Non-prehydrated	Prehydrated
GCL-1	50	0.3	2.2×10^{-11}	1.1×10^{-10}	2.3×10^{-11}	1.1×10^{-10}
		1.2	7.3×10^{-11}	9.3×10^{-11}	7.3×10^{-11}	9.4×10^{-11}
	200	0.3	2.1×10^{-11}	5.7×10^{-12}	2.2×10^{-11}	6.5×10^{-12}
		1.2	3.8×10^{-11}	2.5×10^{-12}	3.9×10^{-11}	2.9×10^{-12}
GCL-3	50	0.3	1.7×10^{-11}	2.5×10^{-11}	1.9×10^{-11}	2.7×10^{-11}
		1.2	1.8×10^{-11}	2.0×10^{-10}	2.0×10^{-11}	2.0×10^{-10}
	200	0.3	1.8×10^{-11}	1.3×10^{-11}	1.9×10^{-11}	1.5×10^{-11}
		1.2	1.5×10^{-11}	7.0×10^{-12}	1.6×10^{-11}	7.8×10^{-12}
GCL-2 (test 9)	50	0.3	2.2×10^{-11}	----	2.5×10^{-11}	----
GCL-2 (test 10, specimen inverted)	50	0.3	1.0×10^{-11}	----	1.3×10^{-11}	----
GCL-2 (test 11)	25	0.3	3.2×10^{-11}	----	3.4×10^{-11}	----
GCL-2 (test 11 bis)	25	0.3	5.0×10^{-11}	----	5.3×10^{-11}	----

Table 6.7 – Test results sorted by confining stress

GCLs	Test conditions		Effective transmissivity (m^2 s^{-1})	
	Specimens status	Hydraulic head (m)	Stress = 50 kPa	Stress = 200 kPa
GCL-1	Non-prehydrated	0.3	2.2×10^{-11}	2.1×10^{-11}
		1.2	7.3×10^{-11}	3.8×10^{-11}
	Prehydrated	0.3	1.1×10^{-10}	5.7×10^{-12}
		1.2	9.3×10^{-11}	2.5×10^{-12}
GCL-3	Non-prehydrated	0.3	1.7×10^{-11}	1.8×10^{-11}
		1.2	1.8×10^{-11}	1.5×10^{-11}
	Prehydrated	0.3	2.5×10^{-11}	1.3×10^{-11}
		1.2	2.0×10^{-10}	7.0×10^{-12}

Table 6.8 – Test results sorted by hydraulic head

GCLs	Test conditions		Effective transmissivity (m^2 s^{-1})	
	Specimens status	Confining stress (kPa)	Hydraulic head = 0.3 m	Hydraulic head = 1.2 m
GCL-1	Non-prehydrated	50	2.2×10^{-11}	7.3×10^{-11}
		200	2.1×10^{-11}	3.8×10^{-11}
	Prehydrated	50	1.1×10^{-10}	9.3×10^{-11}
		200	5.7×10^{-12}	2.5×10^{-12}
GCL-3	Non-prehydrated	50	1.7×10^{-11}	1.8×10^{-11}
		200	1.8×10^{-11}	1.5×10^{-11}
	Prehydrated	50	2.5×10^{-11}	2.0×10^{-10}
		200	1.3×10^{-11}	7.0×10^{-12}

6.4.4.1.4 Soil water content

The soil below the GCL was also analysed in terms of water content. Table 6.9 shows the initial water content, the final water content and the differences obtained between the initial and the final water contents of the soil specimens. As can be observed, for soil S-1, this parameter increased in all tests, suggesting that the soil absorbed water during the tests.

For S-2, the variations between the initial and final water content were smaller than for S-1. For two tests, the water content of the soil even decreased, suggesting that the soil lost water during those tests.

Results obtained need to be analysed with caution, because, to determine the soil water content, the wet mass of the soil was determined by weighting the soil inside the test cell. If for the initial water content, the measurement is accurate, as the cell is totally dry, for the final water content, this measurement may not be very accurate, since it is impossible to guaranty that the cell is totally dry. Consequently, the final water contents of the soil may be overestimated in some tests. Based on the discussion above and on results summarised in Table 6.9, it can be concluded that the variations between initial and final water contents of the soil were negligible in small-scale tests.

Table 6.9 – Summary of the soil water contents

Test No.	Soil	Initial water content (%)	Final water content (%)	Difference (%) (final minus initial)
1	S-1	15.2	16.6	1.4
2	S-1	15.3	15.7	0.4
3	S-1	15.4	16.0	0.6
4	S-1	15.2	15.9	0.7
5	S-1	14.9	16.6	1.7
6	S-1	15.2	17.2	2.0
7	S-1	14.8	16.5	1.7
8	S-1	15.1	15.5	0.3
9	S-2	9.9	11.6	1.7
10	S-2	9.5	9.8	0.3
11	S-2	10.2	10.6	0.4
11bis	S-2	12.3	12.0	-0.3
12	S-2	9.5	10.5	1.0
13	S-2	9.5	10.2	0.7
14	S-2	9.7	10.1	0.4
15	S-2	9.6	9.8	0.2
16	S-2	9.7	9.8	0.1
17	S-2	9.6	10.6	1.0
18	S-2	10.0	10.1	0.1
19	S-2	10.2	9.7	-0.5

6.4.4.2 Intermediate-scale test

6.4.4.2.1 Flow rate

The evolution of the influent flow rate for the intermediate-scale test is depicted in Figure 6.24. Again, values of flow rates contain the error bars corresponding to the uncertainty calculated according to Appendix D.

The flow decreased with time until a steady state was reached. As in this test the flow was very small, to reduce the scatter on flow measurements, the values of total flow rates plotted in this figure were re-calculated on a weekly basis.

As regards the flow rate at the downstream side of the cell, no water was ever collected during the testing time in the container located at the bottom of the cell.

The final flow rate, obtained as the mean value of at least the last ten consecutive flow measurements, over a minimum time period of 10 days, was equal to 2.7×10^{-12} m^3 s^{-1}.

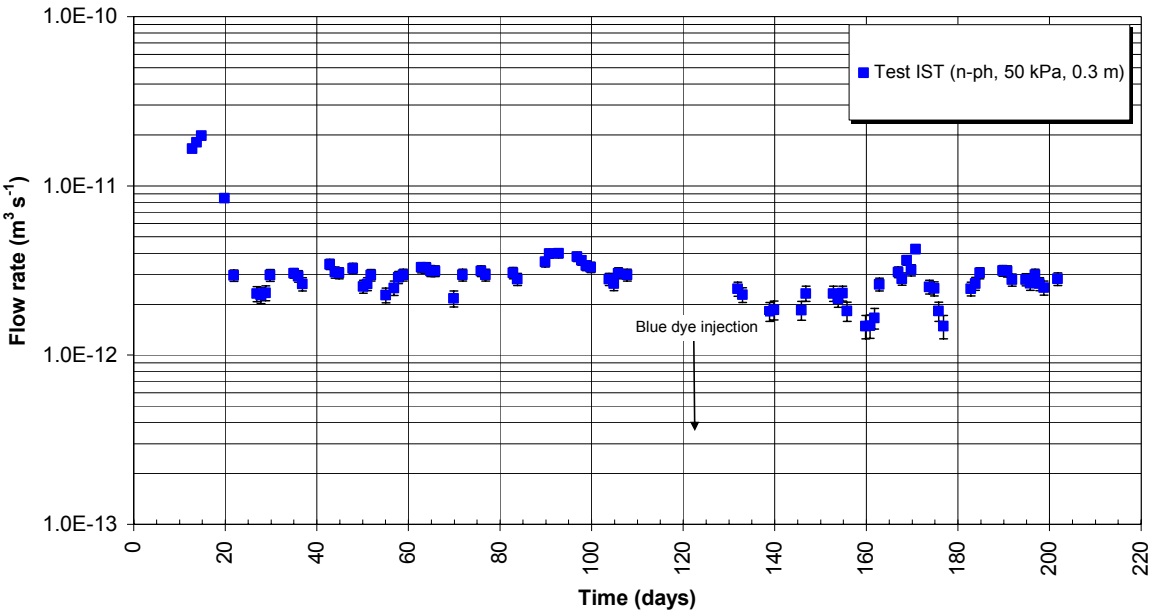

Figure 6.24 – Evolution of the flow rate for the intermediate-scale test

6.4.4.2.2 Wetted area

As no flow was observed at the cell boundary where free flow is allowed, the size of the wetted area is unknown. Following the same procedure as in the small-scale tests, the blue dye was injected in influent flow after the steady state achievement (see Figure 6.24). Results obtained are illustrated in Figure 6.25. The blue dye involved an area with a radius of about 1 cm. It should be noted that around the blue circle there is a grey coloration on a larger radius that could correspond to the wetted area obtained in the earlier phase of the test, when the flow rate was higher. This clearly shows that the wetted area evolves in time. The issue is to know if the equilibrium had already been attained, i.e. if the testing time was long enough to let the final wetted area be achieved.

Figure 6.25 – View of the wetted area observed in intermediate-scale test

In addition, results of the final water content of the GCL specimen measured thanks to circular sub-specimens cut from the GCL suggest a higher wetted area in the neighbourhood of the hole as can be observed in Figure 6.26, even if it is not the only location in the specimen where the water content is high. Circular sub-specimen cut for measuring the final water content of the GCL are represented by the red circles overlapped in this figure. The peculiar distribution of the final water content in the GCL may be related with some scatter observed both in the mass per unit area and in the thickness of the sub-specimens. Measurements of mass per unit area carried out in the same sub-specimens than those that were used to estimate the final water content are illustrated in Figure 6.27. Similar findings, not included here for the sake of brevity, were observed for the thickness. Results obtained tend to confirm that the scatter observed in the water content may be related with the scatter observed simultaneously in the mass per unit area and in the thickness of the GCL.

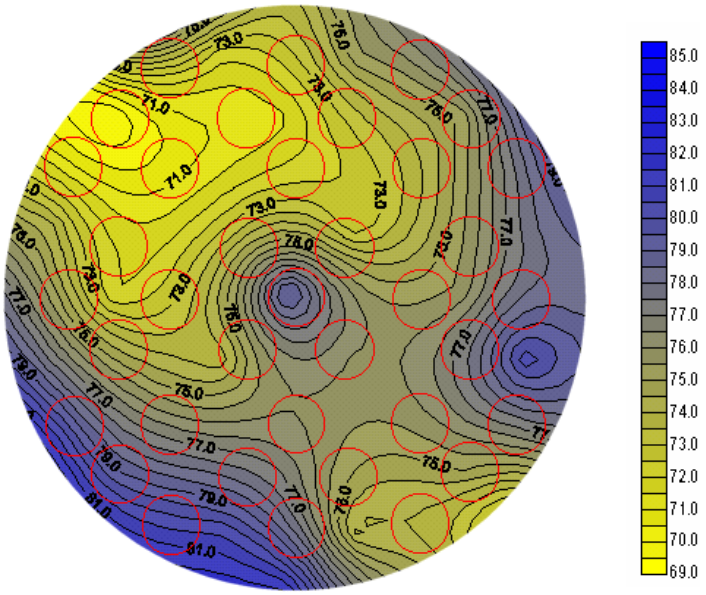

Figure 6.26 – Final water content of the GCL in intermediate-scale test

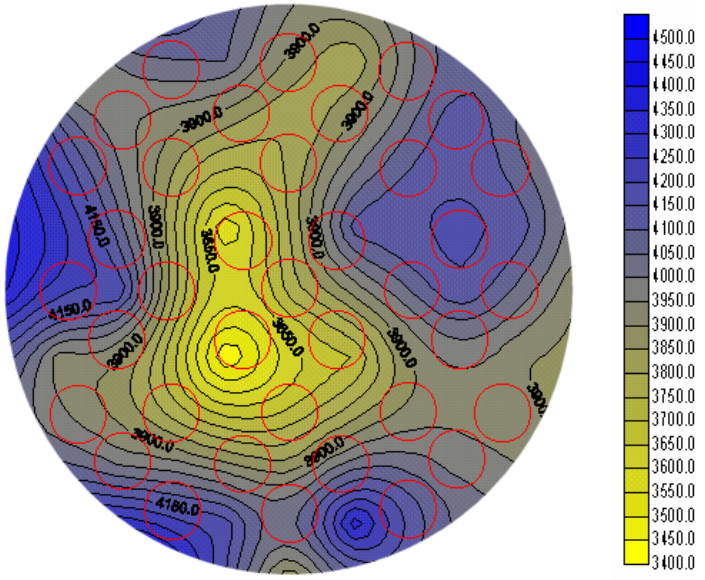

Figure 6.27 – Mass per unit of area of the GCL in intermediate-scale test

The value of the wetted radius can also be estimated by solving Equation (4.33). Based on this approach, the value of R_c obtained was 5.6 cm. This value is about five times higher than the one that could be observed thanks to the blue dye, which brings back the issue previously addressed, regarding the equilibrium of the wetted area.

Based on discussion above, to calculate the interface transmissivity, we adopted the value estimated using Equation (4.33), since it is more conservative than the one observed thanks to the blue dye.

6.4.4.2.3 Transmissivity

Based on the mean final flow rate and on the estimated radius of the wetted area (Sections 6.4.4.2.1 and 6.4.4.2.2), the transmissivity of the interface between the GCL and the geomembrane was evaluated by solving Equation (4.36). A transmissivity equal to 4.5×10^{-12} m^2 s^{-1} was obtained for the intermediate-scale test.

6.4.4.2.4 Soil water content

As for small-scale tests, the soil below the GCL was analysed in terms of water content. Figure 6.28 shows the initial and final values obtained from soil specimen collected at the soil surface.

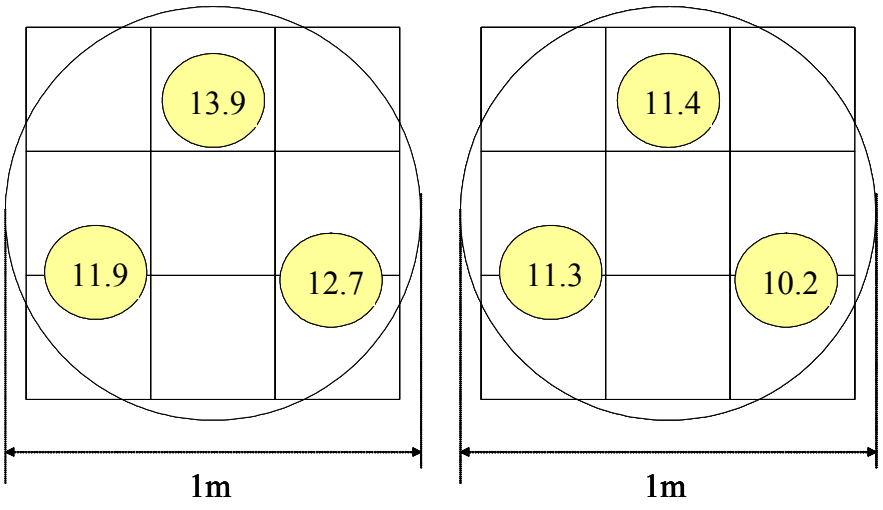

(a) Initial water content (b) Final water content

Figure 6.28 – Initial and final water contents of the soil in intermediate-scale test

Results obtained show that the water content of the soil decreased during the test, indicating that the soil lost water. This decrease seems to be linked with the increase in water content achieved by the GCL. The initial water content of the GCL was 9.5 % and after 6.5 months of testing it was 76.7 % (mean values). This behaviour of the GCL is consistent with the findings

obtained in Section 6.3.3, according to which GCLs present high values of suctions at their natural water content. Hence, GCLs are able to absorb water from the soil in order to reach pore pressure equilibrium. Results obtained are also consistent with the results obtained by Daniel et al. (1993) who observed that the GCLs absorb water from the soil. Daniel et al. (1993) placed specimens of GCLs on sand soils with water contents ranging from 1 to 17 % and measured the uptake of water in the GCL. They observed that after about four weeks, soils as dry as 1 % can result in GCL hydration to 50 %, whereas soils with a water content equal to 17 % can result in GCL hydration up to 175 %.

6.4.4.3 Large scale-test

6.4.4.3.1 Flow rate

Figure 6.29 illustrates the evolution of the flow rate for the large-scale test. As for small-scale tests, to reduce the scatter on flow measurements, the total flow rate was re-calculated on a 24 hour basis. During testing time, the air dissolved in tap water accumulated into the upper point of the pipe connecting the Mariotte bottle to the hole of the geomembrane. As a result, occasionally, it was necessary to remove the air from the pipe in order to guarantee that there was no interruption in water supply. For that, the hydraulic head was substantially increased (for about 2 meters) during a couple of minutes to force the air bubbles to escape through the purge also connected to the geomembrane hole. As can be observed in Figure 6.29, after this operation, the flow rate through the composite liner increased. It then stabilised again after a certain time.

The final flow rate obtained in large-scale test was 2.5×10^{-11} m^3 s^{-1}. This value corresponds to a mean value of at least the last ten consecutive flow measurements over a minimum period of 10 days.

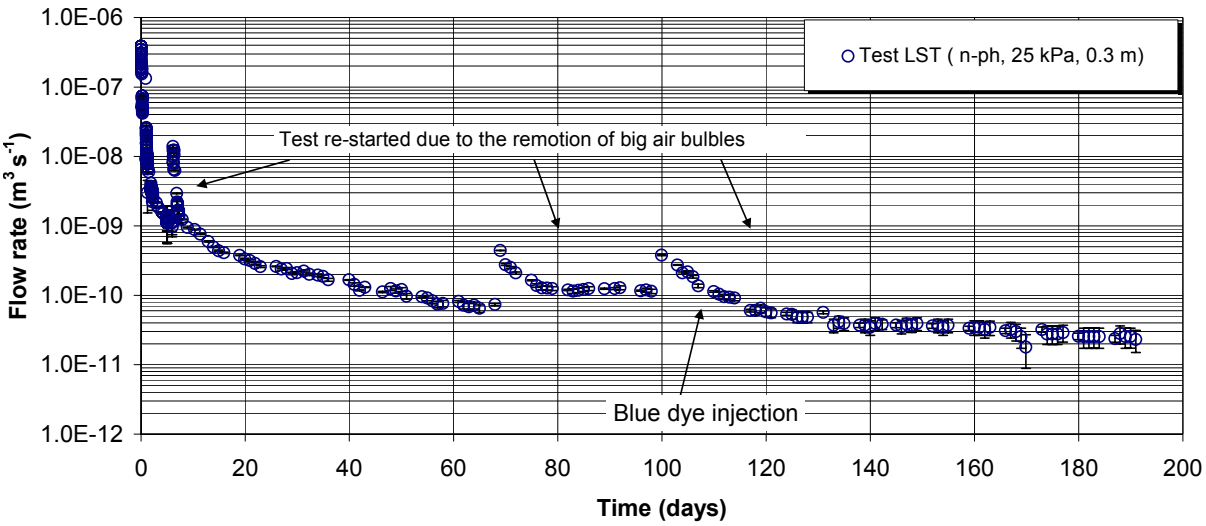

Figure 6.29 – Evolution of the flow rate for the large-scale test

6.4.4.3.2 Wetted area

As for the intermediate-scale tests, the radius of the wetted area is unknown *a priori*, as no edge effects could be noticed. To overcome this, once again some blue dye was injected in influent flow after the steady state achievement (see Figure 6.29). As can be observed in right side of the Figure 6.30, the wetted area is included in a circle with an approximately 0.11 m radius, which is not far from the wetted radius in small-scale tests.

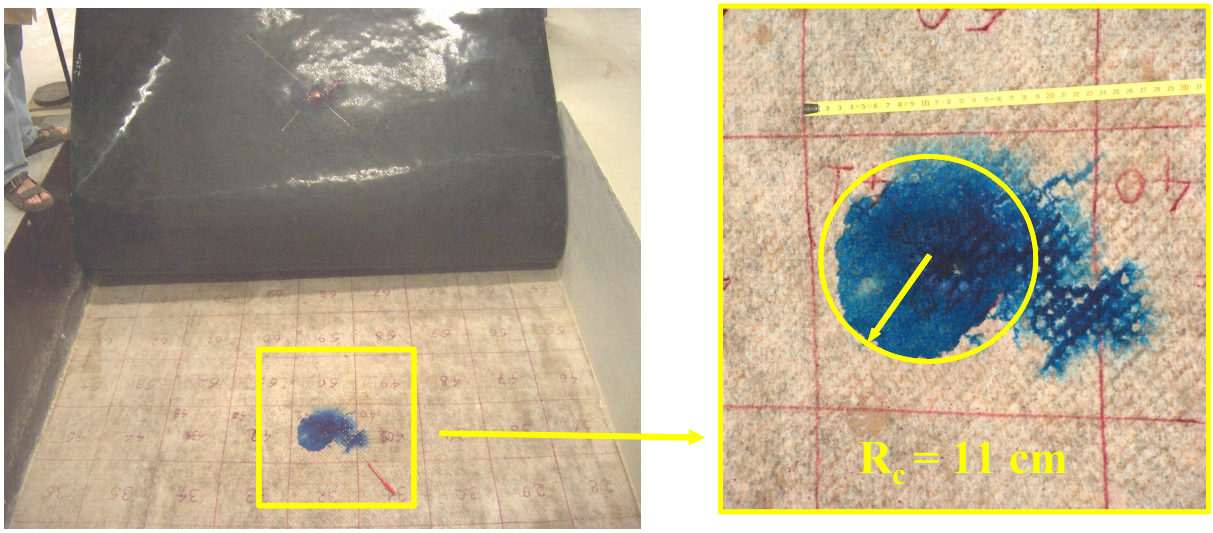

Figure 6.30 – View of the wetted area observed in large-scale test

The dimensions and shape of the wetted area in large-scale test seem to be confirmed by the results of the final water content of the GCL, measured over 91 squares of approximately 23.4×23.4 cm^2 each, cut from the GCL specimen according to the grid shown in left side of the Figure 6.30. Results of final water content measurements are depicted in Figure 6.31. As can be seen, the highest water contents were found near the hole.

It should be noted that observed dimensions for the wetted area are less than the ones estimated using Equation (4.33), although in the same order of magnitude. According to the calculation done using this equation, the radius of the wetted area would be 17.4 cm. Differences between observed and estimated values can be explained by the assumptions done in calculations, such as, for example, the uniformity of the flow in the interface, the saturation of GCL, etc. Furthermore, again, there is no guaranty that the wetted area observed thanks to blue dye is the final one. A longer testing time could increase the value of the radius of the wetted area.

Based on these findings and for maintaining the coherence with the approach adopted in intermediate-scale test, the radius of the wetted area estimated by solving Equation (4.33) was adopted also in this test to calculate the interface transmissivity.

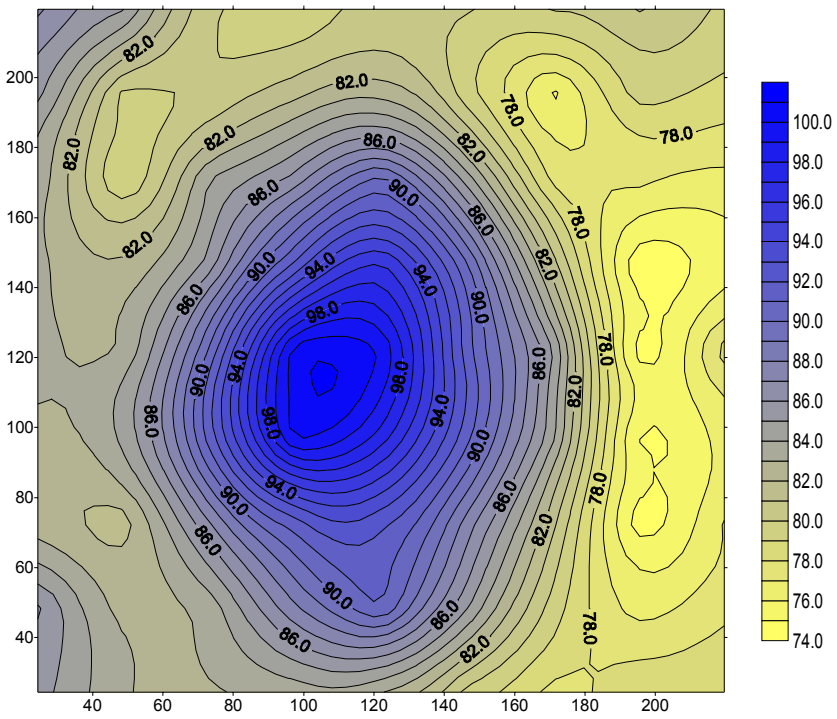

Figure 6.31 – Final water content of the GCL in large-scale test

6.4.4.3.3 Transmissivity

Once again, the interface transmissivity was estimated by solving Equation (4.36), being based on the mean final flow rate and on the estimated radius of the wetted area indicated in Sections 6.4.4.3.1 and 6.4.4.3.2, respectively. A transmissivity equal to 5.7×10^{-11} m^2 s^{-1} was obtained for the large-scale test.

6.4.4.3.4 Soil water content

Figure 6.32 shows the initial and the final water contents obtained from soil specimens collected in soil surface.

The final water contents of the soil specimen are less than the initial ones, indicating that the soil lost water in this test. Again, this decrease was related with the increase in water content of the GCL, which due to its value of suction is able to absorb water from the soil. The initial water content of the GCL was 11.4 % and the final water content, after 6 months of testing, was 83.5 % (mean values). This increase in water content of the GCL is relatively higher than the one obtained in intermediate-scale test. This may be due to the fact that in the intermediate-scale test the GCL was submitted to a confining stress of 50 kPa, while in the large-scale test the GCL was submitted to a confining stress of 25 kPa.

These findings are consistent with the data presented by Giroud & Daniel (2004). According to these authors, the volumetric content of hydration water, i.e. the amount of water used to hydrate the GCL, decreases with increasing values of the confining stress.

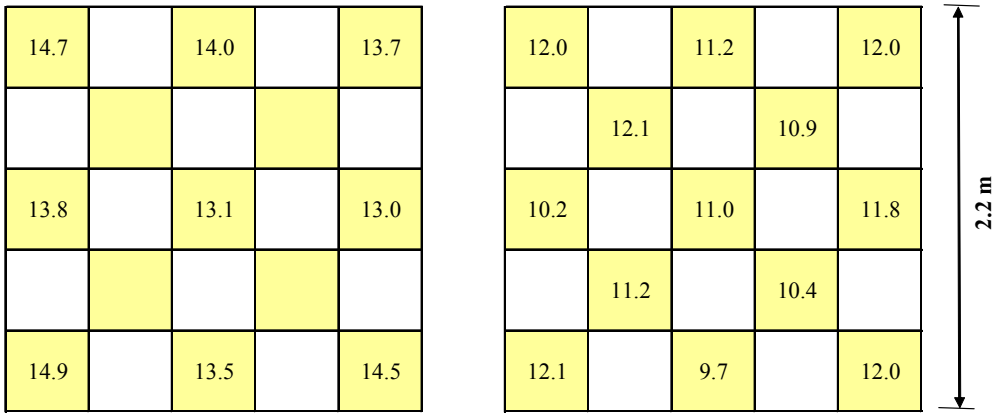

Figure 6.32 – Initial and final water contents of the soil in large-scale test

6.4.5 Discussion

6.4.5.1 Repeatability

By observing Tables 6.5 and 6.6, it can be seen that both the final flow rate and the transmissivity were similar in tests 11 and 11bis, by taking into account the uncertainties associated to these measurements. The final flow rates obtained in these tests were, respectively, equal to 1.5×10^{-11} and to 2.4×10^{-11} m^3 s^{-1}. Corresponding transmissivities were equal to 3.2×10^{-11} and to 5.0×10^{-11} m^2 s^{-1}.

These results tend to confirm the good repeatability of the test method, observed in the evolution of the flow rate during the testing time. Nonetheless, as in this study the repeatability was checked just for one test condition, this point should be further investigated.

6.4.5.2 Influence of the soil on the transmissivity value

By knowing that in the present study, on the one hand, two soils were used, which were characterised by two different hydraulic conductivities and, on the other hand, the thickness of the soil layer was not equal in small, intermediate and large-scale tests, the influence of these two parameters on interface transmissivity needs to be addressed. For that purpose, two numerical parametric studies were carried out.

The first one consisted in estimating the transmissivity using Equation (4.27), for different hydraulic conductivities, by maintaining constant the other input parameters necessary to solve that equation. Besides the hydraulic conductivity of the soils used in this study (8×10^{-11} and 3×10^{-10} m s^{-1}), the hydraulic conductivities that will be considered for developing the empirical equations in Section 6.5 were also used (i.e. 1×10^{-8}, 1×10^{-9}, 1×10^{-10} m s^{-1}). The other input parameters that were kept constant in calculations included: soil thickness equal to 4.5×10^{-2} m; GCL hydraulic conductivity equal to 5×10^{-11} m s^{-1}; GCL thickness equal to

6×10^{-3} m; hole radius equal to 1.5×10^{-3} m; radius of the wetted area equal to 0.1 m; hydraulic head equal to 0.3 m; and flow rate equal to 1×10^{-11} m^3 s^{-1}.

Table 6.10 shows the results obtained in this parametric study. They indicate that the hydraulic conductivity of the soil under the GCL has a minor effect on interface transmissivity.

Table 6.10 – Influence of the soil hydraulic conductivity on interface transmissivity

Soil hydraulic conductivity ($m\ s^{-1}$)	Transmissivity ($m^2\ s^{-1}$)
8×10^{-11}	2.1×10^{-11}
3×10^{-10}	1.9×10^{-11}
1×10^{-8}	1.7×10^{-11}
1×10^{-9}	1.8×10^{-11}
1×10^{-10}	2.1×10^{-11}

The second parametric study consisted also in estimating the transmissivity using Equation (4.27), for different soil thickness, by maintaining constant the other input parameters necessary to solve that equation. Besides the soil thickness used in tests at three scales (i.e. 0.045 m, for small-scale tests and 0.27 m, for intermediate and large-scale tests), other values were used, from the range that will be used for developing the empirical equations in Section 6.5, namely: 0.5 m, 1 m and 5 m. The other input parameters that were kept constant in calculations included: soil hydraulic conductivity equal to 1.0×10^{-9} m s^{-1}; GCL hydraulic conductivity equal to 5×10^{-11} m s^{-1}; GCL thickness equal to 6×10^{-3} m; hole radius equal to 1.5×10^{-3} m; radius of the wetted area equal to 0.1 m, hydraulic head equal to 0.3 m; and flow rate equal to 1×10^{-11} m^3 s^{-1}.

Table 6.11 shows the results obtained in this parametric study. They show that the variation in soil thickness has a negligible influence on the interface transmissivity.

Table 6.11 – Influence of the soil thickness on interface transmissivity

Soil thickness (m)	Transmissivity ($m^2\ s^{-1}$)
0.045	1.8×10^{-11}
0.27	1.6×10^{-11}
0.5	1.5×10^{-11}
1	1.5×10^{-11}
5	1.4×10^{-11}

Based on results obtained in the parametric studies conducted, it can be assumed that the variations both in the hydraulic conductivity and in the soil thickness have a minor impact on

interface transmissivity. Thus, variations in interface transmissivity, which can be obtained in tests at different scales, cannot be linked with the differences in these parameters.

6.4.5.3 Influence of the type of geotextile (nonwoven/woven) facing the geomembrane

A comparison between results obtained in tests 9 and 10 (see Figure 6.19) suggests that there is an influence exerted by the way the GCL is installed. Contrary to what could be expected, during the 350 first hours of test, the specimen with the woven in contact with the geomembrane presented a higher flow rate than the specimen with the nonwoven side up. This unexpected behaviour may be due to bentonite piping. Effluent flow collected at the downstream side of the cell during the first phase of test 10 contained some bentonite that migrated from the GCL as can be seen in Figure 6.33. This GCL has powdered bentonite that apparently is looser than the granular one. Bentonite loss might also occur due to transport, handling and placement of the specimen in cell. As a result, flow paths could be created into the GCL through which the water could flow and a high radial flow rate was obtained during the beginning of test 10. It should be noted that, after the first 80 hours, the flow stabilised for about 200 hours, between 100 and 300 hours, and then dropped to an identical value as the one obtained in tests run with the nonwoven geotextile facing the geomembrane. To check the possibility of occurrence of subsequent drops in flow, test 10 was run for about 1000 hours, but the flow rate remained stabilised during the rest of the testing time.

The behaviour exhibited by the flow rate in test 10, between 100 and 300 hours, may be the result of self-healing of the GCL, which may occur as the bentonite becomes hydrated. Self-healing of GCLs was reported by Orsini & Rowe (2001) and by Rowe et al. (2002), within the scope of a testing program conducted for the study of internal erosion of this type of liner.

Figure 6.33 – Effluent flow collected during the first phase of test 10

The ratio between the final flow rates of the test carried out with the nonwoven geotextile facing the geomembrane (test 9) to that of the test conducted with the woven geotextile (test 10) is 2.0. A similar ratio was obtained in terms of transmissivity. Taking into account the uncertainties associated to these measurements, the differences obtained can be considered as insignificant.

This finding is consistent with the results obtained by Harpur et al. (1993). It is also in agreement with the results obtained in preliminary tests performed within the scope of the present research, as reported by Touze-Folz et al. (2002a). For the geotextile mass per unit of area investigated, these results tend to show that the type of geotextile has a minor effect on the interface transmissivity, on the long term.

6.4.5.4 Influence of the type of bentonite (granular versus powdered)

Comparing the results obtained in tests 1 and 9 (Figure 6.34), it can be found that the flow rate and the transmissivity were identical in both tests. Similar final flow rates and transmissivities were also obtained in these tests. These results suggest that the nature of bentonite (granular or powdered) has no influence on these parameters. This point should be investigated for other products before establishing a generalisation of that result.

These results differ from the results obtained by Harpur et al. (1993), which obtained a transmissivity about one order of magnitude lower for GCL with the powdered bentonite than for GCL with the granular bentonite. Differences between the results obtained in this study and the results obtained by Harpur et al. (1993) might be related with the differences in GCLs studied. Also, the test procedure was different. For small flows, Harpur et al. (1993) performed falling head tests, estimating the flow rate based on water fall in a 7 mm diameter capillary pipe during a certain time interval, whereas in this study, only constant head tests were performed. Therefore, the flow rate measurements were here always taken in steady state conditions. It seems that further research on this topic is needed before some general trends can be established.

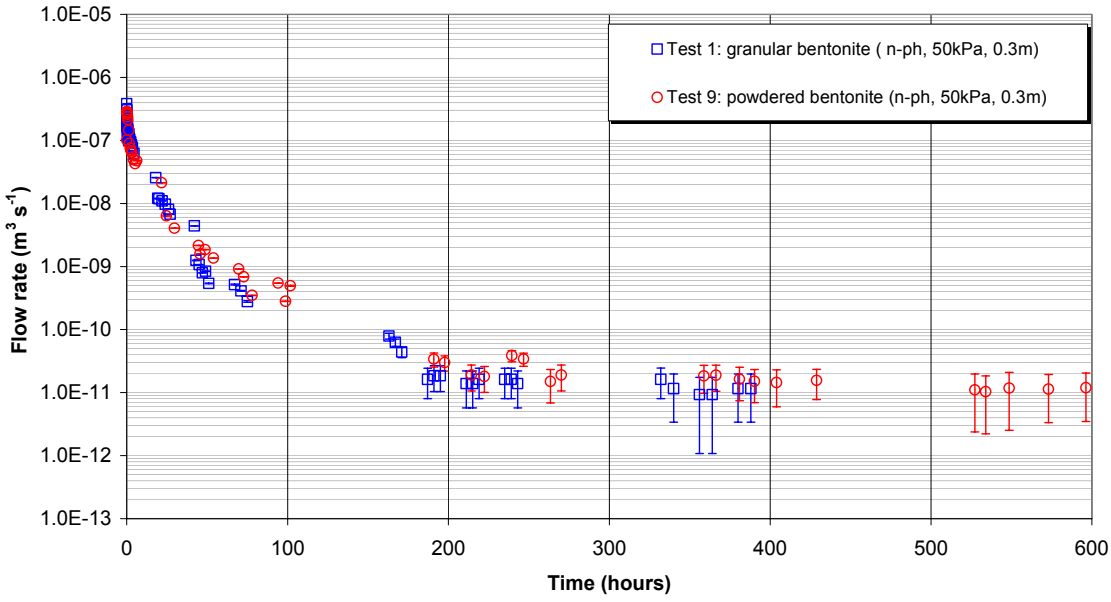

Figure 6.34 – Comparison of the results in tests carried out with granular and powdered bentonite in GCLs

6.4.5.5 Influence of prehydration and of confining stress

The transmissivity results (see Tables 6.6 to 6.8) tend to confirm that they are influenced by both the initial water content of GCL and the confining stress. Similar transmissivities were found in tests carried out with non-prehydrated and prehydrated GCLs, under a low confining stress. In contrast, higher transmissivities were found in tests conducted with non-prehydrated rather than with prehydrated specimens under a high confining stress. The ratio between the tests carried out with non-prehydrated specimens to that of the tests carried out with prehydrated specimens ranged from 0.1 to 0.8, for tests conducted at 50 kPa, and from 1.3 to 15.4, for tests conducted at 200 kPa. Therefore, it seems that prehydration has a small impact on transmissivity for tests carried out under a low confining stress, but seems to have an important impact for tests carried out under a high confining stress.

On the other hand, the increase in confining stress has a negligible effect on transmissivity when non-prehydrated GCLs are used, whereas it has a high impact on transmissivity when prehydrated specimens are used. For the latter, transmissivity was in general higher under a normal stress of 50 kPa than under a normal stress of 200 kPa, except for GCL-3 tested with a hydraulic head of 0.3 m. In this particular case, differences obtained were small. However, due to the significant uncertainties associated to flow rate measurements and, therefore, to transmissivity, no conclusions can be drawn. Disregarding these results, for prehydrated GCLs, the ratio between transmissivity of tests carried out under a confining stress of 50 kPa to that of tests conducted under a confining stress of 200 kPa ranged from 19.1 to 37.4.

Differences obtained may be related with the prehydration process. Prehydrated specimens were kept under stress during one week, for water content homogenisation purposes, before being installed in the test cell. As a result, according to findings by Lake & Rowe (2000), for the confining stress applied, prehydrated specimens may not swell significantly after being installed in test cell, as their thickness is nearly stabilised after the water content homogenisation period. It follows that no significant variations in the quality of contact between GCL and geomembrane are expected due to GCL swelling. In this circumstance, in tests carried out under 50 kPa, the interface may be thicker than in tests carried out under 200 kPa, which, according to Equation (4.52), leads to a high transmissivity.

In opposition, non-prehydrated specimens hydrate and swell in the test cell during the entire test and thus the quality of the contact with geomembrane improves both under low and high confining stress. It follows that similar transmissivities can be found regardless of the confining stress applied. These results are consistent with the findings reported by Harpur et al. (1993), while they tested non-prehydrated GCLs.

Based on the above findings, it seems difficult to conclude if it is advantageous to prehydrate the GCLs after their installation as recommended by the *Comité Français des Géosynthétiques* (1998). The coupled effect of water content and confining stress on the transmissivity needs further research. There should be more experimental work, using a wide range of water contents, confining stress and GCLs, to clarify if there is a couple water content/stress after which it is undoubtedly beneficial to hydrate the GCLs.

6.4.5.6 Influence of the hydraulic head

The increase in hydraulic head from 0.3 m to 1.2 m seems to have a smaller impact on non-prehydrated specimens than on prehydrated GCLs. The ratio between the transmissivity

of tests carried out with a hydraulic head of 0.3 m to that of tests conducted under a hydraulic head of 1.2 m ranged from 0.3 to 1.1, for non-prehydrated specimens and from 0.3 to 2.3, for prehydrated ones. However, as the higher ratios correspond in general to tests carried out under high confining stresses, where bigger uncertainties on flow rate measurements were found, differences obtained in transmissivity between these two hydraulic heads can be considered unimportant. More experimental data would be necessary to better know the influence of hydraulic head on transmissivity.

6.4.5.7 Comparison between different scale tests

6.4.5.7.1 Intermediate-scale versus small-scale

Comparing the results obtained in intermediate-scale test and test 9, it is found that both the final flow rate and the interface transmissivity are about half an order of magnitude higher in small-scale tests than in intermediate scale test (transmissivity equal to 2.2×10^{-11} m^2 s^{-1}, for test 9 and equal to 0.5×10^{-11} m^2 s^{-1}, for intermediate-scale test). Considering the uncertainties obtained in these measurements, as well as the assumptions made for calculating the transmissivity (e.g. saturated hydraulic conductivity of the GCL, constant GCL thickness, etc.), the difference found between these two scale tests can be considered as slight, although the results obtained in small-scale tests are overestimated as compared with the results obtained intermediate-scale test.

This overestimation is confirmed when looking at the wetted areas. Indeed, in intermediate-scale test the radius of the wetted area was about 10 times less than in small-scale tests. However, it should be noted that these tests were carried out in different time frames. Smaller wetted areas and, consequently, flow rates might be obtained also in small-scale tests if longer testing times would be considered. In addition, the fact that in intermediate-scale test be possible to observe a grey coloration on a larger radius around the wetted area identified thanks to blue dye (see Figure 6.25) suggests that, in the beginning, when the flow was higher, there was a larger wetted area. Hence, a smaller wetted area could be obtained in intermediate-scale test if longer tests could be performed. On the other hand, one does not know if the time was long enough in intermediate-scale test for the dye to reach the edge of the wetted area. Nevertheless, results obtain tend to show that transmissivities obtained in small-scale tests represent an upper bond. Numerical modelling of flow in unsteady state conditions could bring some light on the evolution of the wetted area, as well as on the evolution of the flow rate over time.

6.4.5.7.2 Large-scale versus small-scale

Comparing the results obtained in large-scale test and test 11 or test 11bis, it can be observed that the final flow rate is identical, both in the large and in the small-scale tests, considering the uncertainty associated to these measurements. As regards transmissivity, similar values were also obtained (3.2×10^{-11} m^2 $s^{-1}$and 5.0×10^{-11} m^2 s^{-1}, respectively for tests 11 and 11bis and 5.7×10^{-11} m^2 s^{-1}, for large-scale test). Nonetheless, a closer look at Figure 6.29 suggests that the fact that the large-scale test was re-started several times increased the flow. In fact, it can be observed that the flow was still decreasing after six months of testing. This tends to indicate that a lower flow rate could have been obtained if the test had been longer.

Comparisons can also be done in terms of wetted area. In these tests, a similar radius of the wetted areas was identified. However, as previously hypothesised, the large wetted area found in large-scale test could decrease in time if a longer test would have been carried out. Furthermore, it is unclear if the wetted area obtained corresponds to the large flow rate measured when restarting the test or to the flow rate at a quasi steady state. Also, there is no guarantee that the final wetted area had already been attained in the small-scale tests. As large wetted areas mean large transmissivities and large flow rates, values obtained both in large-scale and in small-scale tests may be overestimated. More experimental data would be necessary to better know the behaviour of flow rates on the long term. Knowledge on this topic can also be achieved through numerical modelling.

6.4.5.7.3 Summary of Section 6.4.5.7

Discussions addressed in Sections 6.4.5.7.1 and 6.4.5.7.2 tend to show that, for confining stresses considered in this study (25 and 50 kPa), transmissivity obtained in small-scale tests can be seen as an upper bond of the transmissivity obtained in intermediate and large-scale tests. This suggests that predictions on flow rates though composite liners due to geomembrane defects, which are based on transmissivity values obtained in small-scale tests, are conservative.

6.4.5.8 Comparisons with results reported in literature

6.4.5.8.1 Laboratory studies

Results obtained in this study are consistent with the results reported by Harpur et al. (1993): the flow rates decreased throughout the tests until they reached a steady state. Nevertheless, it should be noted that tests carried out by Harpur et al. (1993) lasted two weeks both for tests conducted with the nonwoven and woven geotextile facing the geomembrane. This testing period was adopted by these authors based on the fact that calculated apparent transmissivity was found to vary somewhat above and below a certain average value, near the end of this period. Testing times longer than two weeks were not investigated. However, results obtained in test 10, carried out with the woven geotextile facing the geomembrane, and at low confining stress (tests 11 and 11bis) showed that two weeks may not be enough to reach a steady state in these cases. It follows that some tests performed by Harpur et al. (1993) may have probably terminated before the steady state had been truly reached. Therefore, lower final flow rates and corresponding interface transmissivities, could have been obtained in tests carried out at a low confining stress and with woven geotextiles facing the geomembrane.

In overall terms, the transmissivity values given by Harpur et al. (1993) have a wide range than the ones obtained in this study. Values given by these authors were in the range 6×10^{-12} to 2×10^{-10} $m^2\ s^{-1}$, whereas the values obtained here with non-prehydrated GCLs vary between 1.5×10^{-11} and 7.3×10^{-11} $m^2\ s^{-1}$. These differences can be due to the fact that the normal stress was uniformly applied in the tests performed by Harpur et al. (1993), whereas, in the present work, that stress was applied in a limited number of contact points, as there is a granular layer on top of the geomembrane. This difference could also be related to the fact that Harpur et al. (1993) measured the flow in a falling head test, through a capillary pipe that is less accurate than a Mariotte bottle, which could induce some scatter on test results.

Regarding the results reported by Koerner & Koerner (2002), by comparing the flow rate obtained by these authors with the final flow rate obtained in tests 5 and 16, it is found that both results are in the same order of magnitude. The ratio between the flow rate of tests conducted by Koerner & Koerner (2002) to that of test 5 (GCL-1) and test 16 (GCL-3) is equal to 0.6 and 2.5, respectively.

6.4.5.8.2 Field studies

Flow rates measured in laboratory through a 3 mm diameter circular hole in the geomembrane can also be compared with the mean flow rates measured in secondary leachate collection system of landfills constructed with double composite liner systems (recall Section 4.7). For comparison purposes, flows will be expressed in litres per hectare/day (lphd). In this framework, two hole densities are considered: 2.5 holes per hectare, following the suggestion given by Giroud & Bonaparte (1989), and 15.3 holes per hectare, considering the literature review done in Section 2.3.1.3.3. Minimum and maximum values of flow rates obtained in laboratory tests conducted in small-scale tests are considered to calculate flow rates, for these two hole densities. Table 6.12 summarises results obtained.

Table 6.12 – Calculated flow rates for two hole densities of 2.5 and 15.3 holes/ha, based on flow rates measured in the laboratory through a 3 mm diameter circular hole

GCL status	Flow rate measured in the present study ($m^3 s^{-1}$)		Calculated flow rate for 2.5 holes/ha (lphd)	Calculated flow rate for 15.3 holes/ha (lphd)
Non-prehydrated	Minimum	5.6×10^{-12}	0.001	0.007
	Maximum	1.3×10^{-10}	0.029	0.174
Prehydrated	Minimum	2.9×10^{-12}	0.001	0.004
	Maximum	3.6×10^{-10}	0.077	0.472

It can be seen that calculated flow rates are in the range of 0.001 to 0.077 lphd assuming a hole density of 2.5 holes per hectare, and in the range of 0.004 to 0.472 lphd assuming a hole density of 15.3 holes per hectare. These flow rates are not in contradiction with the lower limit of a recent study sponsored by USEPA and reported by Majdi et al. (2002). According to this study, the flow rate ranged from 0 to 11 lphd, during the active period and from 0 to 2 lphd, during the post-closure period. The difference between the values estimated based on laboratory tests and the ones reported from field studies may be related with the fact that the laboratory tests covered only a small range of possibilities with respect to shape, location and size of the holes, which may not be representative of what happens in the field, as discussed in Chapter 2. For instance, a hole in a wrinkled geomembrane or a defective seam would increase substantially the flow rate, as discussed by Rowe (1998) and by Touze-Foltz et al. (1999). These findings tend to confirm the need for further studies on flow rates through composite liners when the geomembrane exhibits wrinkles or defects of infinite length.

6.4.5.9 Comparison with field contact conditions

There are two approaches for calculating the interface transmissivity. It can be estimated either based on experimental measurements of flow rate such as the ones described in this study, or through mathematical expressions by knowing the hydraulic conductivity of the soil liner above the geomembrane. As mentioned in Section 4.4.5, the mathematical expressions currently available were defined for soil liners and cover three contact conditions: poor, good and excellent.

The values of interface transmissivity obtained in this study are plotted against the hydraulic conductivity of GCLs (see Table 6.1) together with the synthetic results obtained using Equations (4.56) to (4.58), respectively for poor, good and excellent contact conditions in Figure 6.35. This figure also includes the results reported by Touze-Foltz et al. (2002a), obtained in preliminary tests conducted within the scope of this research with composite involving either a needlepunched GCL (GCL-A) or a stitched bonded GCL (GCL-B). The results from Harpur et al. (1993) and from Koerner & Koerner (2002) are not plotted in the figure because, in the first case, there is no information available concerning the hydraulic conductivity of tested GCLs, and in the second, also there is no data regarding the wetted area, which makes it difficult to estimate the corresponding transmissivity.

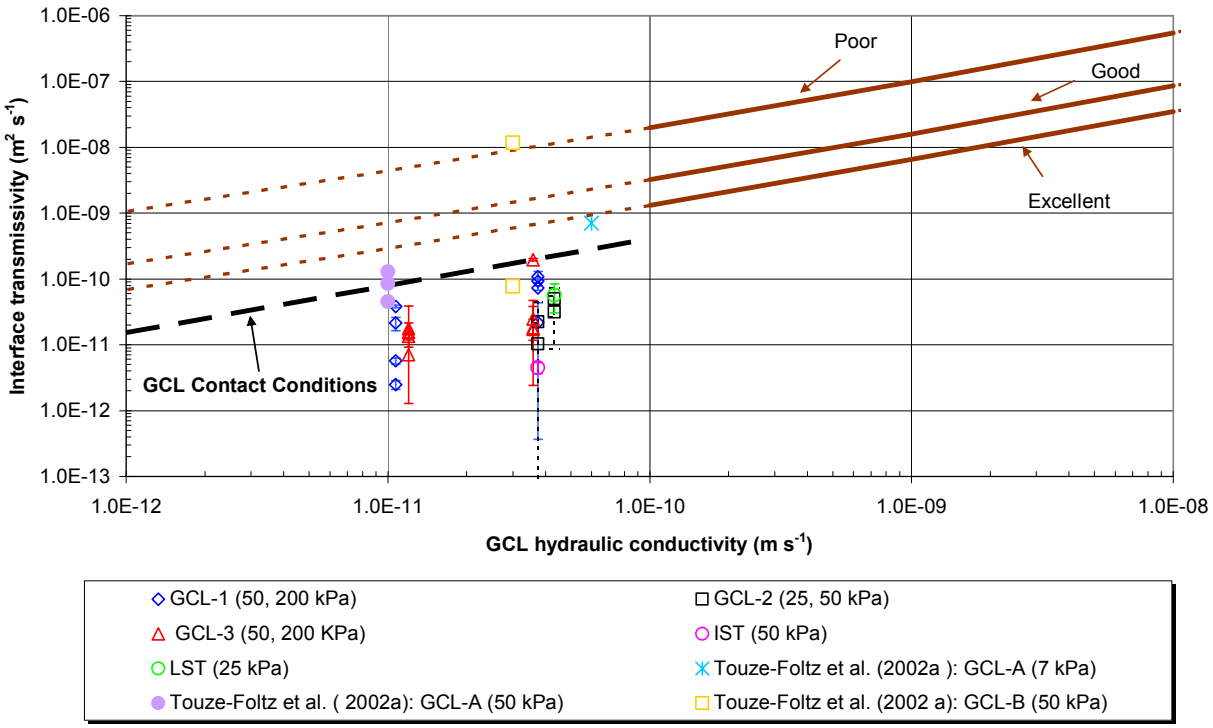

Figure 6.35 – Comparison of experimental results to poor, good, and excellent field contact conditions

The values of transmissivity reported by Touze-Foltz et al. (2002a) were calculated based on flow rate measurements carried out through falling head tests. Those measurements were not

accurate enough. Thus, results reported by Touze-Foltz et al. (2002a) will be disregarded in the subsequent discussion.

The error bars included in Figure 6.35 correspond to uncertainties estimated for transmissivities obtained in this study according to the methodology described in Appendix D. As can be seen in the figure, uncertainties are lower for GCL-1, as compared with uncertainties for GCL-2 and GCL-3. This is related with the uncertainties obtained for flow rates.

Focusing on the results obtained in the present study, it can be seen that the empirical equations for estimating the interface transmissivity, which are based on the hydraulic conductivity of the GCL, overestimate the value of this parameter, even assuming an excellent contact condition for composite liners involving GCLs. As the interface transmissivity is an input parameter in analytical solutions to predict the flow rate though composite liners (see Section 4.5.2), it follows that the flow rate can also be overestimated.

Based on these results, a new definition of contact conditions, herein called as "GCL contact condition", seems to be necessary to determine an interface transmissivity representative of the contact between a geomembrane and a GCL.

Following the rationale given by Rowe (1998) and by Touze-Foltz & Giroud (2003), who proposed quantitative definitions of contact conditions based on the relationship between the interface transmissivity and the hydraulic conductivity of the soil liner, the GCL contact conditions can be defined through a mathematical expression. The latter is based on experimental data obtained in this study, both for the interface transmissivity and for the hydraulic conductivity of the GCLs.

In an attempt to obtain an expression consistent with the existing expressions that relate the interface transmissivity and soil layer hydraulic conductivity, it is assumed that the GCL contact condition is represented by a quasi-straight line parallel to the quasi-straight line representing the poor, good and excellent contact conditions in Figure 6.35 and passing through the highest value of transmissivity obtained in the present work (black dashed line in the figure). From a mathematical point of view, the GCL contact conditions can be represented by the expression below:

$$\log \theta = -2.2322 + 0.7155 \log k_{GCL} \tag{6.4}$$

where θ is the interface transmissivity, and k_{GCL} is the hydraulic conductivity of the GCL component of the composite liner. This equation can only be used in the following units: θ ($m^2 s^{-1}$), k_{GCL} ($m s^{-1}$).

This definition of GCL contact condition in quantitative terms is very important as it can be used for estimating the interface transmissivity for composite liners involving GCL, and thus to predict accurately the flow rate through analytical solutions.

6.4.6 Summary of Section 6.4

Section 6.4 presented and discussed the experimental work performed on flow rates through composite liners due to defects in the geomembrane. Composite liners consisting of a geomembrane over a GCL over a compacted soil liner were operated at three different scales: small (0.2 m diameter circular specimens), intermediate (1 m diameter circular specimen), and large (2.2 m width square specimen). The flow rate through these composite liners due to a circular hole in the geomembrane was measured. The purpose of these tests was to examine the influence of prehydration of the GCLs, of confining stress, and of hydraulic head on flow rates through composite liners due to defects in the geomembrane, as well as to compare different scale test results and, thus, to check the feasibility of an extrapolation of results obtained on small-scale tests to field conditions.

Test results were observed in terms of flow rate, wetted areas, transmissivity and soil water content. Results were then interpreted, mainly, in terms of transmissivity, since this is a key parameter in the development of empirical equations for predicting the flow rate through composite liners involving GCLs (see Section 6.5). To assist the interpretation of results, preliminary tests were carried out to study: the repeatability of the test method (small-scale tests), the influence of the hydraulic conductivity of the soil and of soil thickness, the influence of the type of the geotextile (woven or nonwoven) in contact with the geomembrane, as well as the influence of the nature of the bentonite (granular or powdered) on the transmissivity.

The most significant points to be drawn from the discussion addressed in Section 6.4.5 are as follows:

- The test method used to perform the small-scale tests seems to be repeatable;
- The hydraulic conductivity and the thickness of the soil seem to have a slight influence on the transmissivity;
- The type of geotextile (woven or nonwoven) in contact with the geomembrane seems to have a minor effect on the interface transmissivity, on the long term, suggesting that rather than the characteristics of the upper geotextile, the characteristics of the interface are the ones that actually affect the flow rate through composite liners due to defects in the geomembranes, on the long term;
- For the GCLs under study in the present work, the nature of the bentonite (granular or powdered) seems to have no significant effect on the flow rate and on corresponding interface transmissivity;
- It seems that, as for the effect on the transmissivity, it is important to take into account both the initial water content (prehydration versus non-prehydration) and the confining stress. The prehydration seems to have a minor impact on transmissivity for GCLs under a low confining stress, but it seems to have a great impact for GCLs under a high confining stress, regardless of the hydraulic head applied. On the other hand, the increase in confining stress from 50kPa to 200 kPa does not seem to affect significantly the value of transmissivity for non-prehydrated GCLs. Similar transmissivity was found for both confining stresses, regardless of the hydraulic head. Conversely, it seems to have a great impact on transmissivity for prehydrated GCLs. The transmissivity was one order of magnitude higher in the tests conducted under a confining stress of 50 kPa than in the tests carried out at 200 kPa. Differences obtained were related to the prehydration process, which seems to have serious implications on the quality of contact between the GCL and the geomembrane, and, consequently, on transmissivity. Clearly, more research on the

influence of the set water content/confining stress on the flow rate through composite liners is needed;

- The increase in the hydraulic head from 0.3 m to 1.2 m seems to have a smaller impact on the transmissivity of non-prehydrated specimens than on the one of prehydrated GCLs. Nonetheless, by taking into account the uncertainties associated to transmissivity in these tests, differences can be considered insignificant. More experimental data would be useful to fully understand the influence of hydraulic head on transmissivity;
- Comparisons between both intermediate-scale and small-scale tests, and large-scale and small-scale tests suggest that for the confining stresses considered in this study (25 and 50 kPa), the transmissivity obtained in small-scale tests can be seen as an upper limit of the transmissivity obtained in intermediate-scale and large-scale tests. This finding tends to show that predictions on flow rates through composite liners due to defects in the geomembrane, which are based on transmissivity values obtained in small-scale tests, are conservative;
- Transmissivity values obtained by Harpur et al. (1993) cover a broader range (6×10^{-12} to 2×10^{-10} m^2 s^{-1}) than the ones obtained in the present work with non-prehydrated GCLs (1.5×10^{-11} and 7.3×10^{-11} m^2 s^{-1}). This may be due to the fact that the normal stress was uniformly applied by Harpur et al. (1993), contrary to the present work in which the normal stress was applied through a granular cover plate, in a limited number of points. The difference can also be related to the fact that we have not tested as many different GCLs as those authors have;
- Calculated flow rates for field conditions, based on laboratory measurements carried out in this study and assuming a hole density of 15.3 holes/ha (in agreement with the literature review carried out in Chapter 2), are less than the ones measured in field studies. This may be related with the fact that the present work considered only the case of a 3 mm diameter circular hole in the geomembrane. A hole in a wrinkled geomembrane or a defective seam would augment the flow rate, as emphasised by Rowe (1998) and by Touze-Foltz et al. (1999). Clearly, more studies involving different types of defects in geomembranes are needed; and
- A comparison between the transmissivity obtained in tests at different scales and the field contact conditions, as defined in Section 4.5.3.1, shows that all experimental values obtained in this study are below the line of excellent contact conditions, regardless of the initial water content, the confining stress, and the hydraulic head used in the tests conducted. These results suggest that the existing mathematical expressions to estimate the transmissivity, based on hydraulic conductivity of the GCL liner, overestimate the interface transmissivity. Therefore, predictions of flow rate through composite liners involving GCLs, based on analytical solutions, may be inaccurate. Accordingly, a new contact condition, termed as "GCL contact condition", defined in quantitative terms and based on the experimental data obtained, is proposed in this study to evaluate the interface transmissivity for composite liners involving GCLs. This can be seen as a step forward for accurate predictions of flow rate as the interface transmissivity is an input parameter in analytical solutions used to perform these predictions.

Despite the clear improvement resulting from the definition of the GCL contact condition, a limitation of the analytical solutions is their complexity. Simple tools such as empirical equations are often used by the design engineers to predict the flow rate. In this context, new empirical equations for predicting the flow rate through composite liners, consisting of a geomembrane over a GCL over a CCL, are developed in the next section, for three different types of geomembrane defects: circular defects, defects of infinite length and damaged wrinkles.

6.5 EMPIRICAL EQUATIONS FOR EVALUATING THE FLOW RATE THROUGH COMPOSITE LINERS CONSISTING OF A GEOMEMBRANE OVER A GCL OVER A CCL

Two sets of equations are developed to calculate the flow rate through composite liners consisting of a geomembrane over a GCL over a CCL. The first set corresponds to entirely new equations, developed based on the methodology used by Touze-Foltz & Giroud (2003) for composite liners consisting of a geomembrane and a CCL. This set of equations is herein termed as new equations. The second set of equations corresponds to a modification of the empirical equations proposed by Touze-Foltz & Giroud (2003) to consider the GCL contact conditions (GCL CC). This set of equations differs from the original equations only in the value of the contact factor, which from a physical point of view expresses the features of the interface. They are herein termed as Touze-Foltz & Giroud (2003) modified GCL CC.

Definitions, parameters and assumptions relevant to the equations presented in this study are shown in Section 6.5.1. The methodology used for the development of the new empirical equations is briefly described in Section 6.5.2. The modification of Touze-Foltz & Giroud (2003) equations is presented in Section 6.5.3. A summary of the empirical equations obtained in this work is presented in Section 6.5.4. A discussion of these equations is presented in Section 6.5.5. Finally, conclusions are drawn in Section 6.5.6.

6.5.1 Definitions, parameters, and assumptions

6.5.1.1 Types and size of geomembrane defects

The defects in geomembrane are viewed from two standpoints: type and size. Regarding the type, the ones as follows will be considered in this study: (i) circular defects located in a flat area of the geomembrane (e.g. punctures); (ii) defects of infinite length located in a flat area of the geomembrane (e.g. defective seams and long cuts or tears); and (iii) defects of any shape located on wrinkles in the geomembrane resulting in what is herein termed as damaged wrinkles. Defects of infinite length and damaged wrinkles are grouped under the generic term "two-dimensional defect".

The sizes of the defects considered will be identical to the ones adopted by Touze-Foltz & Giroud (2003) to develop empirical equations for composite liners comprising a geomembrane and a CCL for the sake of consistency, which is:

- circular defects having radii between 1×10^{-3} and 5.64×10^{-3} m;
- defects of infinite length having widths between 2×10^{-3} and 2×10^{-2} m; and
- wrinkle widths ranging from 0.1 to 0.6 m.

6.5.1.2 Hydraulic head above the geomembrane

As mentioned in Chapter 2, leachate head above the geomembrane must not exceed 0.3 m according to most landfill regulations. However, large heads can be found in landfills as a result, for example, of inadequate performance of the leachate collection system, as reported by Rowe (1998).

To cover a hydraulic head range representing most situations for landfill design and for the sake of consistency with Touze-Foltz & Giroud (2003), values ranging from 0.03 to 3 m will be considered in this study.

6.5.1.3 Hydraulic conductivity and thickness of the GCL and CCL

For composite liners consisting of a geomembrane over a GCL over a CCL the hydraulic conductivity and the thickness to be used in flow rate calculations are the equivalent hydraulic conductivity and the equivalent thickness, determined using Equation (4.48) and Equation (4.49), respectively.

Discussions presented in Chapter 2 (see Figure 2.20) tend to show that the hydraulic conductivity of GCLs can vary between 1×10^{-12} and 1×10^{-10} m s^{-1}. Thus, this is the range of hydraulic conductivity used in this study. As regards the soil layer above the GCL, the same range of values adopted by Touze-Foltz & Giroud (2003), to develop empirical equation for composite liners comprising a geomembrane and a CCL, is considered herein, as the one between 1×10^{-10} and 1×10^{-8} m s^{-1}.

Regarding thickness of these layers, values ranging from 0.3 to 5 m are considered for soil layer. This range was chosen because it covers most landfill regulations, as well as the applications of composite liners in other facilities such as reservoirs. For GCLs, values ranging from 6×10^{-3} to 14×10^{-3} m are considered in this study. This range covers the GCL thicknesses that may be expected in landfills as result of the coupling effect between confining stress and swelling, according to the results obtained by Lake & Rowe (2000) in constant stress swell tests.

To sum up, the following range of parameters is considered in developing the empirical equations:

- circular defects having radii between 1×10^{-3} and 5.64×10^{-3} m;
- defects of infinite length having widths between 2×10^{-3} and 2×10^{-2} m;
- wrinkle widths ranging from 0.1 to 0.6 m;
- hydraulic heads ranging from 0.03 to 3 m;
- hydraulic conductivities of the GCL component of the composite liner ranging from 1×10^{-12} to 1×10^{-10} m s^{-1};
- hydraulic conductivities of the soil component of the composite liner ranging from 1×10^{-10} to 1×10^{-8} m s^{-1};
- thickness values of the GCL component of the composite liner ranging from 6×10^{-3} to 14×10^{-3} m; and
- thickness values of the soil layer component of the composite liner ranging from 0.3 to 5 m.

6.5.2 New equations

6.5.2.1 Methodology

6.5.2.1.1 Approach

The notion behind the methodology consists in developing empirical equations that are simple and give flow rate values as close as possible to the values rigorously calculated using available analytical solutions. The same approach is used for circular defects, defects of infinite length, and damaged wrinkles in order to avoid inconsistency such as the one found by Touze-Foltz (2001) and Foose et al. (2001), i.e. even considering the same contact conditions, the empirical equations for circular defects and the empirical equations for defects of infinite length lead to different values of interface transmissivity.

As mentioned, the methodology used for developing this set of new equations derives mainly from the methodology adopted by Touze-Foltz & Giroud (2003). Essentially, it consists of selecting a mathematical expression for the empirical equations and selecting values for the unknowns of the empirical equations such that flow rates calculated using the empirical equations are as close as possible to flow rates rigorously calculated using existing analytical solutions. In this context, the first step consists in selecting the same form of mathematical expression for the empirical equations developed herein for all types of defects: circular, infinite length, and damaged wrinkles, considering the GCL contact conditions defined in Section 6.4.5.9. In order to be consistent with Touze-Foltz & Giroud (2003), the form of mathematical expression adopted for the empirical equations is presented below:

$$Q = C_c\, h_w^{\chi}\, a^{\xi}\, k_S^{\kappa} \left[1 + \lambda \left(\frac{h_w}{H_s} \right)^{\mu} \right] \qquad \text{for circular defects} \tag{6.5}$$

$$Q_L = C_{td}\, h_w^{\chi}\, b^{\xi}\, k_S^{\kappa} \left[1 + \lambda \left(\frac{h_w}{H_s} \right)^{\mu} \right] \qquad \text{for two-dimensional defects} \tag{6.6}$$

where Q is the rate of flow through a composite liner due to a circular defect in the geomembrane component of the composite liner; Q_L is the rate of flow per unit length through a composite liner due to a two-dimensional defect in the geomembrane component of the composite liner; C_c and C_{td} are the contact condition factor, for circular defects and two-dimensional defects, respectively; h_w is the hydraulic head on top of the geomembrane; a is the circular defect area; b is the width of the two-dimensional defect; k_s is the equivalent hydraulic conductivity of the soil liner (GCL+CCL); λ is a factor; H_s is the equivalent thickness of the soil liner (GCL+CCL); and χ, ξ, κ and μ are exponents. Equations (6.5) and (6.6) can only be used with the SI units as follows: Q ($m^3\ s^{-1}$), Q_L ($m^2\ s^{-1}$), h_w (m), a (m^2),

b (m), k_s (m s^{-1}), and H_s (m); dimension of C_c and C_{td} are variable; χ, ξ, κ, λ and μ are dimensionless.

In these equations, the term in brackets is the average hydraulic gradient, i_s, in the soil liner (GCL+CCL):

$$i_s = 1 + \lambda \left(\frac{h_w}{H_s} \right)^{\mu} \tag{6.7}$$

6.5.2.1.2 Analytical solutions

The analytical solutions used to evaluate the proposed empirical equations are Equation (4.27), for circular defects and Equation (4.47), for two-dimensional defects, according to Section 4.5.2. Regarding the latter, it is important to remember that there is no fundamental difference between the two types of two-dimensional defects since it is assumed that the holes in a wrinkle do not control the flow, and no assumption is made regarding the height or the shape of the wrinkle. Therefore, the two types of two-dimensional defects are defined by one characteristic: their width, b (see Figure 4.9). Nonetheless, there will be two empirical equations for two-dimensional defects, one for the defects of infinite length, and another for the damaged wrinkles, because these empirical equations can only be used in a narrow range of values of the parameters. The ranges of widths of defects of infinite length and damaged wrinkles do not overlap, as indicated in Section 6.5.1.1.

An important aspect related with the analytical solutions is the value of the interface transmissivity. This parameter was calculated using the Equation (6.4), which is proposed in this study for GCL contact conditions (see Section 6.4.5.9).

6.5.2.1.3 Determination of the unknowns of the empirical equations

By adopting the same procedure as the one used by Touze-Foltz & Giroud (2003), the values of the unknown exponents and factors of Equations (6.5) or (6.6), i.e. χ, ξ, κ, C_c (or C_{td}), λ and μ, are determined by comparison. That comparison is done between the values of Q, calculated using the empirical Equation (6.5) – or Q_L, calculated using the empirical Equation (6.6) – with the values of Q, calculated using the analytical solution expressed by Equation (4.27) – or the values of Q_L, calculated using the analytical solution expressed by Equation (4.47).

This general methodology would give a range of values for each exponent and factor. For each exponent or factor, a value located within the given range is selected. In this study, the selected value was the mean value of the calculated cases.

Determination of the unknowns of the empirical equations is done in three steps: (i) determination of the exponents χ, ξ and κ; (ii) determination of the contact factor (C_c or C_{td}); and (iii) determination of the factor λ and exponent μ. This methodology is used for developing the empirical equations in the subsequent sections.

6.5.2.2 Determination of the empirical equations

6.5.2.2.1 Determination of the exponents

For a given hydraulic gradient, Equations (6.5) and (6.6) show that the only unknowns in the empirical equation are the exponents χ, ξ and κ. By selecting three values for the hydraulic gradient in such a way that covers the range of hydraulic heads and soil liner thickness (GCL+CCL) considered in this study (1.1, 2 and 4, according to preliminary calculations done in this work), systematic calculations were performed using the analytical solutions (Equations 4.27 or 4.47, depending on the type of defect). For each set of values of a (or b), and k_s, the only variable is h_w. Therefore, Equation (6.5), or Equation (6.6), becomes (Touze-Foltz & Giroud 2003):

$$Q = M\, h_w^{\chi} \tag{6.8}$$

where M is a parameter that has a constant value in this case. Equation (6.8) can be written as follows (Touze-Foltz & Giroud 2003):

$$\log Q = \log\ M + \chi \log h_w \tag{6.9}$$

Equation (6.9) means that, if the empirical equation were absolutely equivalent to the analytical solution, there would be a linear relationship, with a slope χ, between Q and h_w in logarithmic scale. In fact, the empirical equation is not absolutely equivalent to the analytical solution and a linear regression analysis was used to obtain an approximate value of χ for each set of values of a (or b, depending on the type of defect) and k_s. The mean value of χ was selected. The same methodology was then used to determine ξ and κ. Table 6.13 shows the mean values thus obtained.

Table 6.13 - Exponents χ, ξ and κ obtained for different types of defects

Type of defect	χ	ξ	κ
Circular defect	0.07	0.87	0.64
Defect of infinite length	0.015	0.49	0.80
Damaged wrinkle	0.31	0.30	0.88

6.5.2.2.2 Determination of the contact condition factor

It is assumed that the contact condition factor, C_c or C_{td}, depends only on interface transmissivity. Based on Equations (6.5) and (6.6), the contact condition factor can be determined for values of hydraulic gradient equal to 1, once the exponents χ, ξ and κ are known.

The hydraulic gradient is equal to 1 when the ratio between the hydraulic head and the equivalent thickness of the soil liner (GCL+ CCL) is small (see Equation (6.7)). Accordingly, calculations were performed for the lowest hydraulic head, 0.03 m, and for the largest equivalent soil liner thickness considered in this study, about 5 m, using the analytical solutions expressed by Equation (4.27) and Equation (4.47), respectively for circular defects or for two dimensional defects, and for various sets of h_w , a (or b) and k_s.

Values of the contact factor, C_c or C_{tw}, were then derived from the calculated values of Q and the values of χ, ξ and κ, determined as discussed in Section 6.5.2.2.1. Following the approach indicated by Touze-Foltz & Giroud (2003), the least square method was used to obtain the values of C_c (or C_{tw}), which leads to the minimum difference between analytical solutions and empirical equations for the calculations performed. The values below were obtained:

- 0.0002, for circular defects;
- 0.016, for defects of infinite length; and
- 0.202, for damaged wrinkles.

6.5.2.2.3 Determination of the unknowns in the average hydraulic gradient

For determining the unknowns in the average hydraulic gradient, λ and μ, various values of Q were first calculated using Equation (4.27), for various sets of h_w , a and k_s indicated in Section 6.5.1. For the values of Q thus determined, the corresponding hydraulic gradients were calculated using the equation below:

$$i_s = \frac{Q}{C_c h_w^{\chi} a^{\xi} k_s^{\kappa}} \tag{6.10}$$

In addition, for each set of values of h_w, a and k_s, values of the hydraulic gradient were also calculated using the empirical method, i.e. Equation (6.7), with arbitrarily selected initial values for λ and μ. Then, the least square method was used to obtain the values of λ and μ through an iterative process, solving successively for λ and μ. This leads to the minimum sum of differences between, on one hand, the hydraulic gradient calculated using Equation (6.7) and, on the other hand, the hydraulic gradients calculated using Equation (6.10). The same approach was used for two-dimensional defects. Table 6.14 shows the values thus obtained.

Table 6.14 - Factor λ and exponent μ obtained for different types of defects

Type of defect	λ	μ
Circular defect	0.31	0.79
Defect of infinite length	0.35	0.94
Damaged wrinkle	0.20	1.25

6.5.3 Modification of Touze-Foltz & Giroud (2003) equations

Considering that the features of the interface are the key issue on the flow rate through composite liners due to defects in the geomembrane, equations by Touze-Foltz & Giroud (2003) are modified to take into account the characteristics of the interface between a geomembrane and a GCL. The contact factor was thus recalculated for the GCL contact condition by using the methodology described in Section 6.5.2.2.2. The values below were obtained:

- 0.0024, for circular defects;
- 0.05, for defects of infinite length; and
- 0.22, for damaged wrinkles.

6.5.4 Summary of the empirical equations

Table 6.15 summarises the empirical equations obtained in this study, both the new equations and the Touze-Foltz & Giroud modified GCL CC.

It should be noted that these empirical equations can only be used for values of the parameters listed in Section 6.5.1.

Furthermore, it must be pointed out that the equations for two-dimensional defects (defects of infinite length and damaged wrinkles) only account for flow perpendicular to the longitudinal direction of the defect. Therefore, these equations should only be used in cases where the ratio between the length and the width of the defect is large. If the ratio between the length and the width of the defect is small, the magnitude of the flow that takes place at the two ends of the defect will not be negligible, as highlighted by Touze-Foltz & Giroud (2003).

Table 6.15 - Empirical equations obtained for estimating the flow rate through composite liners consisting of a geomembrane over a GCL over a CCL

Type of defect		Empirical equation
Circular defect	New equation	$Q = 0.0002 h_w^{0.87} a^{0.07} k_s^{0.64} \left[1 + 0.31 \left(\frac{h_w}{H_s} \right)^{0.79} \right]$
	Touze-Foltz & Giroud (2003) modified GCL CC	$Q = 0.0024\, h_w^{0.90} a^{0.1} k_s^{0.74} \left[1 + 0.1 \left(\frac{h_w}{H_s} \right)^{0.95} \right]$
Defect of infinite length	New equation	$Q_L = 0.016 h_w^{0.49} b^{0.015} k_s^{0.80} \left[1 + 0.35 \left(\frac{h_w}{H_s} \right)^{0.94} \right]$
	Touze-Foltz & Giroud (2003) modified GCL CC	$Q_L = 0.05\, h_w^{0.45} b^{0.004} k_s^{0.87} \left[1 + 0.52 \left(\frac{h_w}{H_s} \right)^{0.59} \right]$
Damaged wrinkle	New equation	$Q_L = 0.202 h_w^{0.30} b^{0.31} k_s^{0.88} \left[1 + 0.20 \left(\frac{h_w}{H_s} \right)^{1.25} \right]$
	Touze-Foltz & Giroud (2003) modified GCL CC	$Q_L = 0.22 h_w^{0.45} b^{0.1} k_s^{0.87} \left[1 + 0.28 \left(\frac{h_w}{H_s} \right)^{0.82} \right]$

The following symbols are used in this table: Q = flow rate; Q_L = flow rate per unit length; h_w = hydraulic head on top of geomembrane; a = circular defect area; b = width of defect of infinite length or damaged wrinkle; k_s = equivalent hydraulic conductivity of the soil liner (GCL + CCL); H_s = equivalent thickness of the soil liner (GCL+CCL), and GCL CC = GCL contact condition. These equations must be used with the following units: Q ($m^3\ s^{-1}$), Q_L ($m^2\ s^{-1}$), h_w (m), a (m^2), b (m), k_s ($m\ s^{-1}$), and H_s (m).

6.5.5 Discussion of the empirical equations

Considering that several approximations were done to develop the empirical equations, it is important to verify that the flow rate values obtained with the empirical equations are a good approximation of the flow rates rigorously calculated using analytical solutions. The accuracy of the empirical equations is observed from two perspectives. First, systematic comparisons are done between flow rates calculated using empirical equations and analytical solutions. Second, the flow rates calculated using empirical equations are compared with the flow rates obtained in intermediate-scale and large-scale tests.

Regarding the first perspective, Figures 6.36 to 6.38 show the percentage of cases studied (i.e. percentage of flow rates calculated for different sets of parameters), as a function of the relative difference between the flow rate calculated using analytical solutions and empirical equations, for different types of defects. For comparison purposes, these figures also include flow rates calculated using the empirical equations reported in the literature and that are applicable to the range of parameters used in this study, namely the Equation by Gundseal (2001), for circular defects, and the Equation by Foose et al. (2001), for defects of infinite length. Recalling Section 4.5.3.2, the empirical equation by Gundseal (2001) is applicable to circular defects with radii between 0.25 mm and 12.5 mm. The Equation by Foose et al. (2001) is applicable when the ratio between the hydraulic conductivity of the interface and that of the soil component of the composite liner is higher than 3×10^4 (see

second footnote of Table 4.3), which is always the case for the range of parameter values considered in this study. Lastly, Figures 6.36 to 6.38 also include the flow rates predicted using the empirical equations by Touze-Foltz & Giroud (2003), by assuming excellent contact conditions (ECC), which appear to be the closest ones to the GCL contact condition.

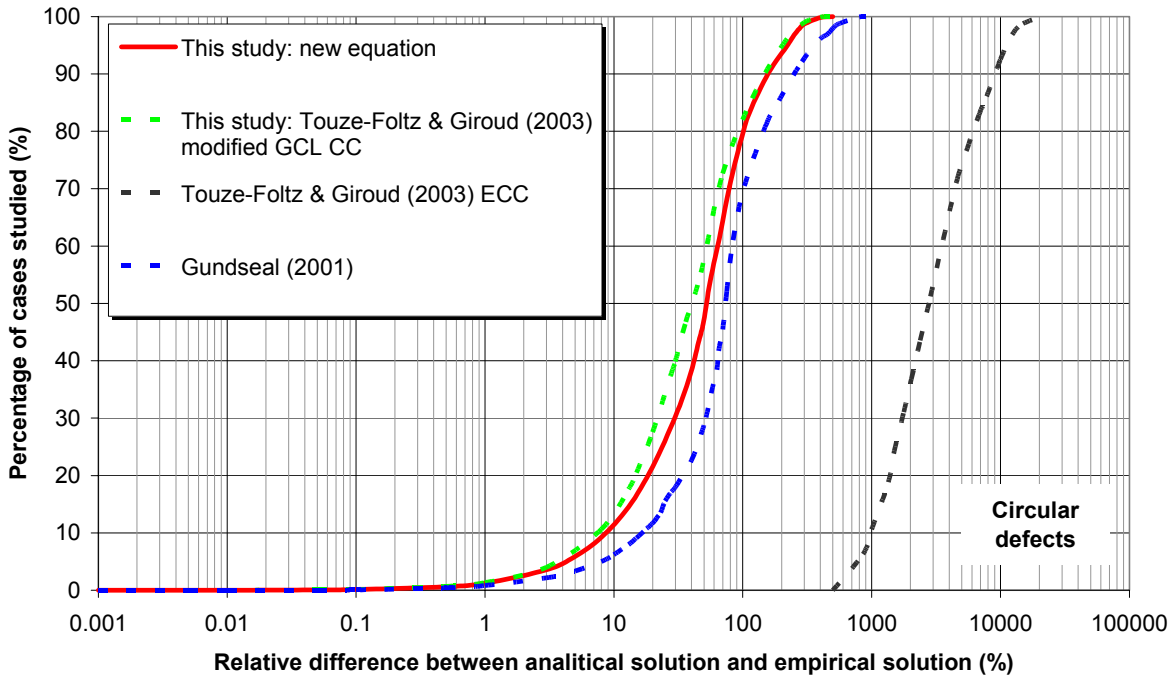

Figure 6.36 - Relative difference between analytical solution and empirical equations for circular defects

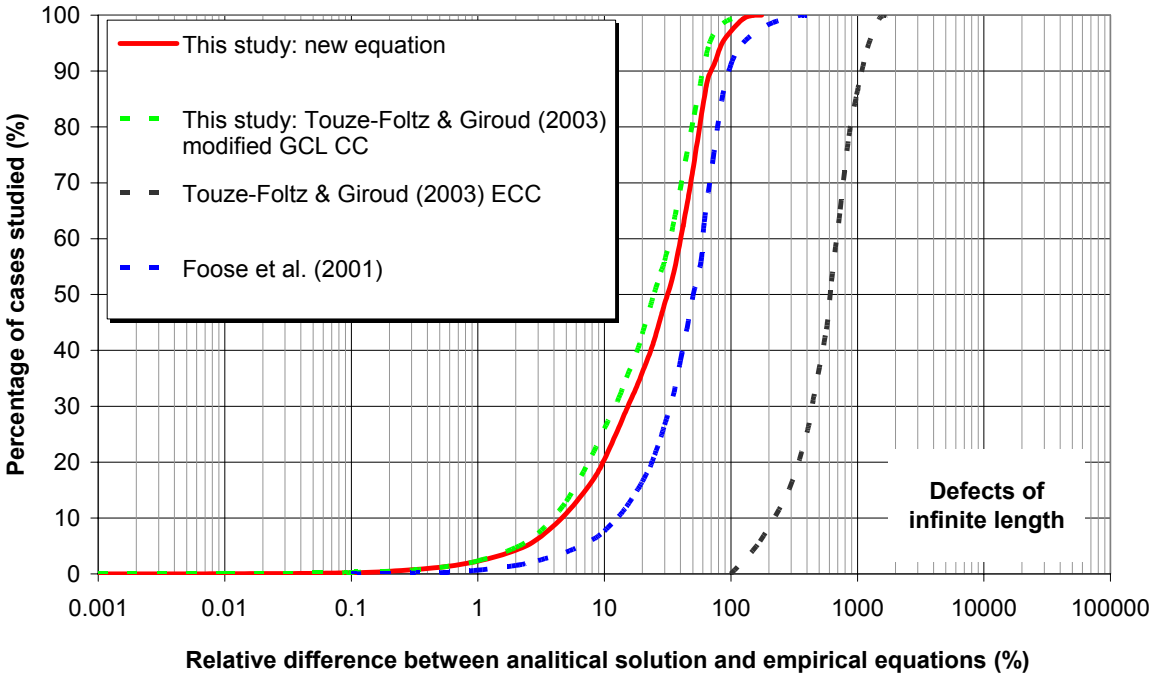

Figure 6.37 - Relative difference between analytical solution and empirical equations for defects of infinite length

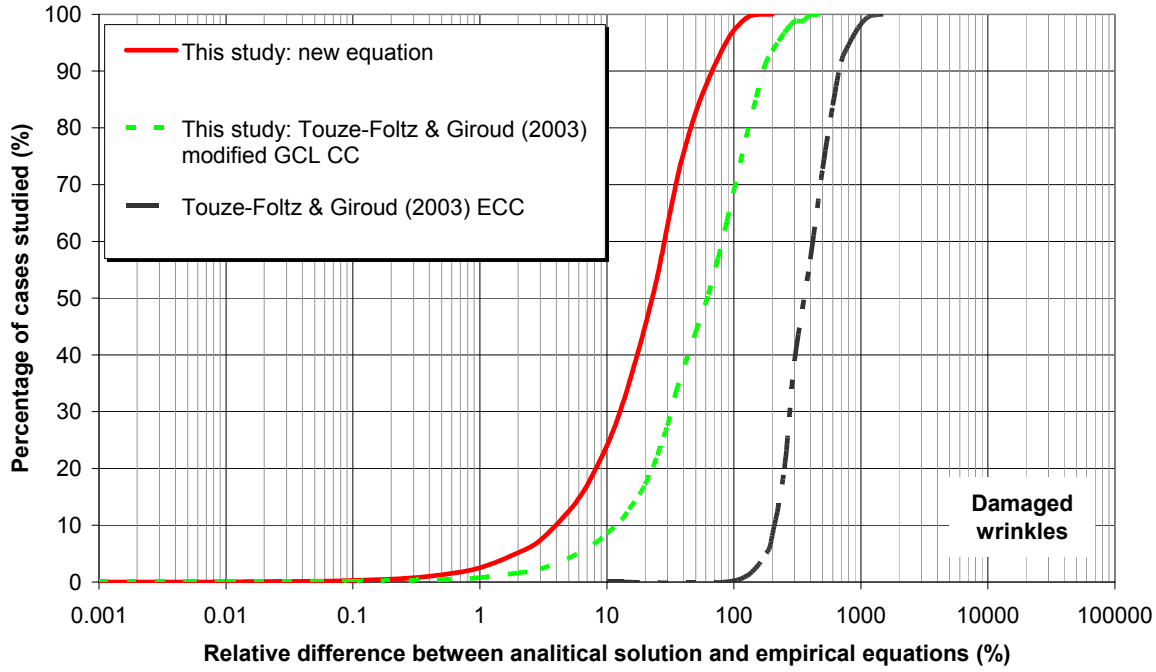

Figure 6.38 - Relative difference between analytical solution and empirical equations for damaged wrinkles

For circular defects, Figure 6.36 shows that, for the cases studied, empirical equations obtained in this study (new equation and Touze-Foltz & Giroud (2003) modified GCL CC) led to similar flow rates. The relative difference between flow rates rigorously calculated using the analytical solution and approximate flow rates calculated using the empirical equations obtained in this study is identical. The curves almost overlap. It can also be seen that the empirical equations presented in this study are more accurate than the empirical equations by Gundseal (2001) and by Touze-Foltz & Giroud (2003) ECC. For the latter, the relative differences are always higher than 1000 %.

These results suggest that both empirical equations obtained in this study can be used to predict the flow rate due to circular defects in the geomembrane. It also indicates that the predictions based on the empirical equation by Touze-Foltz & Giroud (2003) ECC significantly overestimate the flow rate though composite liners consisting of a geomembrane over a GCL over a CCL.

For defects of infinite length, Figure 6.37 shows that, for the cases studied, empirical equations obtained in this study (new equation and Touze-Foltz & Giroud (2003) modified GCL CC) led to identical flow rates. The relative difference between flow rates rigorously calculated using the analytical solution and approximate flow rates calculated using the empirical equations obtained in this study is similar. Significant relative differences can be observed between flow rates calculated using the analytical solution and the flow rates calculated using either the equation proposed by Foose et al. (2001) or the empirical equation proposed by Touze-Foltz & Giroud (2003) ECC. For the latter, this difference is always higher than 100 %.

These findings tend to show that, for defects of infinite length, the empirical equations presented in this study are more accurate than the empirical equations by Foose et al. (2001) and by Touze-Foltz & Giroud (2003) ECC.

For damaged wrinkles, Figure 6.38 shows that, in about 85 % of the cases, the relative difference between flow rates rigorously calculated using the analytical solution and approximate flow rates calculated using the new equation empirical equation developed in this study is less than 50 %. It also shows that, for damaged wrinkles, the new equation is the most accurate.

The accuracy of the empirical equations developed in this study was at last studied by comparing the flow rates predicted for circular defects with the flow rates obtained in intermediate-scale and large-scale tests. Comparisons carried out are in Table 6.16 and Table 6.17.

Table 6.16 – Comparison between the flow rates calculated using the empirical equations for circular defects and the ones obtained in intermediate-scale tests

Empirical equation		**Flow rate calculated ($m^3 s^{-1}$)**	**Flow rate measured ($m^3 s^{-1}$)**	**Relative difference (%)**
This study	New equation	2.9×10^{-11}	2.7×10^{-12}	957
	Touze-Foltz & Giroud (2003) modified GCL CC	2.1×10^{-11}		682
Touze-Foltz & Giroud (2003) ECC		8.6×10^{-10}		31 168

Table 6.17 – Comparison between the flow rates calculated using the empirical equations for circular defects and the ones obtained in large-scale test

Empirical equation		**Flow rate calculated ($m^3 s^{-1}$)**	**Flow rate measured ($m^3 s^{-1}$)**	**Relative difference (%)**
This study	New equation	2.9×10^{-11}	2.5×10^{-11}	15
	Touze-Foltz & Giroud (2003) modified GCL CC	2.2×10^{-11}		15
Touze-Foltz & Giroud (2003) ECC		8.6×10^{-10}		3 313

From the observation of Table 6.16, there can be seen that the relative difference between the flow rate measured in the intermediate-scale test and the flow rate calculated using the empirical equations obtained in this study is much less (about 960 %) than the relative difference obtained between the flow rate measured and the flow rate calculated using the empirical equation proposed by Touze-Foltz & Giroud (2003) ECC, for excellent contact condition (about 31 168 %), which is considered to be the closest one to the GCL contact conditions.

The same finding can be drawn from the large-scale test (Table 6.17). In this case, the relative difference between the flow rate measured and the flow rate calculated using the empirical equations obtained in this study is about 15 %. On the contrary, the relative difference between the flow rate measured and the flow rate calculated using the empirical equation

proposed by Touze-Foltz & Giroud (2003) ECC is about 3 300 %. These results show that there is a good agreement between flow rates calculated using the empirical equations presented here and the flow rates obtained in the large-scale test.

Clearly, for composite liners involving GCLs, the empirical equations presented in this study are more accurate than the previously published empirical equations, even when assuming excellent contact conditions. In fact, these represent an improvement in available tools for calculating the flow rate through composite liners consisting of a geomembrane over a GCL over a CCL.

On the other hand, the good agreement found, in the case of circular defects and defects of infinite length, between the flow rates calculated using the empirical equations developed in this work, and the flow rates calculated using Touze-Foltz & Giroud (2003) modified GCL CC, suggests that changing the contact factor is enough to improve the existing empirical equations. For the range of parameters used in this work, changes in exponents and in the hydraulic gradient factor did not improve significantly the accuracy of the empirical equations for predicting the flow rate through composite liners due to circular defects and defects of infinite length.

Based on the above discussion and taking into account that both the exponents and the hydraulic gradient factor of the empirical equations by Touze-Foltz & Giroud (2003) are familiar to design engineers, for circular defects and for defects of infinite length, it is suggested to adopt the empirical equations obtained in this study by modifying the contact factor, i.e. equations termed as Touze-Foltz & Giroud (2003) modified GCL CC. For damaged wrinkles the new empirical equation, developed according to Section 6.5.2.2, is recommend as it proved to be in better agreement with the analytical solution.

Table 6.18 summarises the final empirical equations recommended in this study for predicting the flow rate through composite liners consisting of a geomembrane over a GCL over a CCL.

Table 6.18- Recommended empirical equations for estimating the flow rate through composite liners consisting of a geomembrane over a GCL over a CCL

Type of defect	**Empirical equation**
Circular defect	$Q = 0.0024\, h_w^{0.90} a^{0.1} k_s^{0.74} \left[1 + 0.1 \left(\frac{h_w}{H_s} \right)^{0.95} \right]$
Defect of infinite length	$Q_L = 0.05\, h_w^{0.45} a^{0.004} k_s^{0.87} \left[1 + 0.52 \left(\frac{h_w}{H_s} \right)^{0.59} \right]$
Damaged wrinkle	$Q_L = 0.202\, h_w^{0.30} a^{0.31} k_s^{0.88} \left[1 + 0.20 \left(\frac{h_w}{H_s} \right)^{1.25} \right]$

The symbols as follows are used in this table: Q = flow rate; Q_L = flow rate per unit length; h_w = hydraulic head on top of geomembrane; a = circular defect area; b = width of defect of infinite length or damaged wrinkle; k_s = equivalent hydraulic conductivity of the soil liner (GCL + CCL); and H_s = equivalent thickness of the soil liner (GCL+CCL). These equations must be used with the units as follows: Q ($m^3\ s^{-1}$), Q_L ($m^2\ s^{-1}$), h_w (m), a (m^2), b (m), k_s ($m\ s^{-1}$), and H_s (m).

6.5.6 Summary of Section 6.5

Section 6.5 focused on the development of the empirical equations for predicting the flow rate through composite liners consisting of a geomembrane over a GCL over a CCL. Two sets of equations were developed. One corresponding to entirely new equations, developed based on the methodology used by Touze-Foltz & Giroud (2003). The other set was obtained modifying the empirical equations proposed by Touze-Foltz & Giroud (2003) by recalculating the contact factor to take into account the GCL contact condition. Circular defects, defects of infinite length and damaged wrinkles were considered.

In order to study the accuracy of these empirical equations, flow rates calculated using the two sets of equations were compared with the flow rates obtained using both analytical solutions and previously published empirical equations, as well as with the flow rates measured in the intermediate-scale and large-scale tests.

For the range of parameters used in the present work, it was observed that the empirical equations presented in this study are in better agreement than the empirical equations reported in literature, both with the analytical solutions and with the flow rates measured experimentally. Relative differences between the flow rate measured in large-scale test and the flow rate calculated using the empirical equations obtained in this study were about 15 %. This tends to validate the empirical equations proposed in this study from an experimental point of view.

For circular defects and defects of infinite length it was found that empirical equations presented in this study (new equation and Touze-Foltz & Giroud (2003) modified GCL CC) led to similar flow rates. This suggests that, for these types of defects, both equations can be used for predicting the flow rates. For damaged wrinkle, the new equation proved to be the most accurate.

Based on the above findings, for circular defects and for defects of infinite length, modified equations were recommended for predicting the flow rate composite liners consisting of a geomembrane over a GCL over a CCL. For damaged wrinkles, the new equation is suggested.

Equations proposed here provide engineers with simple empirical equations that can give a good approximation of flow rates through composite liners consisting of a geomembrane over a GCL over a CCL, as compared with the previous equations reported in literature. This represents an improvement in available tools for predicting flow rates with the advantage that were validated experimentally.

6.6 SUMMARY AND CONCLUSIONS

This chapter first presented the experimental work carried out to assess the water retention curves (relationship between the volumetric water content and suction) of GCLs. The suitability of the filter paper method to assess the suction of GCLs was addressed. Results obtained suggest that the filter paper is appropriate to measure the suction of GCLs. Based on this finding, suctions and correspondent volumetric water contents were measured, without stress, for three different products. Water retention curves of GCLs could thus be determined based on experimental data. Its knowledge, often represented by the van Genuchten parameters, is necessary in modelling the flow rate through composite liners under unsaturated conditions. This is the case of the GCLs on the short term, as they are typically installed in landfill bottom lining systems at their natural water content.

Then, Section 6.4 presented and discussed the experimental work performed on flow rates through composite liners due to defects in the geomembrane. Composite liners consisting of a geomembrane over a GCL over a CCL were simulated in tests at three scales: small (circular specimens 0.2 m in diameter), intermediate (circular specimen 1 m in diameter), and large (square specimen 2.2 m in width). The tests conducted aimed at studying the influence of the prehydration of the GCLs, the influence of the confining stress, and the influence of the hydraulic head on flow rates through composite liners due to defects in the geomembrane, as well as at comparing different scale test results and thus check the feasibility of an extrapolation of results obtained on small-scale tests to field conditions.

Final flow rates, obtained in steady state conditions, together with the radius of the wetted areas, were used to calculate the transmissivity of the interface between the geomembrane and the GCL through analytical solutions. Transmissivity was then used for interpreting the test results. The main conclusions that can be drawn from the experimental work performed are as follows: (i) it seems that, as for the effect on the transmissivity, it is important to consider the relationship between the initial water content of the GCLs (prehydration versus non-prehydration) and the confining stress. The prehydration seems to have a minor impact on transmissivity for GCLs under a low confining stress, but it seems to have a significant impact for GCLs under a high confining stress. In addition, the increase in the confining stress from 50kPa to 200 kPa does not seem to affect significantly the value of transmissivity for non-prehydrated, whereas it seems to affect seriously the transmissivity of prehydrated GCLs; (ii) the increase in hydraulic head from 0.3 m to 1.2 m seems to have smaller impact on the transmissivity of the non-prehydrated specimens than on the prehydrated GCLs. However, due to the high uncertainties associated to the transmissivity, the differences may be considered unimportant; (iii) the comparisons between, on the one hand, intermediate-scale and small-scale tests and, on the other hand, large-scale and small-scale tests suggest that for the confining stresses considered in this study, i.e. 25 and 50 kPa, the transmissivity obtained in small-scale tests can be seen as an upper limit of the transmissivity obtained in intermediate-scale and large-scale tests. Thus, predictions on flow rates through composite liners due to defects in the geomembrane, based on transmissivity values obtained in small-scale tests, are conservative; and (iv) a comparison between the transmissivity obtained in tests at different scales and the field contact conditions shows that all experimental values obtained in the present study are below the line of excellent contact conditions. This has serious implications on values of flow rate calculated using analytical solutions, because the transmissivity is an input parameter in those solutions.

Based on this latter finding, a new contact condition, termed as “GCL contact condition”, was defined based on the experimental data obtained in this study. It is expressed by an equation that related the hydraulic conductivity of the GCLs with the transmissivity. The extension of the contact conditions for GCLs is a step forward for accurate predictions of the flow rate through composite liners involving GCLs.

Despite the improvement achieved by the definition of the GCL contact conditions, analytical solutions for calculating the flow rate are complex. Alternative tools, simple but giving a good approximation of the flow rate as compared with analytical solutions, are often used by the design engineers. As for composite liners consisting of a geomembrane over a GCL over a CCL there was a lack on this type of tool, empirical equations for predicting the flow rate were developed in Section 6.5, for three types of defects (circular defects, defects of infinite length and damaged wrinkles).

Flow rates calculated using the empirical equations developed in this study are in better agreement with the flow rates measured experimentally than the empirical equations reported

in literature. These equations correspond thus to an improvement in available tools for predicting the flow rate through composite liners involving GCLs.

7 CONCLUSIONS AND PERSPECTIVES

7.1 CONCLUSIONS

This dissertation concerns investigations into fluid migration through geomembrane seams and through composite liners involving geomembranes and GCLs. The research was undertaken to address the problems of geomembrane seams in terms of fluid-tightness and of flow rate through composite liners due to defects in the geomembrane. Original laboratory tests, modelling both the gas migration through high density polyethylene geomembranes seams and the flow rate through composite liners comprising a geomembrane over a GCL over a compacted clay liner due to circular defects in geomembranes, were performed. Advances were achieved in experimental modelling of the fluid migration through geomembranes liners. This led to a better understanding of the fundamental processes involved in leachate migration in landfill liners. In addition, empirical equations were developed for predicting the flow rate through the above mentioned type of composite liners, which provides engineers with simple design tools and can thus contribute to construct safer landfill bottom liners.

Gas migration through geomembrane seams was addressed through gas permeation pouch tests carried out using pouch specimens consisting of true seams made by the thermal-hot dual wedge method. In situ, the quality of this type of seams is typically evaluated by the results of the pressurised dual test method. This method provides only qualitative information about the fluid-tightness of the seams despite their importance to ensure the performance of the geomembrane as barriers. Therefore, small-scale gas permeation pouch laboratory tests were conducted using a 1.2 m permeation cell, for assessing quantitatively the quality of the geomembrane seams. Another goal of these tests was to study the appropriateness of the pressurised dual method. Two different gases (nitrogen and carbon dioxide) were used. In addition, large-scale gas permeation pouch tests were performed both in laboratory, using a 10 m long specimen, and in field conditions, using a 5 m long specimen exposed to weather conditions. The aim of the large-scale tests was to complement the small-scale tests and to study the suitability of the gas permeation pouch test to control the quality of the thermal-hot dual wedge seams in situ, as an alternative to the pressurised dual method. Also, the mechanical strength of the seams was studied through peel and shear tests, in order to investigate a possible correlation between gas permeation pouch test results and mechanical strength of the seams.

The results obtained in gas permeation pouch tests were interpreted in terms of permeation coefficients, evaluated in pseudo steady state conditions, and in terms of time constant, estimated in unsteady state conditions. The most significant findings to be drawn from the results obtained are as follows: (i) the gas permeation pouch test was able to identify poor seams which would have been accepted in the field after a control based on the pressurised dual seam method, suggesting that the tools presently used on site need to be improved; (ii) the comparison between the results of gas permeation pouch tests and mechanical tests showed that the poorest seam from a mechanical point of view is also the poorest from a gas

permeation point of view; this comparison also suggests that mechanical tests are better adapted than gas permeation pouch test to optimise seam parameters and to compare aged specimens in landfills to new specimens; (iii) gas permeance was approximately half an order of magnitude higher to carbon dioxide than to nitrogen; and (iv) it appears that it is possible to assess the quality of double thermal-hot dual wedge seams, from a non-destructive test conducted on site, by determining the time constant.

Based on the above findings, it can be concluded that the gas permeation pouch test may be a useful tool to assess the quality of seams by quantitative measurement of the time constant, providing an essential and complementary test to the mechanical tests.

Regarding the flow rates through composite liners involving GCLs, the literature review carried out suggests that the amount of liquid flow at the interface between the geomembrane and the GCL depends on many parameters, such as the hydraulic conductivity of the GCL, the liquid head on top of the liner, the confining stress over the liner system, the contact conditions between the geomembrane and the GCL, the thickness of the liner system, the type and location of the defect in the geomembrane, etc.

The effect of the hydraulic conductivity of GCLs is difficult to address as it is not constant. These materials are typically installed in landfills at their natural water content. Therefore, the saturated hydraulic conductivity is not representative of the field conditions, at least in the short period before GCLs reaching saturation. The unsaturated hydraulic conductivity can be estimated by predictive methods based on knowledge of the relationship between the suction and the volumetric water content, known as water retention curve and often represented by the van Genuchten parameters.

Data on GCLs' suction is scarce and thus experiments studying the suitability of the filter paper method for evaluating the suction of the GCLs were performed. The results obtained showed that the filter paper method can be used for measuring the suction of these products. Based on this finding, suction measurements were carried out, under no stress, for three products. Correspondent volumetric water contents were also estimated experimentally. Water retention curves were determined and then the van Genuchten parameters were evaluated by fitting a theoretical water retention curve to the experimental data.

The relative importance of GCLs prehydration, liquid head above the liner, and confining stress over the liner system, for the flow rate through composite liners due to defects in the geomembrane, was studied through laboratory tests. Composite liners comprising a geomembrane, with a circular hole, over a GCL over a compacted clay liner, were simulated in tests at three scales, and the flow rate at the interface between the geomembrane and the GCL was measured. Small-scale tests were performed using a 0.2 m diameter cell. An intermediate-scale test was conducted using a 1 m diameter cell, and a large-scale test was performed in a square 2.2 m wide test facility. The intermediate and large-scale tests were intended to complement the small-scale tests and to check the feasibility of an extrapolation of the results obtained on small-scale tests to field conditions.

Final flow rates, obtained in steady state conditions, together with the observation of the wetted areas, made possible to estimate the transmissivity values of the interface between the

GCL and the geomembrane. These values were then used for interpreting the test results.

The influence of the prehydration of the GCL was studied by carrying out tests either with non-prehydrated (natural water content) or with prehydrated specimens (moistened to water content of 100%). The effect of the confining stress was addressed by performing tests under 50 kPa and 200 kPa. Finally, the influence of the hydraulic head was examined conducting tests with two hydraulic heads: 0.3 and 1.2 m.

The main findings to be drawn from the results can be summarised as follows: (i) it seems that, as for the effect on the transmissivity, it is important to take into account the relationship between the initial water content and the confining stress. The transmissivity does not seem to be affected by prehydration when low confining stresses are used, whereas it seems to be affected when high confining stresses are used. In addition, the transmissivity does not seem to be influenced by the increase in the confining stress when non-prehydrated GCLs are used, but it seems to be significantly affected when prehydrated GCLs are used. The differences obtained might be related with the prehydration process, which seems to have a significant influence on the quality of the contact between the geomembrane and the GCL and, therefore, on the transmissivity; (ii) the transmissivity does not seem to be significantly influenced by the increase in hydraulic head; (iii) the comparisons between, on the one hand, intermediate and small-scale tests and, on the other hand, large and small-scale tests, suggest that, for the confining stresses considered in this study (25 and 50 kPa), the transmissivity obtained in small-scale tests can be seen as an upper limit of the transmissivity obtained in intermediate and large scale tests, which indicates that predictions on flow rates through composite liners, due to defects in the geomembrane, based on transmissivity values obtained in small-scale tests are conservative; and (iv) the flow rates calculated for field conditions, based on the experimental data obtained in this work, and assuming a hole density of 15.3 holes per hectare (in accordance with the literature review carried out on this topic), are less than the ones measured in field studies. This discrepancy can be attributed to the fact that, in the present study, only circular holes in the geomembrane were considered. Higher flow rates would have been obtained if long defects or a damaged wrinkle had been considered.

Based on transmissivity values obtained experimentally, empirical equations for predicting the flow rate through composite liners comprising a geomembrane over a GCL over a compacted clay liner were developed. Equations were presented respectively for circular defects, for defects of infinite length, and for damaged wrinkles, as it was observed that accurate predictions of flow rate could be obtained if more than one type of defects are considered. For the range of parameters used to develop these equations, it was found that the empirical equations presented in this study are in better agreement than the empirical equations reported in literature, both with the analytical solutions and with the flow rates measured experimentally. Relative differences between the flow rate measured in large-scale test and the flow rate calculated using the empirical equations obtained in this study was about 15 %, which tends to validate these empirical equations from an experimental point of view. The equations proposed here provide engineers with simple tools that give a good approximation of flow rates through composite liners consisting of a geomembrane over a GCL over a CCL as compared with the previous equations reported in literature. This represents an improvement in the existing methods for predicting the flow rates through this

type of composite liners.

7.2 PERSPECTIVES

The investigation of fluid migration through geomembrane seams warrants further work. It would be appropriate to use geomembranes manufactured with different raw materials rather than to use high density polyethylene, as well as to consider other types of seams, such as for example, the extrusion seams.

The gas permeation pouch test can also be used as a tool for studying the long-term behaviour of thermal-hot dual wedge seams exposed to sunlight. Over the last years, geomembranes have been used in landfill facility elements, which are often permanently exposed to sunlight without any external protection (e.g. leachate lagoons). There have been some studies on the long term mechanical behaviour of geomembrane seams exposed to sunlight, but the evolution of the fluid-tightness remains unstudied. Seams are vulnerable areas due to the mechanical and thermal solicitations during the seaming process. A study in this topic can be carried out in complement to a research programme in progress at *Laboratório Nacional de Engenharia Civil* to address the evolution of the mechanical properties of 2mm-thick high density polyethylene geomembrane seams exposed to sunlight for several years, in several Portuguese landfills.

The investigation about flow rate through composite liners due to defects in geomembranes needs to be extended to include other GCLs, as well as other geomembranes, such as for example textured geomembranes. In addition, as the transmissivity depends on the hydraulic conductivity of the GCL, which seems to increase with the increase in the concentration and cation valence of the permeant liquid, the effect of the permeant liquid on the interface transmissivity should be examined.

The numerical modelling of the flow rate through composite liners comprising unsaturated GCLs needs also to be addressed. This can serve to understand which is the long-term influence on flow rates and wetted areas of the variation in transmissivity observed on short-term, particularly the variations related with the coupled effect between the confining stress and water content of the GCLs. As in field conditions GCLs are usually under stress, a critical point for the numerical modelling is to know the retention curves of the GCLs under stress. Actually, as a consequence of this study, suction measurements for GCLs under stress, based on the filter paper method, are already under way and the numerical modelling on this issue will be carried out in a near future.

The empirical equations for calculating the flow rate through composite liners due to geomembrane defects can be extended to composite liners consisting of just a geomembrane over a GCL.

REFERENCES

Air Liquide, 2002, *Encyclopédie des Gaz*, Elsevier.

Alexiew, N., 2000, New Perspectives for Geosynthetic Clay Liners Using Calcium Bentonite. *Proceedings of EuroGeo 2*, Vol. 2, Bologna, Italy, pp. 707-712.

ASTM D 1434, *Standard Test Method for Determining Gas Permeability Characteristics of Plastic Films and Sheeting*, American Society for Testing and Materials, West Conshohocken, Pennsylvania, USA.

ASTM D 4437, *Determining the Integrity of Field Seams Used in Joining Flexible Polymeric Sheet Geomembranes*, American Society for Testing and Materials, West Conshohocken, Pennsylvania, USA.

ASTM D 5199, *Standard Test Method for Measuring Nominal Thickness of Geotextiles and Geomembranes,* American Society for Testing and Materials, West Conshohocken, Pennsylvania, USA.

ASTM D 5298, *Standard Test Method for Measurement of Soil Potential (suction) using Filter Paper*, American Society for Testing and Materials, West Conshohocken, Pennsylvania, USA.

ASTM D 5887, *Standard Test Method for Measurement of Index Flux Through Saturated Geosynthetic Clay Liner Specimens Using a Flexible Wall Permeameter*, American Society for Testing and Materials, West Conshohocken, Pennsylvania, USA.

ASTM D 638, *Standard Test Method for Tensile Properties of Plastics*, American Society for Testing and Materials, West Conshohocken, Pennsylvania, USA.

ASTM D 6747, *Standard Guide for Selection of Techniques for Electrical Detection of Potential Leaks Paths in Geomembrane*, American Society for Testing and Materials, West Conshohocken, Pennsylvania, USA.

ASTM E 96, *Test Method for Water Vapour Transmission Materials*, American Society for Testing and Materials, West Conshohocken, Pennsylvania, USA.

August, H. & Tatzky, R., 1984, Permeabilities of Commercially Available Polymeric Liners for Hazardous Landfill Leachate, *Proceedings of International Conference on Geomembranes*, Denver, USA, pp. 163-168.

Babu, G.L.S., Sporer, H. & Gartung, E., 2002, Desiccation Behaviour of Selected Geosynthetic Clay Liner, *Proceedings of the International Symposium IS Nuremberg 2002*, Nuremberg, Germany, pp. 295-302.

Barroso, M.C.P., 2001, *Verificação da Estanqueidade da Geomembrana Superior do Revestimento Basal de Duas Lagoas em Alcochete*, LNEC, Nota Técnica 21/01-NP, Proc^{o} 054/1/14632, 6 p. (in Portuguese).

Benneton, J.P. & Gerard, Y., 2002, Mechanical Strength Evaluation of Geomembrane Welds-Welding Factors, *Proceedings of Seventh International Conference on Geosynthetics*, Vol. 4, Nice, France, pp. 1411-1414.

Benson, C.H., Daniel, D.E. & Boutwell, G.P., 1999, Field Performance of Compacted Clay Liners, *Journal of Geotechnical and Geoenvironmental Engineering*, Vol. 125, No. 5, pp. 390-403.

Bonaparte, R. & Gross, B.A., 1990, Field Behavior of Double-Liner Systems, Waste *Containment Systems: Construction, Regulation, and Performance*, Bonaparte. R., Editor, ASCE Geotechnical Special Publication No. 26, Proceedings of a symposium held in San Francisco, USA, pp. 52-83.

Bonaparte, R. & Gross, B.A., 1993, LDCRS Flows from Double-Lined Landfills and Surface Impoundments, *United States Environmental Protection Agency Report EPA/600/SR-93/070*, Cincinnati, OH, USA, 65 p.

Bonaparte, R., Daniel, D. & Koerner, R.M., 2002, *Assessment and Recommendations for Improving the Performance of Waste Containment Systems*, United States Environmental Protection Agency Report EPA/600/R-02/099, Cincinnati, OH, USA.

Bonaparte, R., Othman, M.A., Rad, N.S., Swan, R.H. & Vander Linde, D.L., 1996, Evaluation of Various Aspects of GCL Performance, Appendix F in Report of 1995 *Workshop on Geosynthetic Clay Liners*, D.E. Daniel and H.B. Scranton, United States Environmental Protection Agency Report EPA/600/R-96/149, Cincinnati, OH, USA, pp. F1-F34

Bouazza, A. Zornberg, J.G. & Adam, D., 2002a, Geosynthetics in Waste Containment Facilities: Recent Advances. Keynote Paper, *Proceedings of Seventh International Conference on Geosynthetics*, Vol. 2, Nice, France, pp. 445-511.

Bouazza, A., 2002, Geosynthetic Clay Liners, *Geotextiles and Geomembranes*, No. 20, pp. 3-17.

Bouazza, A., Vangpaisal, T. & Rahman, F., 2002b, Gas Migration through Needle Punched Geosynthetic Clay Liners, *Proceedings of the International Symposium IS Nuremberg 2002*, Nuremberg, Germany, pp. 165-176.

Broad, M & Laine, D.L., 1995, Coralling Liner Nightmares, *MSW Management*, Nov./Dec. 95, pp. 48-40.

Brown, K.W., Thomas, J.C., Lytton, R.L., Jayawickrama, P. & Bhart, S., 1987, *Quantification of Leakage Rates through Holes in Landfill Liners*, United States Environmental Protection Agency Report CR810940, Cincinnati, OH, 147 p.

Cartaud, F., Touze-Foltz, N. & Duval, Y., 2005, Experimental Investigation of the Influence of a Geotextile Beneath the Geomembrane in a Composite Liner on the Leakage through a Hole in the Geomembrane, *Geotextiles and Geomembranes,* Vol. 23, No. 2, 27 pages

Castro, E., 1974, *Mecânica dos Solos-Conceitos Fundamentais*, Edições LNEC, 161 p. (in Portuguese).

Chandler, R.J. & Gutierrez, C.I., 1986, The Filter-Paper Method of Suction Measurement, *Géotechnique*, Vol. XXXVI, No. 2, pp. 265-268.

Chul Joo, J., Kim, J.Y. & Nam, K., 2001, Mathematical Modelling of Organic Chemical Permeation through Flexible Membrane Liners, *Proceedings of Eight International Waste Management and Landfill Symposium*, Vol. 3, Cagliari, Sardinia, Italy, pp. 237-244.

Colucci, P. & Lavagnolo, M. C., 1995, Three Years Field Experience in Electrical Control of Synthetic Landfill Liners, *Proceedings of Fifth International Landfill Symposium: Sardinia '95*, Vol. 2, Cagliari, Sardinia, Italy, pp. 437-452.

Comité Français des Géosynthétiques, 1998*, Recommandation Générales pour la Réalisation d'Etanchéité par Géosynthétiques Bentonitiques*, Fascicule n°12, Bagneux, 56 p. (in French).

Comité Français des Géosynthétiques, 2003, *Présentation de Méthods de Détection et de Localisation de Défauts dans les Dispositifs d'Etanchéité par Géomembranes*. 44 p. (in French).

Daniel, D.E. & Koerner, R.M., 1993, Quality Assurance and Quality Control for Waste Containment Facilities. United States Environmental Protection Agency Report EPA/600/R-93/182, Cincinnati, OH, USA, 305 p.

Daniel, D.E., 1982, Measurement of Hydraulic Conductivity of Unsaturated Soils with Thermocouple Psychrometers, *Soil Science Society of America Journal*, Vol. 20, No. 6, pp. 1125-1129.

Daniel, D.E., 1993, *Geotechnical Practice for Waste Disposal*, Edited by David E. Daniel, Published by Chapman & Hall, London, U.K., 683 p.

Daniel, D.E., 1996, Geosynthetic Clay Liners, Part Two: Hydraulic Properties, *Geotechnical Fabrics Report*, June/July, pp. 22-26.

Daniel, D.E., 1998, Landfills for Solid and Liquid Wastes, *Proceedings of Third International Congress on Environmental Geotechnics*, Balkema, Vol. 4, Lisbon, Portugal, pp. 1231-1246.

Daniel, D.E., Shan, H-Y. & Anderson, J.D., 1993, Effects of Partial Wetting on the Performance of the Bentonite Component of a Geosynthetic Clay Liner. *Proceedings of Geosyntheitcs'93*, Vol. 3, IFAI, St. Paul, USA, pp. 1482-1496.

Darilek, G.T. & Miller, L. V., 1998, Comparison of Dye Testing and Electrical Leak Location Testing of a Solid Waste Liner System, *Proceedings of Sixth International Conference on Geosynthetics*, Vol. 1, Atlanta, USA, pp. 273-276.

Darilek, G.T., Laine D. & Parra, J.O., 1989, The Electrical Leak Location Method for Geomembrane Liners, *Proceedings of Geosynthetics'89*, Vol. 2, IFAI, San Diego, USA, pp. 456-462.

Didier, G. & Comeaga, L., 1997, Influence of Initial Hydration Conditions on GCL Leachate Permeability, Testing and Acceptance Criteria for Geosynthetic Clay Liners, *ASTM STP 1308*, Larry W. Well, Ed., American Society for Testing and Materials, pp. 181-195.

Didier, G., Bouazza, A. & Cazaux, D., 2000, Gas Permeability of Geosynthetic Clay Liners, *Geotextiles and Geomembranes*, Vol. 18, No. 2-4, pp. 235-250.

Durin L., 1999, Transferts d'Eau et de Contaminants Organiques dans les Structures d'Etanchéité Synthétiques et Minérales des Centres de Stockage de Déchets Ménagers, Thèse de Docteur, Université de Paris-Sud Orsay, Paris, France, 290 p. (in French).

Durin, L., Touze, N. & Duquennoi, C., 1998, Water and Organic Solvents Transport Partrameters in Geomembranes, *Proceedings of Sixth International Conference on Geosynthetics*, Vol. 1, Atlanta, USA, pp. 249-256.

Egloffstein, T., 1997, Geosynthetic Clay Liners, Part Six: Ion Exchange, *Geotechnical Fabric Report*, June/July, pp. 38-43.

Egloffstein, T., 2001, Natural Bentonites – Influence of the Ion Exchange and Partial Desiccation on Permeability and Self-Healing Capacity of Bentonites Used in GCLs, *Geotextiles and Geomembranes*, No. 19, pp. 427-444.

Egloffstein, T., 2002, Bentonite as Sealing Material in Geosynthetic Clay Liners – Influence of Electrolytic Concentration, the Ion Exchange and Ion Exchange with Simultaneous Partial Desiccation on Permeability, *Proceedings of the International Symposium IS Nuremberg 2002*, Nuremberg, Germany, pp. 141-153.

Eloy-Giorni, C., Pelte, T., Pierson P. & Margrita, R., 1996, Water Diffusion through Geomembranes Under Hydraulic Pressure, *Geosynthetics International*, Vol. 3, No. 6, pp. 741-769.

EN 964, *Geotextiles and Geotextile-Related Products – Determination of Thickness at Specified Pressures – Part 1: Single Layers*, European Committee for Standardization (CEN), Brussels, Belgium.

Encyclopedia of Polymer Science and Technology, 1964, John Wiley and Sons.

Estornell, P. & Daniel, D., 1992, Hydraulic Conductivity of Three Geosynthetic Clay Liners, *Journal of Geotechnical Engineering*, Vol. 18, No. 10, pp. 1592-1606.

Estrin, D. & Rowe, R.K., 1995, Landfill Design and the Regulatory System, *Proceedings of Fifth International landfill Symposium: Sardinia'95*, Vol 3, Cagliari, Sardinia, Italy, pp. 15- 26.

European Directive No. 1999/31/EC, 1999, *Directive on the Landfill of Waste*, Official Journal of the European Communities, L182/1-L182/19.

Fang, H.-Y., 1997, *Introduction to Environmental Geotechology*, CRC Press LLC, 652 p.

Fawcett, R.G. & Collis-George, G.N., 1967, A Filter-Paper Method for Determining the Moisture Charcteristics of Soil, *Australian Journal of Experimental Agriculture and Animal Husbandry*, Vol. 7, pp. 162-167.

Foose, G.J., Benson, C.H. & Edil, T.B., 2001, Predicting Leakage through Composite Landfill Liners, *Journal of Geotechnical and Geoenvironmental Engineering*, Vol. 127, No. 6, pp. 510-520.

Fox, P.J., Olsta, J.T. & Chiu, P., 2002, Internal and Interface Shear Strengths of Needle-Punched Geosynthetic Clay Liners, *Proceedings of Seventh International Conference on Geosynthetics*, Vol. 2, Nice, France, pp. 667-671.

Fredlund, D. G. & Rahardjo, H., 1993, *Soil Mechanics Principles for Unsaturated Soils*, John Wiley & Sons. NY, 517 p.

Fukuoka, M., 1986, Large Scale Permeability Test for Geomembrane Subgrade System, *Proceedings of Third International Conference on Geotextiles*, Vienna, Austria, pp. 917-922.

Giroud, J.P. & Bonaparte, R., 1989, Leakage through Liners Constructed with Geomembranes - Part II. Composite Liners, *Geotextiles and Geomembranes*, Vol. 8, No. 2, pp. 71-111.

Giroud, J.P. & Daniel, D.E., 2004, Liquid Migration in an Encapsulated Bentonite Layer Due to Geomembrane Defects, *Geosynthetics International*, Vol. 11, No. 4, pp. 311-329.

Giroud, J.P. & Touze-Foltz, N., 2003, Geomembranes in Landfills: Discussion at the Seventh International Conference on Geosynthetics, *Geosynthetic International*, Vol. 10, No. 4, pp. 124-133.

Giroud, J.P. &. Touze-Foltz, N., 2005, Equations for Calculating the Rate of Liquid Flow through Geomembrane Defects of Uniform Width and Finite or Infinite Length, Paper submitted to *Geosynthetics International*.

Giroud, J.P., 1997, Equations for Calculating the Rate of Liquid Migration Through Composite Liners Due to Geomembrane Defects, *Geosynthetics International*, Vol. 4, No. 3-4, pp. 335-348.

Giroud, J.P., Badu-Tweneboah, K. & Bonaparte, R., 1992, Rate of Leakage through a Composite Liner Due to Geomembrane Defects, *Geotextiles and Geomembranes*, Vol. 11, No. 1, pp. 1-28.

Giroud, J.P., Khatami, A. & Badu-Tweneboah, K., 1989, Evaluation of the Rate of Leakage through Composite Liners, *Geotextiles and Geomembranes*, Vol. 8, pp. 337-340.

Giroud, J.P., Soderman, K.L., Khire, M.V. & Badu-Tweneboah, K., 1998, New Developments in Landfill Liner Leakage Evaluation, *Proceedings of Sixth international Conference on Geosynthetics*, Vol. 1, IFAI, Atlanta, USA, pp. 261-268.

Gomes, C. F., 1986, *Argilas. O que são e para que servem.* Fundação Calouste Gulbenkian, Lisboa, Portugal, 457 p. (in Portuguese).

Gross, B.A., Bonaparte, R. & Giroud, J.P., 1990, Evaluation of Flow from Landfill Leakage Detection Layers", Fourth International Conference on Geotextiles, Vol. 2, The Hague, pp. 481-486.

Guide EA - 4/02, 1999, *Expression of the Uncertainty of Measurements in Calibration*, drafted by EAL Task Force for revision of WECC Doc. 19-1990 on behalf of the EAL Committee 2 (Calibration and Testing Activities).

Gundseal, 2001*, The GSE GundSeal GCL Design Manual.*

Hamblin, A. P., 1981, Filter-Paper Method for Routine Measurement of Field Water Potential, *Journal of Hydrology*, Vol. 53, pp. 355-360.

Harpur, W.A. & Wilson-Fahmy, R.F. & Koerner, R.M., 1993, Evaluation of the Contact Between Geosynthetic Clay Liners and Geomembranes in Terms of Transmissivity, *Geosynthetic Liner Systems: Innovations, Concerns and Design*, Edited by Koerner & Wilson-Fahmy, Proceedings of a Geosynthetic Liner Systems Seminar held in Philadelphia, USA, pp. 143-154.

Haxo, H.E. & Pierson, P., 1991, Permeability Testing, *Geomembranes Identification and Performance Testing*, Chapter 10, Edited by A. Rollin and J. M. Rigo, pp. 219-240.

Haxo, H.E., 1990, Determining the Transport through Geomembranes of Various Permeants in Different Applications, *Proceedings of ASTM Symposium on Geosynthetic Testing for Waste Containment Applications*, Las Vegas, USA.

Haxo, H.E., Jr & Kamp, C.L., 1990, Destructive Testing of Geomembranes Seams: Shear and Peel Testing of Seam Strength, *Geotextile and Geomembranes*, No. 9, pp. 369-404.

Haxo, H.E., Miedema, J.A. & Nelson, N.A., 1984, Permeability of Polymeric Membrane Lining Materials, *Proceedings of International Conference on Geomembranes*, Vol. I, IFAI, Denver, St. Paul, USA, pp. 151-156.

Hurtado-Gimeno, C., 1999, Perméation Gazeuse des Géomembranes Soudées, Mémoire de DEA, Univerité Joseph Fourier, Grenoble, France, 44 p. (in French).

IGS, 2000, *Recommended Descriptions of Geosynthetics Functions, Geosynthetics Terminology, Mathematical and Graphycal Symbols*, Fourth Edition.

Ingold, T.S., 1994, *Geotextiles and Geomembranes Manual,* Elsevier Advanced Technology, 610 p.

Iryo, T. & Rowe, R.K., 2004, Numerical Study of Infiltration into a Soil – Column, *Geosynthetics International*, Vol. 11., No. 5, pp. 377-389.

Jayawickrama, P.W., Brown, K.W., Thomas, J.C. & Lytton, R.L., 1988, *Journal of Environmental Engineering*, Vol. 114, No.6, pp. 1401-1420.

Jo, H.Y., Katsumi, T., Benson, C.H., & Edil, T.B., 2001, Hydraulic Conductivity and Swelling of Nonprehydrated GCLs Permeated with Single-species Salt Solutions, *Journal of Geotechnical and Geoenvironmental Engineering*, Vol. 127, No. 7, pp. 557-567.

Katsumi, T., Ogawa, A. & Fukagawa, R., 2004, Effect of Chemical Solutions on Hydraulic Barriers Performance of Clay Geosynthetic Barriers, *Proceedings of EuroGeo 3*, Vol. 2, Munich, Germany, pp. 701-706.

Koerner, G.R. & Allen, S., 1997, The water Vapor Transmission Testing Controversy, *Geotechnical Fabric Report*, March, pp. 8-12.

Koerner, G.R. & Koerner, R.M., 2002, Geomembrane Leakage Arising from Broken Needles with GCLs, *Proceedings of the International Symposium IS Nuremberg 2002*, Nuremberg, Germany, pp. 209-217.

Koerner, R.M., 1997, Perspectives on Geosynthetic Clay Liners. Testing and Acceptance Criteria for Geosynthetic Clay liners, *ASTM STP 1308*, Larry W. Well, Ed., American Society for Testing and Materials, pp. 3-20.

Koerner, R.M., 1998, *Designing with Geosynthetics*, Prentice Hall, Fourth Edition, 761 p.

Koerner, R.M., 2000, Emerging and Future Developments of Selected Geosynthetics Applications, *Journal of Geotechnical and Geoenvironmental Engineering*, Vol. 126, No. 4, pp. 293-306.

Laine, D.L. & Darilek, G.T., 1993, Locating Leaks in Geomembrane Liners of Landfill Covered with Protective Soil, *Proceedings of Geosynthetics'93,* Vol. 3, Vancouver, Canada, pp. 1403-1412.

Laine, D.L. & Miklas, M.P.J., 1989, Detection and Location of Leaks in Geomembrane Liners Using an Electrical Method, *Proceedings of Tenth National Conference, Superfund'89*, Washington, USA, pp. 35-40.

Laine, D.L. & Mosley, N.G., 1993, Leak Location Survey of a Soil Covered Geomembrane at a Landfill Site in the UK, *Proceedings of GREEN'93*, pp. 151-156.

Laine, D.L., 1991, Analysis of Pinehole Seam Leaks Located in Geomembrane Liners Using the Electrical Leak Location Method: Case Histories, *Proceedings of Geosynthetics'9*1, Atlanta, USA, pp.239-253.

Lake, C.B. & Rowe, R.K., 2000, Diffusion of Sodium and Chlorite through Geosynthetic Clay Liners, *Geotextiles and Geomembranes*, Vol. 18, No. 2-4, pp. 103-131.

Lambert, S., 1994, Estude de lá Perméabilité aux Gaz des Géomembranes, Mémoire de DEA, Univerité Joseph Fourier, Grenoble, France, 50 p. (in French).

Liu, Z.Y., 1998, A Scheme of Using Geosynthetics to Treat Cracks on a Reservoir Blanket, *Sixth International Conference on Geosynthetics*, IFAI Atlanta, Georgia, USA, pp. 1121-1124.

Luders, G., 2000, Quality Assurance in Hot Wedge Welding of HDPE Geomembranes, *Proceedings of EuroGeo 2*, Vol. 2, Bologna, Italy, pp. 591-596.

Majdi, A.O., Gross, B.A., Bonaparte, R. & Warren, D., 2002, *Evaluation of Liquids Management Data for Double-Lined Landfills*, Appendix E of United States Environmental Protection Agency Report EPA/600/R-02/099, Cincinnati, OH, USA, 206 p.

Manassero, M., Benson, C. H. & Bouazza, 2000, Solid Waste Containment Systems, *Proceedings of International Conference on Geotechnical & Geological Engineering*, Vol. 1, Melbourne, Australia, pp. 520-642.

Manassero, M., Parker, R., Pasqualini, E., Szabò, I.; Almeida, M.S.S., Bouazza, A., Daniel, D.E. & Rowe, R. K., 1998, Controlled Landfill Design (Geotechnical Aspects), *Proceedings of Environmental Geotechnics*, Vol. 3, LNEC, Lisbon, Portugal, pp. 1001-1035.

Matrecon, 1988, *Lining of Waste Containment and other Impoundment Facilities*, United States Environmental Protection Agency Report EPA/600/2-88/052, Cincinnati, OH, USA.

McQueen, I.S. & Miller, R.F., 1968, Calibration and Evaluation of a Wide-Range Gravimetric Method for Measuring Moisture Stress, *Soil Science Society of America Journal*, No. 106, pp. 225-231.

MEDD, 2002, *Guide de Recommandations à L'usage des Tiers-experts pour L'évaluation de "L'équivalence" en Étanchéité Passive de Centre de Stockage*, Version 1, 20 p. (in French).

Mualem Y., 1976, A New Model for Predicting the Hydraulic Conductivity of Unsaturated Porous Media, *Water Resource Research*, Vol. 12, p. 513-522.

Mueller, W.; Jakob, I., Tatzky-Gerth, R. & August, H., 1998, Solubilities, Diffusion and Partition Coefficients of Organic Pollutants in HDPE Geomembranes: Experimental Results and Calculations, *Proceedings of Sixth International Conference on Geosynthetics*, Vol. 1, Atlanta, USA, pp. 239-248.

Navarro, N., 1999, Quantification des Débits de Fuite dans les Etanchéités Composites de Centres de Stockage de Déchets, Master of Science Géomatériaux, Ecole Nationale Supérieure des Mines de Paris, France, 63 p. (in French).

Needham, A. D., Gallagher, E.M.G., & Smith, J.W.N., 2004, Prediction of the Long Term Generation of Defects in HDPE Liners, *Proceedings of EuroGeo 3*, Vol. 2, Munich, Germany, pp. 507-514.

NF P 84-502.1, *Geomembranes, Essais sur Joints. Partie 1: Détermination des Caractéristiques en Traction-Cisaillement*, Afnor, 1993, 13 pages.

NF P 84-502.2, *Geomembranes, Essais sur Joints. Partie 2: Détermination de la Résistance en Traction-Pelage*, Afnor, 1993, 17 pages.

Nosko, V. & Touze-Foltz, N., 2000, Geomembrane Liner Failure: Modelling of its Influence on Contaminant Transfer, *Proceedings of EuroGeo 2*, Vol. 2, Bologna, Italy, pp. 557-560.

NSF 54, 1993, *Flexible Membrane Liners*, National Sanitation Foundation, Ann Arbor, Michigan, USA, 30 p.

Oliveira, M. & Lopes, M.L., 2002, Geocompósitos Bentoníticos – Análise de Alguns Aspectos do Comportamento Mecânico, *8º Congresso Nacional de Geotecnia*, Vol. 3, LNEC, Lisboa, Portugal, pp. 1851-1861 (in Portuguese).

Orsini, C. & Rowe, K.K., 2001, Testing Procedure and Results for the Study of Internal Erosion of Geosynthetic Clay Liners, *Proceedings of Goesynthetics 2001 Conference*, Porland, USA, pp. 189-201.

Oweis, I.S. & Khera, R.P., 1998, *Geotechnology of Waste Management*, Second Edition, International Thomson Publishing, Boston, MA.

Pardo de Santayana, F.& Barroso, M.C.P., 2002, *Assessoria Geotécnica nas Fases de Projecto e Construção do Aterro de Resíduos do Oeste*, LNEC, Relatório158/02 – Chefia, Proc. 050/1/14316, 47 p. (in Portuguese).

Pardo de Santayana, F.& Lopes, M.G., 2003, Geotechnical Aspects and Construction Quality Assurance Plans for MSW Landfills Recently Built in Portugal, *Proceedings of XIIIth European Conference on Soil Mechanics and Geotechnical Engineering*, Vol. 1, Prague, Czech Republic, pp. 199-204.

Park, G.S., 1986, Transport Principles-Solution, Diffusion and Permeation in Polymer Membranes, *Synthetic Membranes: Science, Engineering and Applications*, P.M. Bugay et al. (eds.), D. Reidel Publishing Company, pp. 57-107.

Park, J.K. & Nibras, M., 1993, Mass Flux of Organic Chemicals through Polyethylene Geomembranes, *Water Environment Research*, Vol. 65, No. 3, pp. 227-237.

Park, J.K., Sakti, J.P. & Hoopes, J.A., 1995, Effectiveness of Geomembranes as Barriers for Organic Coumpounds. *Proceedings of Geosynthetics'95*, Vol. 3, Nashville, Tennessee, USA, pp. 879-891.

Peggs, I. D., 1996b, A Reassessment of HDPE Geomembrane Specifications, *Proceedings of Geosynthetics: Applications, Design and Construction*, Balkema, Rotterdam, Nederland, pp.693-695.

Peggs, I.D., 1989, Destructive Testing of Polyethylene Geomembrane Seams: Various Methods to Evaluate Seam Strength, *Seaming of Geosynthetics*, Elsevier Science Publishing Co., Inc., NY, USA, pp 125-133.

Peggs, I.D., 1994a, Testing Program to Assure the Durability of Geomembranes, *Landfilling of Waste: Barriers*, Edited by T.H. Christensen; R. Cossu and R. Stegmann, Published by E & FN Spon, pp.413-429.

Peggs, I.D., 1994b, HDPE Geomembrane Seams: Acceptance Criteria and Critical Defects, *Geosynthetic Liner Systems: Innovations, Concerns and Designs*, Edited by R. M. Koerner and R. F. Wilson-Fahmy, Proceedings of a Geosynthetic Liner Systems Seminar held in Philadelphia, USA, pp. 25-32.

Peggs, I.D., 1996a, Defect Identification, Leak Location, and Leak Monitoring in Geomembrane, *Proceedings of Geosynthetics: Applications, Design and Construction*, Balkema, Rotterdam, Nederland, pp. 611-618.

Peggs, I.D., 1997, A Comprehensive Generic CQA Plan for HDPE Geomembranes, *Proceedings of Geosynthetics Asia'97*, Bangalore, India, pp. 403-408.

Peggs, I.D., 2001, Three Challenging Electrical Integrity/Leak Surveys on Uncovered and Deep Water-Covered Liners, *Proceedings of the Geosynthetics Conference 2001*, IFAI, Portland, Oregon, USA, pp. 245-262.

Petle, T., 1993, Étude Théorique et Expérimental de la Fonction Étanchéité et de Comportement Thermique des Géomembranes. Thèse de Doctorat, Laboratorie de Géology et de Mécanique. Grenoble, Université Joseph Fourier-Grenoble I. France, 253 p. (in French).

Petrov , R.J. & Rowe, R.K., 1997, Geosynthetic Clay Liner – Chemical Compatibility by Hydraulic Conductivity Testing: Factors Impacting its Performance, *Canadian Geotechnical Journal*, Vol. 34, No. 6, pp. 863-885.

Petrov, R.J., Rowe, R.K. & Quigley, R.M., 1997a, Comparison of Laboratory Measured GCL Hydraulic Conductivity Based on Three Permeameter Types, *Geotechnical Testing Journal*, Vol. 20, No. 1, pp. 49-62.

Petrov, R.J., Rowe, R.K. & Quigley, R.M., 1997b, Selected Factors Influencing GCL Hydraulic Conductivity, *Journal of Geotechnical and Geoenvironmental Engineering*, Vol. 123, No. 8, pp. 683-695.

Pierson, P. & Duquennoi, C. 2000, Perméabilité et Durabilité des Géomembranes, *Séminaire la Notation d'Equivalence en Etanchéité-Drainage*, Cemagref, Paris, France, pp. 85-94. (in French).

Rad, N.S., Jacobsen, B.D. & Bachus, R.C., 1994, Compatibility of Geosynthetic Clay Liners with Organic and Inorganic Permeants, *Proceedings of Fifth International Conference on Geosynthetics*, Singapore, pp. 1165-1168.

Reddi, L.N. & Inyang, H.I., 2000, *Geoenvironmental Engineering. Principles and Applications.* Headquarters, Marcel Dekker, Inc., 494 p.

Reid, J.M., Prausnitz, J.M & Poling, B.E., 1987, *Properties of Gases and Liquids*, Fourth Edition.

Rogers, C.E., 1985, Permeation of Gases and Vapours in Polymers, *Polymer Permeability*, Comyn, J. (Ed.), Elsevier Applied Science Publishers, London, U.K., Chapter 2, pp. 1-77.

Rollin, A.L. & Fayoux, D., 1991, Geomembrane Seaming Techniques, *Geomembrane Identification and Performance Testing*, RILEM, Edited by A. Rollin and J-M. Rigo, pp.59-79.

Rollin, A.L., Jacquelin, T., Forget, B. & Saunier, 2004, A Guide to Detect Leaks on Installed Geomembranes, *Proceedings of EuroGeo 3*, Vol. 1 , Munich, Germany, pp. 235-239.

Rollin, A.L., Marcotte, M. & Chaput, L., 2002b, Lessons Learned from Geo-electrical Leaks Surveys, *Proceedings of Seventh International Conference on Geosynthetics*, Vol. 2, Nice, France, pp. 527-530.

Rollin, A.L., Marcotte, M., Jacqueline, T. & Chaput, L., 1999, Leak Location in Exposed Geomembrane Liners Using an Electrical Leak Detection Technique, *Proceedings of Geosynthetic'99*, Industrial Fabrics Association International, Vol. 2, Boston, USA, pp. 615-626.

Rollin, A.L., Pierson, P. & Lambert, S., 2002a, *Géomembranes-Guide de Choix Sous l'Angle des Matéraiux*, Presses Internationales Polytechnique, 274 p.

Rollin, A.L., Vidovic, A. & Ciubotariu, V., 1994, Assessment of HDPE Geomembrane Seams, *Landfilling of Waste: Barriers*, Edited by T.H. Christensen; R. Cossu and R. Stegmann, Published by E & FN Spon, pp. 377-391.

Rollin, A.L., Vidovic, A. & Denis, R., 1989, Evaluation of HDPE Geomembrane Field Welding Techniques: Need to Improve Reliability of Quality Seams, *Proceedings of Geosynthetics'89*, San Diego, USA, pp. 443-455.

Rowe, R.K., 1998, Geosynthetics and the Minimization of Contaminant Migration through Barrier Systems Beneath Solid Waste, Keynote paper, *Proceedings of the Sixth International Conference on Geosynthetics,* Vol. 1, Atlanta, USA, pp. 27-103.

Rowe, R.K., 1999, Solid Waste Disposal Facilities for Urban Environments, *Proceedings of XI Pan American Conference on Soil Mechanics and Geotechnical Engineering*, Vol. 4, Foz do Iguassu, Brasil, pp. 89-111.

Rowe, R.K., Orsini, C. & Maubeuge, K., 2002, An Examination of the Potential Erosion of GCLs Placed Directly Over a Geonet, *Proceedings of Seventh International Conference on Geosynthetics*, Vol. 2, Nice, France, pp. 791-795.

Rowe, R.K., Quigley, R. M. & Booker, J.R., 1995, *Clayey Barrier Systems for Waste Disposal Facilities*, Published by E & FN Spon, an imprint of Chapman & Hall, First Edition, 390 p.

Ruhl, J.L. & Daniel, D.E., 1997, Geosynthetic Clay Liners Permeated with Chemical Solutions and Leachates, *Journal of Geotechnical and Geoenvironmental Engineering*, Vol. 123, No. 4, pp. 369-381.

Sangam, H.P. & Rowe, R.K , 2001a, The Role of HDPE Geomembranes in Retarding the Diffusive Migration of Organic Contaminants through Composite Liners Systems, *Proceedings of Eighth International Waste Management and Landfill Symposium*, Vol. 3, Cagliari, Sardinia, Italy, pp. 245-254.

Sangam, H.P. & Rowe, R.K., 2001b, Migration of Dilute Aqueous Organic Pollutants through HDPE Geomembranes, *Geotextiles and Geomembranes*, Vol. 19, pp. 329-357.

Shackelford, C.D., Benson, CH., Katsumi, T., Edil, T.B. & Lin, L., 2000, Evaluating the Hydraulic Conductivity of GCLs Permeated with Non-Standard Liquids, *Geotextiles and Geomembranes*, No. 18, pp. 133-161.

Shan, H-Y. & Lai, Y-J., 2002, Effect of Hydrating Liquid on Hydraulic Properties of Geosynthetic Clay Liners, *Geotextiles and Geomembranes*, No. 20, pp. 19-38.

Snow, M., Bishop, Keenan, R., 1999, Case History of Geomembrane Damage Assessement. *Proceedings of Geosynthetics'99*, Vol. 1, Boston, USA, pp. 635-644.

Southen, J.M. & Rowe, R.K., 2002, Desiccation Behaviour of Composite Landfill Lining Systems Under Thermal Gradients, *Proceedings of the International Symposium IS Nuremberg 2002*, Nuremberg, Germany, pp. 265-274.

Southen, J.M. & Rowe, R.K., 2004, Investigation of the Behavior of Geosynthetic Clay Liners Subjected to Thermal Gradients in Basal Liner Applications, *Journal of ASTM International*, Vol 1, No. 2.

Southen, J.M., Rowe, R.K. & Maubeuge, K., 2004, The Prediction of Thermally-Induced Desiccation in Geosynthetic Clay Liners Used in Landfill Basal Liners Applications, *Proceedings of EuroGeo 3*, Vol. 1, Munich, Germany, pp. 311-320.

Stormont, J.C., Henry, K.S. & Evans, T.M., 1997, Water Retention Functions of Four Nonwoven Polypropylene Geotextiles, *Geosynthetics International*, Vol. 4, No.6, pp. 661-672.

Struve, F., 1994, Consistent Wedge Welders, *Geosynthetic Liner Systems: Innovations, Concerns and Designs*, Edited by R. M. Koerner and R. F. Wilson-Fahmy, Proceedings of a Geosynthetic Liner Systems Seminar held in Philadelphia, USA, pp 9-23.

Swyka, M.A., Hullings, D.A., Iosue, G. & Peggs, I.D., 1999, Overview of Landfill Liner Leak Location Technologies, *Proceedings of Waste Technical Conference,* New Orleans, USA, 10 p.

Tedder, R.B., 1997, Evaluating the Performance of Florida Double-Lined Landfills, *Proceedings of Geosynthetics 97 Conference*, Long Beach, CA, USA, Vol. 1, pp. 425-438.

Touze-Foltz, N., 2001, Modélisation des Transferts Advectifs dans les Etanchéités Composites de Centres de Stockage de Déchets, Thèse de Doctorat, Spécialité Géologie de l'Ingénieur, Ecole Nationale Supérieure des Mines de Paris, France, 288 p. (in French).

Touze-Foltz, N., 2002a, Evaluation of the Hydraulic Transmissivity in Soil Liners-Geomembrane Interfaces, *Proceedings of Seventh International Conference on Geosynthetics*, Vol. 2, Nice, France, pp. 799-803.

Touze-Foltz, N., 2002b, The Influence of Non-Uniform Transmissivity vis-à-vis Hole Location, *Geotextiles and Geomembranes*, Vol. 20, No. 4, pp. 263-277.

Touze-Foltz, N., Darlot, O. & Barroso, M., 2002a, Experimental Investigation of the Influence of the Pre-hydration of GCLs on the Leakage Rates through Composite Liners, *Proceedings of the International Symposium IS Nuremberg 2002*, Nuremberg, Germany, pp. 265-274.

Touze-Foltz, N., Giroud, J.P., 2003, Empirical Equations for Calculating the Rate of Liquid Flow through Composite Liners Due to Geomembrane Defects, *Geosynthetics International*, Vol. 10, No. 6, pp. 215-233.

Touze-Foltz, N., Nosko, V. & Morcet, M., 2002b, Hydraulic Performance of a Composite Bottom Liner in a Municipal Solid Waste Landfill, *Proceedings of Seventh International Conference on Geosynthetics*, Vol. 2, Nice, France, pp. 535-538.

Touze-Foltz, N., Rowe, R.K. & Duquennoi, C., 1999, Liquid Flow Through Composite Liners due to Geomembrane Defects: Analytical Solutions for Axi-symmetric and Two-dimensional Problems, *Geosynthetics International*, Vol. 6., No. 6, pp. 455-479 (Erratum: 2000, Vol. 7, No. 1, p. 77).

Touze-Foltz, N., Rowe, R.K. & Navarro, N., 2001, Liquid Flow through Composite Liners due to Geomembrane Defects: Nonuniform Hydraulic Transmissivity at the Liner Interface, *Geosynthetics International*, Vol. 8, No. 1, pp. 1-26.

Triplett, E.J. & Fox, P.J., 2001, Shear Strength of HDPE Geomembrane/Geosynthetic Clay Liner Interfaces, *Journal of Geotechnical and Geoenvironmental Engineering*, Vol. 127, No. 6, pp. 543-552.

USEPA, 1998, Solid Waste Disposal Facility Criteria Technical Manual, United States Environmental Protection Agency Report EPA/530/R/93/017, Cincinnati, OH, USA.

Van Genuchten, M.,Th., 1980, A Closed Form Equation for Predicting the Hydraulic Conductivity of Unsaturated Soils. *Soil Science Society of America Journal*, Vol. 44, pp. 892-898.

Van Genuchten, M.Th., Leij, F.J. & Yates, S.R., 1991, *The RETC Code for Quantifying the Hydraulic Functions of Unsaturated Soils*, United States Environmental Protection Agency Report EPA/600/2-91/065, Cincinnati, OH, USA.

Vangpaisal, T. & Bouazza, A., 2004, Gas Permeability of Partially Hydrated Geosynthetic Clay Liners. *Journal of Geotechnical and Geoenvironmental Engineering*, Vol. 130, No. 1, pp. 93-102.

Vangpaisal, T., Bouazza, A. & Kodikara, 2002, Gas Permeability of a Needle Punched Geosynthetic Clay Liner Subjected to Wetting and Drying, *Proceedings of Seventh International Conference on Geosynthetics*, Vol. 2, Nice, France, pp. 841-845.

Vasko, S.M., Jo, H.Y., Benson, C.G., Edil, T.B. & Katsumi, T., 2001, Hydraulic Conductivity of Partially Prehydrated Geosynthetic Clay Liners Permeated with Aqueous Calcium Cholorite Solutions, *Proceedings of Goesynthetics 2001 Conference*, Porland, USA, pp. 685-699.

Von Maubeuge, K. & Heerten, G., 1994, Needle Punched Geosynthetic Clay Liners, *Proceedings of 8th GRI Conference*, Philadelphia, USA, pp. 129-207.

White, C.C. & Barker, R.D., 1997, Electrical Leak Detection System for Landfill Liners: a Case History. *GWMR*, pp. 153-159.

Yong, R., Mohamed, A.M.O., Warkentin, B.P., 1992, *Principles of Contaminant Transport in Soils*, Elsevier, 327 p.

Zanzinger, H. & Alexiew, N., 2002, New Shear Creep Tests on Stitch-Bonded GCLs: Important Results, *Proceedings of Seventh International Conference on Geosynthetics*, Vol. 2, Nice, France, pp. 845-849.

APPENDIXES

APPENDIX A: CALCULATION OF THE PARTIAL PRESSURE OF NITROGEN OUTSIDE THE SPECIMEN WHEN PLACED IN ATMOSPHERE

The atmosphere consists of nitrogen (N_2, number of moles: n_{N2}), water vapour (W, number of moles: n_W) and other gases (OG, number of moles: n_{OG}). The partial pressure of nitrogen outside the specimen, p_{Gout}, when placed in atmosphere is then:

$$p_{Gout} = \left(\frac{n_{N2}}{n_{N2} + n_W + n_{OG}} \right) p_{atm} \tag{A.1}$$

where p_{atm} is the atmospheric pressure. The Equation (A.1) can also be written as follows:

$$p_{Gout} = \frac{p_{atm}}{\left(\frac{n_W}{n_{N2} + n_{OG}} \right)\left(\frac{n_{N2} + n_{OG}}{n_{N2}} \right) + \left(\frac{n_{N2} + n_{OG}}{n_{N2}} \right)} \tag{A.2}$$

In Equation (A.2), the ratio $\left(\frac{n_W}{n_{N2} + n_{OG}} \right)$ can be expressed as a function of the specific humidity r. This is the ratio of the mass of water vapour on the mass of dry air (nitrogen + other gases), which can be easily obtained from the psychometric chart, when temperature and relative humidity of atmosphere are recorded:

$$r = \left(\frac{n_W M_{water}}{n_{N2} M_{N2} + n_{OG} M_{OG}} \right) p_{atm} \tag{A.3}$$

where M_{water}, M_{N2} and M_{OG} are the molar masses of water, nitrogen and other gases, respectively.

The concept of dry air molar mass M_{air} is generally used:

$$M_{air} = \frac{n_{N2} M_{N2} + n_{OG} M_{OG}}{n_{N2} + n_{OG}} \tag{A.4}$$

leading to the following by combining Equations (A.3) and (A.4):

$$\frac{n_W}{n_{N2} + n_{OG}} = r \frac{M_{air}}{M_{water}} = 1.61r \tag{A.5}$$

considering M_{air} = 29g and M_{water} = 18g .

In Equation (A.2), the ratio $\left(\frac{n_{N2}}{n_{N2} + n_{OG}} \right)$ is equal to 0.7808. By combining Equations (A.2) and (A.5), it is possible to express p_{Gout} as a function of p_{atm} and r:

$$p_{Gout} = \frac{0.7808}{1 + 1.61r} p_{atm} \tag{A.6}$$

APPENDIX B: CALCULATION OF THE PARTIAL GAS PRESSURE IN THE SPECIMEN WHEN IMMERSED IN WATER

The partial gas pressure, $p_{Gin}(t)$, depends on the mole quantity, $n_G(t)$, in the specimen. This quantity is determined from the same quantity calculated in the preceding step: $n_G(t-\delta t)$, from equation $n_G(t) = n_G(t-\delta t) - f_G'\,\delta t$, which implies that f_G' is known. Since the quantity $p_{Gin}(t)$ is required for the calculation of f_G', it is necessary to determine $p_{Gin}(t)$ directly from $n_G(t-\delta t)$, as follows:

$$p_{Gin}(t) = \left[\frac{n_G(t-\delta t)}{n_{G+W}(t-\delta t)}\right] p_{G+W}(t) \qquad \text{(B.1)}$$

In equation (B.1), $p_{G+W}(t)$ is the absolute total pressure measured inside the pouch specimen, n_G is the mole quantity of gas G, and n_{G+W} is the total mole quantity in the specimen (elements G and W). At time t, the pressure ratio $\left[\frac{p_{Gin}(t)}{p_{G+W}(t)}\right]$ is assumed to be approximately the same as the mole quantity ratio at time $t-\delta t$: $\left[\frac{n_G(t-\delta t)}{n_{G+W}(t-\delta t)}\right]$, which is acceptable if the registering time step δt is small enough. The different steps of calculation are then:

(a) At time $t = 0$

$$n_G(0) = n_{G+W}(0) = \frac{p_{G+W}(0)\,V}{RT} \qquad \text{(B.2)}$$

$$n_W(0) = 0 \qquad \text{(B.3)}$$

$$f_G'(0) = f_G\,\frac{\Delta p_G'(0)}{\Delta p_G}, \text{ where } \Delta p_G'(0) = p_{Gin}(0) = p_{G+W}(0) \qquad \text{(B.4)}$$

f_G and Δp_G were determined after the experiment where the pouch specimen is immersed in gas *G*.

(b) At time $t = \delta t$

$$n_G(\delta t) = n_G(0) - f_G'(0)\delta t \tag{B.5}$$

$$n_{G+W}(\delta t) = \frac{p_{G+W}(\delta t)V}{RT} \tag{B.6}$$

$$n_W(\delta t) = \left[n_{G+W}(\delta t) - n_G(\delta t)\right] \tag{B.7}$$

$$\Delta p_G'(\delta t) = p_{Gin}(\delta t) = \frac{n_G(0)}{n_{G+W}(0)}\, p_{G+W}(\delta t) = p_{G+W}(\delta t) \tag{B.8}$$

$$f_G'(\delta t) = f_G \frac{\Delta p_G'(\delta t)}{\Delta p_G} \tag{B.9}$$

(c) At time $t = 2\delta t$

$$n_G(2\delta t) = n_G(\delta t) - f_G'(\delta t)\, \delta t \tag{B.10}$$

$$n_{G+W}(2\delta t) = \frac{p_{G+W}(2\delta t)\, V}{R\, T} \tag{B.11}$$

$$n_W(2\delta t) = \left[n_{G+W}(2\delta t) - n_G(2\delta t)\right] \tag{B.12}$$

$$\Delta p_G'(2\delta t) = p_{Gin}(2\delta t) = \frac{n_G(\delta t)}{n_{G+W}(\delta t)}\, p_{G+W}(2\delta t) \tag{B.13}$$

$$f_G'(2\delta t) = f_G \frac{\Delta p_G'(2\delta t)}{\Delta p_G} \tag{B.14}$$

Etc., for other steps.

APPENDIX C: EVOLUTION OF ABSOLUTE GAS PRESSURE INSIDE THE SPECIMENS DURING THE TESTS IN AIR AND IN WATER AND GAS QUANTITY PERMEATING THROUGH THE SPECIMENS DURING THE TESTS IN AIR

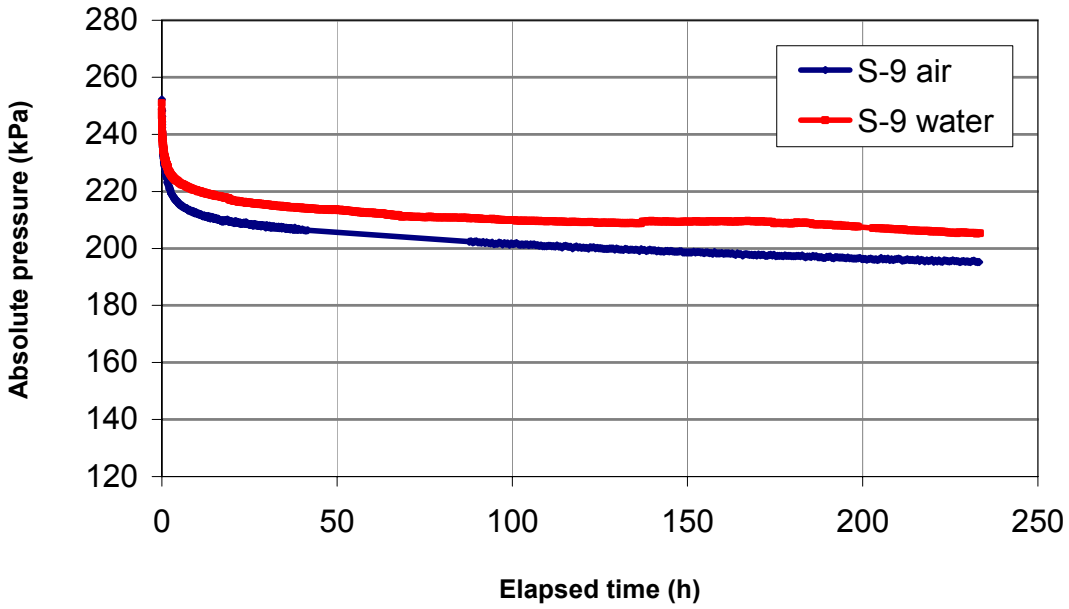

Figure C.1 – Decrease in the absolute pressure of nitrogen for S-9 during the test in air and in water

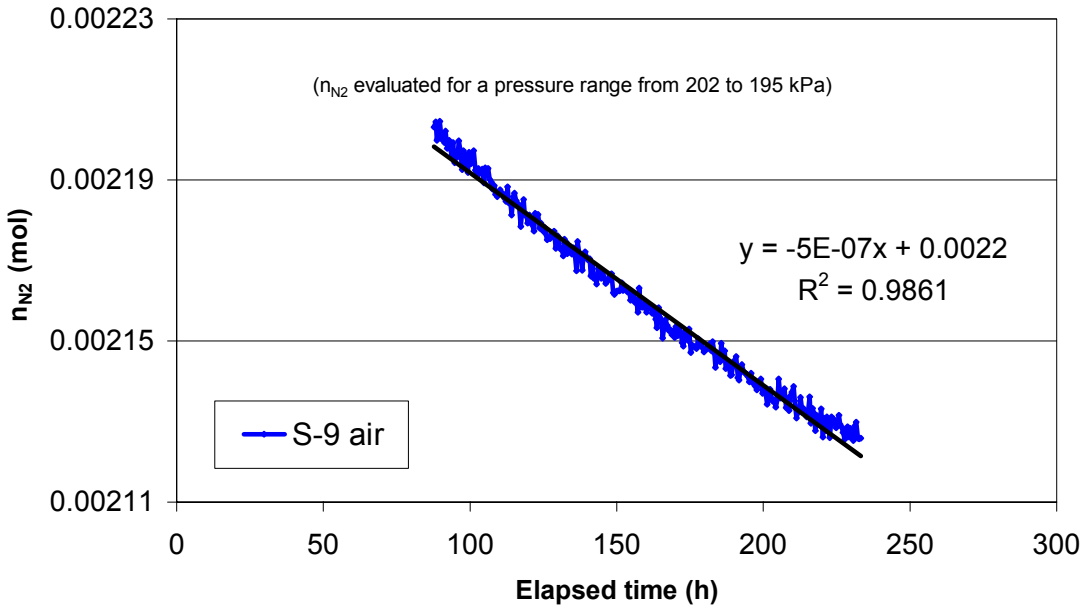

Figure C.2 – Nitrogen quantity permeating through the S-9 in test carried out with the specimen in air

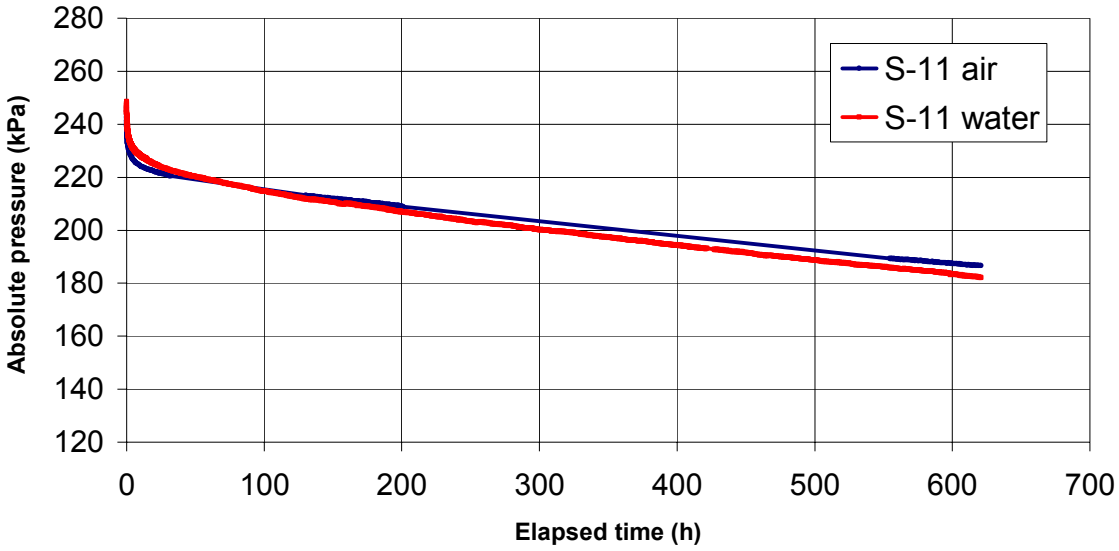

Figure C.3 – Decrease in the absolute pressure of nitrogen for S-11 during the test in air and in water

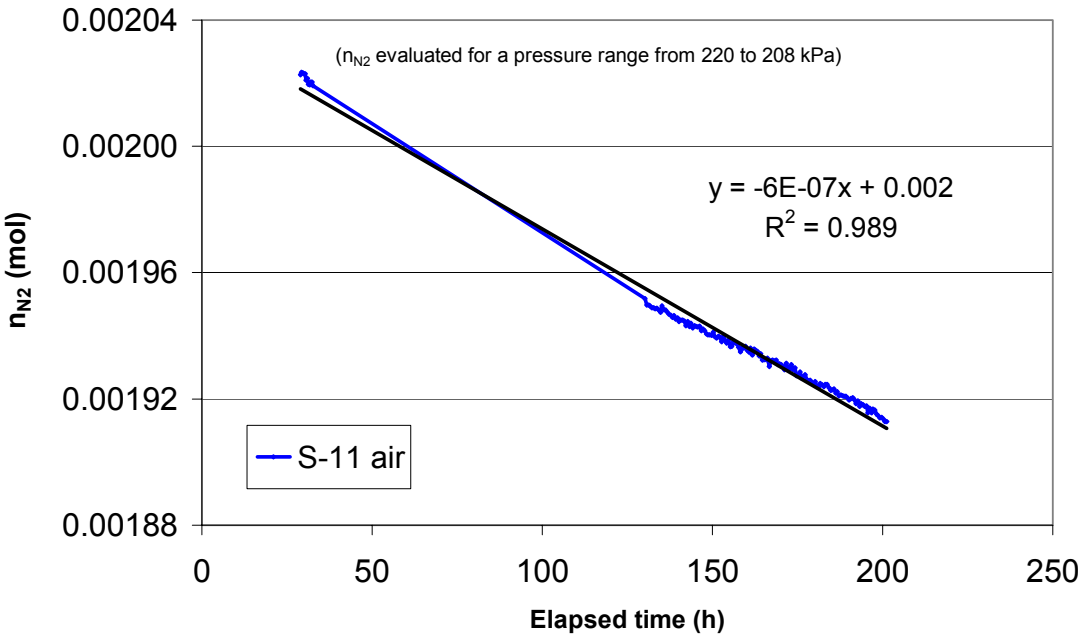

Figure C.4 – Nitrogen quantity permeating through the S-11 in test carried out with the specimen in air

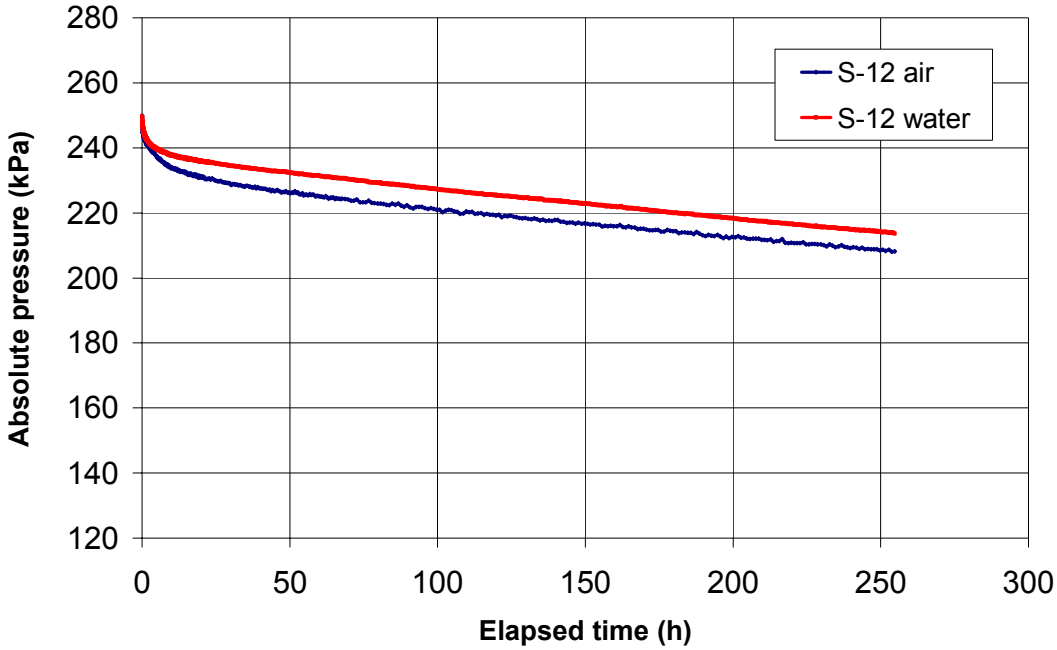

Figure C.5 – Decrease in the absolute pressure of nitrogen for S-12 during the test in air and in water

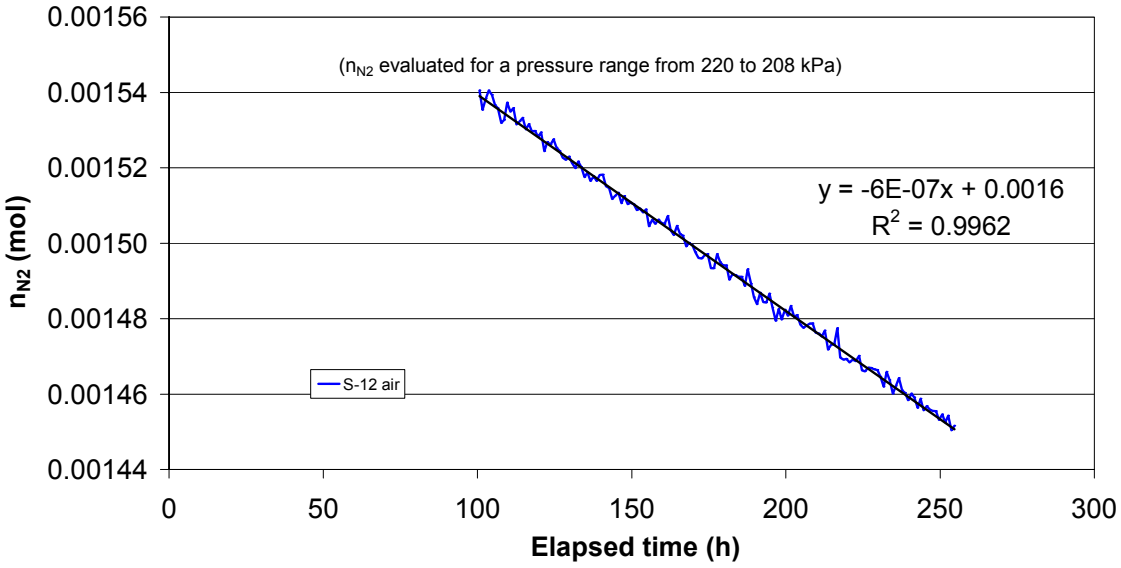

Figure C.6 – Nitrogen quantity permeating through the S-12 in test carried out with the specimen in air

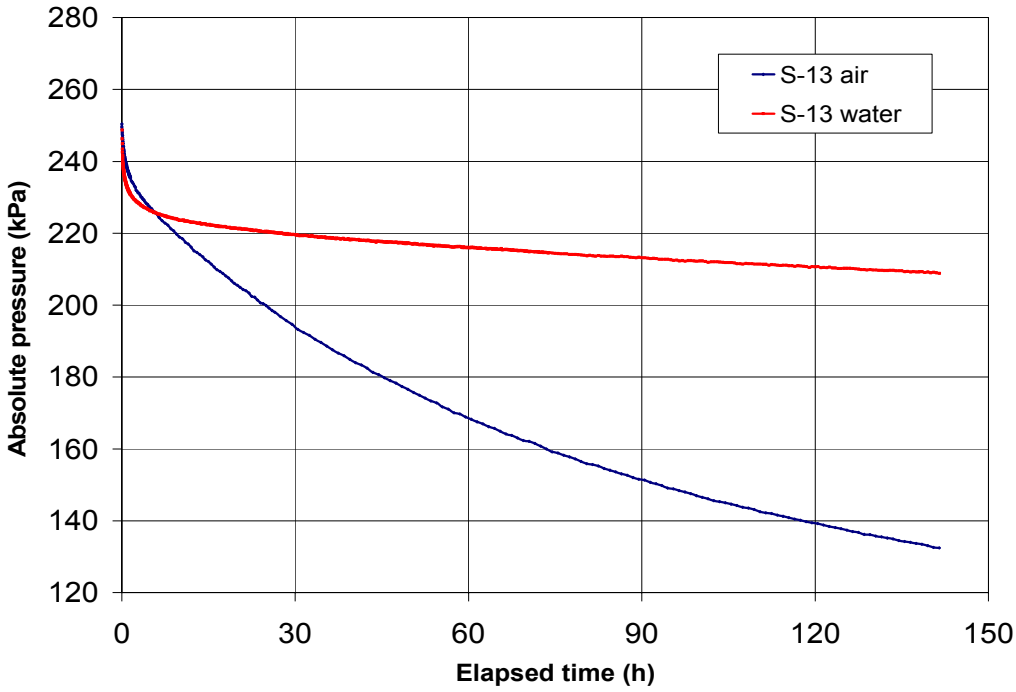

Figure C.7 – Decrease in the absolute pressure of nitrogen for S-13 during the test in air and in water

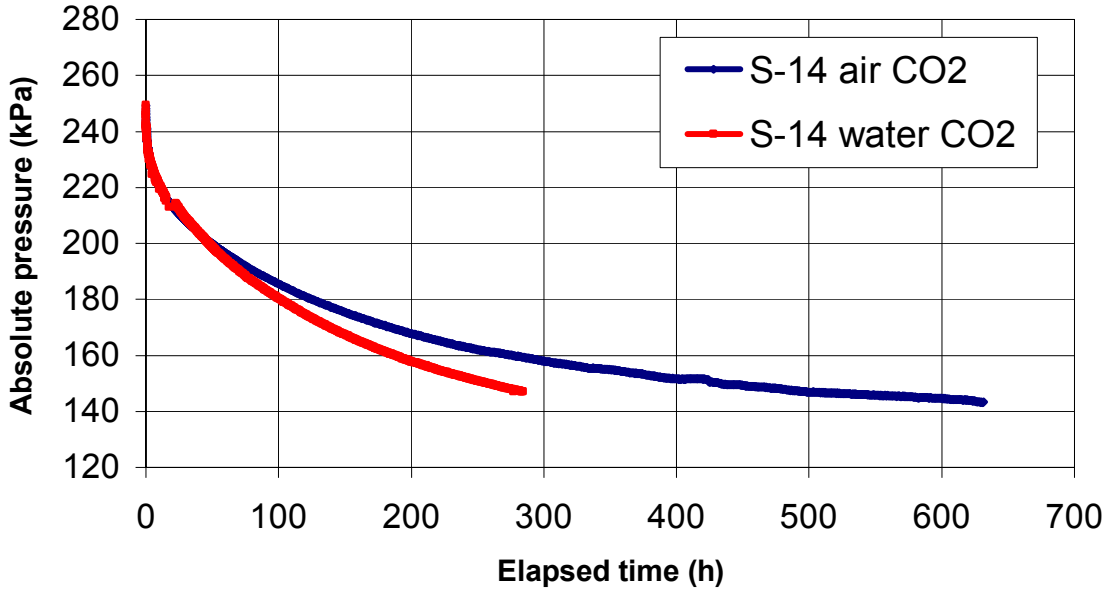

Figure C.8 – Decrease in the absolute pressure of carbon dioxide for S-14 during the test in air and in water

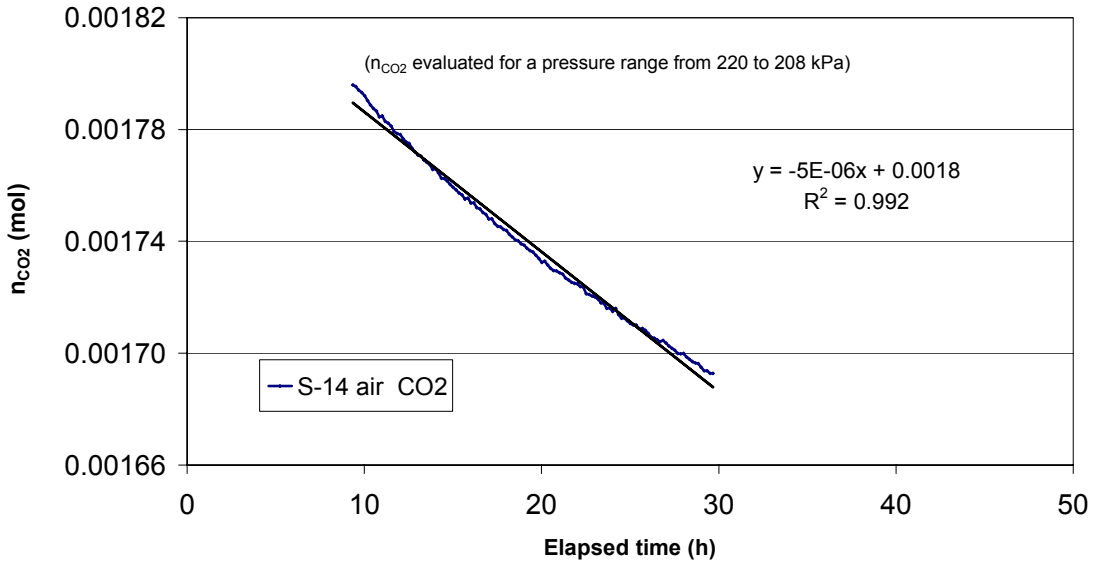

Figure C.9 – Carbon dioxide quantity permeating through the S-14 in test carried out with the specimen in air

APPENDIX D: DETERMINATION OF THE UNCERTAINTIES

1 THEORETICAL BACKGROUND

1.1 Definitions

The uncertainty of measurement is a parameter associated with the result of a measurement that characterizes the dispersion of the values that could reasonably be attributed to the measurand (Guide EA-4/02 1999).

The measurand (output quantity), Y, is a particular quantity that is subject to measurement. It depends on a number of input quantities ($X_1, \ldots X_N$) according to the functional relationship $Y = f(X_1, \ldots, X_N)$, which represents the procedure of measurement and the method of evaluation (Guide EA-4/02 1999).

According to the Guide EA-4/02 (1999), for a random variable, the variance of its distribution or positive square root of the variance (standard deviation) is used as a measure of the dispersion of values. The standard uncertainty of measurement associated with the output estimate or measurement result (y), indicated by $u(y)$, is the standard deviation of the measurand Y. It is to be calculated from the estimates x_i of the input quantities X_i and their associated standard uncertainties $u(x_i)$.

1.2 Methods for evaluating the uncertainty of a measurement related with input quantities

The uncertainty of measurement associated with the input estimates is evaluated according to either a "Type A" or a "Type B" method of determination. The first is the method of evaluating the uncertainty by the statistical analysis of a series of observations. The standard uncertainty is the experimental standard deviation of the mean that follows from an averaging methodology or an appropriate regression analysis. The "Type B" evaluation of standard uncertainty is the method of evaluating the uncertainty by a means other than the statistical analysis of a series of observations. It is based on other scientific knowledge (Guide EA-4/02 1999).

For a proper use of the available information for a Type B evaluation of standard uncertainty of a measurement, the following cases must be distinguished (Guide EA-4/02 1999):

(1) when only a single value is known for a quantity X_i such as, for example, a single measured value, a resultant value of a previous measurement, a reference value from the literature, or a correlation value, this value will be used for x_i. The standard uncertainty $u(x_i)$ associated with x_i is to be adopted where it is given. Otherwise, it has to be calculated from unequivocal uncertainty data. If data of this kind are not available, the uncertainty has to be assessed on the basis of experience;
(2) when a probability distribution function (PDF) can be assumed for a quantity X_i, based either on theory or on experience, then, appropriate expectation or expected value and

square root of the variance of this distribution has to be taken as the estimate x_i and associated standard uncertainty $u(x_i)$, respectively.

(3) if only upper and lower limits, a_+ and a_-, can be estimated for the value of the quantity X_i, (for example: manufacturer's specifications of a measuring instrument, a temperature range, a rounding or truncation error resulting from automated data reduction), a probability distribution with a constant probability density between these limits (rectangular probability distribution, has to be assumed for the possible variability of the input quantity X_i. According to the case (2) above, this leads to:

$$x_i = \frac{1}{2}(a_+ + a_-) \tag{D.1}$$

for the estimated value and to:

$$u(x_i) = \sqrt{\frac{1}{12}(a_+ + a_-)^2} \tag{D.2}$$

for the square of the standard uncertainty. If the difference between the limiting values is termed by $2a$, equation (D.2) yields:

$$u(x_i) = \frac{a}{\sqrt{3}} \tag{D.3}$$

The rectangular distribution is a reasonable description from a probability point of view of the inadequate knowledge about the input quantity X_i in the absence of any other information than its limits of variability.

1.3 Sources of uncertainty of measurement

The uncertainty of the result of a measurement reflects the lack of complete knowledge of the value of the output quantity, for which an infinite amount of information would be required. The phenomena that contribute to the uncertainty and thus to the fact that the result of a measurement cannot be characterized by a unique value, are called sources of uncertainty. In practice, there are many sources of uncertainty in a measurement, including: incomplete

definition of the measurand; imperfect realization of the definition of the measurand; non-representative sampling; inadequately known effects of environmental conditions or their imperfect measurements; personal bias; finite instrument resolution; approximations and assumptions incorporated in the measurement method and procedure, etc.

The main possible sources of uncertainty in the measurements carried out in the experimental work described in the present study that contribute to uncertainty budget include: resolution of each equipment used, results of calibrations, approximations and assumptions incorporated in the measurement methods and procedures, and operator influence. The corrected input quantity (x_c) is then equal to the sum corrections due to resolution (δx_{res}), calibrations (δx_{cal}), approximations and assumptions incorporated in the measurement methods and procedures (δx_{meth}), and operator (δx_{ope}):

$$x_c = x_{read} + \delta x_{res} + \delta x_{cal} + \delta x_{meth} + \delta x_{ope} \quad \text{(D.4)}$$

1.4 Evaluation of standard uncertainty of the input quantities

In the present study, the evaluation of standard uncertainty of the input quantities is evaluated based on experience, i.e., using methods Type B. This is done with the identification of all sources of uncertainty.

Assuming non co-related input quantities, the standard uncertainty of the input quantities is given by:

$$u(x_c) = \sqrt{\sum_{i=1}^{N} u^2(x_i)} \quad \text{(D.5)}$$

Equation (D.5) can be re-written as follows:

$$u(x_c) = \sqrt{u^2(x_{read}) + u^2(\delta x_{res}) + u^2(\delta x_{cal}) + u^2(\delta x_{meth}) + u^2(\delta x_{ope})} \quad \text{(D.6)}$$

1.5 Evaluation of standard uncertainty of the output estimate

The evaluation of standard uncertainty of the output estimate is calculated using the equation $y = f(x_1, \ldots, x_N)$ and applying the law of propagation of uncertainties. For non co-related input quantities, the square of the standard uncertainty associated with output estimate y is given by:

$$u(y) = \sqrt{\sum_{i=1}^{N} \left(\frac{\partial f}{\partial x_i} \right)^2 (x_i)^2} \qquad \text{(D.7)}$$

where

$$\frac{\partial f}{\partial x_i} = \left. \frac{\partial f}{\partial X_i} \right|_{X_1 = x_1, \ldots, X_N = x_N} = c_i \qquad \text{(D.8)}$$

and c_i is the sensitivity coefficient associated with the input estimated x_i, which corresponds to the partial derivative of the model function f with respect to X_i estimated at input estimates x_i.

1.6 Evaluation of expanded uncertainty of measurement

From a practical point of view, the values of the standard uncertainty of the output estimate, *u(y)*, are comparable to one standard deviation, what corresponds to a coverage probability of approximately 68%. If a high level of coverage probability is required, the uncertainty might be expanded to a required level, which can be done by multiplying the standard uncertainty, *u(y)*, of the output estimate, *y*, by a coverage factor *k*:

$$U = k\, u(y) \qquad \text{(D.9)}$$

A coverage factor of equal to 2 corresponds to a coverage probability of approximately 95%, and of equal to 3 corresponds to a coverage probability of approximately 99%.

1.7 Summary

To estimate the uncertainty of measurement the following steps must be considered:

- definition of the functional relationship between the output quantity and the input quantities;
- identify and apply all significant corrections;
- list all sources of uncertainty;
- for input quantities for which the probability distribution function (PDF) is known or can be assumed, calculate the expectation and the standard uncertainty $u(x_i)$ according to Section 1.2, item (2). If only upper and lower limits are given or can be estimated, calculate the standard uncertainty $u(x_i)$ in accordance with Section 1.2, item (3);
- calculate the uncertainty of input quantities;
- estimate the standard uncertainty of output estimated; and
- if a level of coverage probability higher than 68% is required, calculate the expanded uncertainty U by multiplying the standard uncertainty $u(y)$ associated with the output estimate by a coverage factor k.

The methodology outlined is used to estimate the uncertainties associated to the gas permeation through geomembrane seams as well as to the flow rate through composite liners due to geomembrane defects and corresponding interface transmissivity. The uncertainties of the output estimate are calculated for a coverage probability of 68% (coverage factor $k = 1$), that means the uncertainties are comparable to one standard deviation.

2 UNCERTAINTIES OVER THE PERMEANCE AND GAS FLUX THROUGH GEOMEMBRANE SEAMS

2.1 Definitions of the functional relationships

To measure the gas flux, f_G, and the permeance, P_G, through geomembrane seams, gas permeation pouch tests were carried out in two scales: small-scale and large-scale. In tests carried out in small-scale these coefficients were assessed assuming that pseudo steady state conditions were attained. For the large-scale test, it was impossible to find a reasonable period of time in which the pseudo steady state conditions could be assumed. Under unsteady state conditions, time constant, τ, was used to characterise the response of the specimen to the migration of gas throughout the seam.

The gas flux, f_G, was estimated as from ideal gas law, through the equation below:

$$f_G = \frac{V}{TR}\frac{\Delta p_{Gin}}{\Delta t} \tag{D.10}$$

where p_{Gin} is the gas absolute pressure (relative pressure + atmospheric pressure) inside the specimen (Pa); V is the specimen inner volume (m^3); R is the universal gas constant

(8.3143 m^3 Pa mol^{-1} K^{-1}); T is the specimen absolute temperature *(K),* and t is the time (s).

The temperature, as well as the relative and atmospheric pressures were directly read using pressure transducers (see Table D.1). The volume was estimated indirectly by adding the volume of specimen without pressure ($V_{prel=0}$) to the variation in the volume of the specimen due to the pressurization ($dV_{prel=150\ kPa}$), as shown below:

$$V = V_{p_{rel}=0} + dV_{p_{rel}=150kPa} \tag{D.11}$$

where $V_{prel=0}$ was estimated by weighing the specimen full of water and dry:

$$V_{p_{rel}=0} = \frac{m}{\rho_w} \tag{D.12}$$

where m is the mass of the specimen and ρ_w is the mass density of the water.

The volume of the specimen due to the pressurization was estimated thanks to a capillary pipe connected to a pressure transducer. Transducer readings were converted into height of water in the capillary pipe and then multiplied by the area of the pipe to obtain the volume change due to gas specimen pressurization (150 kPa):

$$dV_{p_{rel}=150kPa} = \Delta h_{cap.pipe}\, A_{cap.pipe} \tag{D.13}$$

The mean gas permeance per unit of length was then determined using the equation below:

$$\overline{P_G} = \frac{f_G}{\overline{\Delta p_G}\, L} \tag{D.14}$$

where L equals to the length of the specimen and $\overline{\Delta p_G}$ is the gas mean partial pressure difference inside and outside the specimen, which can be determined through the Equation (D.15):

$$\overline{\Delta p_G} = \overline{p_{Gin}} - p_{Gout} \tag{D.15}$$

where $\overline{p_{Gin}}$ is the gas mean absolute pressure inside the specimen and p_{Gout} is the gas absolute pressure outside the specimen, both values were calculated for pseudo steady state conditions. For carbon dioxide, p_{Gout} is zero, whereas for nitrogen gas, the gas absolute pressure outside the specimen was estimated using the equation below (details on Appendix A):

$$p_{Gout} = 0.7808 \frac{\overline{p_{atm}}}{1 + 1.61\, r} \tag{D.16}$$

where $\overline{p_{atm}}$ is the mean atmospheric pressure and r can be estimated through the psychometric chart, knowing the relative humidity (RH) and the air temperature. The RH and the air temperature were also automatically measured using the devices indicated on Table D.1.

Regarding the time constant parameter, τ, assessed in unsteady state conditions, it can be estimated as follows:

$$\ln Z(t) = \frac{-t}{\tau} \tag{D.17}$$

with

$$Z(t) = \frac{p_{Gin}(t) - p_{Gout}}{p_{Gin}(0) - p_{Gout}} \tag{D.18}$$

where $p_{Gin}(t)$ is the gas absolute pressure inside the specimen at time t (Pa); $p_{Gin}(0)$ is the gas absolute pressure inside the specimen at time t equal to zero (Pa); and p_{Gout} is the gas absolute pressure outside the pouch specimen (Pa).

The quantities measured, represented by equations (D.10), (D.14) and (D.17) can be modelled by the equations below:

$$f_G = f_1(\Delta p_{Gin}, V, T, R, \Delta t) \tag{D.19}$$

$$\overline{P_G} = f_2(f_G, \overline{\Delta p_G}, L) \tag{D.20}$$

$$\tau = f_3(p_{Gin}, p_{Gout}, t) \tag{D.21}$$

2.2 Corrections, sources of uncertainty and uncertainty of input quantities

The quantities required for evaluating f_G, P_G and τ are automatically read and recorded thanks to data acquisition systems. Table D.1 presents the devices used for measuring the different quantities in small-scale tests. Different devices were used in large-scale tests (Table D.2), for some quantities, such as: the absolute pressure inside the specimen, the atmospheric pressure, the air temperature and the relative humidity.

Table D.1 - Equipment used in small-scale tests

Parameters under measurement	Objectives	Equipment used
Relative pressure (p_{rel}) (kPa)	Determination of f_G, at any given time	Pressure transducer Model TJE, Sensotec Range: 0-25PSI (172kPa) Accuracy: ± 0.1% F. S. (full scale) p_{rel}= 23.034U+0.8508 (Pa/Volt)
Time (t) (s)	Determination of f_G	Timer counter (computer)
Variation of water in capillarity pipe ($\Delta h_{cap.pipe}$) (cm)	Determination of the variation of volume of the specimen due to pressurization (dVp_{rel}= 150kPa = $\Delta h_{cap.pipe} A_{cap.pipe}$) ($A_{cap.pipe}$= 0.2496 cm^2)	Pressure transducer Model P3091, Schaevitz Range: 0-25 cm of H_2O Accuracy: ± 0.5% $h_{cap.pipe}$= 2.8451U-Cte (cm/Volt)
Atmospheric pressure (p_{atm}) (kPa)	Determination of f_G, at any given time	Pressure transducer Model Tb 303 Bourdon Sedeme Range: 0-115kPa Accuracy: ± 0.2% p_{atm}= 10.714U + 62.634 (Pa/Volt)
Air temperature (t_{air}) (ºC)	Determination of f_G, at any given time	Temperature transducer Model Cuproswem Range: -50 to 150 ºC Accuracy: ± 0.01ºC t_{air}= 1.002 $t_{displayed}$ − 0.864
Relative humidity (RH) (%)	Assessment of the gas partial pressure (Δp_G), required for calculating the P_G	Humidity Sensor Model HIH-3605-A Range: 0-100% Accuracy: ± 2% R.H. RH= 30.6638U-24.482 (%/Volt)
Mass (M) (g)	Determination of the initial volume of the specimen before pressurization Vp_{rel}=0 (weight specimen full of water – weight of dry pouch)	Balance BP 3100P Range: 0-3100g Scale interval (range): d=0.01 (<600g)
Length (L) (m)	Determination of the length of the specimens, required for calculating the P_G	Meter rule (Sartorius) Range: 0.001 m –1 m Resolution: 0.001 m

Table D.2 - Equipment used in large-scale tests

Parameters under measurement	Objectives	Equipment used
Absolute pressure (p_{abs}) (kPa)	Determination of f_G, at any given time	Pressure transducer Model PMP 4070 druck Range: 0-3.5 bar (350 kPa) Accuracy: ± 0.04% F. S. (full scale) p_{abs}= 35000 U(Pa/Volt)
Atmospheric pressure (p_{atm}) (kPa)	Determination of f_G, at any given time	Sensor Model Rotronic BM 90 Range: 0-200kPa Accuracy: ± 0.01kPa
Air temperature (t_{air}) (ºC)	Determination of f_G, at any given time	Sensor Model Rotronic BM 90 Range: -50 to 150 ºC Accuracy: ± 0.1ºC
Relative humidity (*RH*) (%)	Assessment of the gas partial pressure (Δp_G), required for calculating the P_G	Sensor Model Rotronic BM 90 Range: 0-100% Accuracy: ± 0.1% R.H.

The evaluation of the standard uncertainty associated to f_G requires the determination of the corrected value x_c of each input quantity, namely: V (M, and $\Delta h_{cap.\ pipe}$), p_{abs}, and t, according to the Equation (D.6). Table D.3 to Table D.9 present the values of standard uncertainty for different input quantities.

It should be noted that, for the instruments that have calibration certificates, the reported uncertainty is typically the expanded uncertainty of measurement multiplied by a coverage factor *k=2*, which for a normal distribution corresponds to a coverage probability of approximately 95%. Whenever the uncertainties are evaluated to a coverage factor probability of 65%, the contribution of the calibration for output standard uncertainty must be divided by 2, i.e. $u_i(y) = U/2$, if *k=2*.

Table D.3 - Standard uncertainty for *M*

Quantity X_i=M	Limits (m) or uncertainties	Probability distribution function	Standard input uncertainty $u(x_i)$	Sensitivity coefficient c_i	Contribution to the output standard uncertainty $u_i(y)$
δM_{res}	± 0.005 g	rectangular	$\pm \frac{m}{\sqrt{3}}$	1.0	0.003 g
δM_{cal}	$U(M_{cal})$ = ± 0.01 g (k=2)	-	-	-	0.005 g
δM_{meth}	± 0.05 g	rectangular	$\pm \frac{m}{\sqrt{3}}$	1.0	0.029 g
δM_{ope}	-	Normal (95%)	$\pm \frac{m}{2}$	1.0	-
M	-	-		-	0.029 g

Table D.4 - Standard uncertainty for $h_{cap.pipe}$

Quantity $X_i=h_{cap.pipe}$	Limits (h) or uncertainties	Probability distribution function	Standard input uncertainty $u(x_i)$	Sensitivity coefficient c_i	Contribution to the output standard uncertainty $u_i(y)$
$\delta h_{cap.pipe-res}$	± 0.05 cm	rectangular	$\pm \frac{h}{\sqrt{3}}$	1.0	0.03 cm
$\delta h_{cap.pipe-cal}$	$U(h)$ = ± 0.1 cm (k=2)	-	-	-	0.05 cm
$\delta h_{cap.pipe-meth}$	± 0.2 cm	rectangular	$\pm \frac{h}{\sqrt{3}}$	1.0	0.17 cm
$\delta h_{cap.pipe-ope}$	± 0.1 cm	normal (95%)	$\pm \frac{h}{2}$	1.0	0.05 cm
$h_{cap.pipe}$	-	-	-	-	0.19 cm

Table D.5 - Standard uncertainty for p_{rel}

Quantity $X_i=p_{rel}$	Limits ($p_{relative}$) or uncertainties	Probability distribution function	Standard input uncertainty $u(x_i)$	Sensitivity coefficient c_i	Contribution to the output standard uncertainty $u_i(y)$
$\delta p_{rel-res}$	± 0.5 kPa	rectangular	$\pm \frac{p_{relative}}{\sqrt{3}}$	1.0	0.29 kPa
$\delta p_{rel-cal}$	$U(p_{relative})$ = ± 1 kPa (k=2)	-	-	-	0.50 kPa
$\delta p_{rel-meth}$	± 1 kPa	rectangular	$\pm \frac{p_{relative}}{\sqrt{3}}$	1.0	0.58 kPa
$\delta p_{rel-ope}$	-	normal (95%)	$\pm \frac{p_{relative}}{2}$	1.0	-
$\delta p_{rel-temp}$	0.66 kPa	normal (95%)	$\pm \frac{p_{relative}}{2}$	1.0	0.33 kPa
p_{rel}	-	-	-	-	0.88 kPa

Table D.6 - Standard uncertainty for p_{atm}

Quantity $X_i=p_{atm}$	Limits ($p_{atmosph}$) or uncertainties	Probability distribution function	Standard input uncertainty $u(x_i)$	Sensitivity coefficient c_i	Contribution to the output standard uncertainty $u_i(y)$
$\delta p_{atm-res}$	± 0.5 kPa	rectangular	$\pm \frac{p_{atmosph}}{\sqrt{3}}$	1.0	0.29 kPa
$\delta p_{atm-cal}$	$U(p_{atmosph})$ = ± 1 kPa (k=2)	-	-	-	0.50 kPa
$\delta p_{atm-meth}$	± 1 kPa	rectangular	$\pm \frac{p_{atmosph}}{\sqrt{3}}$	1.0	0.58 kPa
$\delta p_{atm-ope}$	-	normal (95%)	$\pm \frac{p_{atmosph}}{2}$	1.0	-
p_{atm}	-	-	-	-	0.82 kPa

Table D.7 - Standard uncertainty for t_{air}

Quantity $X_i=t_{air}$	Limits (t_a) or uncertainties	Probability distribution function	Standard input uncertainty $u(x_i)$	Sensitivity coefficient c_i	Contribution to the output standard uncertainty $u_i(y)$
$\delta t_{air\text{-}res}$	± 0.25 ºC	rectangular	$\pm \frac{t_a}{\sqrt{3}}$	1.0	0.14 ºC
$\delta t_{air\text{-}cal}$	$U(t_a)$ = ± 0.5 ºC (k=2)	-	-	-	0.25 ºC
$\delta t_{air\text{-}meth}$	± 1 ºC	rectangular	$\pm \frac{t_a}{\sqrt{3}}$	1.0	0.58 ºC
$\delta t_{air\text{-}ope}$	-	normal (95%)	$\pm \frac{t_a}{2}$	1.0	-
t_{air}	-	-	-	-	0.65 ºC

Table D.8 - Standard uncertainty for t

Quantity $X_i=t$	Limits ($time$) or uncertainties	Probability distribution function	Standard input uncertainty $u(x_i)$	Sensitivity coefficient c_i	Contribution to the output standard uncertainty $u_i(y)$
δt_{res}	± 0.5 s	rectangular	$\pm \frac{time}{\sqrt{3}}$	1.0	0.29 s
δt_{cal}	-	-	$\pm \frac{time}{2}$	-	-
δt_{meth}	± 1 s	rectangular	$\pm \frac{time}{\sqrt{3}}$	1.0	0.58 s
δt_{ope}	-	normal (95%)	$\pm \frac{time}{2}$	1.0	-
t	-	-	-	-	0.65 s

Table D.9 - Standard uncertainty for p_{abs} (large-scale tests)

Quantity $X_i=p_{abs}$	Limits ($p_{absolute}$) or uncertainties	Probability distribution function	Standard input uncertainty $u(x_i)$	Sensitivity coefficient c_i	Contribution to the output standard uncertainty $u_i(y)$
$\delta p_{abs\text{-}res}$	± 0.5 kPa	rectangular	$\pm \frac{p_{absolute}}{\sqrt{3}}$	1.0	0.29 kPa
$\delta p_{abs\text{-}cal}$	$U(p_{absolute})$ = ± 1 kPa (k=2)	-	-	-	0.50 kPa
$\delta p_{abs\text{-}meth}$	± 1 kPa	rectangular	$\pm \frac{p_{absolute}}{\sqrt{3}}$	1.0	0.58 kPa
$\delta p_{abs\text{-}ope}$	-	normal (95%)	$\pm \frac{p_{absolute}}{2}$	1.0	-
$\delta p_{abs\text{-}instrumentation}$	± 0.14 kPa	normal (95%)	$\pm \frac{p_{absolute}}{2}$	1.0	0.08 kPa
p_{abs}	-	-	-	-	0.94 kPa

Concerning permeance, P_G, the evaluation of standard uncertainties requires as well the determination of corrected values x_c, according to Equation (D.6). In this case, input quantities include f_G, L and Δp_G. Table D.10 presents the values of standard uncertainty for L. As regards Δp_G, it is necessary to correct p_{Gin} (Table D.5 and Table D.6) and p_{Gout} (recall Equation (D.16)), which is linked with the atmospheric pressure (p_{atm}), air temperature (t_{air}) and relative humidity (RH). Values of p_{atm} and t_{air} can be corrected based on Table D.6 and Table D.7, respectively. Regarding RH, it can be corrected based on Table D.11.

Table D.10 - Standard uncertainty for L

Quantity $X_i=L$	Limits (l) or uncertainties	Probability distribution function	Standard input uncertainty $u(x_i)$	Sensitivity coefficient c_i	Contribution to the output standard uncertainty $u_i(y)$
δL_{res}	± 0.5 mm	rectangular	$\pm \frac{l}{\sqrt{3}}$	1.0	0.29 mm
δL_{cal}	$U(l)$ = ± 1 mm (k=2)	-	-	-	0.50 mm
δL_{meth}	± 1 mm	rectangular	$\pm \frac{l}{\sqrt{3}}$	1.0	0.58 mm
δL_{ope}	± 1 mm	normal (95%)	$\pm \frac{l}{2}$	1.0	0.50 mm
L	-	-	-	-	0.96 mm

Table D.11 - Standard uncertainty for RH

Quantity $X_i=RH$	Limits (rh) or uncertainties	Probability distribution function	Standard input uncertainty $u(x_i)$	Sensitivity coefficient c_i	Contribution to the output standard uncertainty $u_i(y)$
δRH_{res}	± 1%	rectangular	$\pm \frac{rh}{\sqrt{3}}$	1.0	0.58 %
δRH_{cal}	$U(rh)$ = ± 2 % (k=2)	-	-	-	1.0 %
δRH_{meth}	-	rectangular	$\pm \frac{rh}{\sqrt{3}}$	1.0	-
δRH_{ope}	-	normal (95%)	$\pm \frac{rh}{2}$	1.0	-
RH	-	-	-	-	1.15 %

2.3 Estimation of the standard uncertainty of the output estimate

Once the corrections of all input quantities are known, the standard uncertainty of output estimate can be evaluated. Recalling the equation $f_G = \frac{V}{TR}\frac{\Delta p_{Gin}}{\Delta t}$, making $\frac{\Delta p_{Gin}}{\Delta t} = \vartheta$, with $\Delta p_{Gin} = \Delta p_{rel}$, the standard uncertainty for the gas flux, f_G, can be estimated as follows:

$$u(f_G) = \sqrt{\left(\frac{\partial f_G}{\partial \vartheta}\right)^2 u^2(\vartheta) + \left(\frac{\partial f_G}{\partial V}\right)^2 u^2(V) + \left(\frac{\partial f_G}{\partial T}\right)^2 u^2(T)} \qquad \text{(D.22)}$$

or

$$u(f_G) = \sqrt{\left(\frac{V}{RT}\right)^2 u^2(\vartheta) + \left(\frac{\vartheta}{RT}\right)^2 u^2(V) + \left(\frac{V\vartheta}{RT^2}\right)^2 u^2(T)}$$

or

$$u(f_G) = \frac{1}{RT}\sqrt{V^2 u^2(\vartheta) + \vartheta^2 u^2(V) + \left(\frac{V\vartheta}{T}\right)^2 u^2(T)}$$

The quantity $u(\vartheta)$ can be estimated based on a graphical method, by plotting $p_{rel} \pm u(p_{rel})$ versus $t \pm u(t)$, where $u(p_{rel})$ can be estimated from

Table D.5 and $u(t)$ is estimated from Table D.7. The quantity $u(T)$ can be assessed from Table D.7, and, finally, the quantity $u(V)$ can be estimated through the equation below (recall Equations (D.11) to (D.13)):

$$u^2(V) = u^2(V_{p_{rel}=0}) + u^2(dV_{p_{rel}=150kPa}) \qquad \text{(D.23)}$$

where $u^2(V_{prel=0}) = \frac{1}{\rho_w^2}u^2(m)$ and $u^2(dV_{p_{rel}=150kPa}) = A^2 u^2(\Delta h_{cappipe})$. The area of the capillary pipe, A, is constant, therefore the uncertainty associated to its measurement can be neglected ($u(A)$=0). In addition, $\Delta h_{cap.pipe} = \left[h_{cap.pipe}(t_2) - h_{cap.pipe}(t_1)\right]$ and $u\left[h_{cap.pipe}(t_2)\right] = u\left[h_{cap.pipe}(t_1)\right]$. The uncertainty of the capillarity pipe is then $u^2(\Delta h_{cap.pipe}) = 2u^2(h_{cap.pipe})$. The Equation (D.23) can then be written as follows:

$$u^2(V) = \frac{1}{\rho_w{}^2} u^2(m) + A^2\, 2u^2(h_{cap.pipe}) \tag{D.24}$$

For the mean permeance $\overline{P_G}$, recalling the equation $\overline{P_G} = \frac{f_G}{\overline{\Delta p_G} L}$, the standard uncertainty of the output estimate can be calculated using the equation below:

$$u(\overline{P_G}) = \sqrt{\left(\frac{\partial \overline{P_G}}{\partial f_G}\right)^2 u^2(f_G) + \left(\frac{\partial \overline{P_G}}{\partial \overline{\Delta p_G}}\right)^2 u^2(\overline{\Delta p_G}) + \left(\frac{\partial \overline{P_G}}{\partial L}\right)^2 u^2(L)} \tag{D.25}$$

or

$$u(\overline{P_G}) = \sqrt{\left(\frac{1}{\overline{\Delta p_G} L}\right)^2 u^2(f_G) + \left(-\frac{f_G}{(\overline{\Delta p_G})^2 L}\right)^2 u^2(\overline{\Delta p_G}) + \left(-\frac{f_G}{(L)^2 \overline{\Delta p_G}}\right)^2 u^2(L)}$$

or

$$u(\overline{P_G}) = \frac{1}{\overline{\Delta p_G} L}\sqrt{u^2(f_G) + \left(-\frac{f_G}{\overline{\Delta p_G}}\right)^2 u^2(\overline{\Delta p_G}) + \left(-\frac{f_G}{L}\right)^2 u^2(L)}$$

The quantity $u(f_G)$ is evaluated through Equation (D.22), the quantity $u(L)$ can be determined from Table D.10, and the quantity $u(\overline{\Delta p_G})$ can be estimated through the expression below (recall Equation (D.15)):

$$u^2(\overline{\Delta p_G}) = u^2(p_{Gin}) + u^2(p_{Gout}) \tag{D.26}$$

where $u^2(p_{Gin}) = u^2(p_{rel}) + u^2(p_{atm})$ and $u^2(p_{Gout})$ can be estimated based on the following expression:

$$u^2(p_{Gout}) = \left(\frac{\partial p_{G\,out}}{\partial p_{atm}}\right)^2 u^2(p_{atm}) + \left(\frac{\partial p_{Gout}}{\partial r}\right)^2 u^2(r) \tag{D.27}$$

or

$$u^2(p_{Gout}) = \left(\frac{0.7808}{1+1.61r}\right)^2 u^2(p_{atm}) + \left[-\frac{0.7808\,(1.61\,\overline{p_{atm}})}{(1+1.61r)^2}\right]^2 u^2(r) \qquad \text{(D.28)}$$

with $u(p_{atm})$ being estimated based on Table D.6. Regarding $u(r)$, first, its variability was graphically determined, by plotting $RH \pm u(RH)$ against $t_{air} \pm u(t_{air})$, with $u(RH)$ and $u(t_{air})$ being determined from Table D.11 and Table D.7, respectively. The correspondent $u(r)$ was then estimated based on a psychometric chart. A value of 0.0018 ($g_{water}/g_{dry\ air}$) was obtained. The Equation (D.26) can then be re-written as follows:

$$u^2(\overline{\Delta p_G}) = u^2(p_{rel}) + u^2(p_{atm}) + \left(\frac{0.7808}{1+1.61r}\right)^2 u^2(p_{atm}) + \left[-\frac{0.7808\,(1.61\,\overline{p_{atm}})}{(1+1.61r)^2}\right]^2 u^2(r) \qquad \text{(D.29)}$$

Finally, the standard uncertainty for time constant, τ, was evaluated graphically, by plotting $t \pm u(t)$ versus $\ln Z \pm u(\ln Z)$. The quantity $u(t)$ is determined from Table D.8, whereas $u(\ln Z)$ can be obtained as follows:

$$u(\ln Z) = \sqrt{\left[\frac{\partial(\ln Z)}{\partial p_{Gin}(t)}\right]^2 u^2[p_{Gin}(t)] + \left[\frac{\partial(\ln Z)}{\partial p_{Gout}}\right]^2 u^2(p_{Gout}) + \left[\frac{\partial(\ln Z)}{\partial p_{Gin}(0)}\right]^2 u^2[p_{Gin}(0)]} \qquad \text{(D.30)}$$

or

$$u(\ln Z) = \sqrt{\left[\frac{1}{p_{Gin}(t) - p_{Gout}}\right]^2 u^2[p_{Gin}(t)] + \left[\frac{-\left(p_{Gin}(0) - p_{Gin}(t)\right)}{\left(p_{Gin}(t) - p_{Gout}\right)\left(p_{Gin}(0) - p_{Gout}\right)}\right]^2 u^2(p_{Gout}) +}$$

$$+ \sqrt{\left[\frac{-1}{\left(p_{Gin}(0) - p_{Gout}\right)}\right]^2 u^2[p_{Gin}(0)]}$$

where the $u^2(p_{Gin}) = u^2(p_{rel}) + u^2(p_{atm})$ and $u^2(p_{Gout})$ are either zero for carbon dioxide or for nitrogen and can be estimated from Equation (D.28).

To sum up, the standard uncertainty for the gas flux, f_G, is estimated thanks to Equation (D.20), for the permeance, P_G, thanks to Equation (D.23), and for the time constant, τ, it will be based on graphical method. Values obtained are included in experimental results through the error bars displayed in Figures 5.13, 5.15, 5.16 and 5.17 (Chapter 5).

3 UNCERTAINTIES OVER THE FLOW RATE AND THE INTERFACE TRANSMISSIVITY

3.1 Definitions of the functional relationships

To measure the flow rate, constant head tests were run at three different scales in LNEC (Portugal) and in Cemagref (France). Water flow measurement was conducted in two different ways. First, during the first few hours of testing, when there was a relatively large volume of effluent water, the water was collected at the downstream side of the cell and weighted. As the water flow decreased, the measurements were done using a Mariotte bottle attached to the top of the cell due to its higher accuracy at low flow rates.

For the first case, the flow collected at the interface, $Q_r(R_c)$, is radial and the flow rate can be calculated using the following equation:

$$Q_r\left(R_c\right) = \frac{M}{\rho_w t} \tag{D.31}$$

where M is the mass of water collected during a time interval t and ρ_w is the mass density of the water.

When a Mariotte bottle is used for measuring the flow, a total flow, Q, is measured and the flow rate can be obtained using the expression below:

$$Q = \frac{\Delta V}{t} \tag{D.32}$$

where ΔV is the variation of volume in the Mariotte bottle during a considered time interval t.

The quantities measured, represented by Equations (D.31) and (D.32), can be modeled through the equations below:

$$Q_r\left(R_c\right) = f_1\left(M, \rho_w, t\right) \tag{D.33}$$

$$Q = f_2\left(\Delta V, t\right) \tag{D.34}$$

3.2 Corrections, sources of uncertainty and uncertainty of input quantities

For the radial flow, $Q_r(R_c)$, different balances were used to weigh the water collected at the interface. In France, the balance Metter PB 3002 S was used (masses less than 3000g). In Portugal, the balance OHAUS was used (masses less than 4000g).

For total flow, Q, the measurements were done using a Mariotte bottle. Different Mariotte bottles could be used depending on the influent volume, namely 50ml, 100ml and 200ml or 400ml.

For time measurements, a chronometer was used in the two cases.

The evaluation of standard uncertainty associated to radial flow, $Q_r(R_c)$, requires the determination of the corrected value (x_c) of each input quantity, namely mass (M) and time (t), according to the Equation (D.6). Tables D.12 to D.14 present the standard uncertainty for different input quantities.

Table D.12 - Standard uncertainty for M: balance Mettler PB 3002 S (France, intermediate scale tests)

Quantity $X_i=M$	Limits (m) or uncertainties	Probability distribution function	Standard input uncertainty $u(x_i)$	Sensitivity coefficient c_i	Contribution to the output standard uncertainty $u_i(y)$
δM_{res}	± 0.005 g	rectangular	$\pm \frac{m}{\sqrt{3}}$	1.0	0.003 g
δM_{cal}	$u(m)$= ± 0.030 g	-	-	-	0.030 g
δM_{meth}	0 g	rectangular	$\pm \frac{m}{\sqrt{3}}$	1.0	0 g
δM_{ope}	-	normal (95%)	$\pm \frac{m}{2}$	1.0	-
M	-	-	-	-	0.030 g

Table D.13 - Standard uncertainty for M: balance OHAUS (Portugal)

Quantity $X_i=M$	Limits (m) or uncertainties	Probability distribution function	Standard input uncertainty $u(x_i)$	Sensitivity coefficient c_i	Contribution to the output standard uncertainty $u_i(y)$
δM_{res}	± 0.005 g	rectangular	$\pm \frac{m}{\sqrt{3}}$	1.0	0.005 g
δM_{cal}	$u(m)$= ± 0.035 g	-	-	-	0.035 g
δM_{meth}	0 g	rectangular	$\pm \frac{m}{\sqrt{3}}$	1.0	0 g
δM_{ope}	-	normal (95%)	$\pm \frac{m}{2}$	1.0	-
M	-	-	-	-	0.035 g

Table D.14 - Standard uncertainty for t

Quantity $X_i=t$	Limits (*time*) or uncertainties	Probability distribution function	Standard input uncertainty $u(x_i)$	Sensitivity coefficient c_i	Contribution to the output standard uncertainty $u_i(y)$
δt_{res}	± 0.005 s	rectangular	$\pm \frac{time}{\sqrt{3}}$	1.0	0.003 s
δt_{cal}	-	-	-	-	-
δt_{meth}	± 0.01 s	rectangular	$\pm \frac{time}{\sqrt{3}}$	1.0	0.006 s
δt_{ope}	± 1 s	normal (95%)	$\pm \frac{time}{2}$	1.0	0.500 s
t	-	-	-	-	0.50 s

The evaluation of standard uncertainty associated to total flow, Q, requires the determination of the corrected value (x_c) of each input quantity, namely volume (V) and time (t), according to the Equation (D.6). Tables D.15 to D.18 present the values of the standard uncertainty for different input quantities.

Table D.15 - Standard uncertainty for V: Mariotte bottle of 50 ml

Quantity $X_i=V$	Limits (v) or uncertainties	Probability distribution function	Standard input uncertainty $u(x_i)$	Sensitivity coefficient c_i	Contribution to the output standard uncertainty $u_i(y)$
δV_{res}	± 0.05 ml	rectangular	$\pm \frac{v}{\sqrt{3}}$	1.0	0.03 ml
δV_{cal}	$u(v)$= ± 0.030 g or ml	-	-	-	0.03 ml
δV_{meth}	± 0.11 ml	rectangular	$\pm \frac{v}{\sqrt{3}}$	1.0	0.06 ml
δV_{ope}	± 0.1 ml	normal (95%)	$\pm \frac{v}{2}$	1.0	0.05 ml
V	-	-	-	-	0.09 ml

Table D.16 - Standard uncertainty for V: Mariotte bottle of 100ml

Quantity $X_i=V$	Limits (v) or uncertainties	Probability distribution function	Standard input uncertainty $u(x_i)$	Sensitivity coefficient c_i	Contribution to the output standard uncertainty $u_i(y)$
δV_{res}	± 0.1 ml	rectangular	$\pm \frac{v}{\sqrt{3}}$	1.0	0.06 ml
δV_{cal}	$u(v)$= ± 0.035 g or ml	-	-	-	0.035 ml
δV_{meth}	± 0.85 ml	rectangular	$\pm \frac{v}{\sqrt{3}}$	1.0	0.49 ml
δV_{ope}	± 0.1 ml	normal (95%)	$\pm \frac{v}{2}$	1.0	0.050 ml
V	-	-	-	-	0.50 ml

Table D.17 - Standard uncertainty for V: Mariotte bottle of 200ml

Quantity $X_i=V$	Limits (v) or uncertainties	Probability distribution function	Standard input uncertainty $u(x_i)$	Sensitivity coefficient c_i	Contribution to the output standard uncertainty $u_i(y)$
δV_{res}	± 0.2 ml	rectangular	$\pm \frac{v}{\sqrt{3}}$	1.0	0.11 ml
δV_{cal}	$u(v)$= ± 0.035 g	-	-	-	0.04 ml
δV_{meth}	± 0.61 ml	rectangular	$\pm \frac{v}{\sqrt{3}}$	1.0	0.35 ml
δV_{ope}	± 0.2 ml	normal (95%)	$\pm \frac{v}{2}$	1.0	0.10
V	-	-	-	-	0.39 ml

Table D.18 - Standard uncertainty for V: Mariotte bottle of 400ml

Quantity $X_i=V$	Limits (v) or uncertainties	Probability distribution function	Standard input uncertainty $u(x_i)$	Sensitivity coefficient c_i	Contribution to the output standard uncertainty $u_i(y)$
δV_{res}	± 0.5 ml	rectangular	$\pm \frac{v}{\sqrt{3}}$	1.0	0.29 ml
δV_{cal}	$u(v)$= ± 0.035 g or ml	-	-	-	0.04 ml
δV_{meth}	± 0.96 ml	Rectangular	$\pm \frac{v}{\sqrt{3}}$	1.0	0.55 ml
δV_{ope}	± 0.5 ml	normal (95%)	$\pm \frac{v}{2}$	1.0	0.25 ml
V	-	-	-	-	0.67 ml

3.3 Estimating the standard uncertainty of the output estimate

For the flow collected at the interface, $Q_r(R_c)$, the standard uncertainty can be estimated through the equation below:

$$u\left[Q_r\left(R_c\right)\right]=\frac{1}{\rho_w}\sqrt{\left[\frac{\partial Q(R_c)}{\partial M}\right]^2 u^2(M)+\left[\frac{\partial Q(R_c)}{\partial t}\right]^2 u^2(t)} \quad \text{(D.35)}$$

or

$$u\left[Q_r\left(R_c\right)\right]=\frac{1}{\rho_w}\sqrt{\frac{1}{t^2}u^2(M)+\frac{M^2}{t^4}u^2(t)}$$

Considering that the time interval correspondent to the time elapsed between two flow measurements is long, when compared to the uncertainty associated to the measurement, it can be considered negligible. The Equation (D.35) can then be simplified as indicated below:

$$u\left[Q_r\left(R_c\right)\right]=\frac{1}{\rho_w t}u(M) \quad \text{(D.36)}$$

with $u(M)$ being determined either based on Table D.12 or on Table D.13.

For the total flow, Q, measured using a Mariotte bottle, the standard uncertainty can be assessed by the equation below:

$$u(Q)=\sqrt{\left(\frac{\partial Q}{\partial V_2}\right)^2 u^2(V_2)+\left(-\frac{\partial Q}{\partial V_1}\right)^2 u^2(V_1)+\left(\frac{\partial Q}{\partial t}\right)^2 u^2(t)} \quad \text{(D.37)}$$

or

$$u(Q)=\sqrt{\left(\frac{1}{t}\right)^2 u^2(V_2)+\left(\frac{-1}{t}\right)^2 u^2(V_1)+(V_2-V_1)^2\left(\frac{1}{-t^2}\right)^2 u^2(t)}$$

The time interval correspondent to the time elapsed between two flow measurements is long, when compared to the uncertainty associated to the measurement, therefore, it can be considered negligible. In this circumstance, the Equation (D.37) can then be simplified as indicated below:

$$u(Q) = \sqrt{\left(\frac{1}{t}\right)^2 u^2(V_2) + \left(\frac{-1}{t}\right)^2 u^2(V_1)} \tag{D.38}$$

In addition, assuming that the uncertainty of V_2 is equal to the uncertainty of V_1, the Equation (D.38) becomes:

$$u(Q) = \sqrt{\frac{2u^2(V)}{t^2}} = \frac{u(V)}{t}\sqrt{2} \tag{D.39}$$

with $u(V)$ being determined from one of the Tables (D.15 to D.18), depending on the Mariotte bottle used during the test.

3.4 Standard uncertainty for the interface transmissivity

The interface transmissivity, θ, is estimated based on the value of the measured final flow rate Q, according to the Equation (D.40):

$$Q = \pi r_0^2 k_s i_s - 2\pi r_0 \theta\beta\left[A_p I_1(\beta r_0) - B_p K_1(\beta r_0)\right] \tag{D.40}$$

with

$$A_p = -\frac{hK_0(\beta R_c) + C\left(K_0(\beta R_c) - K_0(\beta r_0)\right)}{K_0(\beta r_0) I_0(\beta R_c) - K_0(\beta R_c) I_0(\beta r_0)} \tag{D.41}$$

$$B_p = \frac{hI_0(\beta R_c) + C\left(I_0(\beta R_c) - I_0(\beta r_0)\right)}{K_0(\beta r_0) I_0(\beta R_c) - K_0(\beta R_c) I_0(\beta r_0)} \tag{D.42}$$

$$\beta = \sqrt{\frac{k_s}{(H_L + H_f)\theta}} \tag{D.43}$$

$$C = H_L + H_f \tag{D.44}$$

where I_0 and K_0 are modified Bessel functions of zero order; k_s is the equivalent hydraulic conductivity for the GCL and the soil layer; H_L is the GCL thickness; and H_f is the soil layer thickness.

The standard uncertainty of interface transmissivity is estimated indirectly from its potential variability. First, the upper and lower limits of θ were estimated. They correspond to the difference between the maximum θ_{max} and minimum θ_{min} values obtained by taking into account both the uncertainty associated to Q, previously determined in accordance with Section 3.3, and the variability of the hydraulic conductivity of the GCL for each confining stress used in this study and expressed through Figure 2.20 (Chapter 2). For that, Equation (D.40) is solved for the cases as follows:

- Q + u(Q) for k_{GCL} maximum at a specified confining stress according to the Figure 2.20;
- Q + u(Q) for k_{GCL} minimum at a specified confining stress according to the Figure 2.20;
- Q – u(Q) for k_{GCL} maximum at a specified confining stress according to the Figure 2.20;
- Q – u(Q) for k_{GCL} minimum at a specified confining stress according to the Figure 2.20.

Then, according to Section 1.2, the potential variability of the transmissivity was modeled by a rectangular distribution function and uncertainty of interface transmissivity, $u(\theta)$, was estimated as presented in the Table D.19.

Table D.19 - Standard uncertainty for transmissivity, θ

Quantity $X_i=\theta$	Value limits θ_{max} - θ_{min}	Probability distribution function	Standard input uncertainty $u(x_i)$	Sensitivity coefficient c_i	Contribution to the output standard uncertainty $u_i(y)$
$\delta\theta$	θ_{max} - θ_{min}	rectangular	$\frac{\theta_{max} - \theta_{min}}{\sqrt{3}}$	1.0	$u(\theta) = \frac{\theta_{max} - \theta_{min}}{\sqrt{3}}$

To sum up, the standard uncertainty for the radial flow rate, $u[Q_r(R_c)]$, is estimated thanks to Equation (D.36), whereas the standard uncertainty for the total flow rate, $u(Q)$, is estimated thanks to Equation (D.39). As regards the transmissivity, standard uncertainty is estimated based on its potential variability. Values obtained are included in experimental results through the error bars displayed in Figures 6.19 to 6.21, 6.24, 6.29, 6.34 and 6.35 (Chapter 6).

APPENDIX E: PROTOCOL FOR MEASURING GCL SUCTION USING THE FILTER PAPER METHOD[1] UNDER NO CONFINING PRESSURE

1. PRELIMINARY TESTS FOR DETERMINING THE INITIAL WATER CONTENT OF THE GCL (TO ESTIMATE THE MASS OF WATER NECESSARY TO PRE-HYDRATE THE SPECIMENS BY IMMERSION)

- Cut three specimens of GCL (for example, three squares of 5 cm in width);
- Weigh each specimen;
- Place the specimens in the oven (105º C) during at least 16 hours for drying;
- Remove the specimens from the oven, weigh them and calculate the initial moisture content (W_i) of the GCL (W_i = mass of water in the GCL/mass of dry GCL).

2. PRE-HYDRATION OF THE SPECIMENS

- Define the water contents to which the GCL specimens will be pre-hydrated (for example: natural, 15%, 30%, 45%, 60%, 75%, 90%, 105%, 120% and 135%);
- For each defined pre-hydration value, cut two GCL circular specimens with 10 cm in diameter (for each pre-hydration value, a couple of specimens is necessary);
- Weigh all specimens;
- Identify each couple of specimens with the same pre-hydration value writing on each one the information as follows: pre-hydration value, date, and specimen number (1 or 2);
- Based on the pre-estimated initial water content of the GCL and on the mass of the GCL specimens, estimate the mass of water that has to be added to each specimen to reach the defined pre-hydration value;

  Note: if possible, group the GCL specimens by selecting the two specimens of each pre-hydration value with a similar mass to be sure that both have similar immersion times. For the highest pre-hydration values, select the lightest specimens to reduce the immersion time.

- Pre-hydrate the GCL specimens by immersing them into distilled water (for the lowest pre-hydration values, a spray can be used); the immersion time depends on the mass of each specimen. Therefore, it is necessary to successively weigh it until the correspondent wet mass is reached; the pre-hydration values of the GCL specimens must be confirmed by determining its water content at the end of the suction measurements;

[1] Based on the ASTM D 5298 – 94.

- Wrap the two GCL specimens with the same pre-hydration value in a plastic film; then, insert the wrapped specimens in a watertight plastic bag; finally, place it in a air-tight container in a location with temperature variations less than 3º C; the container shall be labelled with the information as follows: date, pre-hydration value, and test number;
- Keep the GCL specimens in the containers for a minimum of **7** days to homogenise the water content.

3. FILTER PAPER PREPARATION (WHATMAN® NO. 42)

- Three stacked filter papers are necessary for each pre-hydration value; the outer filter papers are 7.0 cm in diameter and should be slightly larger in diameter than the center filter paper; this can be accomplished by cutting the center paper with a diameter of 5.5 cm; this operation shall be performed using gloves in order to prevent the filter paper contamination; the outer filter papers prevent the GCL contamination of the center filter paper used for analysis of the matric suction;
- Dry all filter papers for testing, at least for 16 hours or overnight, in the drying oven (105º C);
- After drying, place the filter paper in a desiccant jar over silica gel, as fast as possible (couple of seconds); connect desiccant jar to a vacuum pump, and keep them in vacuum until they are hot (10 to 15 minutes).

4. PROCEDURE FOR DETERMINING THE MATRIC SUCTION

- Remove the three stacked filter papers from the desiccant jar, and immediately (a couple of seconds) insert them between the two GCL specimens with the same pre-hydration value; to avoid the hydration of the filter paper, it is suggested to remove a group of three stacked filter papers each time; press slightly the GCLs specimens to ensure a good contact between the filter papers and the GCL;
- Wrap the "sandwich" formed by the GCL specimens and the filter papers with a plastic film; then, insert the wrapped specimens in a watertight plastic bag; finally, place it in a air-tight container (e.g. Tupperware) in a location with temperature variations less than 3ºC; the container shall be labelled with the information as follows: date, pre-hydration value, and test number;
- The suction of the filter paper and the GCL specimens in the container should be allowed to come to equilibration for a minimum of **7** days;
- At the end of the equilibration period, weigh glass filter paper containers, which will hold the filter papers; determine their mass to the nearest 0.0001 g;
- Estimate the final thickness of each couple of GCL specimens and weigh it for further determination of the water content of the GCL specimens, as section 5 indicates;

- Using tweezers, remove the centre filter paper of the three-layer stack and place it in the glass filter paper container of predetermined mass, put the lid on the glass filter paper container, then weigh it; determine this mass to the nearest 0.0001 g; this entire process must be completed in less than 5 seconds;
- Place the glass filter paper containers in an oven (105ºC), with the lids slightly ajar (or unsealed) to permit moisture to escape, for 16 hours or overnight;
- Remove the glass filter paper containers from the oven, seal them and place the sealed containers in a desiccant jar over silica gel to cool (10 to 15 minutes); after cooling, weigh them (less than 5 seconds); determine the mass to the nearest 0.0001 g.

5. THICKNESS AND WATER CONTENT DETERMINATIONS

- Estimate the final thickness of each couple of GCL specimens (the 2 GCL specimens with the same pre-hydration values); the thickness shall be measured at 1 min; it is suggested to measure the thickness just before removing the filter paper.

  Note: this determination is necessary to determine the volume of the specimens, and the volumetric water content of the GCL, which are necessary to make the "Van Genuchten adjustments".

- To confirm the pre-hydration values and accurately determine the water contents of the GCL specimens; place each couple of GCL specimens in a GCL container of predetermined mass, weigh it, and then place it in the in the drying oven (105º C), at least for 16 hours or overnight.
- Remove each couple of GCL specimens from the oven, weigh it and calculate its water content.

6. SUCTION CALCULATIONS

- Water content of the filter paper by mass, ω_f, can be estimated through the following expression:

$$\omega_f = \frac{M_w}{M_f} \times 100 \qquad \text{(E.1)}$$

where M_w is the mass of water in the filter paper (g), and M_f is mass of dry filter paper (g).

- Convert the filter paper water content (ω_f) into a suction value (ψ) by reference to the calibration curve for filter paper Whatman® No. 42, as the one included in ASTM D 5298 and presented below:

$$\psi = 10^{5.327-0.0779\omega_f} \quad \text{for } \omega_f < 45.3\ \%,$$

or (E.2)

$$\psi = 10^{2.412-0.0135\omega_f} \quad \text{for } \omega_f > 45.3\ \%:$$

Divisão de Edições e Artes Gráficas do LNEC